

DOCTORAT DE L'UNIVERSITE LILLE1

Ecole doctorale: science de la matière, du rayonnement et de l'environnement

Laboratoire d'Océanologie et de Géosciences

Discipline: Géosciences (GEPO)

**Relations entre tectonique, sédimentation, authigenèse et diagenèse
en contexte extensif :
le Jurassique supérieur du Boulonnais (France).**

Par :

Ebraheem HATEM

Directeurs de Thèse :

Nicolas TRIBOVILLARD & Olivier AVERBUCH

Rapporteurs:

François BAUDIN

Jean-François DECONINCK

Examinateurs

Anne BIALKOWSKI

Renaud BOUROULLEC

Alain TENTESAUX

Soutenance le 9 Octobre2015

A : (Ruba, Maria, Aya)

A : (mes parents)

A : mon pays (Syrie)

Merci

Au terme de ce travail, il m'est agréable d'exprimer ma reconnaissance à tous ceux qui, de près ou de loin, ont contribué à sa réalisation.

Je tiens à remercier tout particulièrement :

En premier lieu, je tiens à remercier infiniment mon directeur de thèse, monsieur :

Nicolas TRIBOVILLARD, pour la confiance qu'il m'a accordée en acceptant d'encadrer ce travail doctoral, pour ses multiples conseils et pour toutes les heures qu'il a consacrées à diriger cette recherche. J'aimerais également lui dire à quel point j'ai apprécié sa grande disponibilité et son respect sans faille des délais serrés de relecture des documents que je lui ai adressés. Enfin, j'ai été extrêmement sensible à ses qualités humaines d'écoute et de compréhension tout au long de ce travail doctoral.

Olivier AVERBUCH, en tant que co-directeur de thèse, pour sa disponibilité, son écoute, sa rigueur et sa confiance. Je le remercie également de m'avoir fait découvrir et aimer la tectonique, ainsi que de m'avoir aidé à gérer efficacement cette étude.

Mes sincères remerciements s'adressent également aux personnes ci-dessous, pour accepter de faire partie du jury de ma thèse :

- François BAUDIN: professeur à UPMC, université de Paris 06.
- Jean-François DECONINCK : professeur à la Centre des sciences de la terre, université de Bourgogne.
- Renaud BOUROULLEC : ingénieur géologue à TNO – Pays-Bas.
- Anne BIALKOWSKI : ingénieur géologue à BRGM, Unité Géologie des Bassins et Stockages.
- Alain TRENTESAUX : professeur à LOG UMR CNRS, université de Lille1 Sciences et Technologies

Je voudrais également remercier l'ensemble des personnes ci-dessous pour leur compétence, leurs aides techniques et scientifiques durant ces quatre années, et le temps précieux qu'elles ont pu me consacrer :

-Alain TRENTESAUX pour son aide scientifique.

-François GUILLOT pour l'échantillonnage.

-Viviane BOUT-ROUMAZEILLES, Romain ABRAHAM et Marion DELATTRE pour les analyses d'argiles.

-Sylvie REGNIER, pour la préparation des lames minces.

-Sandra VENTALON et Philippe RECOURT, pour les analyses microscopique.

-Monique Gentric

Je remercie très chaleureusement ma femme (Ruba), qui m'a donné l'espoir et de courage dans les moments les plus difficiles de ma vie.

Je remercie enfin toute ma famille et en particulier : ma mère, mon père, Abir, Ansab, Wihad, Ali, Fahd, Boussaina, ainsi que les parents de ruba qui m'ont soutenu pendant ces quatre années où galères et espoirs étaient tour à tour à l'ordre du jour. Bien qu'éloignés je les ai toujours sentis à mes côtés pour m'encourager et j'espère qu'ils savent à quel point je leur en suis reconnaissant.

Résumé

L'objectif de ce travail est d'évaluer les rôles respectifs des facteurs environnementaux et de la tectonique synsédimentaire en milieu de plate-forme propice à l'accumulation de matière organique. La zone atelier est le Jurassique supérieur du Boulonnais et ses dépôts terrigènes (grès et marnes), accumulés dans un contexte tectonique extensif, à une époque où les variations du niveau marin pouvaient être importantes. Nous montrons que les bancs calcaires et les récifs à huîtres que nous avons étudiés dans ces formations sont d'origine diagénétique très précoce et qu'ils se sont formés à l'interface eau-sédiment ou juste au-dessous. Ces carbonates sont induits par des réactions chimiques bactériennes rendues possibles par des circulations de fluides de long des failles synsédimentaires. Nos résultats montrent également que les conditions de préservation de la matière organique sont soumises à de nombreux facteurs mais nous insistons ici sur le rôle du fer qui, par sa présence, peut empêcher les réactions de sulfuration entre les ions sulfures et les molécules organiques. De ce fait, cette protection naturelle par sulfuration est empêchée et la matière organique est plus intensément reminéralisée. Les sources de fer sont multiples en milieu de plate-forme mais nos travaux suggèrent que les smectites puissent véhiculer du fer alors qu'elles sont souvent interprétées comme des vecteurs de matière organique. Enfin, nous montrons que des gradients de distribution de la smectite peuvent être très marqués sur de courtes distances, malgré la flottabilité de ce minéral. Cette information est utile pour les reconstitutions fondées sur les argiles.

Abstract

The goal of this study was to evaluate the respective roles of environmental factors and synsedimentary tectonic in a platform environment favorable to the accumulation of organic matter. The study area is the Upper Jurassic of the Boulonnais (Northern France) and the terrigenous deposits (sandstone and marl) accumulated in an extensive tectonic context, at a time when the sea level variations could be noticeable. We show that the limestone beds and oyster reefs that we studied are of earliest diagenetic origin and that they were formed at the water-sediment interface or just beneath. These carbonates are induced by bacterial chemical reactions enabled by fluid circulation along synsedimentary faults. Our results also show that the conditions of preservation of organic matter is subject to many factors but we focus here on the role of iron which, by its presence, can prevent sulfuration reaction between sulfide ions and organic molecules. Thus, this natural protection by sulfuration is prevented and the organic material is more intensely mineralized. The sources of iron are multiple in a platform environment but our work suggests that smectites can convey iron while they are often considered to be organic-matter vectors. Finally, we show that smectite distribution gradients can be very marked over short distances in spite of the buoyancy of this mineral. This information is useful for clay-based reconstructions.

Table des matières

Introduction & présentation de la thèse.....	1
Chapitre 1- Contexte géologique, matériel et méthodes	3
Chapitre 2 – Les récifs à huîtres comme indicateurs de suintements de fluides fossiles induites par des failles synsédimentaires.....	15
2.1 – Présentation	15
2.2- <i>Oyster patch reefs as indicators of fossil hydrocarbon seeps induced by synsedimentary faults.....</i>	17
2.3 – Compléments.....	27
Chapitre 3 – Formations de carbonates au cours de la diagénèse précoce dans un environnement de rampe terrigène soumise à des failles synsédimentaires : le rôle des fluides.....	33
3.1 – Présentation.....	33
3.2 – <i>Early diagenetic formation of carbonates in a clastic-dominated ramp environment impacted by synsedimentary faulting-induced fluid seepage - Evidence from the Late Jurassic Boulonnais Basin (N France</i>	37
3.3 – Compléments.....	81
Chapitre 4 – Transect selon un gradient proximal-distal dans les Argiles de Châtillon.....	89
4.1- Présentation.....	89
4.2- <i>Small-scaled lateral variations of an organic-rich formation in a ramp-type depositional environment (the Late Jurassic of the Boulonnais, France): impact of the clastic supply.....</i>	93
4.3 – Compléments.....	113
Chapitre 5 - Quelques observations importantes au cours du terrain.....	117
Conclusion générale.....	123
ANNEXE.....	125
<i>La disponibilité du fer : un contrôle de la composition chimique et de l'empreinte diagénétique des roches riches en matière organique :</i>	
1. Présentation.....	125

<i>2. Iron availability as a dominant control on the primary composition and diagenetic overprint of organic-matter-rich rocks.....</i>	129
---	------------

Les tableaux des résultats analytiques.....	147
--	------------

Introduction & présentation de la thèse

Depuis plus d'un siècle et demi, le Boulonnais a été le sujet de nombreuses études géologiques en raison d'une situation privilégiée. En effet, on y trouve une succession de terrains géologiques qui s'étagent depuis le Dévonien jusqu'au Quaternaire, comme le détaille la notice explicative de la feuille Marquise à 1/50 000 2^e édition (Mansy et al., 2007). Situé aux confins septentrionaux du Basin de Paris, le Boulonnais, par sa morphologie de terminaison péri-anticlinale érodée au cœur (morphologie dite « en boutonnière »), permet l'observation de l'intégralité de cette succession. Une des richesses géologiques de cette région est, en particulier, la qualité de l'enregistrement des dépôts sédimentaires au Jurassique supérieur (voir la figure 1 qui illustre les formations géologiques évoquées ci-dessous). A cette époque, la région est soumise à une subsidence significative en liaison avec les mouvements distensifs contemporains des stades initiaux du rifting de l'Océan Atlantique nord (partie de l'Atlantique située au nord de la faille transformante Terre Neuve-Gibraltar)(Mansy et al., 2003). Dans ce contexte, la zone d'étude est considérée comme ayant été principalement une rampe mixte, silicoclastique et carbonatée (Proust et al., 1995 ; Deconinck et al., 1996) où alternent des formations gréseuses et des formations argileuses, avec quelques intercalations de bancs carbonatés. Les formations riches en argiles du Boulonnais contiennent de la matière organique sédimentaire, ce qui en fait des roches mères d'hydrocarbures potentielles. Les formations gréseuses font des réservoirs possibles. L'ensemble du Jurassique supérieur de cette région peut être compris comme étant un système pétrolier, ce qui en fait un site d'études privilégié.

Cette zone du Boulonnais a fait l'objet de nombreuses études car elle représente un équivalent proximal de la célèbre « Kimmeridge Clay Formation » (KCF), qui a donné naissance au pétrole exploité en Mer du Nord. Sa stratigraphie et les conditions générales de dépôt sont donc relativement déjà bien connues. Nous allons nous attacher dans cette thèse à répondre à des questions liées aux facteurs influençant les dépôts du Jurassique supérieur du Boulonnais, en particulier, pour évaluer l'impact direct et indirect de la tectonique synsédimentaire sur les conditions de dépôts au sens large. L'impact de la tectonique syn-dépôt sur les modalités de l'accumulation sédimentaire dans un bassin en cours de structuration est important à déterminer dans le contexte des systèmes pétroliers (**volume spécial MPG 2014**). En effet, des failles synsédimentaires sont des zones drainantes pour les fluides expulsés au cours de la diagenèse précoce, et ces fluides peuvent être des hydrocarbures. En outre, les fluides mis en circulation au cours des mouvements synsédimentaires peuvent, de par leur chimisme particulier, induire des réactions diagénétiques précoces, comme des cimentations carbonatées. Ces objets carbonatés précoces peuvent éventuellement être des barrières de perméabilité contrariant les circulations ultérieurement de fluides. En outre, savoir décrypter ces objets diagénétiques particuliers peut être un moyen de mettre en évidence des mouvements synsédimentaires, qui sont parfois très discrets.

Dans cette thèse, nous allons étudier l'impact de la tectonique synsédimentaires selon deux approches complémentaires. Nous allons d'abord nous intéresser aux objets carbonatés nés de ces processus précoces, et nous observons ensuite comment la tectonique sédimentaire peut modifier latéralement le dépôt des sédiments en étudiant un transect dans le Boulonnais. De manière plus précise, nous allons chercher l'origine de structures biologiques récemment mises en évidence, qui

se révèlent être des petits biohermes à huîtres, ou aussi appelés « patchs » à huîtres. Pourquoi ces structures spéciales sont-elles presque toujours localisées au sommet de la Formation de Grès de Châtillon (cette formation a été souvent affectée par des failles synsédimentaires) ? Se sont-elles formées en place ? Sont-elles liées à des suintements d'hydrocarbures localisés, à l'image de ce qui est observé dans les champs de « pockmarks » actuels, voire de long de failles synsédimentaires observées dans le Jurassique supérieur du Bassin du Sud-Est de la France ? Nous allons ensuite discuter de la formation des bancs calcaires intercalés au sein de la formation des Bancs Jumeaux. Quelle est la relation entre cette structure et le mouvement de fluides, et, y a-t-il un effet tectonique ou les couches calcaires de Banc Jumeaux résultent-elles d'un épisode favorable à précipitation des carbonates ? Ces bancs Jumeaux carbonatés seront comparés à d'autres bancs calcaires, notamment ceux de la formation des Calcaires du Moulin Wibert.

Ensuite, nous étudierons la formation des Argiles de Châtillon en plusieurs endroits à partir du Cap de la Crèche jusqu'au Cap Gris-Nez. Nous allons nous concentrer sur cette formation qui affleure de façon quasi-continue le long du littoral allant du Cap Gris-Nez à Boulogne-sur-Mer. De plus, cette formation est une roche mère d'hydrocarbures potentielle. Observe-t-on latéralement des variations de faciès, épaisseur de sédiment, de conditions de dépôts (profondeur d'eau, conditions redox) ? Ces variations latérales trouvent-elles un écho dans l'accumulation de matière organique ? Peuvent-elles être rattachées à une activité tectonique synsédimentaire ?

Nous avons pris le parti de présenter cette thèse sous forme d'articles. L'avantage est de produire des informations relativement faciles à délivrer à la communauté concernée. La probabilité d'être lu est ainsi accrue. L'inconvénient de ce mode de présentation de thèse est qu'il conduit à répéter des parties entières communes à chaque article et qu'il peut "hacher" la linéarité du fil conducteur du mémoire de doctorat. Nous nous sommes efforcés de gommer ce dernier défaut. Chaque chapitre repose sur un article, déjà paru ou soumis ou en cours de polissage. L'article, porteur de l'information principale de la recherche, est parfois dépouillé d'informations intéressantes mais omises car jugées non-essentielles. L'article pourra donc être accompagné d'annexes qui n'auraient pas trouvé leur place dans un journal scientifique mais qui méritent d'être portées à la connaissance du lecteur. Chaque chapitre débute en outre par une courte présentation en français donnant l'essentiel en quelques lignes. Les articles ou manuscrits sont rédigés en anglais. Nous avons ajouté en annexe du mémoire un chapitre comprenant une présentation et un article paru à Chemical Geology en 2015. Je n'en suis pas le premier auteur mais j'ai participé activement à l'acquisition des données et l'interprétation des résultats. N'étant pas premier auteur, je n'ai pas souhaité que cet article figure dans le corps du mémoire mais il m'a semblé plus logique de le faire apparaître en annexe. En outre, certaines données et interprétations de cet article sont utiles pour la thèse proprement dite.

Chapitre 1 - Contexte géologique, matériel et méthodes

1.1. Le Boulonnais, contexte géologique

Le Boulonnais est une petite région du nord de la France qui trouve son originalité dans son style géomorphologique de boutonnière (figure 1) (Sommé, 1991). Cette particularité, lié à l'interférence entre la structuration anticlinale acquise au cours de l'épisode compressif tertiaire péri-alpin et l'érosion, met à l'affleurement des terrains d'âges variés (Dévonien à Holocène) et il est ainsi possible d'observer dans d'excellentes conditions les terrains paléozoïques et leur couverture jurassique et crétacée.

Les terrains les plus anciens affleurent dans la région de Marquise. Il s'agit de roches paléozoïques, pour la plupart carbonatées, exploitées au sein de plusieurs grandes carrières. Elles s'étendent du milieu du Dévonien (Givétien) à la fin du Carbonifère (calcaires viséens et molasse houillère du Namuro-Westphalien). Ces séries sont impliquées dans un système d'écailles chevauchantes à vergence vers le N matérialisant le front de la chaîne varisque (e.g. Averbuch et Mansy, 1998 ; Averbuch et al, 2004). La couverture de ces massifs de socle paléozoïque est accessible à partir des affleurements permanents de découverte des grandes carrières qui exploitent les calcaires paléozoïques. La mise à jour de cette couverture a, en particulier, permis l'étude de la base du Dogger (Bajocien supérieur à Bathonien inférieur-moyen) qui forme la séquence basale des séries mésozoïques discordantes sur le socle (Thierry et al., 1996). Le sommet du Malm (Kimméridgien supérieur et Tithonien) est, pour sa part, très bien exposé sur les falaises côtières au nord et au sud de Boulogne-sur-Mer. Le reste de la série (Bathonien supérieur à Kimméridgien inférieur) n'est visible que ponctuellement dans l'intérieur des terres (Sommé, 1991).

Comme le montre la carte géologique simplifiée de la figure 1, cette série de couverture du socle forme l'ensemble sédimentaire le plus complet en bordure sud du Massif de Brabant. L'épaississement des dépôts post-paléozoïques dans le Boulonnais est lié à l'existence d'une aire de sédimentation jurassique contrôlée par un système de failles normales de direction N110-120 et N030 délimitant un golfe subsidant en connexion à l'Ouest à travers la Manche avec le bassin du Weald du sud de l'Angleterre (figure 2) (e.g., Auffret & Colbeaux, 1977 ; Mansy et al., 2003 ; Minguely et al., 2005). Les dépôts jurassiques disparaissent aussi bien vers le Nord (Calais) que vers le Sud (Montreuil) et l'Est (Saint-Omer). Ils ne réapparaissent qu'en sondage à l'extrême sud de la région. La géométrie des aires de sédimentation jurassique se calque ainsi sur la disposition cartographique en boutonnière du massif du Boulonnais (e.g., Minguely, 2007). Dans les zones de lacune des dépôts jurassiques (la plaine des Flandres, l'Artois, l'Avesnois...), on retrouve directement sur le substratum les séries crétacées reposant sur une surface d'érosion majeure à l'échelle du bassin, d'âge fin-jurassique. Celle-ci fait place localement aux dépôts continentaux à faciès Wealdiens du Crétacé inférieur. Ces derniers présentent de très fortes variations d'épaisseurs, variations dont on peut penser qu'elles sont localisées par la présence de failles (par exemple à Wissant, au niveau de la retombée Nord de l'anticlinal du Cap Gris-Nez). L'ensemble est surmonté, en discordance, par la séquence marine de l'Aptien-Albien (sables et argiles et glauconie) et du Crétacé supérieur (faciès crayeux). Cette séquence s'est mise en place lors d'une phase de transgression généralisée sur la bordure nord du bassin de Paris (Minguely, 2007), transgression caractéristique du processus de propagation des dépôts sur les marges du bassin au cours de la phase subsidante post-rift associée à l'océanisation de l'Atlantique nord central (Crosby et al, 2008 ; Bronner et al, 2011).

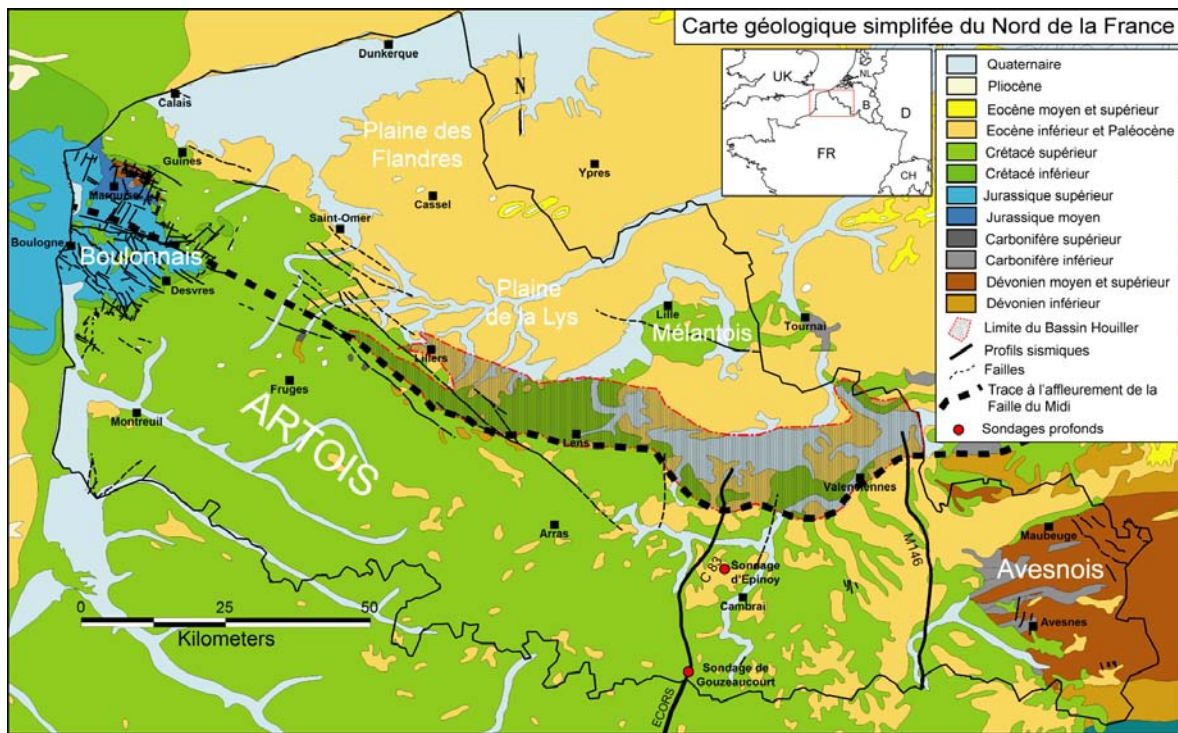


Figure 1. Carte géologique simplifiée du nord de la France (d'après Minguely, 2007 ; modifiée de Laquement et al, 2004).

Cette disposition générale est interprétée comme la superposition d'un épisode compressif tertiaire sur une géométrie initiale de demi-graben de direction E-W, structuré lors de la mise en place du bassin Weald-Boulonnais au Jurassique supérieur et au Crétacé inférieur (figure 2)(Butler and Pullan, 1990 ; Mansy et al, 2003). Ainsi que l'attestent les données géophysiques (Mansy et al, 1997) et les variations brutales d'épaisseur des dépôts, la zone faillée bordière limitant le bassin au nord (la zone faillée Cap Gris Nez-Landrethun)(figure 3) apparaît comme une élément majeur de contrôle de la subsidence du bassin, les zones faillées de Slack-Epitre et de Wimereux-Belle pouvant, quant à elles, être considérées comme des failles normales intra-bassin permettant son aprofondissement en direction du sud (Boulogne sur mer).

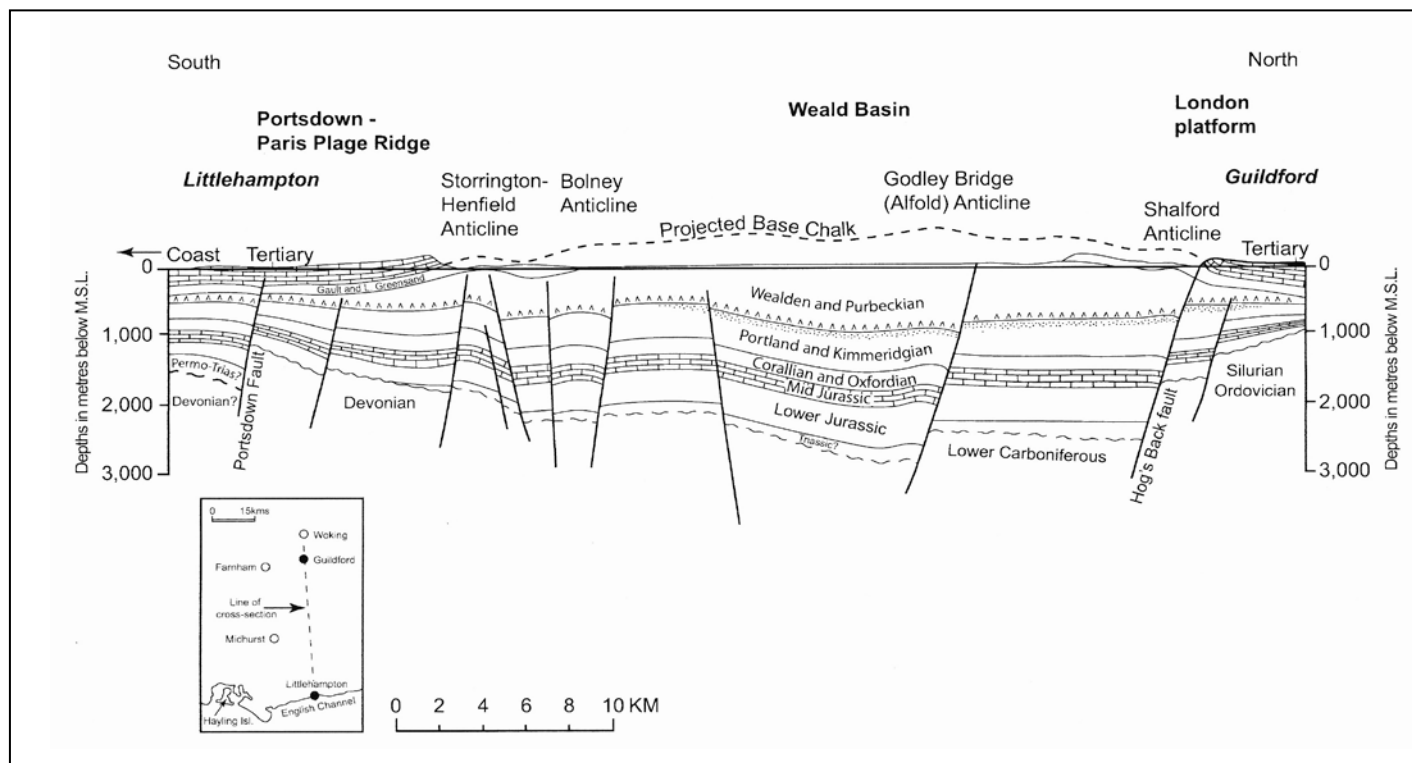
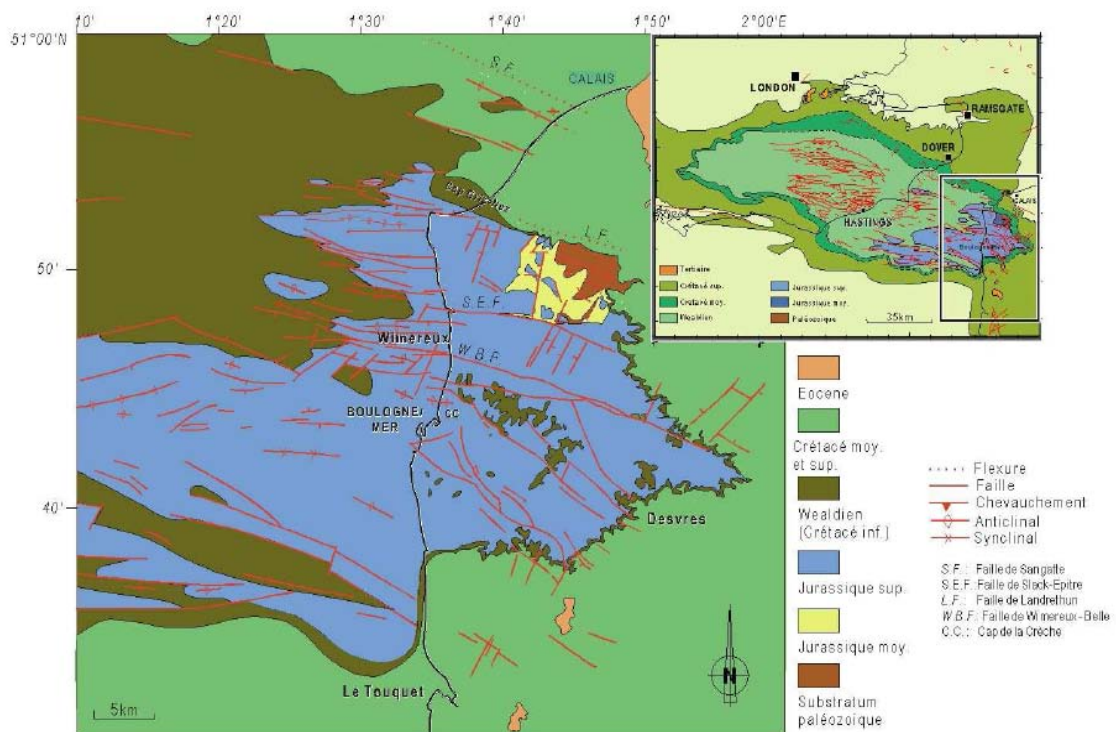


Figure 2: Haut : carte géologique du Boulonnais et de son extension en Manche et au Sud de l'Angleterre (d'après Mansy et al., 2003). Bas : Coupe géologique N-S à travers le bassin du Weald du sud de l'Angleterre établi sur la base de profils sismiques, montrant sa disposition en demi-graben inversé (Butler and Pullan, 1990).

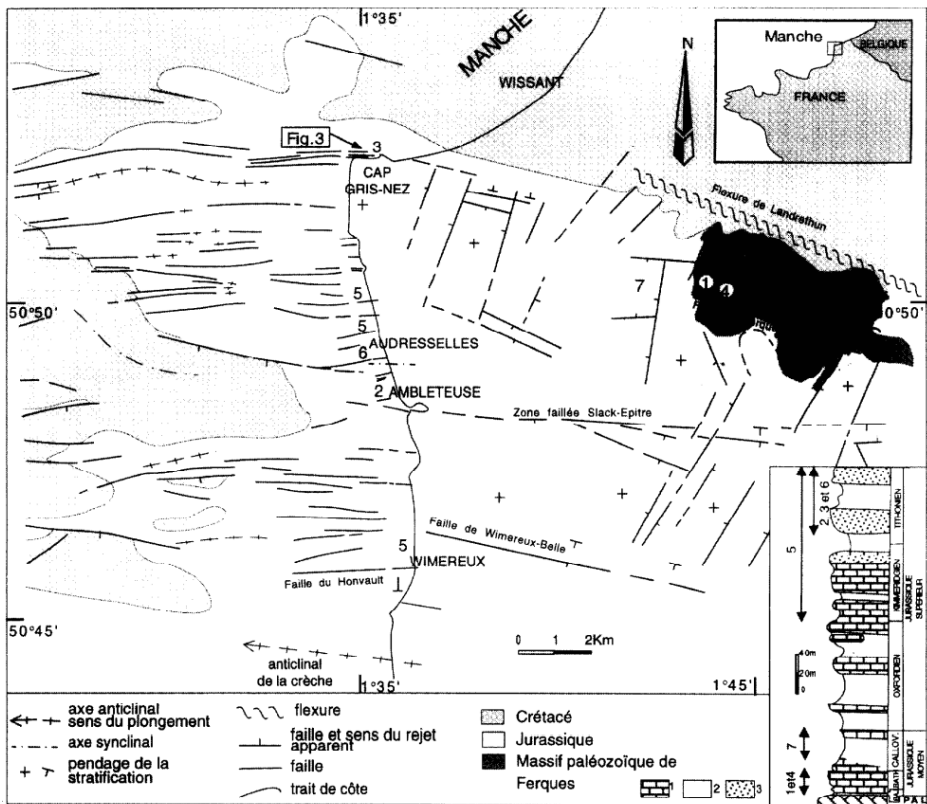


Figure 3. Les grandes structures tectoniques du Boulonnais, d'après l'analyse structurale de terrain et de profils sismiques (Mansy et al., 2007). Colonne lithostratigraphique du jurassique (simplifiée d'après Geyssant et al., 1993 ; Vidier et al., 1995). Faciès dominant : 1 : calcaire, 2 : argileuse, 3 : gréseuse.

Au Cap Gris-Nez, les plis et failles inverses visibles en surface (figure 4), associés à la faille profonde détectée par la géophysique montrent que la marge nord du bassin a été inversée lors de l'événement compressif tertiaire, probablement à partir de l'Eocène moyen. Le dôme résultant moulé sur les failles contrôlant le bassin, aurait été déjà partiellement excavé dès cette époque ainsi que le montrent les données sédimentaires et paléo-pédologiques recueillies à l'intérieur du Boulonnais et au niveau des fosses Dangeard (Van Vliet-lanoe et al., 2003). Cette érosion précoce aurait localisé un paléo-golfe marin conduisant à l'ouverture du Pas-de-Calais dès le Lutétien.

Dans le détail, au niveau du Cap Gris-Nez, on observe, sur l'estran, trois terminaisons péricliniales à rayon de courbure plurimétrique et, sur la falaise, une charnière anticlinale (Lamarche et al., 1996). Les quatre plis d'axe N090 (A figure 4) sont dissymétriques à flanc nord subvertical. Ils sont recoupés par des failles chevauchantes d'orientation N090 qui, latéralement, se raccordent à la stratification matérialisant des niveaux de décollement interstratifiés. L'analyse détaillée des plis et des failles, associée au calcul des paléo-états de contraintes, a permis de préciser les directions d'extension : nord-sud à NW-SE et d'inversion tectonique nord-sud à NNW-SSE. La pérennité des directions structurales dans le Paléozoïque et le Jurassique montre l'origine héritée des structures profondes et leur propagation au sein de la couverture. La structure régionale est constituée de failles en relais, d'âge varisque, dont certaines seront réactivées en failles normales puis inversées, comme le montre la structure de la couverture méso-cénozoïque (Lamarche et al., 1997 ; Mansy et al., 2003 ; Minguely et al., 2010).

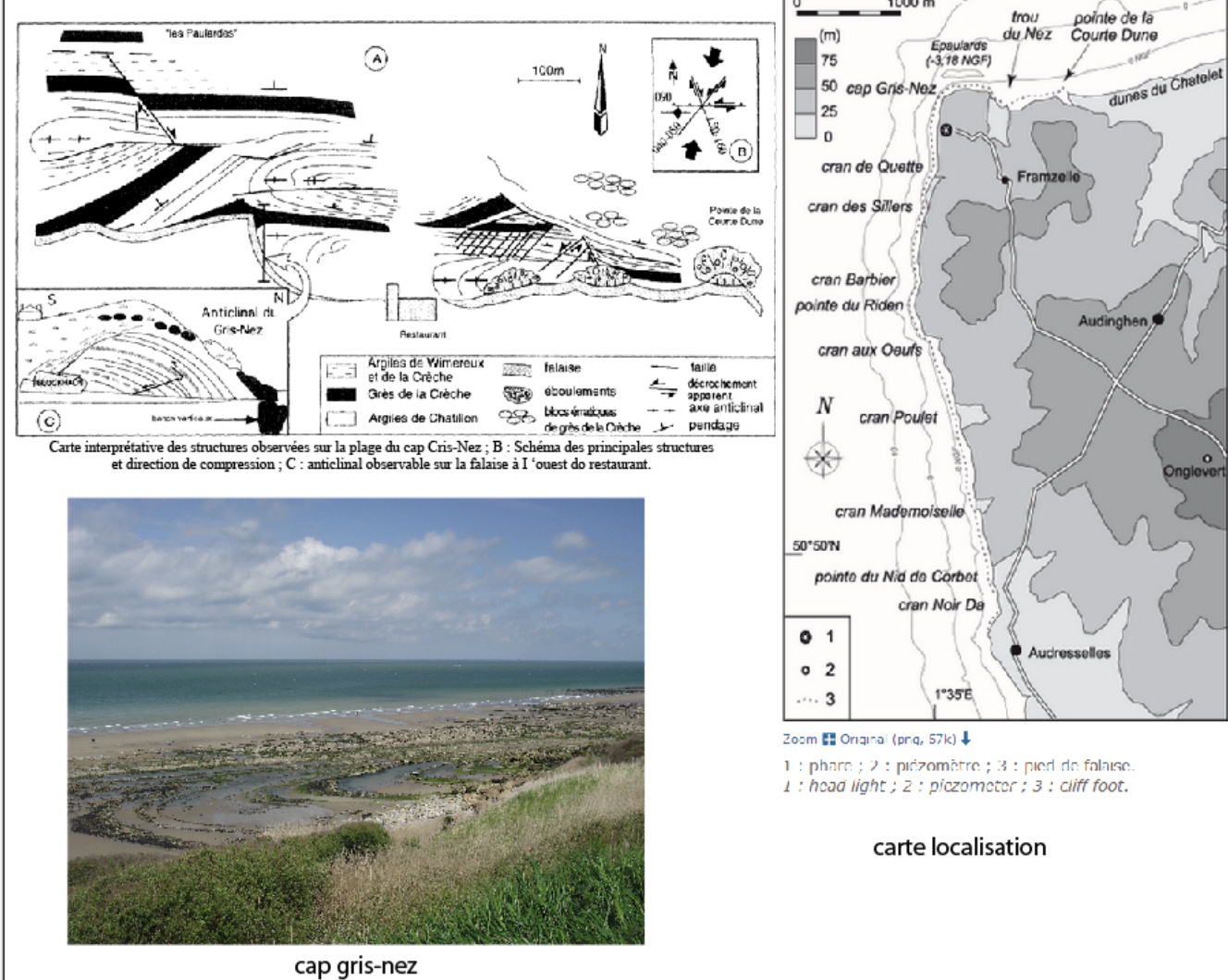


Figure 4 : Carte de localisation, carte interprétative des structures observées sur la plage du cap Cris-Nez (d'après Lamarche et al, 1996) et vue de l'anticinal observable sur l'estran.

A plus grande échelle, le Jurassique est affecté par des plis d'origine et de géométrie variées. On distingue des ondulations de grande longueur d'onde (de l'ordre du kilomètre), d'axe sub-E-W, associés à des crochons localisés le long des failles ; ces ondulations, particulièrement visibles entre Cran aux Œufs et le Cran du Noirda (localisation en Figure 4) sont à relier avec le jeu initial des failles normales (plis de type « roll-over ») : d'autres telles que la flexure de Landrethun (affectant le Crétacé) et l'anticlinal de la Crèche (Figure 3) résulteraient de la déformation souple dans la couverture, lors de l'inversion de failles normales synsédimentaires. Ces failles sont importantes et bien détectées par la géophysique (Mansy & Everaerts, 1997).

La plupart des failles de socle sont aveugles et se traduisent dans la couverture par des flexures ou des plis forcés autour desquels un gradient elliptique de rejet est observé ; l'analyse des cartes gravimétriques transformées a permis de mieux cerner la nature des failles générées lors de l'inversion tectonique. Ces failles s'amortissent latéralement en quelques dizaines de kilomètres, elles ne constituent donc pas une zone faillée continue mais un réseau en échelons, elles sont organisées en réseaux bien réglés, et là où elles sont réactivées, elles possèdent une orientation légèrement différente dans le Boulonnais et dans l'Artois (Everaerts et al, 2001).

L'ensemble de ces données montre ainsi que le bassin jurassique du Boulonnais est un enregistreur majeur du contexte extensif mésozoïque dans le Bassin anglo-parisien, puis de son inversion au Cénozoïque (Colbeaux et al., 1993). L'étude des déformations syn-sédimentaires au sein de la marge nord du bassin et des relations avec la sédimentation et la diagenèse nous permettra de préciser les processus actifs lors de cet événement de structuration initiale du bassin au Jurassique supérieur.

1-2. Stratigraphie et sédimentologie du Jurassique du Boulonnais :

Le Jurassique du Boulonnais est discordant sur le substratum paléozoïque d'âge Silurien à Carbonifère. Il est constitué de trois ensembles lithologiques aux caractères mécaniques différents : (1) le calcaire bathonien, (2) l'ensemble Callovien-Oxfordien à dominante argileuse et (3) une alternance de formations calcaires, gréseuses et argileuses du Kimméridgien-Tithonien (Lamarche et al., 1997).

Au Jurassique supérieur, la région du Boulonnais correspondait à une plateforme épicontinentale soumise à une sédimentation mixte silico-clastique et carbonatée, à proximité du Massif Londres-Brabant (fig. 5). Sur le plan climatique et paléobiologique, le Boulonnais faisait alors partie de la province sub-boréale, zone intermédiaire et fluctuante entre les provinces boréale et téthysienne. L'existence de ces provinces faunistiques oblige à utiliser pour ces périodes plusieurs échelles d'ammonites (Groupe Français d'étude du Jurassique, 1997).

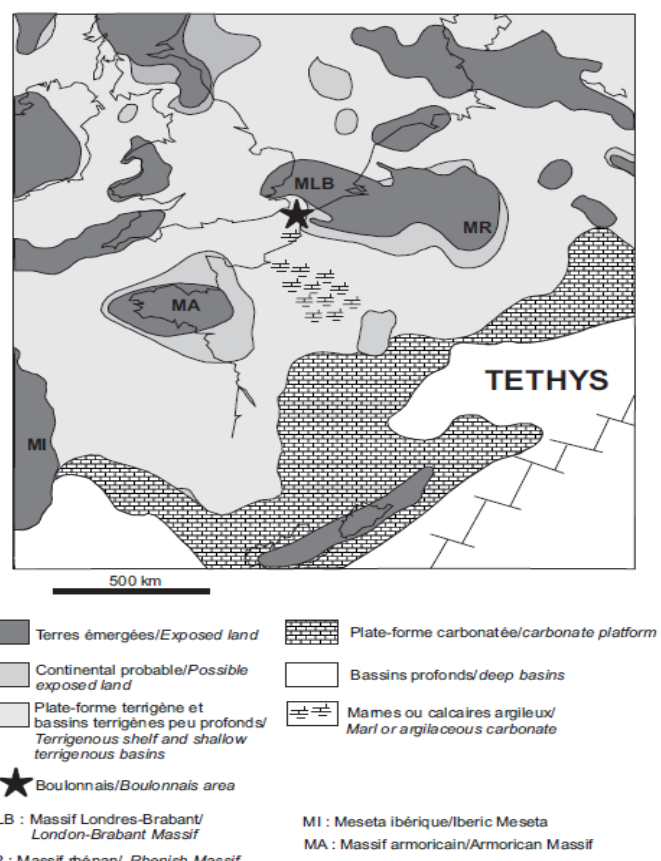


Figure 5: Paléogéographie de l'Europe de l'ouest au Kimméridgien inférieur, d'après (Cecca et al., 1993).

Dans le détail, les noms d'unités lithologiques jurassiques ne sont pas systématiquement libellés comme des formations pour deux raisons. D'une part, ces unités sont discontinues, peu épaisses et sujettes à de fréquents passages latéraux de faciès, difficiles à cartographier. D'autre part, afin de ne pas créer de confusion vis-à-vis des anciennes éditions de cartes et de publication concernant ces unités, les dénominations sont le plus possible fondées sur celles classiquement données par les auteurs.

Dans tout les cas, le lithofaciès, le biofaciès et l'attribution chronostratigraphique de chaque unité cartographiable sont précisément définis et fondés sur les publications les plus récentes (Mansy et al., 2007).

Certaines unités peuvent être subdivisées en sous-unités qui ont valeur de membres:

- 1- **Sables d'Hydrequent (Aalénien – Bajocien supérieur).** Ce sont des sables très fins, de teinte variée à débris charbonneux épars. Quelques passées décimétriques plus argileuses et riches en matière organique sont observées.
- 2- **Calcaires de Leulinghen (Bajocien supérieur à Bathonien supérieur pars).** On range dans cette unité des calcaires variés identifiés par leur position géométrique entre deux discontinuités sédimentaires physiquement bien marquées sur l'ensemble de la feuille de Marquise.
- 3- **Calcaires de Marquise-Rinxent (Bathonien supérieur pars).** Ce sont des calcaires oolitiques à niveaux fossilifères bien individualisés.
- 4- **Marnes des Calhaudes et Calcaires des Pichottes (Bathonien supérieur pars et Callovien inférieur pars).**
- 5- **Argile et marnes du Wast (Callovien inférieur à Oxfordien inférieur).** Cet ensemble, épais de 30 m au moins, à dominante argileuse, est richement fossilifère.
- 6- **Calcaires d'Houllefort et Argiles de Selles (Oxfordien moyen pars).** Ces dépôts sont très discrets à cause de la faible épaisseur des bancs et de leur état d'altération.
- 7- **Calcaires et Argiles du Mont des Boucards (Oxfordien moyen pars et supérieur pars).**
- 8- **Grés de Brunem bert (Oxfordien supérieur pars- kimméridgien inférieur pars).** Cet ensemble se présente comme une masse à dominante calcaire noyée entre deux masses argileuses. C'est donc un repère cartographique intéressant.
- 9- **Argiles du Moulin Wibert :** il s'agit essentiellement d'argiles noires pyriteuses contenant quelques intercalations carbonatées (Oschmann, 1988). L'essentiel des Argiles de Moulin Wibert appartient à la première sous-zone de la zone d'ammonites à Eudoxus (Herbin et al., 1995 ; Deconinck et al., 1996). L'épaisseur de cette formation est variable latéralement dans les affleurements.
- 10 - **Sables ou Grés de Connincthun :** il s'agit d'une formation épaisse de quelques mètres mais qui affleure mal au niveau de l'anticlinal de la Crèche entre Boulogne-sur-Mer et la Pointe de la Crèche. On repère principalement un banc gréso-glaconieux à ciment carbonaté et grains de quartz polycristallins mal classés et rares feldspaths plagioclases. La faune comprend des trigonies et de rares oursins. Aucune ammonite n'a été trouvée dans cette formation, mais elle est attribuée à la zone à Eudoxus (Deconinck et al., 1996).
- 11 - **Calcaires du Moulin Wibert (Kimméridgien supérieur pars) :** épais d'environ 15m, les dépôts sont constitués de nombreux bancs calcaires micritiques et de lumachelles à

Nanogyra virgula, séparés par des intervalles de marnes noires plus ou moins silteuses. Le sommet des Calcaires du Moulin Wibert passe progressivement à des marnes sableuses puis aux Sables et Grès de Châtillon, attribués à la sous-zone à *Contejeani* (dernière sous-zone de la zone à *Eudoxus*) (Deconinck et al., 1996).

12 - Grès de Châtillon (Kimméridgien supérieur pars) (5m). Il s'agit de sables et grès légèrement glauconieux peu fossilières à rides de vagues et à figures de houle.

-Cette formation (4m d'épaisseur) : content de nombreuses figures de courant (rides, stratification entrecroisées et laminations planes). La bioturbation est marquée par des tubes en U, des Rhizocoralliums, des Thalassinoides (Ager & Wallace, 1970).

13 - Argiles de Châtillon (Kimméridgien supérieur pars – Tithonien inférieur pars) Les : Argiles de Châtillon apparemment homogènes présentent en réalité une assez grande variabilité de faciès entre des argiles massives plus ou moins foncées, des argiles noires feuillettées et des argiles particulièrement plastiques en partie responsables des glissements de terrains qui affectent les falaises (Debrabant et al., 1994).

Au sein de ces argiles, on trouve quelques bancs carbonatés de lumachelles à *Nanogyra*, probablement mis en place sous l'influence de courants de tempêtes (Fürsich & Oschmann, 1986).

La limite Kimméridgien/Tithonien est située avec précision au sien des Argiles de Châtillon, dans lesquelles on distingue deux membres : l'inférieur appartient à la zone à *Autissiodorensis* (sous-zone à *Autissiodorensis*) et le supérieur à la zone à *Gigas-Elegans*. Il y a lacune de la partie supérieure de la zone à *Autissiodorensis* (sous-zone à *Irius*) et peut-être de la base de la zone à *Gigas* (Geyssant et al., 1993 ; Deconick et al., 1996)(figure 6).

15 - Grès de la Crèche (Tithonien inférieur) : Les grés de la Crèche sont classiquement divisés en trois sous-unités lithologiques avec de bas en haut :

Grès de la Crèche inférieurs : ce sont des grès en bancs métriques bien individualisés séparés par des sables jaunes fins à boules de grès typiques. Ils montrent des figures sédimentaires diverses et contiennent des niveaux peu épais de sables plus grossier voire graveleux et à galets de quartz.

Les Grés de la Crèche supérieur : ils sont plus calcaires, de teinte verdâtre, en bancs massifs alternant avec des passées argilo-sableuses. Ces bancs sont parfois déformés par des figures d'échappement de fluides. La base est plus gréseuse et glauconieuse que la partie supérieure.

16 - Argiles de la Crèche et Argiles de Wimereux (Tithonien inférieur) (18 m).

Argiles de la Crèche (8 m) : ce sont des argiles noires feuillettées, plus sableuses sur quelques décimètres à la base, à plaquettes gréseuses avec des figures sédimentaires (tempestites) à la partie supérieure.

Argiles de Wimereux (10 m) : ce sont des argiles grises, montrant quelques lits sableux et glauconieux. Elles contiennent un banc repère de calcaire gréseux, légèrement glauconieux et se terminent avec un niveau phosphaté.

Ces deux formations sont séparées par la formation des Bancs Jumeaux qui est la transition entre les Argiles de la Crèche et les Argiles de Wimereux. Cette transition est limitée à la base et au sommet par deux surfaces d'érosions forte caractérisées par l'accumulation de fossiles phosphatés et des nodules, et des galets du quartz. Ces deux niveaux sont appelés P1 et P2, respectivement (Geyssant et al., 1993 ; Herbin et al., 1995 ; Deconinck et al., 1996). La formation des Bancs Jumeaux est d'environ 2 m d'épaisseur (e.g., Tribouillard et al., 2012).

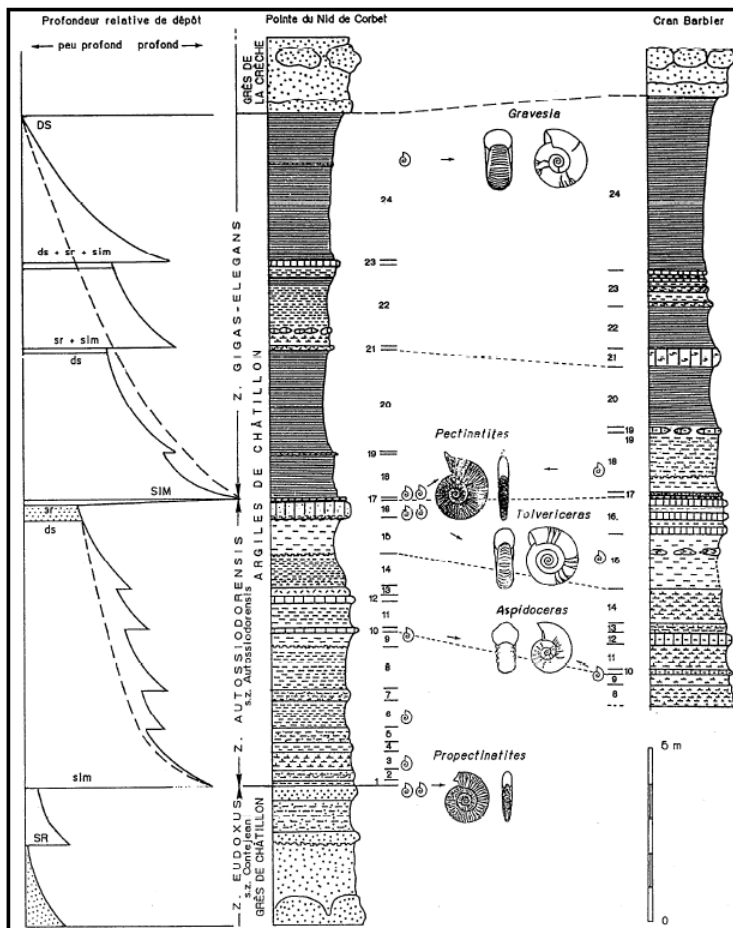


Figure. 6- Coupe des Argiles de Châtillon au nord d'Audresselles (point du Nid de Corbet et Cran Barbier).
Lithologie. Paléoprofondeurs. Influence de variations de paléoprofondeur sur les peuplements d'ammonites.
(Geyssant et al., 1993).

17 - Argiles et calcaires de la Tour de Croï et Grès de la Pointe aux Oies (Tithonien supérieur) (20 m).

Les Argiles et calcaires de la Tour de Croï (10 m) sont faites d'une alternance de bancs irréguliers, nodules, de calcaire ou de grès calcareux, glauconieux épais de quelques décimètres et d'argiles également glauconieuses.

Les Grès de la Pointe aux Oies (10 m) consistent en une alternance de bancs calcaréo-gréseux et de silts verdâtres, irrégulièrement indurés, plus ou moins argileux, glauconieux, dans la partie inférieure.

18 - Calcaires de la Pointe aux Oies (Tithonien terminal, faciès purbeckien) (2m). Ensemble massif de calcaires de teinte crème clair, vacuolaires, à structures en « chou fleur » et en lames millimétriques à plurimillimétriques, localement bréchifiés.

1.3. Matériel et Méthodes générales:

1.3.1. Matériel :

Les échantillons des formations jurassiques étudiées ici proviennent de plusieurs coupes levées : 1/ coupe du cap de la Crèche ($50^{\circ}44'53.69''N$ - $1^{\circ}35'44.14''E$), 2/ coupe du Cran du Noirda ($50^{\circ}49'45.50''N$ - $1^{\circ}35'24.54''E$), 3/ coupe du Cap Gris-Nez ($50^{\circ}52'14.68''N$ - $1^{\circ}35'30.40''E$) sur la plage de la Sirène.

Un log stratigraphique a été dessiné pour chacune des coupes, à partir des notes prises sur le terrain. Environ 200 échantillons ont été sélectionnés et prélevés afin de caractériser les principaux paramètres abordés dans cette étude.

1.3.2. Méthodes :

Une approche multidisciplinaire a été appliquée en veillant à adopter les méthodes appropriées à nos types d'échantillons et les paramètres recherchés. Toutes les méthodes sont recensées et rapidement présentées dans chacun des articles ou manuscrits qui constituent le cœur des chapitres suivants.

Bibliographie

AGER, D., & WALLACE, P. (1970). The distribution and significance of trace fossils in the uppermost Jurassic rocks of the Boulonnais, Northern France. In Crimes and J.C. Harper, eds. *Geological Journal, Special Issue n3*, 117.

AVERBUCH O. & MANSY J-L. (1998). The “Basse-Normandie” duplex (Boulonnais, N France): evidence for an out-of-sequence thrusting overprint. *J. Struct. Geol.*, 20, 33-42.

AVERBUCH O., MANSY J-L., LAMARCHE J., LACQUEMENT F. & HANOT F. (2004). Geometry and kinematics of the Boulonnais fold-and-thrust belt (N France) : implications for the dynamics of the Northern Variscan thrust front. *Geodinamica Acta*, 17, vol 2, 163-178.

AUFFRET, J.-P., & COLBEAUX, J.-P. (1977). Etude structurale du Boulonnais et de son prolongement sous-marin en Manche orientale. *Bulletin de la Société Géologique de la France XIX(5)*, 1047-1055.

BUTLER , M. & PULLAN, C.P. (1990). Tertiary structures and hydrocarbon entrapment in the Weald Basin of southern England. In: Hardman, R.F.P. & Brooks, J. (Eds.), *Tectonic Events Responsible for Britain's Oil and Gas Reserves*, Geological Society, London, Special Publications 55, 371-391.

BRONNER, A., SAUTER, D., MANATSCHAL, G., PERON-PINVIDIC G., MUNSCHY M. (2011). Magmatic breakup as an explanation for magnetic anomalies at magma-poor rifted margins. *Nature geoscience* 4, 549- 553.

CECCA, F., AZEMA, J., FOURCADE, E., BAUDIN, F., GUIRAUD, R., & DE WEVER, P. (1993). Early Kimmeridgian Palaeoenvironment (146 to 144 Ma). In: Dercourt J., Ricou L.E., et Vrielynck B.(eds.). *Atlas Tethys Palaeoenvironnement Maps*, Beicip-Franlab, Rueil-Malmaison.

- COLBEAUX, J.-P., AMEDRO, F., BERGERAT, F., BRACQ, P., CRAMPON, N., DELAY, F. (1993). Un enregistreur des épisodes tectonique dans le bassin de Paris: le Boulonnais. *Bulletin de la société Géologique de France* 164(1) , 93-102.
- CROSBY, A., WHITE, N., EDWARDS, G., SHILLINGTON, D.J. (2008). Evolution of the Newfoundland-Iberia conjugate rifted margins. *Earth and Planetary Science Letters* 273, 214-226.
- DEBRABANT, P., ADIDA, B., PAINSET, J., DECONINCK, J.-F., & RECOURT, P. (1994). Comportement géotechnique des argiles de châillon (Kimméridgien/Tithonien du bas Boulonnais). *Ann.Soc. Géo, du Nord* , 145-153.
- DECONINCK, J.-F., GEYSSANT, J.R., PROUST, J.-N., VIDIER, J.P. (1996) Séimentologie et biostratigraphie des dépôts kimméridgiens et tithoniens du Boulonnais. *Annales de la Société Géologique du Nord*, 4, 157-170.
- EVERAERTS, M., & MANSY, J.-L. (2001). Le filtrage des anomalies gravimétriques; une clé pour la compréhention des structures tectoniques du Boulonnais et de l'Artois. *Bull. Soc. Géol. France*, t .172 n 3 , 267-274.
- FÜRSICH, F., & OSCHMANN, W. (1986). Storm shell beds of *Nanogyra virgula* in the Upper Jurassic of France. *N. Jb. Geol. Paläont., Abh., Stuttgart*, 172, 2 , 141-161.
- GEYSSANT, J.-R., VIDIER, J.-P., HERBIN, J.-P., PROUST, J., & DECONICK, J.-F. (1993). Biostratigraphie et paléoenvironnement des couches de passage Kimméridgien/Tithonien du Boulonnais (Pas de Calais): nouvelles données paléontologiques (ammonites), organisation séquentielle et contenu en matière organique. *Géologie de la France*, 4 , 11-24.
- GROUPE FRANÇAIS D'ETUDE DU JURASSIQUE, .. (1997). Biostratigraphie du Jurassique méditerranéen et ouest-européen : zonations parallèles et distribution des invertébrés et microfossiles. Cariou E. et Hantzpergue P. (coord.). *Bull. Centre. Rech. Elf, Explor. Prod., Mém.* , 17, 440 p., 6 fig., 79 tabl., 42 pl.
- HERBIN, J., FERNANDEZ-MARTINEZ, J., GEYSSANT, J., EL ALBANI, A., DECONINCK, J.-F., PROUST, J.-N. (1995). Sequence stratigraphy of source rocks applied to the study of the Kimmeridgian/Tithonian in the north-west European shelf (Dorset/UK, Yorkshire/UK and Boulonnais/France). *Marine and Petroleum Geology*, 12 , 177-194.
- LACQUEMENT, F., BARCHI, P., & QUESNEL, F. (2004). Carte géologique harmonisée de la région Nord- Pas de Calais. *BRGM/RP53484-FR* , 188.
- LAMARCHE, J., BERGERAT, F., & MANSY, J. (1997). Déformations cassantes et plicatives dans le Jurassique du Boulonnais (France), influence lithostructurale et héritage paléozoïque. *Académie des sciences / Elsevier, Paris* , 57-63.
- LAMARCHE, j., BERGERAT, F., & MANSY, J.-L. (1996). Tectonique plicative et cassante dans le Jurassique du Boulonnais: une histoire Méso-Cénozoïque polyphasée. *Ann.Soc.Géol.du Nord* , 171-179.
- MANSY, J., & EVERAERTS, M. (1997). Reinterpretation de la tectonique du Boulonnais et de l'Artois avec l'apport de la géophysique, In : Colloque Artois-Brabant. *SGF. Mons.*
- MANSY, J.-L., GUENNOC, P., ROBASZYNSKI, F., AMEDRO, F., AUFRRET, J.-P., VIDIER, J.-P. et al. (2007). Carte géologique de la france à 1/50000 (MARQUISE). 49.
- MANSY, J.-L., MANBY, G. M., AVERBUCH, O., EVERAERTS, M., BERGERAT, F., VAN VLIET-LANOË, B. (2003). Dynamics and inversion of the Mesozoic Basin of the Weald-Boulonnais area: role of basement reactivation. *Tectonophysics* 373 , 1-4.

MINGUELY, B. (2007). Caractérisation géométrique 3-D de la couverture sédimentaire Meso-Cénozoïque et du substratum Varisque dans le nord de la France. Apports des données des sondage et des données géophysiques. Thèse de doctorat, Université de Lille.

MINGUELY, B., MANSY, J.-L., EVERAERTS, M., MANBY, G., & AVERBUCH, O. (2005). Apport de la modélisation géophysique pour la compréhension de la structuration du pas de Calais. *comptes Rendus Geosciences*337(3) , 305-313.

MINGUELY B., AVERBUCH O., PATIN M., ROLIN D., HANOT F. & BERGERAT F. (2010). Inversion tectonics at the northern margin of the Paris basin (Northern France) : new evidence from seismic profiles and boreholes interpolation in the Artois area. *Bulletin de la Société Géologique de France*, 181, n° 5, 429-442.

OSCHMANN, W. (1988). kimmeridge Clay sedimntation - Anew cyclic model. *Palaeogeogr., Palaioclimato., Palaeoecol.*,65. 217-251.

PROUST, N., DECONINCK, J.-F., GEYSSANT, J., HERBIN, J.-P., & VIDIER, J.-P. (1995). Sequence analytical approach to the Upper Kimmeridgian-Lower Tithonian storm-dominated ramp deposits of the Boulonnais (Northern France). - A landward time-equivalent to offshore marine source rocks. *Geologisches Rundschau*. 255-271.

SOMME, J. (1991). Le système morphotectonique de boutonnière dans la relief du nord de la france. *Homme et Terre du Nord*,2-3. pp. 171-176.

SUNAMURA, T. (1992). *Geomorphology of rocky coasts. John Wiley & Sons* , 302.

THIERRY, J., VIDIER, J., GARCIA, J., & MARCHAND, D. (1996). Le Dogger du Boulonnais : lithostratigraphie et biostratigraphie et stratigraphie séquentielle des séries à l'affleurement. *Ann. Soc. Géol. Nord* . pp. 127-155.

TRIBOVILLARD, N., SANSJOFRE, P., ADER, M., TRENTESAUX, A., AVERBUCH, O., & BARBECOT, F. (2012). Early diagenetic carbonate bed formation at the sediment-water interface triggered by synsedimentary faults. *Chemical Geology* 300-301 , 1-13.

VAN VLIET-LANOË, B., MANSY, J.-L., HENRIET, J.-P., LAURENT, M., TRENTESAUX, A., & VIDIER, J.-P. (2003). Une inversion tectonique Cénozoïque par étapes: Le Pas de Calais. *Congrès Français de Sédimontologie - Livre des résumés* , 541.

Vidier J.P., Garcia J.P., Thierry J., Fauconnier D. (1995) - Le Dogger du Boulonnais (Nord bassin de Paris) : nouveaux découpages chronologique et séquentiel des formations carbonatées jurassiques en bordure du massif Londres-Brabant. *C. R. Acad. Sci., Fr.*, Paris, 320, 2a, 219-226.

Chapitre 2 – Les récifs à huîtres comme indicateurs de suintements de fluides fossiles induites par des failles synsédimentaires.

2.1 – Présentation

L'essentiel en quelques mots

Les dépôts du Jurassique supérieur du Boulonnais (Nord de la France) représentent l'équivalent latéral proximal de la Kimmeridge Clay Formation ; ils se sont accumulés sur une rampe dominée par des dépôts clastiques affectés par des failles synsédimentaires liées au rifting de l'océan Atlantique. La zone étudiée ici se situe dans la région du Cap Gris-Nez, soit près de la zone de faille de la frontière nord du bassin du Jurassique.

La séquence du Jurassique supérieur contient des récifs à huîtres, fréquemment appelés patches à huîtres, de petites dimensions (<1 m) qui sont spécifiquement observés à la base d'une tendance de l'approfondissement net dans la séquence sédimentaire, cet approfondissement est partiellement induit par l'activité de faille normale (sans oublier bien sûr les mouvements eustatiques du niveau marin).

Les patchs étudiés ont une forme arrondie et sont visibles en de nombreux sites entre Audresselles et le Cap Gris-Nez le long de deux horizons stratigraphiques particuliers : sur le sommet des Grès de Connincthun et des Grès de Châtillon. Les patchs les plus grands sont observés le long de la plage du Cap Gris-Nez où ils peuvent atteindre une taille de 1 m, alors que la gamme de taille habituelle de ces objets est 10-50 cm.

Les patchs sont composés d'innombrables coquilles de *Nanogyra nana* (principalement) qui ne montrent pas une orientation préférentielle et qui sont intégrées dans une matrice carbonatée de micro-sparite, et les valves ne sont pas toujours connectées les unes aux autres. Les patchs diffèrent donc des lumachelle à huîtres qui sont très abondantes dans le Jurassique supérieur du Boulonnais (et qui ne sont pas étudiées ici), de par leur matrice à grain fin.

Nous avons caractérisé les récifs isolés par des méthodes pétrographiques et géochimiques. Des sections minces des patchs à huîtres ont été étudiées à l'aide d'un microscope à cathodoluminescence et un microscope électronique, la teneur en carbonate a été déterminée avec un calcimètre de type Bernard.

Approche microscopique : les différents récifs isolés à différents niveaux stratigraphiques montrent les mêmes caractéristiques microscopiques :

- la matrice est en calcite homogène sous forme de micro-sparite .
- de nombreuses coquilles et des fragments de coquilles constituent l'essentiel des récifs.
- une importante présence de cristaux de quartz de taille allant jusqu'à 500 micron est observée.

En cathodoluminescence, toute la matrice dans toutes les sections était homogène.

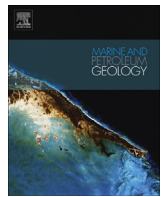
Approche isotopique : à partir de $\delta^{18}\text{O}$ on ne peut faire aucune distinction clairement interprétable entre les compositions de la matrice des récifs, des coquilles elles-mêmes et de leurs remplissages calcitiques quand ils existent.

Pour la pyrite : la valeur $\delta^{34}\text{S}$ de la pyrite des patchs à huîtres montre un fractionnement important (-35 à -43 ‰) par rapport à la valeur des sulfates de l'eau de mer pour le Jurassique supérieur (+15 ‰). Le grand fractionnement isotopique du soufre entre la valeur de l'eau de mer de Jurassique supérieur et de la pyrite de nos échantillons suggère fortement que la réduction de sulfates d'origine bactérienne a exploité un réservoir de sulfate relativement infini, c'est à dire que la sulfato-réduction s'est produite à proximité de la masse d'eau marine, et donc très près de la surface d'eau-sédiment.

Le résultat le plus important est que les analyses isotopique du C montrent que la matrice est nettement appauvrie en ^{13}C , tandis que les coquilles elles-mêmes et leur remplissage éventuel se rapprochent au contraire des valeurs habituelles estimées pour les carbonates de l'eau de mer du Jurassique Supérieur qui ont entre 0 à +2 ‰.

Interprétation - La formation des carbonates authigènes (ici la matrice des récifs à huîtres) a été induite par une augmentation de l'alcalinité, étroitement associée à l'activité de dégradation de matière organique dissoute (éventuellement des hydrocarbures), par les bactéries sulfato-réductrices. La présence et l'activité des bactéries sulfato-réductrices au cours de la diagenèse précoce ont été probablement elles-mêmes induites et alimentées par la circulation de fluides riches en matière organique, en remontant le long des plans de failles synsédimentaires des couches plus profondes, riches en matière organique, qui structuraient le Boulonnais.

Pour conclure : les formations clastiques de la fin du Jurassique dans le Boulonnais, contiennent des objets carbonatés (récifs à huîtres ou bancs carbonatés) qui présentent des caractéristiques communes, en termes de microfaciès et de géochimie, et qui sont d'origine diagénétique. Cette origine est assez discrète (la microsparite peut être confondue avec de la micrite) et l'analyse des données isotopiques est requise pour la mettre en lumière. De tels objets sont peut-être plus abondants qu'on ne le pense dans le registre sédimentaire.



Oyster patch reefs as indicators of fossil hydrocarbon seeps induced by synsedimentary faults



E. Hatem ^a, N. Tribouillard ^{a,*}, O. Averbuch ^a, D. Vidier ^b, P. Sansjofre ^{c,1}, D. Birgel ^d, F. Guillot ^a

^a Université Lille 1, CNRS UMR Géosystèmes 8217, bâtiment SN5, 59655 Villeneuve d'Ascq cedex, France

^b PN82, rue du Calvairé, 62137 Coulogne, France

^c Équipe de géochimie des isotopes stables, Institut de Physique du Globe de Paris (IPGP), CNRS UMR 7154, Sorbonne Paris Cité, Univ Paris Diderot, 75005 Paris, France

^d Department for Geodynamics and Sedimentology, University of Vienna, Althanstrasse 14, A-1090 Vienna, Austria

ARTICLE INFO

Article history:

Received 11 June 2013

Received in revised form

12 November 2013

Accepted 9 December 2013

Available online 18 December 2013

Keywords:

Authigenic carbonates

Hydrocarbon seeps

Sulfate reduction

Late Jurassic

Boulonnais

Stable isotopes

ABSTRACT

The Late Jurassic deposits of the Boulonnais area (N-France) represent the proximal lateral-equivalent of the Kimmeridge Clay Formation; they accumulated on a clastic-dominated ramp subject to synsedimentary faulting as a result of the Atlantic Ocean rifting. In the Gris-Nez Cape area, i.e., close to the northern border fault zone of the Jurassic basin, the Late Jurassic sequence contains small-dimensioned oyster patch reefs (<1 m) that are specifically observed at the base of an abrupt deepening trend in the depositional sequence induced by well-defined pulses of normal fault activity. Petrographic analysis of these patch reefs shows that they are exclusively composed of *Nanogyra nana* embedded in a microsparitic calcite matrix. $\delta^{13}\text{C}$ measurements, carried out within both the matrix and the shells, display significantly lower values in the matrix compared to the oyster shells which suggests that the carbonate matrix precipitation was involving a carbon source different from marine dissolved inorganic carbon, most probably related to sulfate reduction, which is evidenced by light $\delta^{34}\text{S}$ in pyrites. Similarities but also differences with lucinid-rich bioconstructions, namely, the Late Jurassic pseudo-bioherms of Beauvoisin (SE-France) suggest that the patch reefs developed at hydrocarbon seeps are related to synsedimentary faults. The extensional block-faulting segmentation of the northern margin of the Boulonnais Basin in Late Jurassic times is thus believed to have induced a sort of small-dimension hydrocarbon seepage field, recorded by the patch reef distribution.

© 2013 Elsevier Ltd. All rights reserved.

1. Introduction

Fluid flow is a first-order feature of basin evolution. Expulsions are interacting with sediments at the earliest stages of deposition, causing both early and late diagenesis of sediments. This is particularly crucial for basins subjected to extensional tectonic activity, where synsedimentary faults drive early diagenetic fluid circulations. These aspects are of cornerstone importance for petroleum systems. The geological formations of the Late Jurassic times (Kimmeridgian–Tithonian) crop out along the Boulonnais cliffs (Strait of Dover, Northern France; Fig. 1). They represent a proximal equivalent of the Kimmeridge Clay Formation (famous as

a major petroleum source rock) and they accumulated in a clastic-dominated ramp environment subject to dominantly aerobic conditions with some episodes of dissolved oxygen restriction favorable to organic-rich deposition (Wignall, 1991; Ramanampisoa et al., 1992; Proust et al., 1995; Al-Ramadan et al., 2005; Decoyninck et al., 1996; Wignall and Newton, 2001; Williams et al., 2001; Tribouillard et al., 2001, 2004, 2005). The Boulonnais is an excellent example of a small-dimensioned model of petroleum systems involving: 1) fine-grained, clay-dominated, organic-rich formations (termed “Argiles” in the local terminology, e.g., the Argiles de Châtillon Formation) acting as source rocks; and 2) coarser-grained, sandstone-dominated formations (termed “Grès”, e.g., the Grès de Châtillon Formation), acting as possible reservoir rocks. A recent study of the Bancs Jumeaux Formation suggested that synsedimentary tectonics induced fluid circulations through this incipient petroleum system, favoring carbonate precipitation and the formation of indurated carbonate beds, most likely stimulated by bacterial activity (Tribouillard et al., 2012).

* Corresponding author.

E-mail address: Nicolas.Tribouillard@univ-lille1.fr (N. Tribouillard).

¹ Present address: Université de Bretagne Occidentale, Laboratoire des Domaines Océaniques, 29280 Plouzané, France.

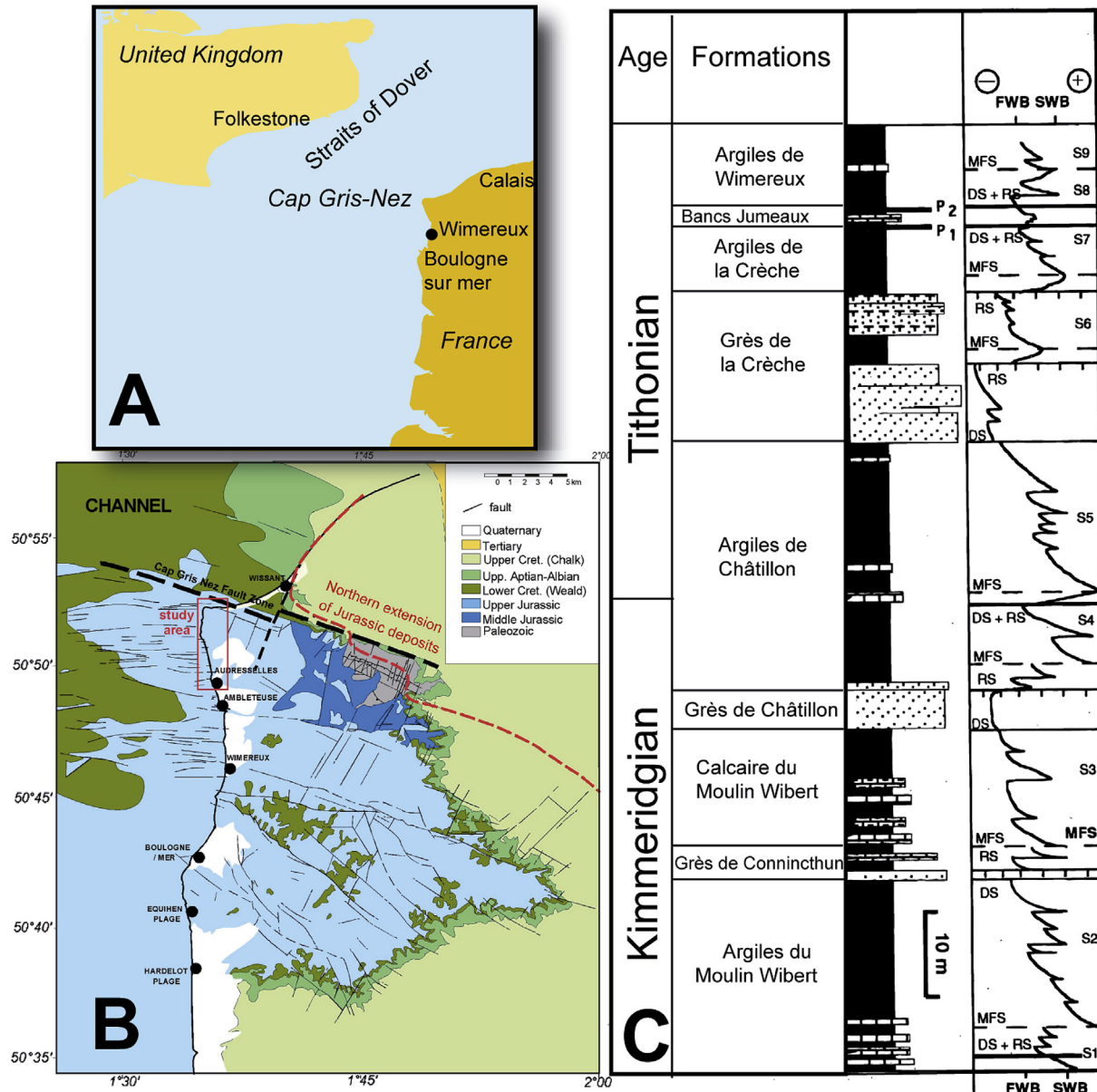


Figure 1. A – Large scale map showing the location of the study area, between the Gris-Nez Cape and the city of Wimereux. B – Geological map of the Boulonnais area (after Mansy et al., 2003). C – Simplified lithostratigraphic log of the Late Jurassic formations cropping alongshore the Boulonnais, showing the sequence stratigraphy framework (after Deconinck et al., 1996). FWB and SWB stand for fair-weather wave base and storm-weather wave base, respectively. P1 and P2 stand for the two horizons rich in phosphatized shells and pebbles.

From a structural point of view, the study area forms the eastern tip of the Weald-Boulonnais basin crossing through the English Channel along a general E–W direction. During the course of the entire Late Jurassic, this basin, alike the Wessex and the North sea basins, was affected by synsedimentary faulting in relation with the northward propagation of rifting along the Atlantic Ocean (Butler and Pullan, 1990; Underhill and Paterson, 1998; Beeley and Norton, 1998; Newell, 2000; Taylor and Sellwood, 2002; Hansen et al., 2002; Mansy et al., 2003; Minguely et al., 2010). This block-faulting geometry had a significant imprint on the subsidence pattern in the basin and, hence, on the depositional contexts. Along the Boulonnais cliffs, this resulted in significant lateral changes of sedimentary thickness and facies of the Kimmeridgian–Tithonian sequence indicating increasingly more proximal conditions toward

the North, up to the Gris-Nez Cape fault zone that represents the present northern onshore extension of the Jurassic deposits (Fig. 1B) (Mansy et al., 2003). One of the main expressions of these lateral depositional variations toward the Gris-Nez Cape fault zone is a progressive increase in the number and thickness of coquina beds into the dominant mudstone–sandstone sequence (Fig. 1C; a coquina is a detrital limestone composed wholly or chiefly of mechanically sorted shell fragments that experienced abrasion and transport before reaching the depositional site; cf., Bates and Jackson, 1987). Actually, in the Gris-Nez Cape area, the Late Jurassic formations contain numerous coquina beds, exclusively composed of the oyster *Nanogyra nana* and representing proximal tempestite deposits (Mansy et al., 2007). Recently, in addition to the coquina beds, occasional, ball- or dome-shaped assemblages of *N.*

nana were observed; they are small-dimensioned, *in situ* formed, oyster patch reefs (Fig. 2A–D and 3A–D; Mansy et al., 2007). The oysters *N. nana* are known to participate commonly to patch-reef building, notably during the Late Jurassic; however, in most patch reefs, *Nanogyra* are accompanied by numerous other organisms, e.g., other genera of oysters, gastropods, serpulids, echinoids, bryozoa, foraminifera, sponges, etc. (e.g., Fürsich, 1981; Helm and Schulke, 1998; Delecat et al., 2001; Wilmsen et al., 2010). In contrast to the faunal composition of most Late Jurassic patch reefs, the Boulonnais patch reefs are rather small and isolated, and are only containing *N. nana* shells preserved in a carbonate-mud matrix (Figs. 2 and 3). The present study focusing on field observations, petrographic, geochemical and isotopic analyses aims at characterizing the development of these patch reefs within the general geological framework of the syn-rift Late Jurassic deposits. Integration of these data and their comparison with the well-studied Beauvoisin “pseudo-bioherms” (biocorstructions) that developed as well along synsedimentary faults in SE France (see section 6.2) will lead us to suggest that these specific ecosystems were controlled by localized fluid expulsion along fractures and faults, favoring bacterial activity at hydrocarbon seep sites through sulfate reduction.

2. The Late Jurassic oyster patch reefs of the Boulonnais: geological context

The Late Jurassic deposits of the Boulonnais form a ca. 100 m-thick sequence, mainly composed of alternating sandstones and black mudstone units as a primary result of the relative sea level oscillations (Fig. 1C). A brief description of the geological formations mentioned in the paper can be found in Table 1. A more detailed description of these formations, cropping out along the Boulonnais shore, may be found in Geyssant et al. (1993),

Deconinck et al. (1996), Proust et al. (1995), Mansy et al. (2007). The studied patch reefs are placed at numerous sites between Audresselles village and Gris-Nez Cape (i.e., in more proximal depositional setting) along two conspicuous stratigraphic horizons: on top of the Grès de Connincthun and Grès de Châtillon formations (see below). The largest patch reefs are cropping out along the beach of the Gris-Nez Cape (Mansy et al., 2007), where they may reach a size of 1 m (Fig. 2), whereas the usual size range of these objects is 10–50 cm.

1) The most common stratigraphic position by far for the patch reefs is the base of the Argiles de Châtillon Formation, a sequence predominated by organic carbon-rich mudstone, generally intercalated between two low-stand sandstone units, namely, the Grès de Châtillon Formation at the base, and the Grès de la Crèche formation at the top (Fig. 1C and Table 1). Both of these clastic-dominated formations mainly consist of brown-to orange-colored sandstones and sandy marlstones with common cross-bedding and wave ripples, as well as intense bioturbation (especially U-shaped and *Rhizocorallium* burrows). Along the cliffs north of Audresselles, some isolated 10–50 cm large patch reefs are observed *in situ* at the base of the first marlstone level of the Argiles de Châtillon, i.e., above an about 30 cm-thick siltstone bed, highly bioturbated, forming the top of the sandstone beds of the Grès de Châtillon Formation (Figs. 4 and 5). Overall, the patch reefs have been extracted from their caging marls by wave erosion and are found as cobbles or boulders directly on the top bed of the Grès de Châtillon on the beach, at the foot of the small cliff. In the Gris-Nez Cape site (“La Sirène” Beach), the Grès de Châtillon Formation does not exist under its common facies due to the more proximal depositional setting (the time-equivalent deposits are possibly lacking in the sedimentary record here). The base of the Argiles de Châtillon



Figure 2. A – Large, *in situ*, patch reef observed on the La Sirène Beach at the foot of the north cliff of the Gris-Nez Cape. B – A block, ripped off by wave erosion, from the large patch reefs of the La Sirène Beach. C – Close-up view of the patch-reef surface. D – A patch reef, smoothed by wave energy on top of a sandstone bed.

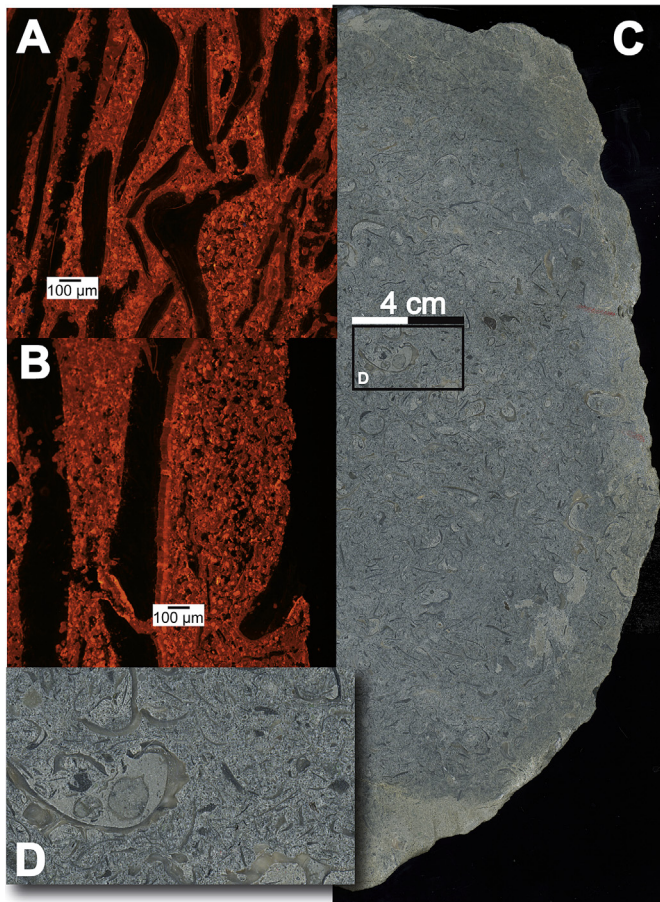


Figure 3. A & B – Cathodoluminescence imaging of thin sections showing the microspar of the calcite matrix and occasional fringes of larger crystals visible on some shells. The shells frequently show microborings. C – Large-scale view of a polished slab of a patch reef. D – Close up from C.

- Formation is marked by a spectacular 1–2 m thick ball-shaped oyster reef sequence (Fig. 2) that can be observed at numerous spots along the shore of the Gris-Nez Cape (Mansy et al., 2007). It is important to note that, at this site, the Late Jurassic rocks are intensely folded and dissected by faults due to their vicinity to the major fault zone of the Gris-Nez Cape (Fig. 1B) that controlled the subsidence pattern during the deposition of the Late Jurassic deposits (Mansy et al., 2003).
- 2) The second stratigraphic position of the observed patch reefs is much less extensive than the first one. This level is situated at the base of the Calcaires du Moulin Wibert Formation (Fig. 1C and Table 1), another mudstone dominated sequence containing, however, numerous carbonate beds. Two small-scale patch reefs were observed on the beach of the Gris-Nez Cape, directly on top of the sandstone bed forming the top of the Grès de Conninchun Formation (Fig. 6A–C).

3. Synsedimentary fluid circulations induced by tectonic activity?

Whatever the stratigraphic position of the observed patch reefs may be, it is noteworthy that they share common paleoenvironmental features. As exemplified by the general sequence-stratigraphy framework (Fig. 1C), the development of patch reefs corresponds to periods of rapid sea-level rise (i.e., at the base of the

Calcaires du Moulin Wibert Formation and at the base of the Argiles de Châtillon Formation). Furthermore, synsedimentary tectonic activity can be observed at the top beds of the sandstone units on which the patch reefs developed (i.e., the Grès de Châtillon and the Grès de Conninchun formations, respectively). Especially along the cliffs north of Audresselles (Fig. 4B), the Grès de Châtillon Formation shows very nice examples of meter-scale syndepositional, south-dipping, normal faults passing upward into a gentle flexure with recurrent southern subsiding panels filled up with sandstone or mudstone sequences of increasing thickness. This is also the case along the Gris-Nez Cape shore, where the top bed of the Grès de Conninchun Formation displays minor 10 cm-scale flexures in the vicinity of a more significant 10 m-scale north-dipping normal fault that also affects the overlying Calcaires du Moulin Wibert Formation (Fig. 6A).

Such observations strongly suggest that the sharp deepening trend at the base of the Calcaires du Moulin Wibert and Argiles de Châtillon formations is controlled by intense tectonic subsidence driven by recurrent pulses of normal fault activity. The related destabilization of the basin floor is likely to have promoted the expulsion of fluids from the deeper lying sediments, which could be a possible driving process for the development of the patch reefs at these specific stratigraphic intervals. The involvement of tectonic-induced fluids into the process controlling the development of observed patch reefs is strengthened by the observation of an isolated patch reef found directly on an N-dipping normal fault scarp just North of Audresselles (Fig. 5B–D). The Grès de Châtillon Formation that forms the footwall of this fault plane, yields very nice examples of sand injectites distributed normal to the fault plane, indicating the expulsion of fluids under pressure expelled away from the fault zone, as the sandstones were not cemented at the time of deposition (i.e., very early in the diagenetic course of the sand bodies).

To further constrain the nature and role of fluids possibly involved in the development of the patch reefs, we conducted a petrographical and geochemical study as explained below.

4. Methods

We characterized the patch reefs by means of petrographical and geochemical methods. Thin sections of the patch reefs were studied using a cathodoluminescence-equipped microscope (Olympus BX41 with a Ctl 8200 MK4 cold-cathode cathodoluminescence device operating at 20 kV) and a scanning electron microscope (FEI Quanta 200 Environmental) equipped with a backscattered electron device and an energy dispersive spectroscopy-probe (X-Flash 3001 Brucker + Quantax 400 software). The carbonate content was determined with a Bernard-type calcimeter (acid digestion followed by CO₂ volume determination; accuracy < 5%). For stable carbon and oxygen isotope analysis, we sampled the shells, shell sparry fillings and the mudstone matrix using a micro-drill, to discriminate between the isotopic signatures of the various carbonate constituents of the patch reefs. The samples were further ground in an agate mortar and sieved to ensure grain size lower than 140 μm. CO₂ was extracted by calcite dissolution with 100% H₃PO₄ (McCreas, 1950) at 25 °C for 12 h in helium flushed Labco Exetainer® vials. Stable carbon and oxygen isotopic compositions of the evolved CO₂ were measured using a gas chromatograph coupled to an isotope ratio mass spectrometer (GC-IRMS) (Analytical Precision 2003, today entitled GV 2003, provided by GV Instruments), with helium as carrier gas. Three internal standards were used to calibrate the δ¹³C_{sample/ref} data provided by the GC-IRMS relative to the V-PDB scale and have been calibrated using two international standards, NBS19 and IAEA-CO1 (IAEA catalog). Results are given in the usual δ-notation relative to the

Table 1

Short description of the Late Jurassic geological formations of the Boulonnais.

Age	Ammonite zone	Formation	Short description
Encompassing the Kimmeridgian–Tithonian boundary	Autissiodorensis to Gigas–Elegans zones	Argiles de Châtillon	The formation consists of claystone and marlstone accumulations with two intervals of laminated paper shales and a laterally variable number of occasional intercalated limestone beds. The marlstones show a gradual enrichment in silt in the upper part of the formation. Storm beds are numerous, notably at the Kimmeridgian–Tithonian Autissiodorensis–Elegans zone) boundary.
Kimmeridgian	Eudoxus Zone, Contejeani subzone	Grès de Châtillon	The formation consists of brown- to orange-colored sandstones and sandy marlstones with common cross-bedding and wave ripples, and intense bioturbation (especially U-shaped and Rhizocorallium burrows).
Kimmeridgian	Eudoxus Zone, Contejeani subzone	Calcaires du Moulin Vibert	Irregular alternation of gray clay, more or less clear, and argillaceous limestones small beds (dm) and thicker beds (0.5–0.8 m). In the upper part of the unit, the beds are coquina.
Kimmeridgian	Eudoxus Zone, Caletanum–Contejeani sub-zones	Grès de Connincthun	The formation is made up with a few sandstone beds that are rich in glauconite and large quartz grains. Abundant bivalves (<i>Trigonia</i>) and occasional echinoids are observed.

international standard V-PDB for $\delta^{13}\text{C}$ and $\delta^{18}\text{O}$. The external reproducibility for $\delta^{13}\text{C}$ and $\delta^{18}\text{O}$ measurements is of $+/-0.1\text{\textperthousand}$ and $+/-0.2\text{\textperthousand}$, respectively (1σ). Each sample was measured twice and the average of two analyses is reported in the figures.

To determine the stable sulfur isotope composition ($\delta^{34}\text{S}$) of pyrite, seven bulk rock samples of patch reefs were decarbonated through HCl digestion to concentrate pyrite. The decarbonated samples were oxidized with O_2 at 1050°C to produce SO_2 that was analyzed using a VG Sira mass spectrometer. The results were expressed in δ conventional notation, relative to the standard V-CDT (Vienna Canon Diablo Troilite). The standard was a Ag_2S

MERCK with $\delta^{34}\text{S} = +3\text{\textperthousand}$ vs. V-CDT. Each sample was measured in duplicate and the average values are reported. The analytical precision of measurements was $\pm 0.3\text{\textperthousand}$; the reproducibility was of $\pm 1\text{\textperthousand}$.

The mineralogical composition of the carbonate was determined using classical X-ray diffraction (XRD) of micro-pulverized samples (Bout-Roumazeilles et al., 1999). To that end, a Bruker D4 Endeavor apparatus was used together with the Macdiff software (Bout-Roumazeilles et al., 1999).

Three patch-reef carbonate specimens were chosen for lipid biomarker analysis and were prepared and decalcified after the method described previously (Birgel et al., 2006). After saponification with 6% KOH in methanol, the samples were extracted three times with a CEM Discovery microwave extraction system at 80°C and 250 W for 15 min with dichloromethane:methanol (3:1). For GC analyses, the total extracts were pre-cleaned by separation into an *n*-hexane soluble and dichloromethane-soluble fraction. The *n*-hexane fraction was further treated and separated by column chromatography into four fractions of increasing polarity (cf. Birgel et al., 2008). The hydrocarbon and carboxylic acid fractions were analyzed by gas chromatography-flame ionization detection (GC-FID) with an Agilent 7820 A GC system at the Department of Geodynamics and Sedimentology, University of Vienna. The GC-FID system was equipped with a 30 m HP-5 MS UI fused silica capillary column (0.25 mm i.d., 0.25 μm film thickness). The carrier gas was helium. The GC temperature program used for all fractions was: 60°C (1 min); from 60°C to 150°C to 320°C at $4^\circ\text{C}/\text{min}$, 25 min isothermal. The aim was to verify whether characteristic microbial molecular fossils were preserved in the carbonates.

5. Results

5.1. Macrofacies

The patch reefs have a rounded shape and are composed of countless shells of *N. nana* that show no visible, preferential orientation. The two valves of the fossils are not always connected to each other. The shells are embedded in a limestone mud (Fig. 3A–D). No other fossils were identified, except for one individual gastropod. Overall, the patch reefs are indurated except for the largest ones, where some “seams” or fissures were observed. They are filled with abundant quartz grains and organic-rich matter. Most likely, these structures result from burrowing activity.

5.2. Microfacies

The various patch reefs at different stratigraphic levels showed the same microfacies features. The carbonate matrix is a

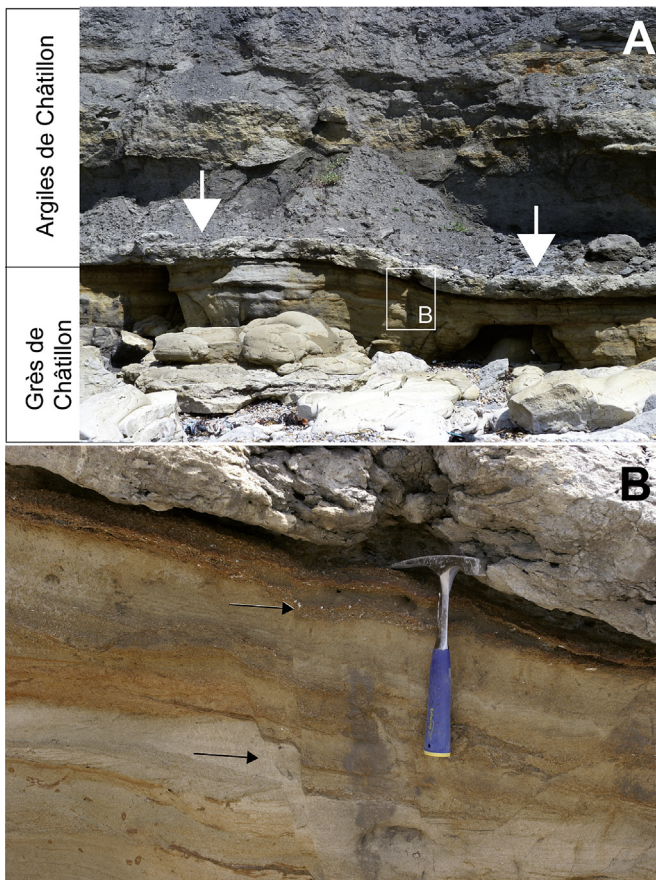


Figure 4. A – The white arrows point to the basal bed of the Argiles de Châtillon Formation, where the patch reefs are rooted. B – The black arrows show the synsedimentary faults visible in the upper part of the Grès de Châtillon Formation. Location: on the beach between the Gris-Nez Cape and the village of Audresselles: black cross in Figure 1B.

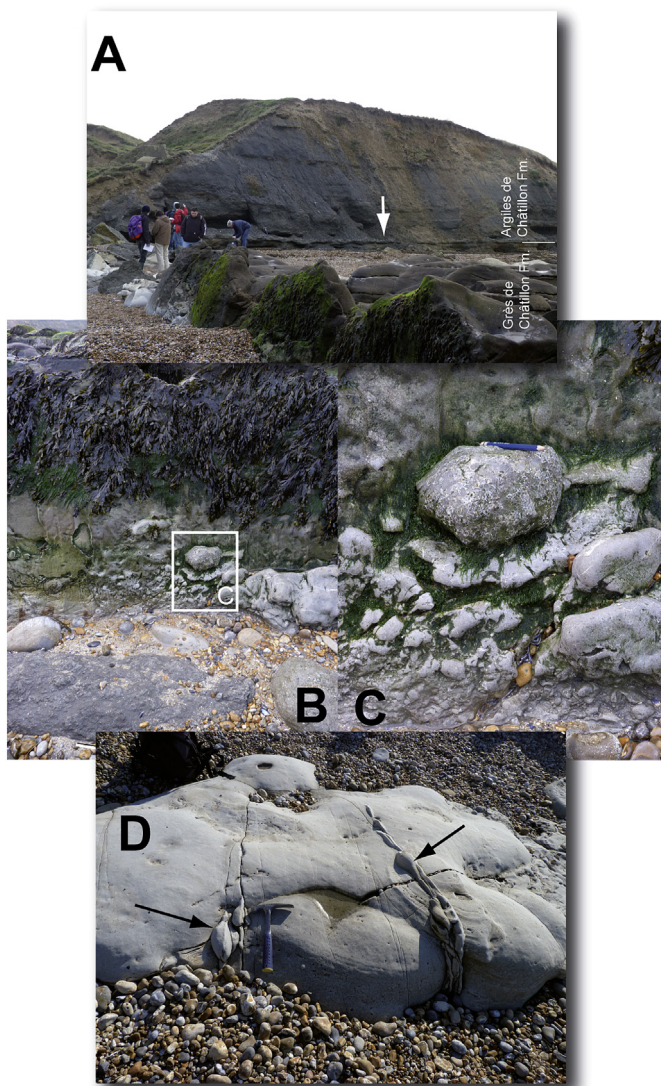


Figure 5. A – The white arrow indicates the basal bed of the Argiles de Châtillon Formation, as in [Figure 4A](#). The picture illustrates the Grès de Châtillon and Argiles de Châtillon formations. In the foreground, covered with green algae, the fault plane of a synsedimentary fault affecting the Grès de Châtillon Fm. On this plane, a small patch reef is rooted (B & C). The synsedimentary fault is accompanied by sand injectites visible in the Grès de Châtillon sandstone beds (D). Location: Cran du Noirda, the beach at the north end of Audresselles ([Fig. 1B](#)).

homogeneous calcite microspar with numerous shells and shell fragments, accompanied by common organic-rich particles and rare pyrite frambooids (packstone–grainstone fabrics; [Fig. 3A, B, D](#)). A fringe of sparitic crystals was frequently but not systematically observed around most shells ([Fig. 3A and B](#)). No coccolith fossils (or molds) could be observed. Cathodoluminescence imaging showed that in all observed thin sections, the color of the calcitic, microsparitic matrix is homogeneous. No luminescence contrast was observed, suggesting that the chemical composition of the carbonate matrix is homogeneous. Shells occasionally showed white, sparitic fillings. Regarding the mineralogy of carbonate, XRD data demonstrated that the microsparite of the matrix is composed of calcite.

5.3. Stable isotopes

The carbonate matrix samples (all but one) show $\delta^{13}\text{C}$ values ranging between $-8.9\text{\textperthousand}$ and $-3.6\text{\textperthousand}$ V-PDB, whereas both shell and

sparry shell-filling samples ranged between $-2.0\text{\textperthousand}$ and $0.6\text{\textperthousand}$ V-PDB ([Fig. 7](#)). No distinction can be made between matrix samples, shell, and shell-filling samples when considering the $\delta^{18}\text{O}$ values ([Fig. 7A and B](#)). The range for all samples varies between $-5.2\text{\textperthousand}$ and $-1.0\text{\textperthousand}$ V-PDB. The two most-depleted samples correspond to shell

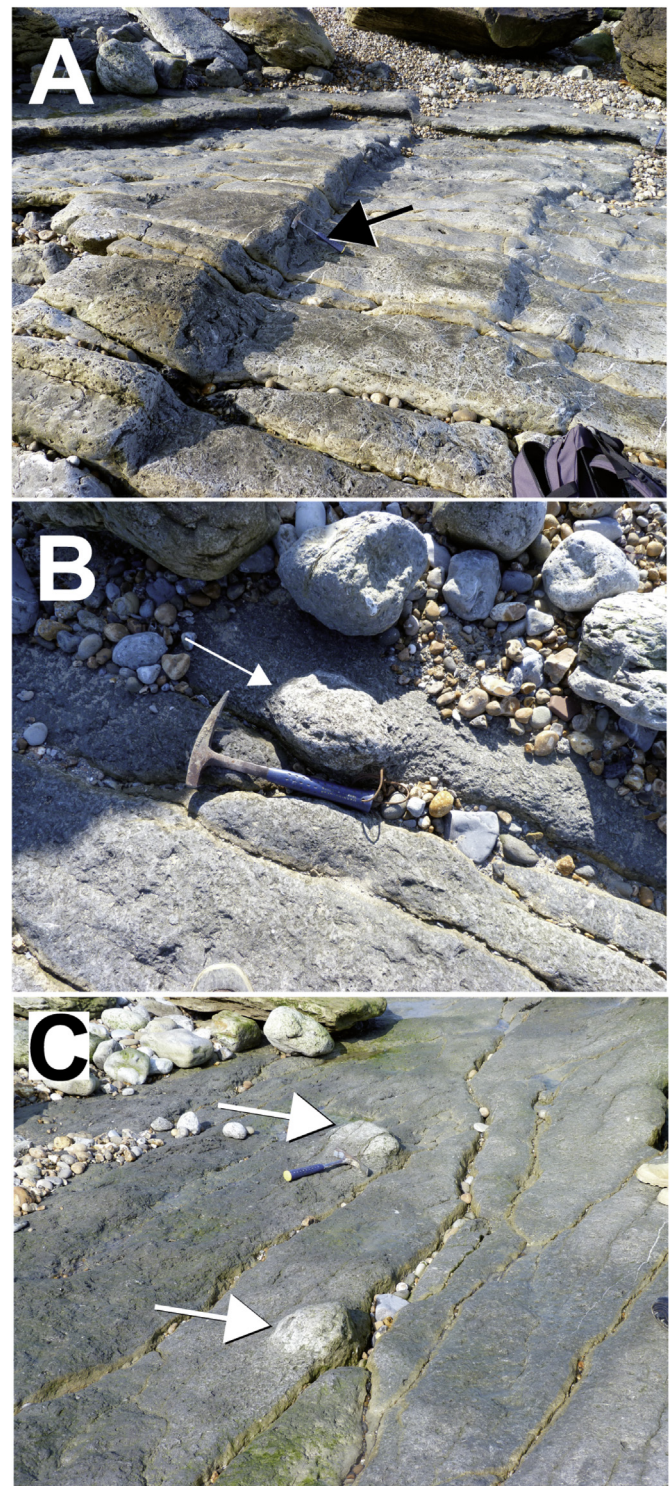


Figure 6. A – Synsedimentary, soft deformations affecting the top sandstone bed of the Grès de Conninckun Formation, producing sorts of stair steps. The black arrow shows the hammer. B & C: patch reefs rooted on the surface of this bed (white arrows). Location: La Sirène Beach, Gris-Nez Cape.

fillings. A positive correlation can be drawn, linking the CaCO_3 content to the $\delta^{18}\text{O}$ values (Fig. 7). For the seven samples ran for sulfur isotope composition of pyrite, the $\delta^{34}\text{S}$ values varied between -42.9‰ and -35.1‰ CDT (Fig. 7C).

At times, molecular fossils of prokaryotes (both bacteria and archaea) can be well preserved in Mesozoic authigenic carbonates (Peckmann et al., 1999; Birgel et al., 2006). Unfortunately, the overall lipid biomarker contents of the patch reef samples were very low and not diagnostic as being derived from bacteria and archaea in both the hydrocarbon and carboxylic acid fractions. Characteristic microbial biomarkers such as terminally-branched fatty acids (sulfate-reducing bacteria) or isoprenoid hydrocarbons

(methanogenic or methanotrophic archaea; see Peckmann and Thiel, 2004 for a review) were not identified or preserved. From the lipid biomarker results we were not able to make any conclusion on the contribution of microbes in the formation of the studied carbonates.

6. Discussion

6.1. Authigenesis in patch reefs

Within the patch reefs, the $\delta^{13}\text{C}$ isotope composition of the fine-grained carbonate matrix is varying significantly from the included

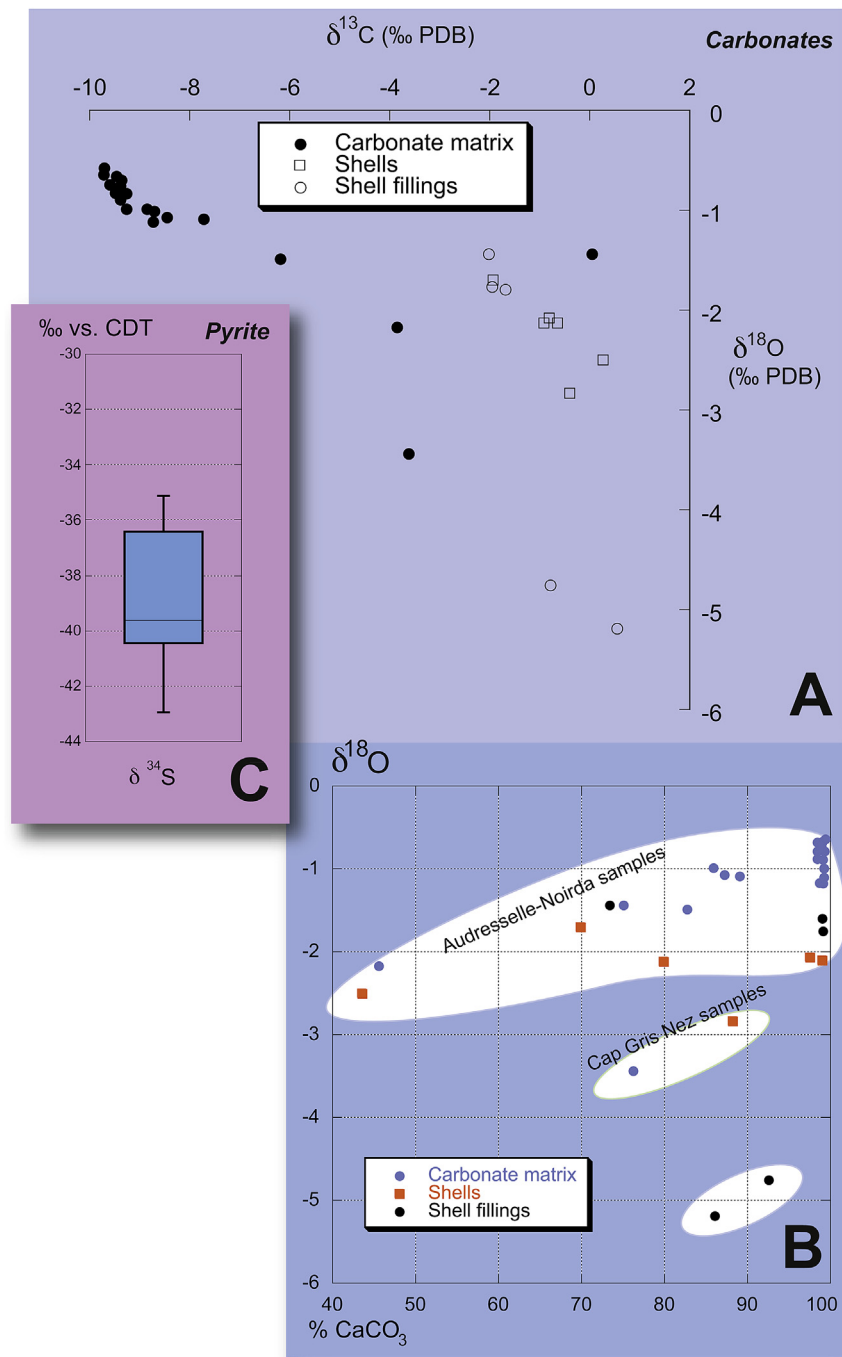
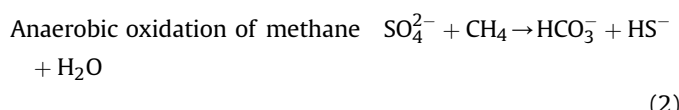
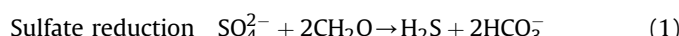
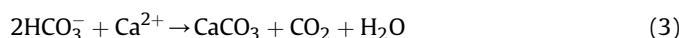


Figure 7. A & B – Carbon and oxygen stable isotope composition of the various carbonate fractions of the patch reefs. C – Box and whiskers-type diagram showing the S isotope composition of pyrite embedded in the patch reefs.

shells. The patch reefs are also varying isotopically from the enclosing marls. The basal marls of the Argiles de Châtillon Formation show $\delta^{13}\text{C}$ values ranging from $-0.2\text{\textperthousand}$ to $2.0\text{\textperthousand}$ (Tribovillard, unpublished data). Overall, the matrix samples are markedly depleted in ^{13}C , while the shell and sparry shell-filling samples resemble the values usually found in Late Jurassic seawater carbonates, which range from 0 to 2\textperthousand (Veizer et al., 1999; Prokoph et al., 2008). The $\delta^{13}\text{C}$ values of the carbonate matrix of the patch reefs are depleted in ^{13}C , pointing to another, more ^{13}C -depleted carbon source than dissolved inorganic carbon (DIC). It is inferred that the patch-reef matrix may be an authigenic carbonate incorporating a fraction of biogenic, ^{13}C -depleted carbon derived from microbial organic-matter remineralization during early diagenesis (cf. Berner, 1980; Folk and Chafetz, 2000; Peckmann and Thiel, 2004; Aloisi et al., 2002, and references therein). Microbes in sediments gain energy by performing various chemical reactions. As a consequence of their metabolism, strong shifts in pH and/or alkalinity are often observed, which may in turn foster or hamper carbonate supersaturation in pore waters, hence calcium carbonate precipitation [see comprehensive syntheses by Megenigal et al. (2003) and Burdige (2006, Chapters 7 and 16) and Soetaert et al. (2007)]. Most of the known bio-induced or bio-mediated chemical reactions leading to authigenic carbonate precipitation function under primarily anaerobic conditions. Two anaerobic, microbially-mediated reactions studied best in the shallow subsurface are bacterial sulfate-reduction (Berner, 1980; Jørgensen, 1982; Burdige, 2006) and sulfate-dependent anaerobic oxidation of methane (AOM), conjointly operated by consortia of anaerobic methane-oxidizing archaea and sulfate-reducing bacteria (e.g., Hinrichs et al., 1999; Boetius et al., 2000). Basically, the reactions of sulfate reduction and anaerobic oxidation of methane can be summarized by the following equations:



In such equations, CH_2O is a simplified, conventional way to represent organic matter. The alkalinity generated by both reactions may favor precipitation of authigenic carbonates in the shallow subsurface of the seafloor (Berner, 1980):



The $\delta^{34}\text{S}$ values for the pyrites extracted from the patch reefs range between $-42.9\text{\textperthousand}$ and $-35.1\text{\textperthousand}$. The $\delta^{34}\text{S}$ value for the Late Jurassic seawater is in average $+15\text{\textperthousand}$ (Prokoph et al., 2008). The significant sulfur isotope fractionation between the Jurassic seawater values and pyrite strongly suggests that bacterial sulfate reduction operated within a comparatively infinite sulfate reservoir, that is, most likely at or very close to the sediment–water interface. Among anaerobic processes, sulfate reduction is most commonly involved into diagenetic carbonate precipitation because sulfate ions are abundant in seawater and sediment pore water (e.g., Jørgensen, 1982; Scotchman, 1991; Peckmann and Thiel, 2004; Pierre et al., 2012).

Based on the abundant literature devoted to microbial activity and authigenic carbonates formed at seep sites (e.g., Hinrichs et al., 1999; De Craen et al., 1999; Boetius et al., 2000; Peckmann and Thiel, 2004; Gontharet et al., 2007, 2009; Ge et al., 2010; Birgel et al., 2011; Chevalier et al., 2011, to mention just a few recent papers), we interpret the localized isotopic anomalies corresponding

to the patch reefs as scattered spots where bacterial activity was fueled by seepage of hydrocarbon-rich fluids, but no (biomarker) evidence for AOM was found (see above). In the patch reefs, specific sulfate-reducing bacteria may have processed the seeping hydrocarbons, as some of them are known to degrade *n*-alkanes and *n*-alkenes (see Grossi et al., 2008 and references therein). Further, activity of sulfate-reducing bacteria is evidenced by abundant pyrite framboids and their specific isotopically-depleted sulfur isotopes. Similar observations were made in other authigenic precipitates, namely phosphorites, where also additional biomarker evidence for sulfate reducers was found (Arning et al., 2009). As a consequence of bacterial activity of sulfate reducers, a localized alkalinity increase led to carbonate precipitation. The $\delta^{13}\text{C}$ signature of the authigenic carbonate was in contrast to the values found for the enclosing marls and that of the shells of the bivalves. These bivalves may have been feeding on the bacterial biomass, but since oysters are so far not known to feed on bacteria or live in chemosymbiosis, they may have simply used the authigenic carbonate as a firm ground. The fact that the $\delta^{13}\text{C}$ is not significantly depleted suggests that the carbonates of the matrix resulted from a mixture of two sources: 1) a light C source such as organic matter remineralization (or even hydrocarbon oxidation) and, 2) a seawater DIC source. The fact that the sparry shell fillings yield more negative $\delta^{18}\text{O}$ values than those of the microsparitic matrix or shells suggests a carbonate precipitation during later diagenesis, with pore-space fluids that had evolved from seawater.

6.2. Patch reefs vs. Beauvoisin pseudo-bioherms

It is tempting to compare the patch reefs of the Boulonnais to the Late-Jurassic pseudo-bioherms of the Beauvoisin site (Vocontian Trough, South-Eastern France), investigated by Bourreau (1977), Gaillard et al. (1985), Gaillard and Rolin (1986), Rolin et al. (1990), Peckmann et al. (1999), Gay (2002), Louis-Schmid et al. (2007) and Tribovillard et al. (2013). These pseudo-bioherms (fossiliferous calcareous bodies with a bioherm shape but no reef-building organisms forming a significant relief at the sediment–water interface) are included in the Terres Noires Formation, a 2500 m-thick marlstone accumulation dated of Bathonian-Kimmeridgian age, and deposited under hemi-pelagic conditions (Tribovillard and Dureux, 1986; Tribovillard, 1988). The pseudo-bioherms are located approximately along or very close to synsedimentary faults that were active during the deposition of the Terres Noires (Gaillard and Rolin, 1988). The proximity of the carbonate precipitates to fault systems is a similarity found as well in the patch reefs. The pseudo-bioherms are lens- or column-shaped carbonate bodies interbedded within marlstones. Their size is (pluri-) metric for both diameter and height. Biogenic remains include mainly numerous bivalve shells (lucinids), pellets and planktonic foraminifers (protoglobigerinids). Gaillard et al. (1992), Peckmann et al. (1999), Louis-Schmid et al. (2007) and Tribovillard et al. (2013) reported isotope data obtained from pseudo-bioherms, carbonate nodules and lucinid shells of Beauvoisin. The limestones are depleted in ^{13}C with $\delta^{13}\text{C}$ ranging from $-24.6\text{\textperthousand}$ to $-9.7\text{\textperthousand}$ PDB. In addition, the typical molecular signature of the AOM consortia was identified (Peckmann et al., 1999). Comparing the sedimentological, faunal and geochemical features of the pseudo-bioherms of Beauvoisin to those of ancient or present sites of hydrocarbon seepage, Rolin et al. (1990) and Gaillard et al. (1992) interpreted the pseudo-bioherms as formed at ancient cold seeps, with carbonate masses and nodules authigenically resulting from bacterial activity, fueled by fluids circulating along synsedimentary faults.

To what extent can the patch reefs be compared to the pseudo-bioherms? Both the Jurassic patch reefs and Beauvoisin pseudo-

bioherms are rich in bivalves, though different groups of bivalves are preserved in the carbonates. In Beauvoisin, lucinids are the only bivalves identified, these bivalves are known to live with endosymbiotic bacteria (Rolin et al., 1990; Gaillard et al., 1992; Callender and Powell, 2000), allowing them to endure anoxic conditions, which is not the case with the patch reef oysters. In addition, the $\delta^{13}\text{C}$ values of the pseudo-bioherms are much more depleted than the ones in the patch reefs. Furthermore, molecular signatures of the AOM-performing consortia were identified in the pseudo-bioherms and were not found in patch reefs (Peckmann et al., 1999). Consequently, AOM cannot be put forward as carbonate forming process in the patch reefs and is in great contrast to the pseudo-bioherms of Beauvoisin. Consequently, activity of sulfate reducing bacteria solely, without AOM involvement, must be retained for the patch reefs. Nevertheless, the major similarity of both the patch reefs and the pseudo-bioherms is their occurrence in the vicinity of synsedimentary faults. During the Late Jurassic, the Boulonnais area was affected by synsedimentary faulting in relation with the rifting of the Atlantic Ocean. The patch reefs are concentrated at stratigraphic levels that were affected by synsedimentary tectonics as well. More conspicuously, patch reefs are observed on a synsedimentary fault plane and on the surface of beds softly deformed by synsedimentary extensional movements (Figs. 5 and 6). Lastly, fluid expulsions associated to synsedimentary tectonics were also held responsible for rendering depositional conditions prone to sulfate reduction, inducing the rapid, authigenic formation of the carbonate beds of the overlying Bancs Jumeaux Formation (Fig. 1C; Tribouillard et al., 2012). Thus, synsedimentary fluid expulsion causing authigenic carbonate precipitation by activity of hydrocarbon-degrading sulfate reducing bacteria is a recurrent feature of the Boulonnais during the latest Jurassic.

7. Conclusion

The late-Jurassic formations of the Boulonnais area show carbonates, either patch reefs or carbonate beds, yielding common facies and microfacial features. Their common and widespread occurrence could be misinterpreted without stable isotope data, pointing to their authigenic origin. The formation of the authigenic carbonate phases was induced by an increase of alkalinity, closely associated to the activity of hydrocarbon-degrading, sulfate reducing bacteria. The presence and activity of sulfate reducing bacteria in early diagenesis was most probably induced and fueled by seepage of hydrocarbon-rich fluids, ascending along synsedimentary fault planes from deeper, organic-rich layers that structured the Boulonnais.

Acknowledgment

We thank Florent Barbecot for his constant support with isotope analyses, Pauline Manet, formerly master student and the members of the technical staff of the Géosystèmes Lab, namely, Marion Delattre, Monique Gentric, Sylvie Regnier, Sandra Ventalon, Romain Abraham and Philippe Recourt. We thank Rudy Swennen and Olivier Lacombe, guest editors of the special Issue of *Marine and Petroleum Geology*. We are indebted to our reviewers — Martin Blumenberg and an anonymous referee — as well as Rudy Swennen for their scientific expertise and editorial work that helped us improve significantly the paper.

References

- Al-Ramadan, K., Morad, S., Proust, J.-N., Al-Aasm, I., 2005. Distribution of diagenetic alterations in siliciclastic shoreface deposits within a sequence stratigraphic framework: evidence from the upper Jurassic Boulonnais, NW France. *J. Sediment. Res.* 75, 943–959.
- Aloisi, G., Bouloubassi, I., Heijmans, S.K., Pancost, R.D., Pierre, C., Sinnige Damste, J.S., Gottschal, J.C., Forney, L.J., Rouchy, J.-M., 2002. CH₄-consuming microorganisms and the formation of carbonate crusts at cold seeps. *Earth Planet. Sci. Lett.* 203, 195–203.
- Arning, E.T., Birgel, D., Brunner, B., Peckmann, J., 2009. Bacterial formation of phosphatic laminites off Peru. *Geobiology* 7, 295–307.
- Bates, R.L., Jackson, J.A., 1987. *Glossary of Geology*, third ed. American Geological Institute, p. 788.
- Beeley, H.S., Norton, M.G., 1998. The structural development of the Central English Channel High — constraints from section restoration. In: Underhill, J.R. (Ed.), *Development, Evolution and Petroleum Geology of the Wessex Basin*, Geological Society, London, Special Publications, vol. 133, pp. 283–298.
- Berner, R.A., 1980. *Early Diagenesis — a Theoretical Approach*. Princeton University Press, p. 241.
- Birgel, D., Feng, D., Roberts, H.H., Peckmann, J., 2011. Changing redox conditions at cold seeps as revealed by authigenic carbonates from Alaminos Canyon, northern Gulf of Mexico. *Chem. Geol.* 285, 82–96.
- Birgel, D., Thiel, V., Hinrichs, K.-U., Elvert, M., Campbell, K.A., Reitner, J., Farmer, J.D., Peckmann, J., 2006. Lipid biomarker patterns of methane-seep microbialites from the Mesozoic convergent margin of California. *Org. Geochem.* 37, 1289–1302.
- Birgel, D., Elvert, M., Han, X., Peckmann, J., 2008. ^{13}C -depleted biphytanic diacids as tracers of past anaerobic oxidation of methane. *Org. Geochem.* 39, 152–156.
- Boetius, A., Ravenschlag, K., Schubert, C.J., Rickert, D., Widdel, F., Gieseke, A., Amann, R., Jørgensen, B.B., Witte, U., Pfannkuch, O., 2000. A marine microbial consortium apparently mediating anaerobic oxidation of methane. *Nature* 407, 623–626.
- Bourseau, J.P., 1977. L'Oxfordien moyen à nodules des "Terres Noires" de Beauvoisin (Drôme). *Nouvelles Arch. Mus. Hist. Lyon* 15, 116.
- Bout-Roumazeilles, V., Cortijo, E., Labeyrie, L., Debrabant, P., 1999. Clay-mineral evidence of nepheloid layer contribution to the Heinrich layers in the Northwest Atlantic. *Palaeogeogr. Palaeocatol. Palaeoecol.* 146, 211–228.
- Burdige, D.J., 2006. *Geochemistry of Marine Sediments*. Princeton University Press, p. 609.
- Butler, M., Pullan, C.P., 1990. Tertiary structures and hydrocarbon entrapment in the Weald Basin of southern England. In: Hardman, R.F.P., Brooks, J. (Eds.), *Tectonic Events Responsible for Britain's Oil and Gas Reserves*, Geological Society, London, Special Publications, vol. 55, pp. 371–391.
- Callender, R., Powell, E.N., 2000. Long-term history of chemoautotrophic clam-dominated faunas of petroleum seeps in the Northwestern Gulf of Mexico. *Facies* 43, 177–204.
- Chevalier, N., Bouloubassi, I., Birgel, D., Crémère, A., Taphanel, M.-H., Pierre, C., 2011. Authigenic carbonates at cold seeps in the Marmara Sea (Turkey): a lipid biomarker and stable carbon and oxygen isotope investigation. *Mar. Geol.* 288, 112–121.
- De Craen, M., Swennen, R., Keppens, E.M., Macaulay, C.I., Kiriakoulakis, K., 1999. Bacterially mediated formation of carbonate concretions in the Oligocene Boom Clay of Northern Belgium. *J. Sediment. Res.* 69, 1098–1106.
- Deconinck, J.-F., Geyssant, J.R., Proust, J.-N., Vidier, J.P., 1996. Sédimentologie et biostratigraphie des dépôts kimméridgiens et tithoniens du Boulonnais. *Ann. Soc. Géol. Nord* 4, 157–170.
- Delecat, S., Peckmann, J., Reitner, J., 2001. Non-rigid cryptic sponges in oyster patch reefs (Lower Kimmeridgian, Langenberg/Oker, Germany). *Facies* 45, 231–254.
- Folk, R.L., Chafetz, H.S., 2000. Bacterially induced microscale and nanoscale carbonate precipitates. In: Riding, R.E., Awramik, S.M. (Eds.), *Microbial Sediments*. Springer, pp. 40–49.
- Fürsich, F.T., 1981. Salinity-controlled benthic associations from the Upper Jurassic of Portugal. *Lethaia* 14, 203–223.
- Gaillard, C., Bourseau, J.P., Boudeulle, M., Pailleret, P., Rio, M., Roux, M., 1985. Les pseudobiohermes de Beauvoisin (Drôme): un site hydrothermal sur la marge tethysienne l'Oxfordien? *Bull. Soc. Géol. France* 8 (1), 69–78.
- Gaillard, C., Rio, M., Rolin, Y., 1992. Fossil chemosynthetic communities related to vents or seeps in sedimentary basins: the pseudobioherms of south-eastern France compared to other world examples. *Palaio* 7, 451–465.
- Gaillard, C., Rolin, Y., 1986. Paléobiocoénoses susceptibles d'être liées à des sources sous-marines en milieu sédimentaire. L'exemple des Terres Noires (SE France) et des teppe butées de la Pierre Shale Formation (Colorado, U.S.A.). *C. R. Acad. Sci. Paris* 303, 1503–1508.
- Gaillard, C., Rolin, Y., 1988. Relation entre tectonique synsédimentaire et pseudobiohermes (Oxfordien de Beauvoisin-Drôme-France). Un argument supplémentaire pour interpréter les pseudobiohermes comme formés au droit de sources sous-marines. *C. R. Acad. Sci. Paris* 307, 1265–1270.
- Gay, A., 2002. Les marqueurs géologiques de la migration et de l'expulsion des fluides sédimentaires sur le plancher des marges passives matures. Exemples dans le Bassin du Congo, vol. 1, p. 426 (Thèse Université de Lille).
- Ge, L., Jiang, S.-Y., Swennen, R., Yang, T., Yang, J.-H., Wu, N.-Y., Liu, J., Chen, D.H., 2010. Chemical environment of cold seep carbonate formation on the northern continental slope of South China Sea: evidence from trace and rare earth element geochemistry. *Mar. Geol.* 277, 21–30.
- Geyssant, J.R., Vidier, J.-P., Herbin, J.-P., Proust, J.-N., Deconinck, J.-F., 1993. Biostratigraphie et paléoenvironnement des couches de passage Kimméridgien/Tithonien du Boulonnais (Pas de Calais): nouvelles données paléontologiques (ammonites), organisation séquentielle et contenu en matière organique. *Géol. France* 4, 11–24.

- Gontharet, S., Pierre, C., Blanc-Valleron, M.-M., Rouchy, J.M., Fouquet, Y., Bayon, G., Foucher, J.P., Woodside, J., Mascle, J., The Nautinil Scientific Party, 2007. Nature and origin of diagenetic carbonate crusts and concretions from mud volcanoes and pockmarks of the Nile deep-sea fan (eastern Mediterranean Sea). Deep Sea Res. Part II: Top. Stud. Oceanogr. 54, 1292–1311.
- Gontharet, S., Stadnitskaia, A., Bouloubassi, I., Pierre, C., Sinninghe Damsté, J.S., 2009. Palaeo methane-seepage history traced by biomarker patterns in a carbonate crust, Nile deep-sea fan (eastern Mediterranean Sea). Mar. Geol. 261, 105–113.
- Grossi, V., Cravo-Laureau, C., Guyoneaud, R., Ranchou-Peyrusse, A., Hirschler-Réa, A., 2008. Metabolism of *n*-alkanes and *n*-alkenes by anaerobic bacteria: a summary. Org. Geochem. 39, 1197–1203.
- Hansen, D.L., Blundell, D.J., Nielsen, S.B., 2002. A model for the evolution of the Weald Basin. Bull. Geol. Soc. Denmark 49, 109–118.
- Helm, C., Schulke, I., 1998. A coral-microbialite patch reef from the Late Jurassic (Florigemma-Bank, Oxfordian) of NW Germany (Süntel Mountains). Facies 39, 75–104.
- Hinrichs, K.-U., Hayes, J., Sylva, S., Brewer, P., DeLong, E., 1999. Methane-consuming archaeabacteria in marine sediments. Nature 398, 802–805.
- Jørgensen, B.B., 1982. Mineralization of organic matter in the sea bed — the role of sulphate reduction. Nature 296, 643–645.
- Louis-Schmid, B., Rais, P., Logvinovich, D., Bernasconi, S.M., Weissert, H., 2007. Impact of methane seeps on the local carbon-isotope record: a case study from a Late Jurassic hemipelagic section. Terra Nova 19, 259–265.
- Mansy, J.-L., Guennoc, P., Robaszynski, F., Amedeo, F., Auffret, J.-P., Vidier, J.-P., Lamarche, J., Lefèvre, D., Sommè, J., Brice, D., Mistiaen, B., Prud'homme, A., Rohart, J.-C., Vachard, D., 2007. Notice explicative, carte géologique de la France (1/50 000), feuille Marquise, second ed. BRGM, Orléans, p. 213.
- Mansy, J.-L., Manby, G.M., Averbuch, O., Everaerts, M., Bergerat, F., Van Vliet-Lanoe, B., Lamarche, J., Vandycke, S., 2003. Dynamics and inversion of the Mesozoic Basin of the Weald-Boulonnais area: role of basement reactivation. Tectonophysics 373, 161–179.
- McCrea, J.M., 1950. On the isotopic chemistry of carbonates and a paleotemperature scale. J. Chem. Phys. 18, 849–857.
- Megonigal, J.P., Hines, M.E., Visscher, P.T., 2003. Anaerobic metabolism: linkages to trace gases and aerobic processes. In: Schlessinger, W.H. (Ed.), Biogeochemistry. In: Holland, H.D., Turekian, K.K. (Eds.), Treatise on Geochemistry, vol. 8. Elsevier-Pergamon, Oxford, pp. 317–424.
- Minguely, B., Averbuch, O., Patin, M., Rolin, D., Hanot, F., Bergerat, F., 2010. Inversion tectonics at the northern margin of the Paris basin (Northern France): new evidence from seismic profiles and boreholes interpolation in the Artois area. Bull. Soc. Géol. France 181 (5), 429–442.
- Newell, A.J., 2000. Fault activity and sedimentation in a marine rift basin (Upper Jurassic, Wessex Basin, UK). J. Geol. Soc. 157, 83–92.
- Peckmann, J., Thiel, V., 2004. Carbon cycling at ancient methane-seeps. Chem. Geol. 205, 443–467.
- Peckmann, J., Thiel, V., Michaelis, W., Clari, P., Gaillard, C., Martire, L., Reitner, J., 1999. Cold seep deposits of Beauvoisin (Oxfordian; southeastern France) and Marmorito (Miocene; northern Italy): microbially authigenic carbonates. Int. J. Earth Sci. 88, 60–75.
- Pierre, C., Blanc-Valleron, M.-M., Demange, J., Boudouma, O., Foucher, J.-P., Pape, T., Himmler, T., Fekete, N., Spiess, V., 2012. Authigenic carbonates from active methane seeps offshore southwest Africa. Geo-Mar. Lett. 32, 501–513.
- Prokoph, A., Shields, G.A., Veizer, J., 2008. Compilation and time-series analysis of a marine carbonate $\delta^{18}\text{O}$, $\delta^{13}\text{C}$, $^{87}\text{Sr}/^{86}\text{Sr}$ and $\delta^{34}\text{S}$ database through Earth history. Earth-Sci. Rev. 87, 113–133.
- Proust, J.-N., Deconinck, J.-F., Geyssant, J.R., Herbin, J.-P., Vidier, J.-P., 1995. Sequence analytical approach to the Upper Kimmeridgian–Lower Tithonian storm-dominated ramp deposits of the Boulonnais (Northern France) — a landward time-equivalent to offshore marine source rocks. Geol. Rundsch. 84, 255–271.
- Ramanampisoa, L., Bertrand, P., Disnar, J.R., Lallier-Vergès, E., Pradier, B., Tribouillard, N., 1992. High-resolution study of an organic-carbon cycle in the Kimmeridge Clays of Yorkshire (Great Britain) — preliminary results of organic geochemistry and petrography. C. R. Acad. Sci. 314 (II), 1493–1498.
- Rolin, Y., Gaillard, C., Roux, M., 1990. Ecologie des pseudobiohermes des Terres Noires jurassiques liés à paléo-sources sous-marines. Le site oxfordien de Beauvoisin (Drôme, Bassin du Sud-Est, France). Palaeogeogr. Palaeoclimatol. Palaeoecol. 80, 79–105.
- Scotchnam, I.C., 1991. The geochemistry of concretions from the Kimmeridge clay formation of southern and eastern England. Sedimentology 38, 79–106.
- Soetaert, K., Hofmann, A.F., Middelburg, J.J., Meysman, F.J.R., Greenwood, J., 2007. The effect of biogeochemical processes on pH. Mar. Chem. 105, 30–51.
- Taylor, S.P., Sellwood, B.W., 2002. The context of lowstand events in the Kimmeridgian (Late Jurassic) sequence stratigraphic evolution of the Wessex–Weald Basin, Southern England. Sediment. Geol. 151, 89–106.
- Tribouillard, N., Ramdani, A., Trentesaux, A., 2005. Controls on organic accumulation in Late Jurassic shales of Northwestern Europe as inferred from trace-metal geochemistry. In: Harris, N. (Ed.), The Deposition of Organic-Carbon-Rich Sediments: Models, Mechanisms, and Consequences, SEPM Special Publication, vol. 82, pp. 145–164.
- Tribouillard, N.-P., 1988. Géochimie organique et minérale dans les Terres Noires calloviennes et oxfordiennes du bassin dauphinois (France SE): mise en évidence de cycles climatiques. Bull. Soc. Géol. France 8 (5), 141–150.
- Tribouillard, N.-P., Ducreux, J.-L., 1986. Mise en évidence de cycles de 100 000 et 400 000 ans dans les Terres Noires du Callovien–Oxfordien de la région de Buis-les-Baronnies (France S-E). C. R. Acad. Sci. Paris II (20), 1508–1512 t. 303.
- Tribouillard, N., Armynot du Châtelet, E., Gay, A., Barbicot, F., Sansjofre, P., Potdevin, J.-L., 2013. Geochemistry of cold seepage-impacted sediments: Per-ascensum or per-descensum trace metal enrichment? Chem. Geol. 340, 1–12.
- Tribouillard, N., Bialkowski, A., Tyson, R.V., Vergès, E., Deconinck, J.-F., 2001. Organic facies and sea level variation in the Late Kimmeridgian of the Boulonnais area (northernmost France). Mar. Petrol. Geol. 18, 371–389.
- Tribouillard, N., Sansjofre, P., Ader, M., Trentesaux, A., Averbuch, O., Barbicot, F., 2012. Early diagenetic carbonate bed formation at the sediment–water interface triggered by synsedimentary faults. Chem. Geol. 300/301, 1–13.
- Tribouillard, N., Trentesaux, A., Ramdani, A., Baudin, F., Riboullau, A., 2004. Contrôles de l'accumulation de matière organique dans la Kimmeridge clay formation (Jurassique supérieur, Yorkshire, G.B.) et son équivalent latéral du Boulonnais: l'apport des éléments traces métalliques. Bull. Soc. Géol. France 175, 491–506.
- Underhill, J.R., Paterson, S., 1998. Genesis of Tectonic inversion structures: seismic evidence for the development of key structures along the Purbeck-Isle of Wight Monocline. J. Geol. Soc. 155, 975–992.
- Veizer, J., Ala, D., Azmy, K., Bruckschen, P., Buhl, D., Bruhn, F., Carden, G.A.F., Diener, A., Ebnet, S., Godderis, Y., Jasper, T., Korte, C., Pawellek, F., Podlaha, O.G., Strauss, H., 1999. $^{87}\text{Sr}/^{86}\text{Sr}$, $^{77}\text{S}\text{r}/^{86}\text{Sr}$, ^{34}S and ^{18}O evolution of Phanerozoic seawater. Chem. Geol. 161, 59–88.
- Wignall, P.B., 1991. Test of the concepts of sequence stratigraphy in the Kimmeridgian (Late Jurassic) of England and northern France. Mar. Petrol. Geol. 8, 430–441.
- Wignall, P.B., Newton, R., 2001. Black shales on the basin margin: a model based on examples from the Upper Jurassic of the Boulonnais, northern France. Sediment. Geol. 144, 335–356.
- Williams, C.J., Hesselbo, S.P., Jenkyns, H.C., Morgans-Bell, H.S., 2001. Quartz silt in mudrocks as a key to sequence stratigraphy (Kimmeridge Clay Formation, Late Jurassic, Wessex Basin, UK). Terra Nova 13, 449–455.
- Wilmsen, M., Fürsich, F.T., Seyed-Emami, K., Majidifard, M., Zamani-Pedram, M., 2010. Facies analysis of a large-scale Jurassic shelf-lagoon: the Kamar-e-Mehdi Formation of east-central Iran. Facies 56, 59–87.

2.3 - Compléments

Des informations, pourtant précieuses, ne peuvent pas toutes trouver place dans les articles scientifiques. Nous complétons donc le papier publié par *Marine and Petroleum Geology* avec des éléments d'informations et d'interprétations complétant l'article central de ce chapitre.

2-3-1 Observation des lames minces :

2-3-1-1 Contenu de quartz

Les faciès observés contiennent tous du quartz. La présence de ce minéral atteste d'un niveau d'énergie du milieu de dépôt. La présence de quartz est a priori antinomique de celle d'une matrice fine, signe, quant à elle, d'un milieu de dépôt calme. Cette contradiction disparaît si l'on considère que la matrice carbonatée à grain fin résulte d'une activité bactérienne relativement indépendante du niveau d'énergie du milieu de dépôt.

Dans nos trois sites étudiés (A : Audresselles, N : Noirda, GN : Gris-Nez), les cristaux de quartz peuvent atteindre dans les deux sites Noirda et Audresselles une taille allant jusqu'à 350 micromètres (en moyenne entre 150-200 microns (Figure 1 (N1, A1)). Au contraire, les cristaux de quartz sont plus petits dans le site du Cap Gris-Nez (généralement de moins de 100 microns ; Figure 1 (GN1), à l'exception de certains cristaux pouvant atteindre jusqu'à 200 microns.



Figure 1 : les cristaux de quartz dans les lames minces des trois sites étudiés : (A : Audresselles, N : Noirda, GN : Gris-Nez).

2-3-1-2 Les coquilles:

L'analyse pétrographique des dômes isolés montre qu'ils sont quasi-exclusivement composés de *Nanogyra nana* noyées dans une matrice de calcite microsparitique (Figure 2). Les dimensions des coquilles sont supérieures à 1 mm et parfois jusqu'à 4-5 mm. En fait, on ne peut pas dire clairement que

les dimensions sur un site de ce qui était le plus grand que les autres, où elles sont à peu près semblables dans tous les sites.

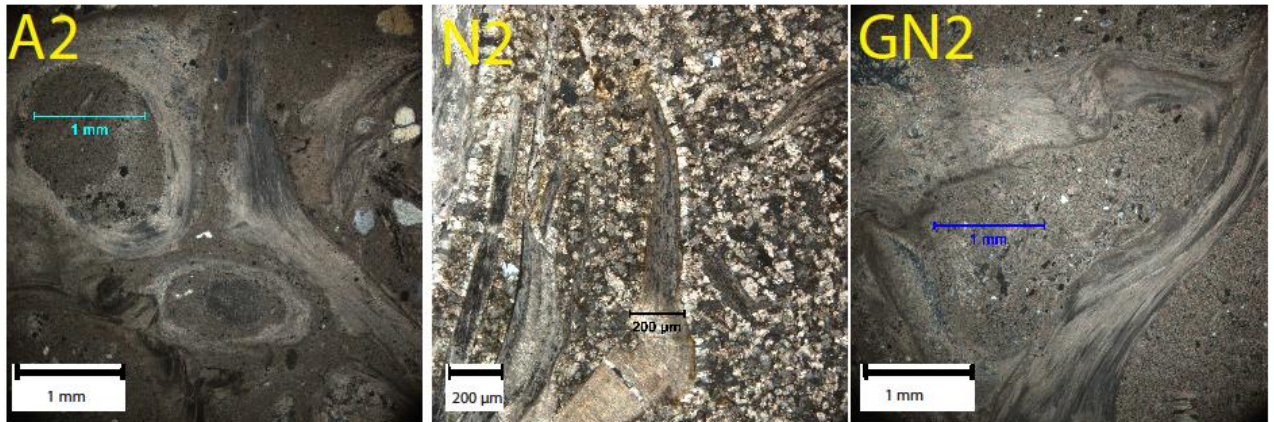


Figure 2 : exemples de coquilles dans les lames minces des trois sites étudiés : (A2 : Audresselles, N2: Noirda, GN2 : Gris-Nez).

2-3-1-3 Le remplissage :

Ce remplissage des coquilles est généralement en sparite. Il se présente surtout en cristaux calcaires ayant des dimensions moyennes d'environ 100 micromètres, et peut atteindre jusqu'à 300 micromètres dans certains cas (Figure 3), à l'exception de quelques rares cas où le remplissage est semblable à la matrice (Figure 2- GN2, A2).

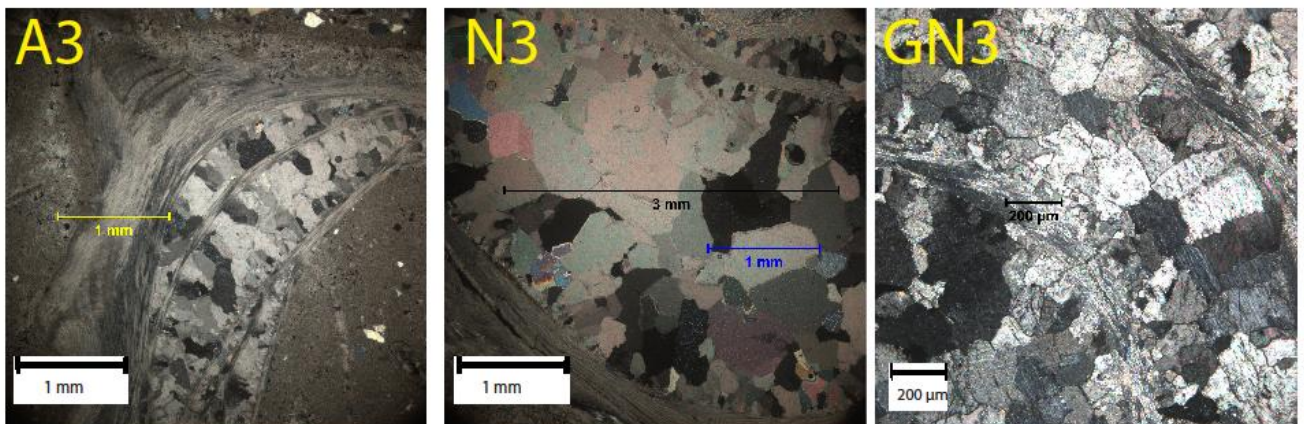


Figure 3 : le remplissage de coquilles dans les lames minces des trois sites étudiés : (A3 : Audresselles, N3: Noirda, GN3 : Gris-Nez).

2-3-2 Cathodoluminecence :

Nous constatons que les coquilles sont entourées par une auréole de cristaux plus grands que ceux de la matrice (Figure 4), qui est souvent composée de deux générations (B) ou trois générations (C), et

plus rarement une seule génération (A). Les cristaux de ces auréoles sont de taille souvent supérieure à 100 micromètres (sparite).

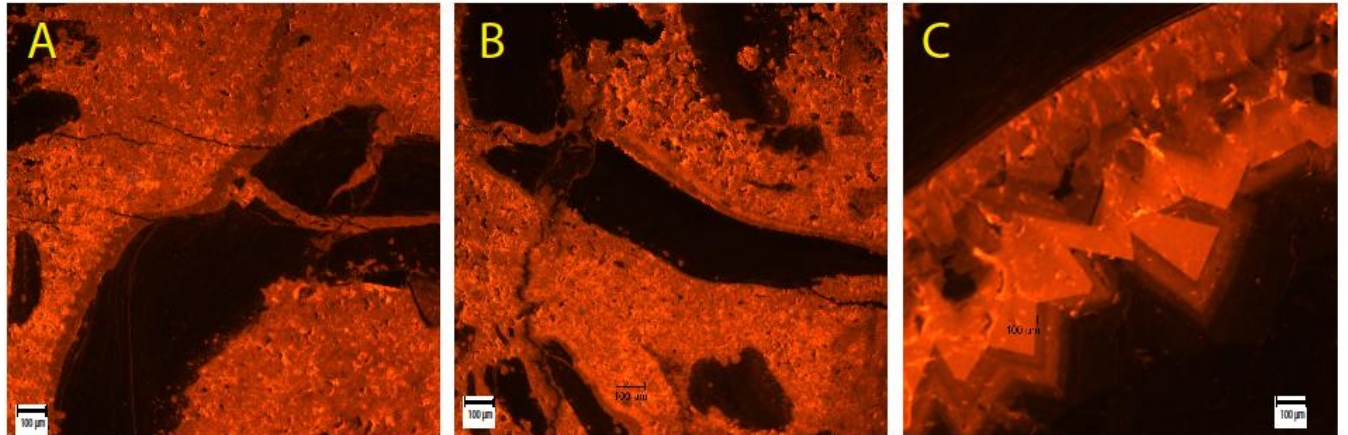


Figure 4 : montre le cadre de la coquille (la génération), A= 1 génération, B= 2 génération, C= 3 génération

2-3-3 Observation macroscopique :

Nous avons fait des sections dans trois dômes de différentes tailles échantillonnées des trois sites différentes (Figure 5), où nous avons trouvé que, malgré la grande différence dans la taille des dômes, qui va de 20 cm à plus de 1 mètre, le contenu de coquilles et de la matrice, et la répartition des coquilles ne sont pas sensiblement différents, ni selon le site d'échantillonnage, ni selon la taille du dôme.

Enfin, on peut observer une relative variété dans la forme des dômes, même si la forme habituelle est plutôt globuleus

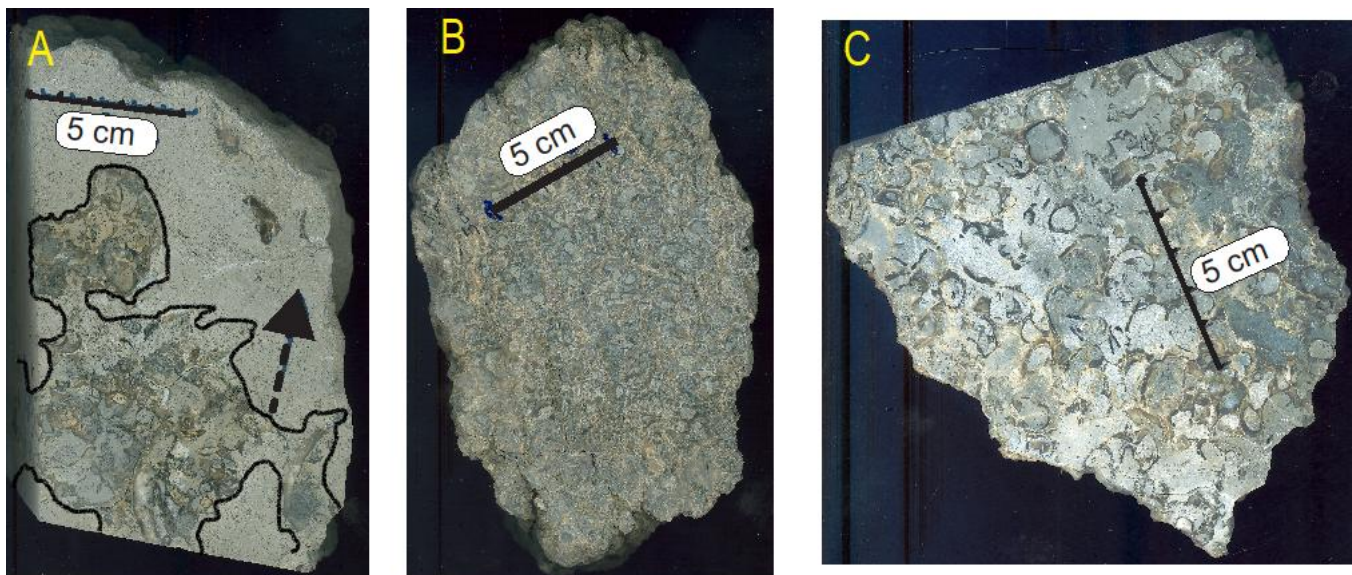


Figure 5 : trois sections montrent des trois sites différents de dômes à huîtres :

A : 300m au nord de la parking du Noirda, B ,C : Cap gris-Nez plage de la Sirène.

2-3-4 Interprétations :

- Nous n'avons trouvé aucune lame mince dépourvue de grain de quartz, ce qui indique que ce type de construction s'est formé dans des conditions de milieu ayant une énergie relativement élevée.
- Selon les observations microscopiques et macroscopique, on peut dire qu'il n'y a pas de relation entre la forme de dômes à huîtres et de leurs tailles et le site des échantillons d'une part, et de leurs contenu interne des coquilles et mode de distribution ou la matrice ou même quartz d'autre part.
- La différence dans la taille des dômes « de quelques centimètres à plus d'un mètre » peut être due à l'intensité et la durée de la poussée des fluides riches en matière organique dissoute ou à leur richesse en éléments nutritifs.
- Les différentes façons de distribuer les assemblages de coquilles régulièrement ou irrégulièrement dans la matrice peuvent être due d'une part à l'intensité du processus de précipitation de la matrice, d'autre part de la régularité ou irrégularité la sortie de fluides hydrocarbonés.

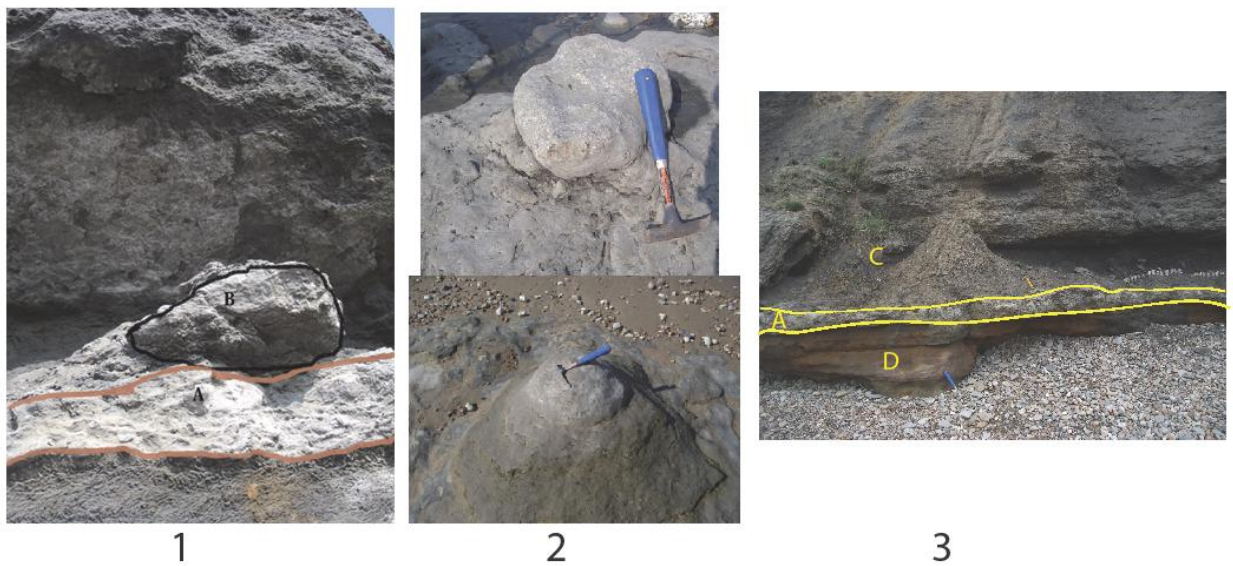


Figure 6 : Certaines des formes différentes de la présence de dômes et des types de positionnement en place.

(1): A le banc carbonaté au dessous du récif à huîtres (300m au nord du parking Noirda), B : un dôme à huîtres sur la falaise du Cran du Noirda. (2) : un dôme sur place (plage du Noirda). (3) : la limite entre les Argiles de Châtillon (C), et le grès de Châtillon (D), représenté d'un banc carbonaté au dessous du récif à huîtres (A).

2-3-5 les tableaux des données isotopiques des (réefs à huître), « Ambleteuse, Noirda et Cap Gris-Nez».

échantillons	Type	$d^{13}\text{C}$	$d^{18}\text{O}$	%CaCO ₃	$d^{18}\text{O}$ matrice	$d^{18}\text{O}$ coquilles	$d^{18}\text{O}$ remplissages de coquille
am01	Matrice de carbonate	-8,87	-0,98	85,79	-0,98		
am02	Matrice de carbonate	-8,47	-1,07	87,16	-1,07		
am03	Matrice de carbonate	-6,20	-1,48	82,67	-1,48		
am04	Matrice de carbonate	-7,73	-1,09	89,07	-1,09		
am05	Matrice de carbonate	0,03	-1,43	75,02	-1,43		
noirda01	Matrice de carbonate	-3,86	-2,17	45,44	-2,17		
cgn03	Matrice de carbonate	-3,63	-3,44	76,15	-3,44		
noirda02	coquille	0,26	-2,50	43,52		-2,50	
am06	coquille	-1,93	-1,70	69,88		-1,70	
cgn01	coquille	-0,40	-2,83	88,10		-2,83	
am07	Remplissage de coquilles	-2,03	-1,43	73,39			-1,43
noirda03	Remplissage de coquilles	0,55	-5,19	86,02			-5,19
cgn02	Remplissage de coquilles	-0,80	-4,75	92,53			-4,75

Chapitre 3 – Formations de carbonates au cours de la diagénèse précoce dans un environnement de rampe terrigène soumise à des failles synsédimentaires : le rôle des fluides

3.1 – Présentation

L'essentiel en quelques lignes

Dans les dépôts du Jurassique supérieur du Boulonnais, on observe surtout des accumulations terrigènes, mais certains objets carbonatés sont visibles à différents niveaux particuliers. Sont-ils mis en place par dépôts sédimentaires ou ont-ils une origine diagénétique ? La question se pose car ces objets carbonatés tranchent fortement par rapport aux sédiments terrigènes (grès et marnes) qui les contiennent. Pour apporter des éléments de réponse, nous avons étudié cinq types d'objets carbonatés, qui représentent tous les objets carbonatés qui apparaissent dans le Jurassique supérieur dans notre zone d'étude, à l'exception des lumachelles mises en place à l'occasion de tempêtes.

- 01- Les récifs à huîtres isolés : visibles à la base de la Formation des Argiles de Châtillon, et à la base des Calcaires du Moulin Wibert.
- 02- Les bancs calcaires de la Formation Calcaires du Moulin Wibert : concernant de 12 bancs calcaires noduleux au Cap Gris-Nez et 10 bancs calcaires noduleux au cap de la Crèche.
- 03- Le banc qui représente la limite entre les Grès de Châtillon et les Argiles de Châtillon.
- 04- Le banc calcaire noduleux de la partie somitale des Argiles de Châtillon.
- 05- Les bancs calcaires de la formation des Bancs jumeaux : il s'agit de trois bancs au Gris-Nez et au nord de Wimereux, tandis que deux bancs seulement affleurent au sud de Wimereux.

Pour la présente étude, nous avons caractérisé les bancs de carbonate appliquant des méthodes pétrographiques et géochimiques, y compris la composition isotopique de C, O et S.

Les résultats :

- Les faciès : dans les cinq types d'objets étudiés, on a trouvé des proportions variables des coquilles et fragments de coquilles, avec des particules de matière organique ligneuses.
- La matrice est toujours en carbonate : une calcite faite de microsparite homogène.
- Du point de vue «couleur», la cathodoluminescence montre que toutes les sections minces de calcite observées sont homogènes (une seule phase de croissance).
- Les valeurs de $\delta^{34}\text{S}$ pour les pyrites extraites des Bancs Jumeaux est entre -29.4‰ et -36.4‰, et pour les récifs ou patchs à huîtres, entre -35.1‰ et -42.9‰, alors que la valeur pour le Jurassique supérieur est estimée à +15‰. On en déduit que la sulfato-réduction bactérienne a exploité un réservoir de sulfate relativement infini, c'est à dire, à l'interface ou très près de l'interface eau-sédiments.

- Dans les récifs à huîtres, la composition isotopique ^{13}C de la matrice de carbonate (entre -8,9 à -3,6 ‰) est significativement différente de celle des coquilles ou du remplissage des coquilles (-

2,0 à + 0,6 ‰). Les échantillons de la matrice sont nettement appauvris en $\delta^{13}\text{C}$, tandis que les échantillons de coquilles ou leur remplissage sont plus proches des valeurs habituellement trouvées dans les carbonates de l'eau de mer du Jurassique supérieur, allant de 0 à 2 ‰.

- La distribution verticale des valeurs de $\delta^{13}\text{C}$ dans les Bancs Jumeaux au Nord de Wimereux montre que les bancs carbonatés diffèrent sensiblement de leurs marnes encaissantes en ceci qu'ils présentent des valeurs de $\delta^{13}\text{C}$ relativement appauvries. L'écart entre les valeurs de $\delta^{13}\text{C}$ dans calcaire et de marnes indique des origines respectives contrastées : les valeurs de $\delta^{13}\text{C}$ de marnes sont conformes à celles attendus pour les carbonates d'eau de mer du Jurassique supérieur. Cela signifie que la majeure partie de la fraction carbonatée des marnes ne présente pas d'influence détectable de ciment diagénétique qui affecterait significativement la signature isotopique. En net contraste, toutes les valeurs de $\delta^{13}\text{C}$ des trois bancs carbonatés sont légèrement, mais significativement plus faible que les valeurs de carbonate marins. Il indique qu'une fraction significative de la teneur en carbonate des bancs est d'origine diagénétique.

Pour la Formation Calcaires du Moulin Wibert, la distribution de taille de grain des intercalations de marnes montre une distribution à deux modes pour la plupart des échantillons. Le principal mode correspond à la classe des silts et le mode accessoire à celle des sables fins à moyens. L'observation de sections de roche montre la présence de relativement gros grains de quartz dans les bancs. Les échantillons de la partie médiane de la formation montrent l'absence de grains de quartz (ni dans les lames minces des bancs carbonatées, ni dans les granulométrie dans les marnes intercalées). On observe ainsi que la distribution stratigraphique de la taille des grains de la fraction clastiques dans les Calcaires du Moulin Wibert n'est pas impactée par les faciès (marnes vs. calcaires). Les bancs de carbonate ne correspondent pas aux conditions de dépôt plus calmes que celles enregistrées par les marnes, malgré leur matrice calcaire finement grenue, évocatrice de conditions de dépôt calmes).

Tous les types d'objets carbonatés de la zone d'étude ont été analysés pour leurs concentrations en éléments majeurs et certains éléments traces ; l'attention a été accordée à ceux qui sont habituellement associés aux carbonates (Ca, Mg, Sr et Mn). Le manganèse ne montre aucune caractéristique particulière, ni de son abondance, ni de son abondance relative dans les bancs ou les récifs à huîtres ou les marnes intercalées. En revanche, les caractéristiques de Mg et Sr sont assez singulières. Comparé leurs abondance par rapport aux marnes encaissantes, tous les objets carbonatés étudiés tombent dans une zone séparée, soit pour le rapport Sr/Ca, soit pour Mg/Ca. Cela indique que tous les objets carbonatés présentent un fort appauvrissement en Sr et Mg.

27 analyses d'isotopes stables de C et O ont été effectuées sur les bancs carbonatés des Bancs Jumeaux affleurant au Cap Gris-Nez. On a trouvé que les gammes de valeurs sont assez similaires à celles des bancs carbonatés des Bancs Jumeaux de Wimereux. Les résultats sont donc cohérents aux extrémités de la zone d'étude.

Pour le banc sommital séparant le Grès de Châtillon de les Argiles de Châtillon, on voit que deux échantillons parmi les six analysés sont les appauvri en $\delta^{13}\text{C}$ comme les échantillons de la matrice les plus appauvris de récifs à huîtres, tandis que les autres concordent bien avec les coquilles et le remplissage sparistique des coquilles.

Pour les bancs noduleux de la partie supérieure de la Formation des Argiles de Châtillon, les valeurs sont assez semblables à celles observées pour les bancs carbonatés de la Formation des Bancs Jumeaux, et en même temps, similaire aux valeurs $\delta^{13}\text{C}$ des coquilles et leur remplissage étudiés dans les récifs à huîtres.

Les valeurs de $\delta^{13}\text{C}$ et de $\delta^{18}\text{O}$ pour les bancs carbonatés des Calcaires du Moulin Wibert sont assez similaires à celles des bancs carbonatés des Bancs Jumeaux ; en revanche, on voit ici le même contraste entre les bancs et les marnes intercalées que celui observé pour les Bancs Jumeaux.

Nous proposons un modèle pour la formation au cours de la diagénèse précoce des bancs carbonatés ou des récifs à huîtres, impliquant une circulation de fluides, elle-même induite par des mouvements tectoniques extensifs, actifs pendant le Jurassique supérieur dans le Boulonnais. Ces fluides riches en carbone organique dissous auraient migré vers la colonne d'eau, soit à des endroits individualisés, soit par imprégnation diffuse dans les sédiments, ou à proximité de l'interface eau-sédiment. Cette dernière situation a provoqué la précipitation de bancs de calcaire à grain fin sur une étendue relativement grande (échelle pluri-km). Plus tard au cours de l'histoire du bassin, ces bancs de formation précoce peuvent avoir agi comme écrans localisés ou barrières de perméabilité qui entravent encore la circulation du fluide, ce qui mérite d'être examinée dans un système pétrolier.

Enfin, les bancs ainsi induits sont assez semblables à des bancs calcaires à grain fin habituels résultant d'un dépôt sédimentaire. Avec l'absence de données isotopiques C, S, O, l'origine diagénétique des bancs ne peut pas être suspectée, sauf sur la base de la présence de microsparite (facile à confondre avec de la micrite, en l'occurrence) et l'apparition inhabituelle des grains de quartz flottant dans une matrice à grain fin.

Dans les descriptions des sites de suintements froids, les objets carbonatés diagénétiques qui y sont associés ne sont généralement pas décrits comme des bancs continus, et les résultats de ce travail suggèrent que l'origine des bancs de calcaire à grain fin intercalés à travers une série dominée par des apports clastiques doive être réévaluée en tenant compte des effets diagénétiques possibles, éventuellement induits par les circulations des fluides contenant du carbone organique.

3.2 – Early diagenetic formation of carbonates in a clastic-dominated ramp environment impacted by synsedimentary faulting-induced fluid seepage - Evidence from the Late Jurassic Boulonnais

Basin (N France)

E. Hatem¹, N. Tribouillard^{1*}, O. Averbuch¹, P. Sansjofre², T. Adatte³, F. Guillot¹, M. Ader⁴, D. Vidier⁵

¹ Université de Lille & CNRS UMR 8187 Laboratoire d'Océanologie et Géosciences, bâtiment SN5, 59655 Villeneuve d'Ascq cedex, France

² Université de Bretagne Occidentale et CNRS UMR 6538, Institut Universitaire Européen de la Mer, Laboratoire Domaines Océaniques, 29280 Plouzane, France

³ Université de Lausanne, Institut des Sciences de la Terre, bâtiment Géopolis, CH-1015 Lausanne Suisse

⁴ Institut de Physique du Globe de Paris & CNRS UMR 7154, Equipe de géochimie des isotopes stables, Sorbonne Paris Cité, Univ Paris Diderot, 75005 Paris, France

⁵ PN82, rue du Calvaire, 62137 Coulogne, France

* corresponding author Nicolas.Tribouillard@univ-lille1.fr

Key words: Authigenic carbonates; cold seeps; synsedimentary faulting; Late Jurassic; Boulonnais; stable isotopes; geochemistry

Abstract. - The Late Jurassic deposits of the Boulonnais area (N-France) represents the proximal lateral-equivalent of the Kimmeridge Clay Formation; they accumulated on a clastic-dominated ramp subject to synsedimentary faulting in relation with the northward propagation of the Atlantic rifting. Within the terrigenous accumulations, some carbonate objects are visible at various conspicuous levels: oyster patch reefs and fine-grained carbonate beds, either continuous, or more or less nodular. Preliminary studies demonstrated that the carbonate beds of the Bancs Jumeaux Formation

as well as the carbonate matrix of the oyster patch reefs are of diagenetic origin. In this paper, we extend the study to many other limestone beds of the Boulonnais with mud- or wackestone texture, examining facies and microfacies through various techniques as well as geochemical data (O, C and S stable isotopes, major and trace elements). We conclude that all examined carbonate bodies are of early diagenetic origin and that they precipitated at, or close to, the sea bed, from seawater mixing with ascending fluids containing isotopically light carbon of organic origin. Fluid circulation was probably induced by the extensional block-faulting segmentation of the northern margin of the Boulonnais Basin in Late Jurassic times. Fluid seepages were either channelized along fault planes or more diffuse, as illustrated by the model we propose.

1. Introduction

Fluid flow is a first-order feature of the evolution of basins, in that fluids may interact with sediments during earliest stages of deposition, conditioning both early and late diagenesis. It is all the more important for basins undergoing extensional tectonics where synsedimentary faults drive fluid circulations contemporaneously with sediment accumulation. These aspects are of cornerstone importance for petroleum systems. The geological formations of the Late Jurassic times (Kimmeridgian-Tithonian) crop out along the Boulonnais cliffs (Strait of Dover, Northern France; Fig. 1). They represent a proximal, lateral equivalent of the Kimmeridge Clay Formation (famous major petroleum source rock) and they accumulated in a clastic-dominated ramp environment subject to dominantly aerobic conditions with some episodes of dissolved oxygen restriction (suboxic conditions) favorable to organic-rich deposition (Proust et al., 1995; Deconinck et al., 1996; Wignall and Newton, 2001; Williams et al., 2001; Tribouillard et al., 2001, 2004, 2005; Al-Ramadan et al., 2005). The Boulonnais is a good, small-dimension model of petroleum systems, comprising: 1) fine-grained, clay-dominated, organic-rich formations (termed "Argiles" in the local terminology, e.g., the Argiles de Châtillon Formation) acting as source rocks; and 2) coarser-grained, sandstone-dominated formations (termed "Grès", e.g., the Grès de Châtillon Formation), acting as possible reservoir rocks.

On a structural point of view, the study area forms the eastern tip of the Weald-Boulonnais basin crossing through the English Channel along a general E-W direction. During the entire course of the Late Jurassic, this basin, alike the Wessex and the North Sea basins, was affected by synsedimentary faulting in relation with the northward propagation of rifting along the Atlantic Ocean (Butler and Pullan, 1990; Underhill and Paterson, 1998; Beeley and Norton, 1998; Newell, 2000; Taylor and Sellwood, 2002; Hansen et al, 2002; Mansy et al., 2003; Minguely et al, 2010). This block-faulting geometry had a significant imprint on the subsidence pattern in the basin and, hence, on the depositional contexts. Recent studies suggested that synsedimentary tectonics induced fluid circulations through this incipient petroleum system, favoring diagenetic precipitation of carbonate beds or isolated bodies (namely, oyster patch reefs), through bacterial activity stimulation (Tribouillard et al., 2012; Hatem et al., 2014). In the present paper, the study is extended to many other carbonate beds throughout the Late Jurassic of the Boulonnais, in order to encompass the various types of limestone beds that are encountered there. The occurrence of such carbonate beds is puzzling and sometimes difficult to interpret on the grounds of the sole sediment accumulation arguments: how can the presence of fine-grained limestone beds be explained when they are intercalated within such a clastic-dominated succession? The objective of the study is to determine whether some or all of the carbonate beds (or bodies) might be of (early) diagenetical origin (except for coquina oyster beds that are storm-induced lumachelles; Fursich and Oschmann, 1986). To that end, facies and microfacies examination, together with geochemical analysis (elemental content and stable isotope composition) have been conducted. Then emphasizing the tectonic framework, we propose a model linking the formation of the carbonate objects to synsedimentary, fault-induced, fluid circulations.

2. Stratigraphy and general description

The Late Jurassic deposits of the Boulonnais form a ca. 100 m-thick sequence, particularly well exposed along the cliffs extending from the Cap Gris-Nez to the north to Boulogne-sur-mer to

the south (Fig. 1). The exposure of different Late Jurassic levels along the cliffs is mainly controlled by a set of WNW-ESE normal faults that parallel the general orientation of the Weald-Boulonnais Basin across the Eastern Channel (see the section of Fig. 1C). The Tertiary inversion of this primary fault network along localized corridors (mainly the northern border fault zone of the basin, i.e., Cap Gris-Nez area) induced the uplift and general folding of the basin allowing the exhumation and the present exposure of the Late Jurassic syn-rift series (Mansy et al, 2003; Minguely et al, 2010). The latter were deposited in a general proximal clastic-dominated environment and are mainly composed of alternating sandstones and black mudstone units as a primary result of the relative sea level oscillations (Figs. 1B & 2). Table 1 provides a quick description of the geological formations quoted in the paper; more detail can be found in Geyssant et al. (1993), Deconinck et al. (1996), Proust et al. (1995), Mansy et al. (2007).

Recent studies focused upon on the oyster patch reefs (Hatem et al., 2014) and peculiar limestone beds of the Bancs Jumeaux Fm. (Tribouillard et al., 2012) included in this clastic-dominated sequence. Since these papers contain an extensive description of these objects, only an overview will be given here, complemented by additional observation of the Bancs Jumeaux Formation (Fm.), cropping out at Cap Gris-Nez (or Gris-Nez Cape). For the present study, we extended our examinations to other carbonate beds visible along the Jurassic cliffs of the Boulonnais, which are described in detail for the first time here.

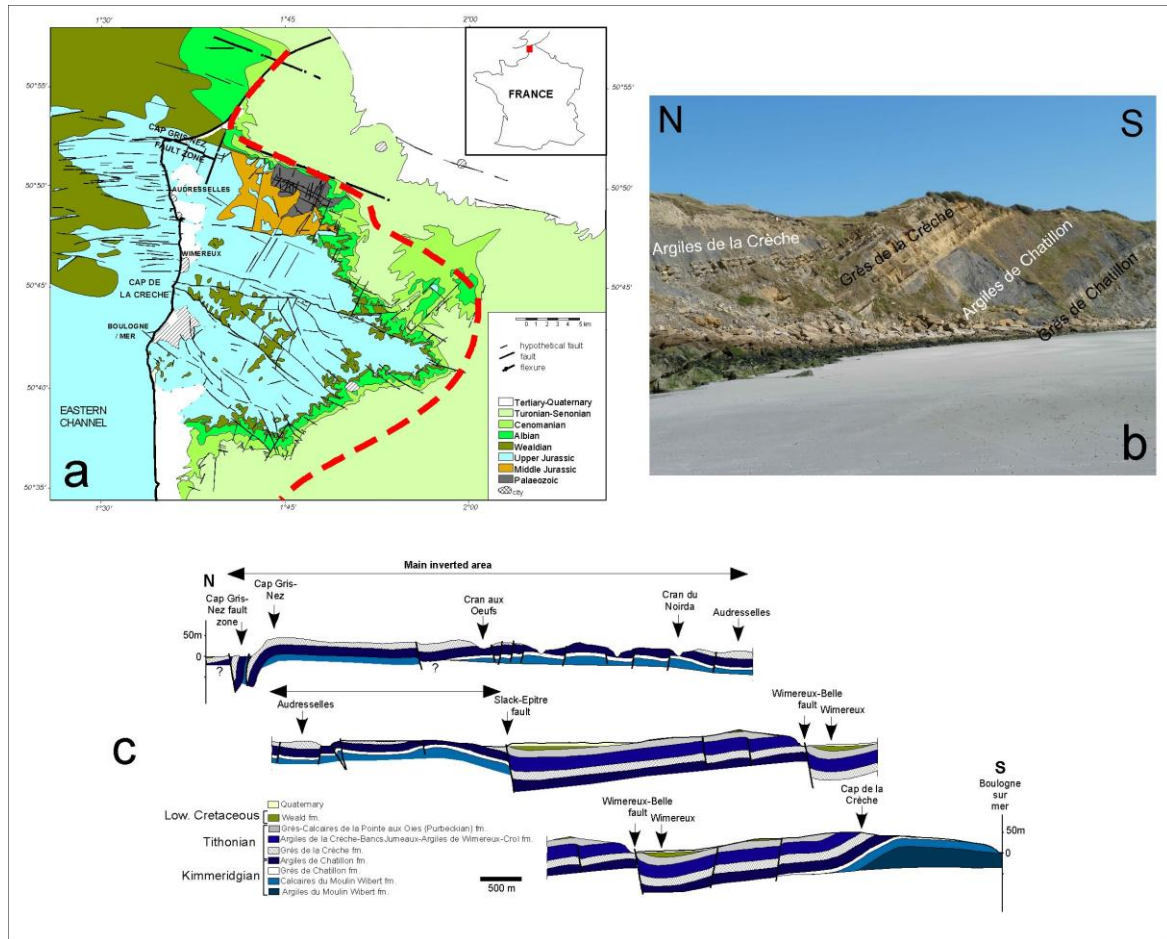


Fig. 1. a: Geological map depicting the general structural and stratigraphical framework of the Boulonnais Basin. The study area corresponds to outcrops of Upper Jurassic rocks exposed along the cliffs from the Cap Gris-Nez fault zone to the city of Boulogne-sur-mer. The red dashed line correspond to the extent of the Jurassic deposits below the Mid-Upper Cretaceous post-rift transgressive sequence. b: Photograph of the Cap de la Crèche section (reference section) illustrating the general clastic-dominated sequence (alternation of sandstone and marlstone formations) characteristic for the Late Jurassic series of the Boulonnais Basin. c: North-South cross section along the cliffs from the Cap Gris-Nez to Boulogne-sur-mer. Note the segmentation of the basin by WNE-ESE trending normal faults coeval with the basin development and the inversion of this fault pattern along localized corridors (mostly along the northern border fault zone, Cap Gris-Nez area).

Figure2

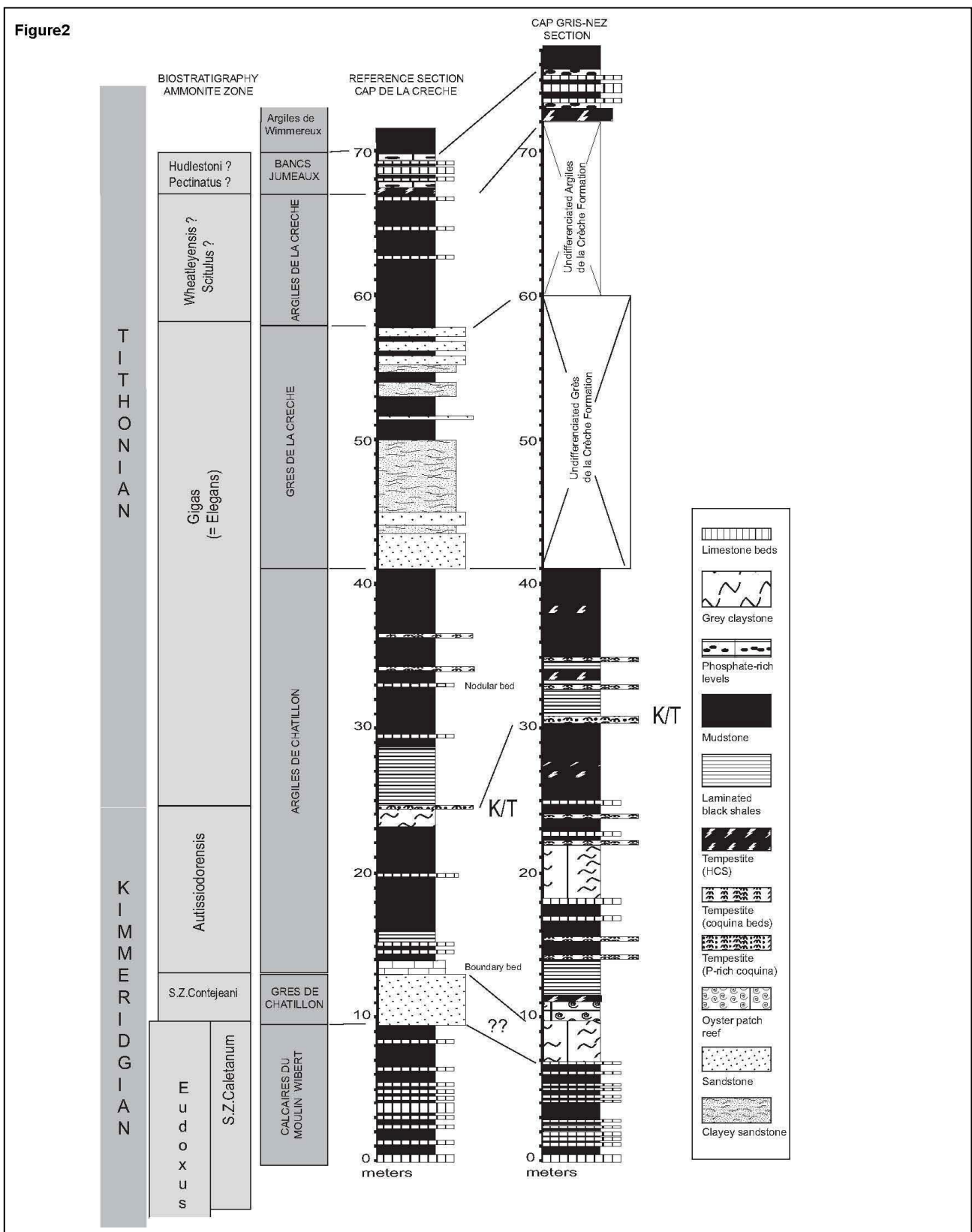


Fig. 2 - Stratigraphic sections of the Late Jurassic sequences under study with correlation of the Cap Gris-Nez sequence with the reference section of the Cap de la Crèche (biostratigraphic zonations based on Geyssant et al, 1993).

2.1. Patch reefs - Recently, occasional, ball- or dome-shaped assemblages of *Nanogyra nana* were observed and interpreted to be small-dimensioned, in-situ formed, oyster patch reefs (Fig. 3). The patch reefs of the Boulonnais are specific in that they are rather small, isolated (except at Cap Gris-Nez where they form kinds of pseudo-bioherms), and essentially made up with *Nanogyra nana* shells (+ up to 10% serpulids and occasional gastropods and forams; Vallone, 2014) and a carbonate fine-grained matrix (Fig. 3). The reef domes may reach a size of 1 meter at Cap Gris-Nez, but the usual size range of these objects is 10 – 50 cm. Such oyster reefs have been observed at various places in the Late Jurassic sequence along the Boulonnais cliffs between the Audresselles village and Cap Gris-Nez, but exclusively along two conspicuous stratigraphic horizons.

1) The most common stratigraphic position for the patch reefs is the base of the Argiles de Châtillon Fm., a sequence dominated by siltstone/mudstone, largely intercalated between two low-stand sandy/sandstone units, namely, the Grès de Châtillon Fm. at the base, and the Grès de la Crèche Fm. at the top (Figs. 1 & 2 and Table 1), both poorly and irregularly cemented. Both these clastic-dominated formations mainly consist of brown- to orange-colored sandstones and sandy marlstones with common cross-bedding and wave ripples, and intense bioturbation (especially U-shaped and *Rhizocorallium* burrows). Isolated 10 – 50 cm large patch reefs are observed in situ at the base of the first marlstone level of the Argiles de Châtillon, i.e., upon an about 30-35 cm-thick sandy limestone bed, highly bioturbated, forming the top of the sandstone beds of the Grès de Châtillon Fm. (Fig. 4; the bed will be referred to as the Boundary bed in what follows). At Cap Gris-Nez site (the “La Sirène” Beach), the Grès de Châtillon Fm. are not visible but the base of the Argiles de Châtillon Fm. is again marked by the presence of patch reefs: a spectacular 1-2 m thick ball-shaped oyster reef sequence (Fig. 3) can be observed extensively along the shore of Cap Gris-Nez (Mansy et al., 2007).

2) The second stratigraphic location of the observed patch reefs is the base of the Calcaires du Moulin Wibert Fm. (Table 1), another mudstone dominated sequence containing, however, numerous carbonate beds (12 or 14 according to the section observed).

Macrofacies. The patch reefs have a rounded shape and are made of countless shells of *Nanogyra nana* that show no visible preferential orientation. The two valves of the fossils are sometimes found in connection (which is never the case in the coquina beds). The shells are embedded in a sparse limestone matrix (Fig. 3).

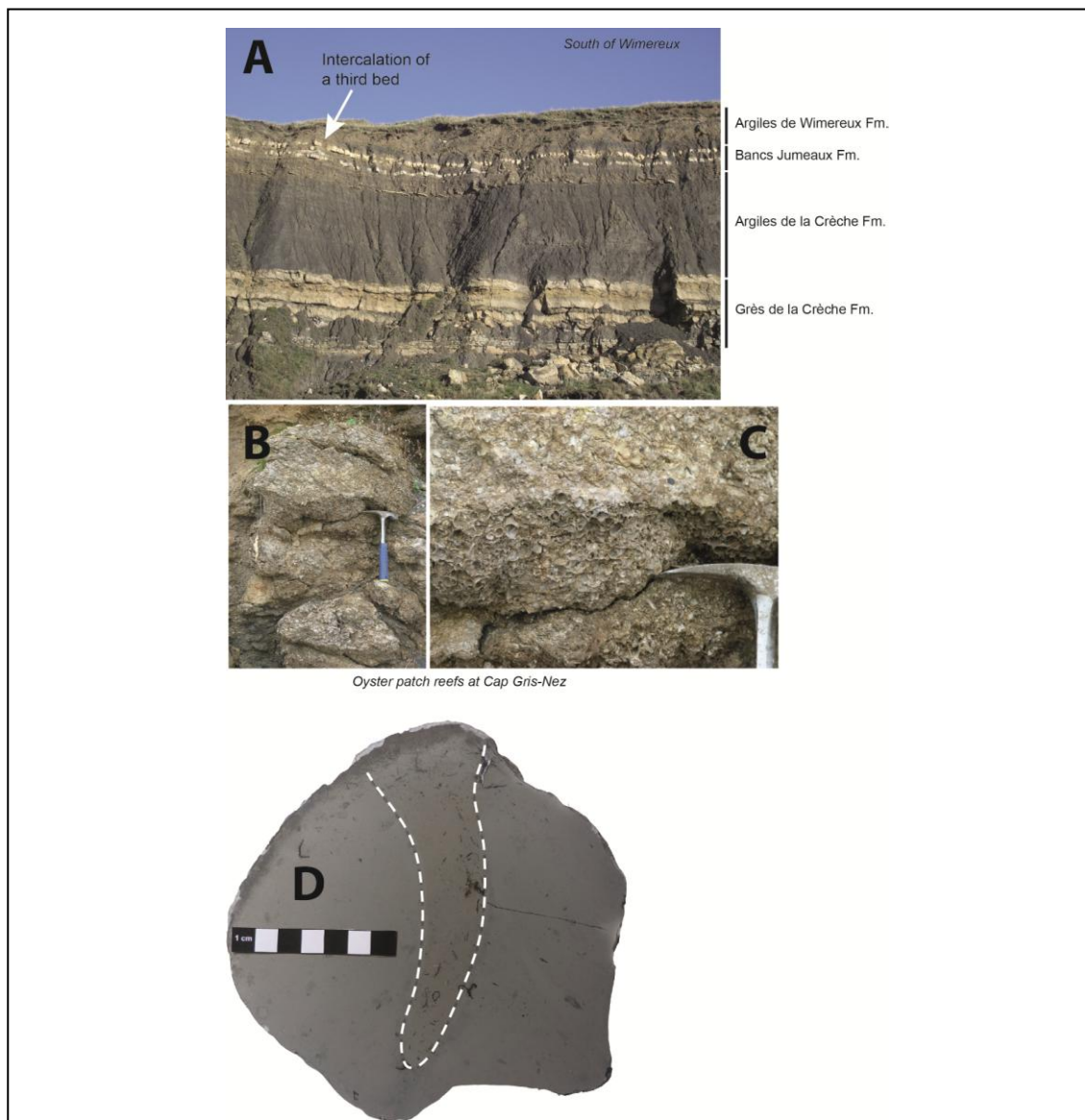


Fig. 3. A: Photograph of the Tithonian part of the sequence under study (see Fig. 2) at Cap de la Crèche focusing on the carbonate beds of the Bancs Jumeaux formation. Note the appearance of a localized third carbonate bed in-between the two classical well-expressed beds. B and C: views of the oyster patch reefs observed in-situ at Cap Gris-Nez (La Sirène Beach) at the base of the Argiles de Châtillon Fm. D: view of a nodule of the medium bed of the Bancs Jumeaux Fm. with a clear-cut burrow (rock sample from the section north of Wimereux; see Fig. 1 for location).

Microfacies. The various patch reefs studied show the same microfacies features. The carbonate matrix is a homogeneous calcite microsparite where plentiful shells and shell fragments, common organic-matter particles and rare pyrite framboids are observed (Fig. 5). A fringe of sparitic crystals is frequently but not systematically observed around most shells. No coccolith fossils (or molds) have been observed (in contrast to what is observed for some of the carbonate beds of the Kimmeridge Clay Fm.). Cathodoluminescence imaging shows that in all observed thin sections, the calcitic, microsparitic matrix is homogeneous. No luminescence contrast was observed, indicating that the chemical composition of the carbonate matrix is homogeneous. Shells occasionally show white, sparitic fillings. Regarding the mineralogy of carbonate, XRD data show that the microsparite of the matrix is exclusively made of calcite. Neither aragonite nor dolomite was identified.

2.2. The two/three beds of the Bancs Jumeaux Formation - The Bancs Jumeaux Fm. is located at the boundary between the Argiles de la Crèche Fm. and the Argiles de Wimereux Fm. (Figs. 2 & 3; Proust et al., 1995; Williams et al., 2001). It is bound at its base and top by two sharp erosional surfaces characterized by accumulations of phosphatic fossils and nodules, and quartz pebbles. These lower and upper P-rich levels are named P1 and P2, respectively. The Bancs Jumeaux Fm. has been interpreted as a transgressive systems tract (Proust et al., 1995; Deconinck et al., 1996; Williams et al., 2001).

North of Wimereux, three limestone beds can be observed for about 300 m alongshore. Three beds are also observed at Cap Gris-Nez. The formation is about 2 m thick (distance separating P1 and P2). The marls are bioturbated, they contain frequent, scattered, wood fragments and bivalve shells (sometimes phosphatic). The lower and upper limestone beds are about 15 cm thick with clear-cut and horizontal boundaries. The intermediate limestone bed is thicker (15-25 cm) and more irregular: although laterally continuous, it has a somewhat nodular structure. The basal two centimeters of the beds are impregnated with the detrital material that makes up the "background" marl sediments, but the tops of the beds are "clean", that is, show no such impregnation. The beds

show a light grey color and some shell fragments are scattered throughout. Bioturbation is evidenced by some mottling and, in one sample of the intermediate bed, the presence occasional large burrows (Fig.3D).

South to Wimereux, the Bancs Jumeaux Fm. comprises only two beds. They are a bit thicker than at Wimereux-North (20 cm) and present sharp boundaries (Fig. 3). They can be observed in the cliff along a distance of about 800 m. The field conditions do not allow us to observe the contact zone between both outcrops (the one with two and the one with three beds), because of the presence of the city of Wimereux, which is bordered by two normal faults (Fig. 1C). However in the south part of the Cap de la Crèche, the outline of a third carbonate bed can be observed locally. See Fig. 3 showing a lenticular, some meter-long carbonate body that may correspond to the medium bed of the succession when the formation yields three beds.

Microfacies. All 3 + 2 limestone beds show the same microfacies features. The limestone is a homogeneous calcite microsparite where common shell fragments and rare pyrite framboids are interspersed (Fig. 5). A fringe of microsparitic crystals is observed around most pyrite framboids. It is emphasized that no coccolith fossils (or molds) could be observed. Bioturbation is visible through the presence of mottling. When examining the burrow illustrated in Fig. 3D, we observe that the microsparite crystals are slightly larger in the burrow infilling than in the hosting microsparite, and that the infilling contains abundant shell fragments and common quartz and glauconite grains. Cathodoluminescence imaging shows that all thin sections are homogeneous. No luminescence contrast was observed, indicating that the chemical composition of the carbonate is homogeneous. This is still true when burrowed portions are compared to unbioturbated "matrix" portions.

These descriptions (macro- and micro-facies), made with outcrops close to Wimereux, also apply to the three carbonate beds of the Bancs Jumeaux Fm. cropping out at the Cap Gris-Nez.

2.3. The Boundary bed - The bed marking the boundary between the Grès de Châtillon Fm. and the overlying Argiles de Châtillon is thick of about 35 cm. It is made of quartz-rich limestone and is

thoroughly bioturbated. Some dm-scale carbonate nodules are included. It overlies the top sandstone levels of the Grès de Châtillon Fm. that are occasionally affected by synsedimentary fault movements (extensional) of small amplitude (Fig. 4). This bed supports oyster patch reefs, as evoked above. It can be observed from the South cliff of the Gris-Nez Cape to Ambleteuse, and again south of the Cap de la Crèche (between Wimereux and Boulogne-sur-mer).

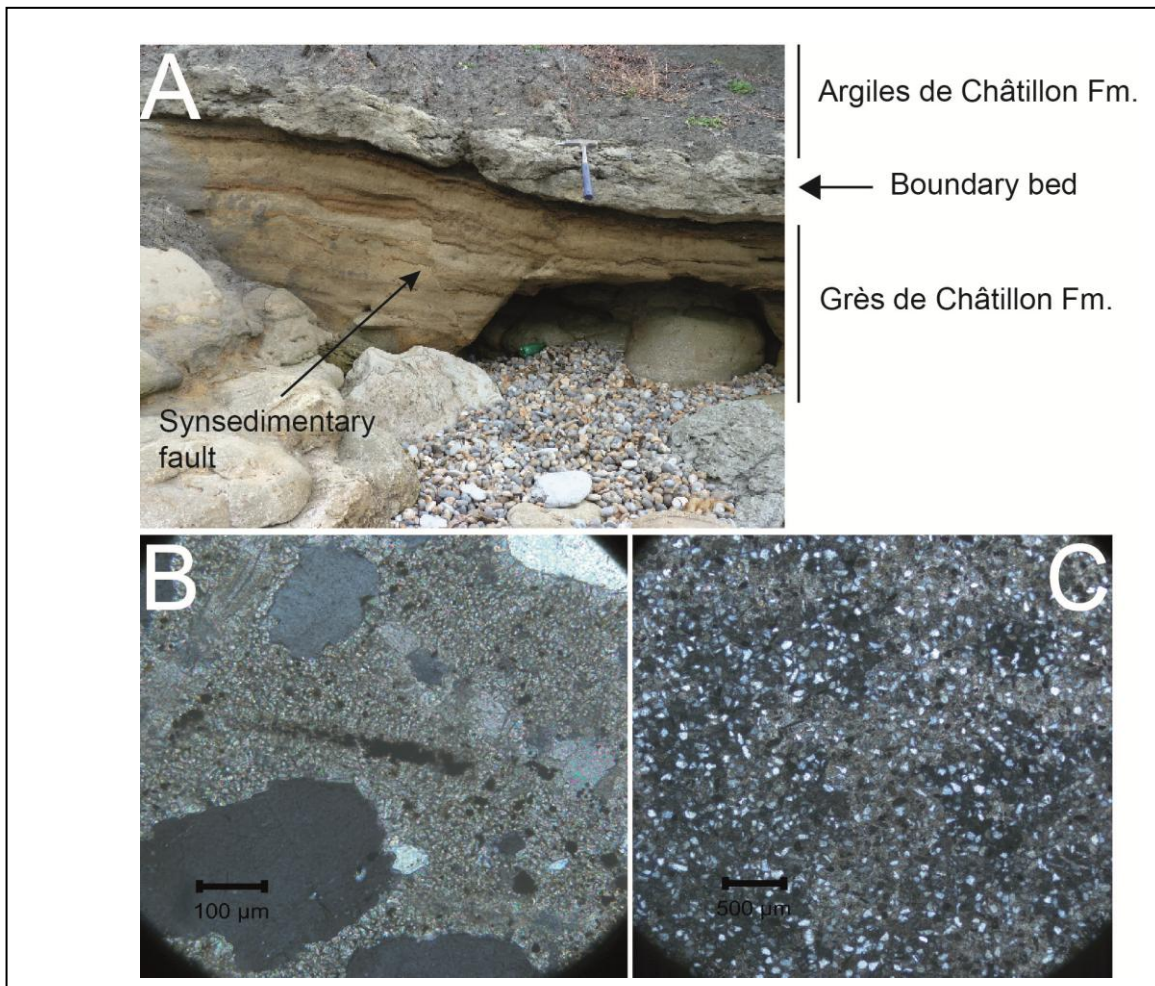


Fig. 4 . A: the Boundary bed with the typical aspect of the transition zone between the Grès de Châtillon and Argiles de Châtillon formations (here affected by synsedimentary faulting). B and C: microfacies of the Boundary bed showing the presence of abundant quartz grains (B and C) and bioturbation (mottling, C).

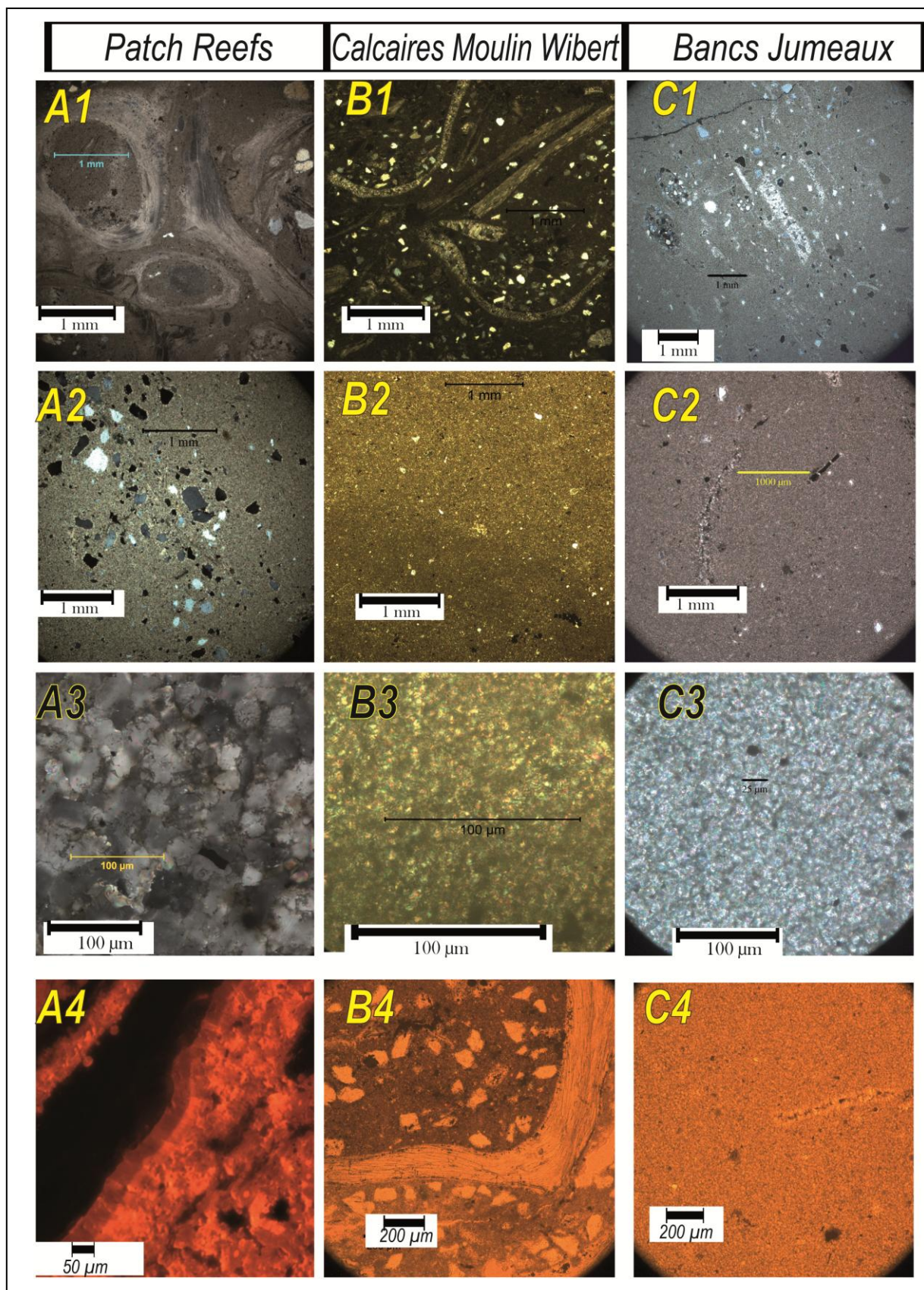


Fig. 5. Thin-section observations of various carbonate objects: oyster patch reefs (A), limestone beds of the *Calcaires du Moulin Wibert* (B) and *Bancs Jumeaux* (C) formations, using normal (A1 to C3) or cathodoluminescence (A4 to C4) illumination.

2.4. The limestone beds of the Calcaires du Moulin Wibert Formation - At Cap Gris-Nez, twelve beds may be identified with variable thickness (20-50 cm) and variable marly interbed distance (Fig. 6A). The aspect of the bed surface, where it is visible, is nodular (Fig. 6B). At the Cap de la Crèche, the beds are less easy to identify (some of them are amalgamated). In the north of the Boulonnais, at Cap Gris-Nez, these beds are lying upon the topmost sandstone bed of the Grès de Conninchun Fm., affected by extensional synsedimentary faults and supporting small oyster patch reefs (Hatem et al., their figure 6).

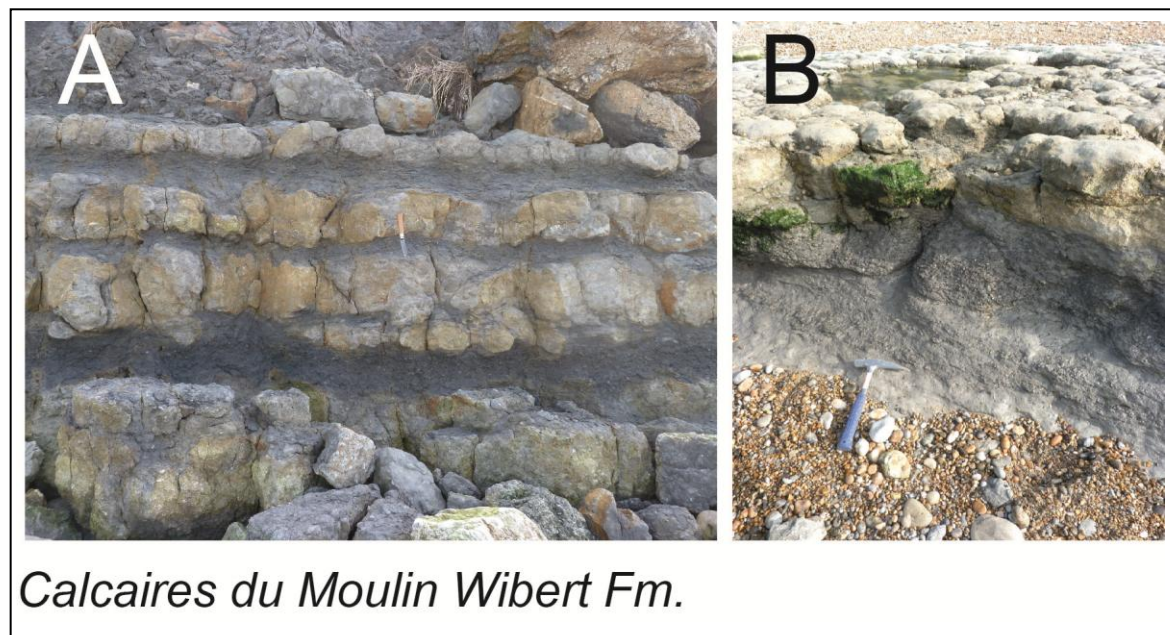


Fig. 6. A and B: typical aspect of the carbonate beds of the Calcaires du Moulin Wibert Fm. (Cap Gris-Nez).

B: nodular aspect of the beds where the bed surface is visible.

2.5. The nodular bed of the uppermost part of the Argiles de Châtillon Fm. - Close to the top of the formation, intercalated among several shell-rich, tempestite beds, a fine-grained carbonate bed is observed along about 2 km (at least) from Audresselles northward (Figs. 7A & 7B). This bed is made of coalescent elongated nodules and is about 20 cm thick. Right in the middle of the bed, a few cm-thick tempestite, made of small, often broken, oyster shells (i.e., a lumachelle) is frequently observed but is not present in each nodule. The base of the lumachelle is an irregular erosional sole and the top is flat (Figs. 7B & 7C).

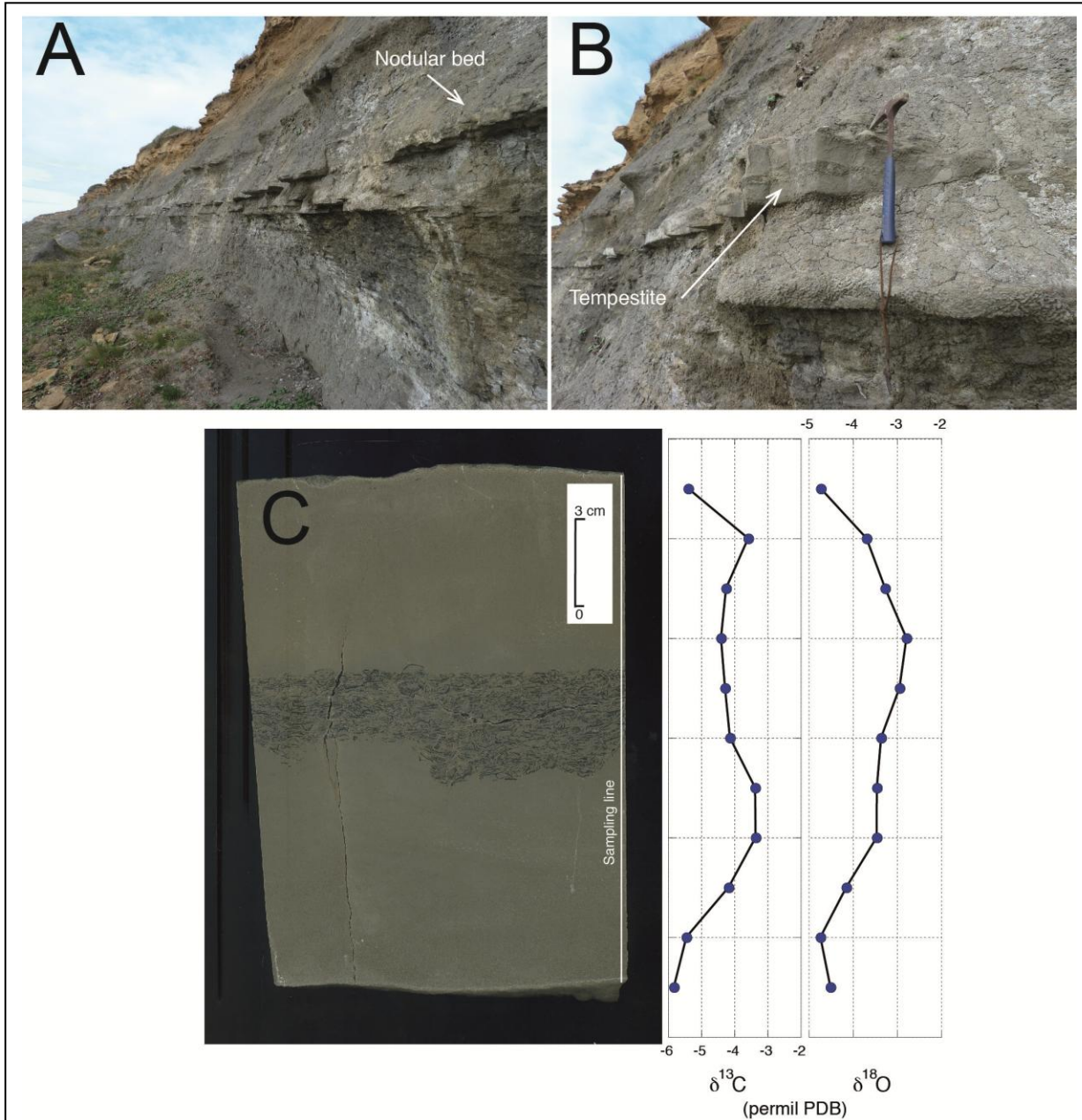


Fig. 7. The nodular bed of the upper part of the Argiles de Châtillon Fm. A: picture showing the large extent of the bed (km-scale) at Audresselles. B: close-up view of the bed with the shell accumulation in the centre. C: polished cross section of the bed with the vertical distribution of the C and O stable isotope data.

Lastly, in addition to all these carbonate beds or reefs for which a diagenetic origin is suspected, numerous lumachelles are present, reaching occasionally 40 cm in thickness. They are more numerous in the north than in the south of the Boulonnais cliffs, in good agreement with the proximal-distal gradient observed from the North to the South of the Boulonnais (Mansy et al.,

2007). The storm-induced lumachelles (Fürsich and Oschmann, 1986) will not be examined here but some analytical measurements were performed for comparison purpose (see below).

3. Interpretations for the carbonate beds of the Bancs Jumeaux Fm. and the patch reefs

The initial studies of the patch reefs (Hatem et al., 2014) and limestone beds of the Bancs Jumeaux Fm. (Tribouillard et al., 2012) led to the following interpretations, based on facies analysis and stable isotope data (Figs. 8A & 8B). We give some detail here because it will simplify the interpretation of the new results of this study.

The limestone beds of the Bancs Jumeaux Fm. are bioturbated. Bioturbation took place as the beds were still soft, as evidenced by the mottled fabric. However the clear edges of the burrow illustrated in Fig. 3D show that the bed was already firm when the burrower intruded. It indicates that the carbonate mass formed early and began to solidify at shallow depth below the sediment-water interface. In other words, the diagenetic carbonate precipitated during early diagenesis at a shallow depth where it could be easily reached by burrowers. The micro-facies observation suggests that the shell fragments and quartz or glauconite grains were injected by bioturbation from the overlying marls down into a carbonate matrix that seems to have been initially pristine. In addition, the color homogeneity of the various limestone beds observed through cathodoluminescence imaging indicates that each bed was formed in a single phase of carbonate precipitation. This observation reinforces the interpretation of the beds forming rapidly with no evidence for subsequent carbonate growth.

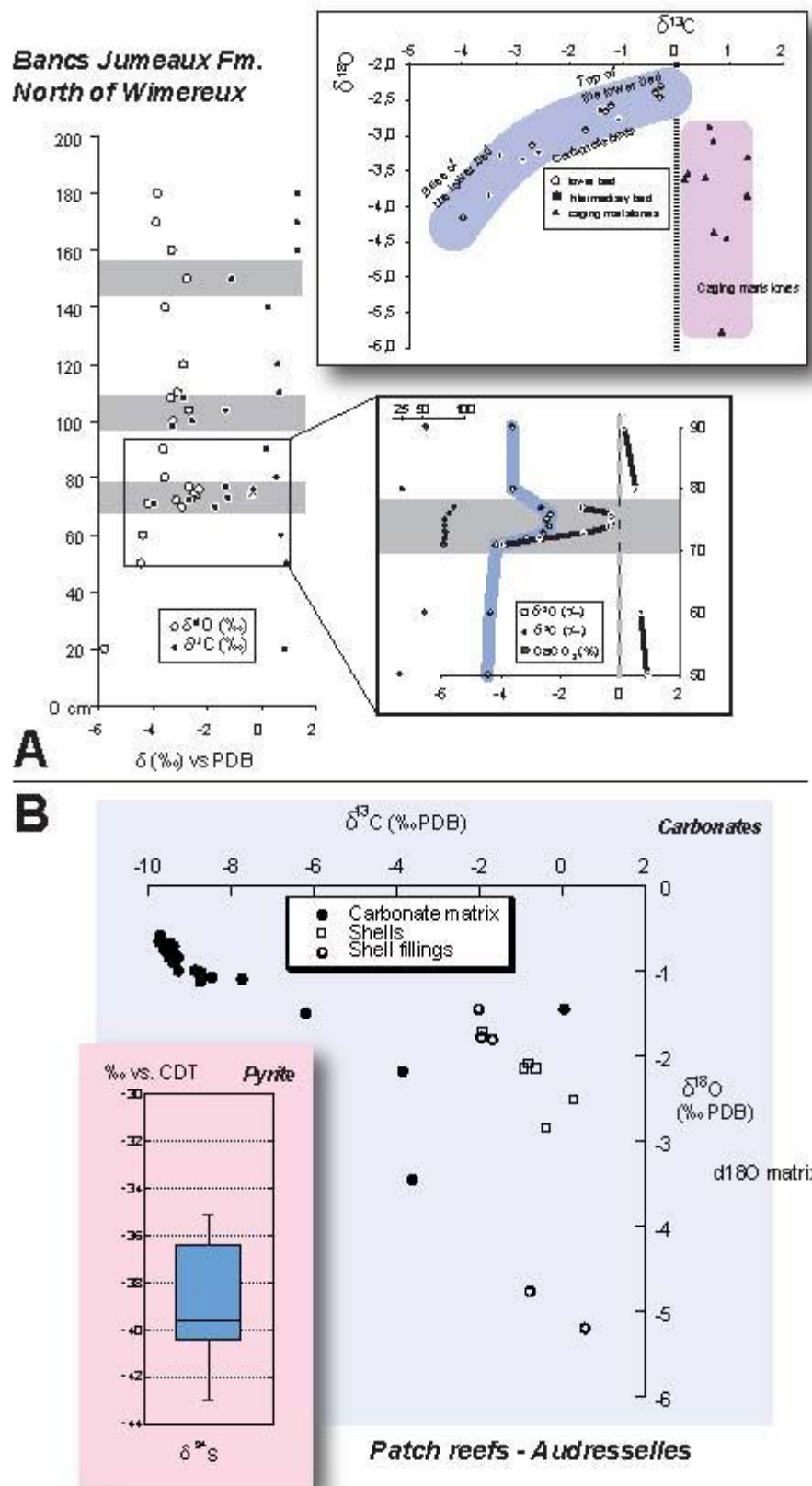


Fig. 8. Recapitulation of the stable isotope dataset initially published in Tribouillard et al. (2012) for the Banks Jumeaux Fm. (A) and Hatem et al. (2014) for the patch reefs (B).

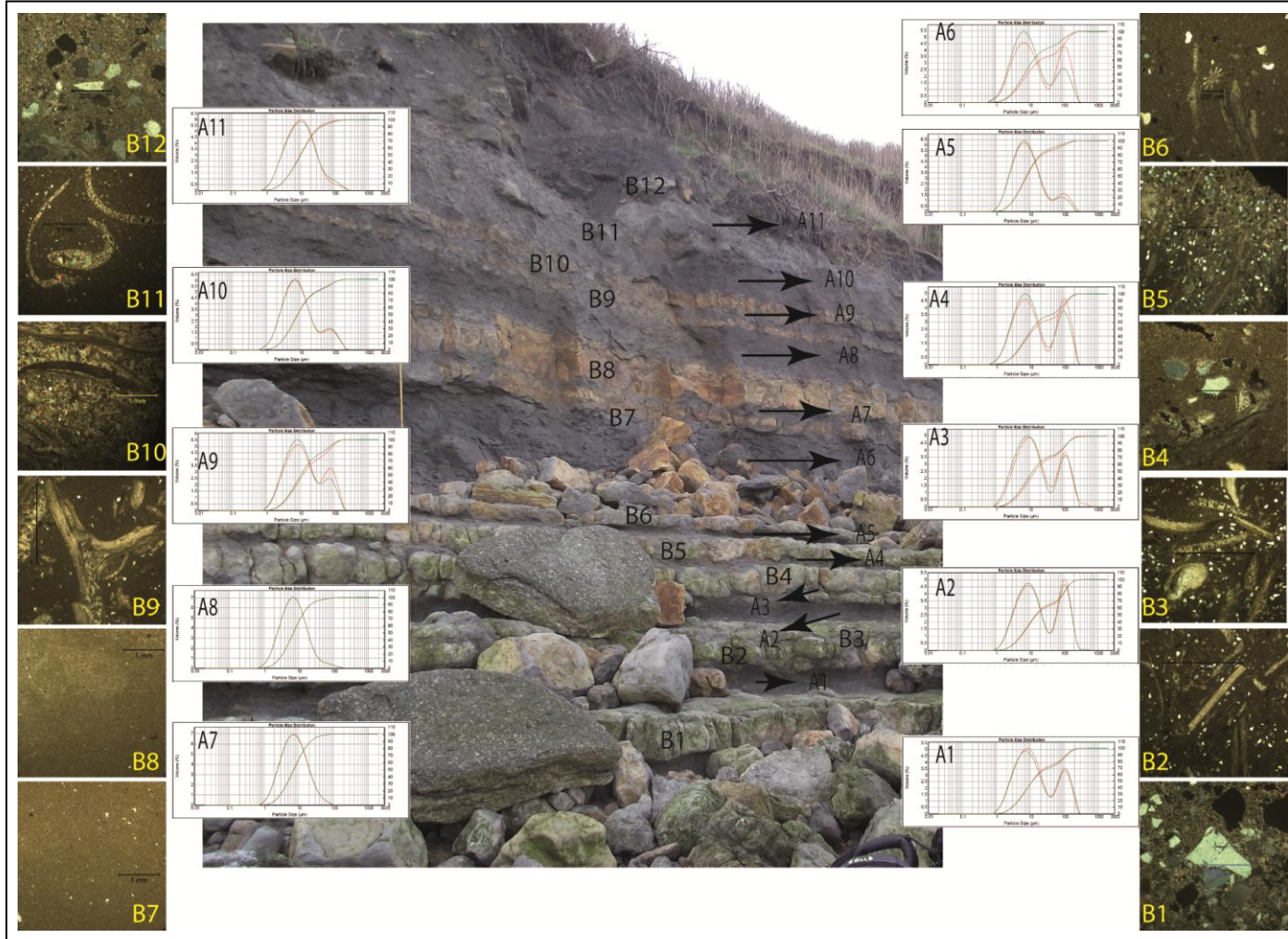


Fig. 9. Mosaic showing the grain-size distribution of the insoluble fraction of the marlstones (series A) and the microfacies of the limestone beds (series B) in the Calcaires du Moulin Wibert Fm. (Cap Gris-Nez).

The $\delta^{34}\text{S}$ values for the pyrites extracted from the Bancs Jumeaux Fm. at Wimereux range between $-29.4\text{\textperthousand}$ and $-36.4\text{\textperthousand}$, while the $\delta^{34}\text{S}$ values for the pyrites extracted from the patch reefs range between $-35.1\text{\textperthousand}$ and $-42.9\text{\textperthousand}$, to be compared to the marine value for the Late Jurassic of about $+15\text{\textperthousand}$ (Prokov et al., 2008). The isotopic values observed here are therefore much depleted relative to seawater values of the Late Jurassic, which indicates a marked fractionation. Pyrite is abundant in the Bancs Jumeaux Fm. (Tribouillard et al., 2008), which indicates that metabolizable organic matter was present (TOC values are ranging between 1 and 2 wt%). Therefore, the marked sulfur isotope fractionation between the seawater values and pyrite (between 45 and 58‰) strongly suggests that bacterial sulfate reduction operated within a comparatively infinite sulfate reservoir,

that is, at or very close to the sediment-water interface. In other words, the process went on during very early diagenesis, with a redox-cline at very shallow depth below the sediment-water interface, and an oxygenated water column above.

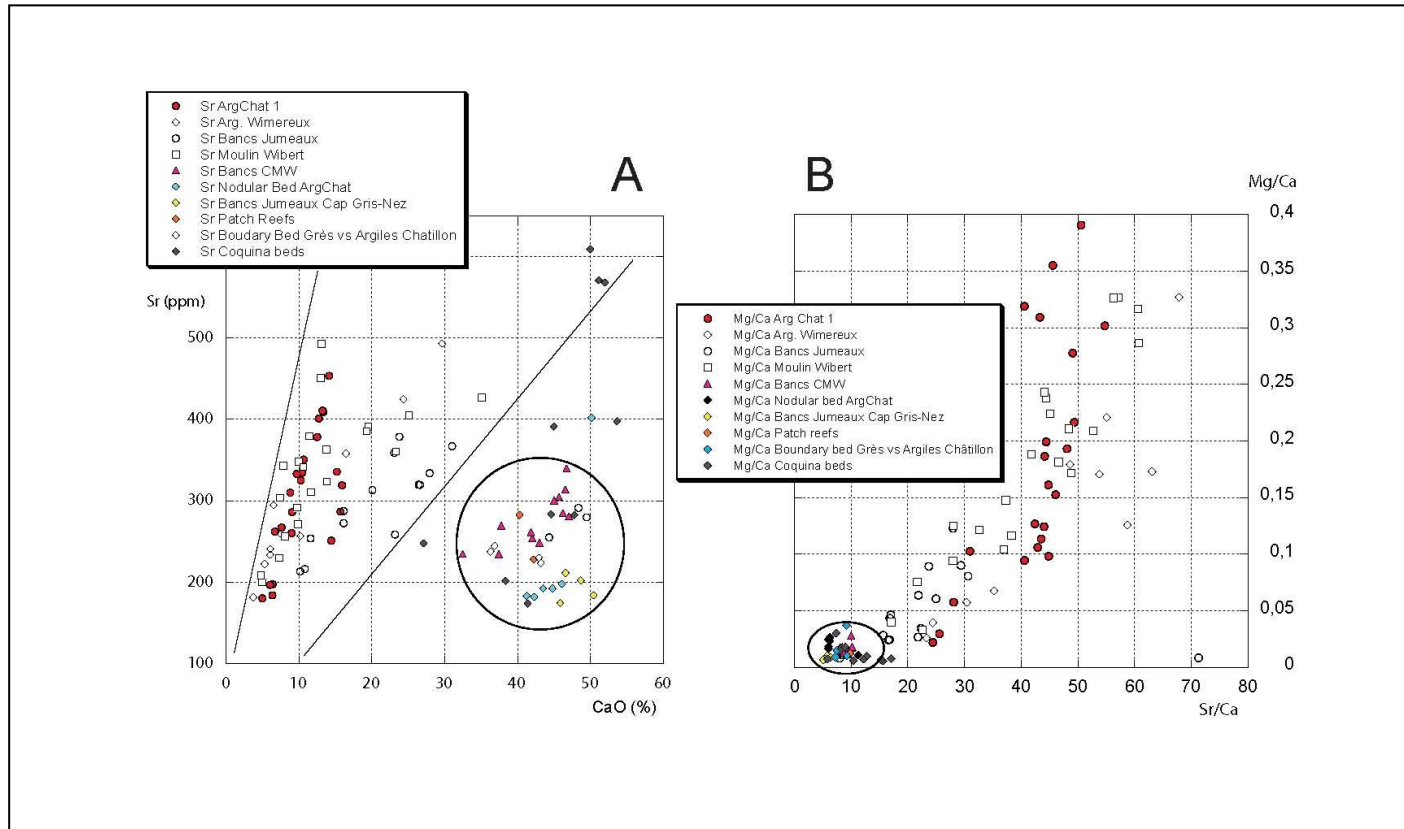


Fig. 10. Crossplots illustrating how the carbonates objects studied here (circles) differ from the caging sediments. A: CaO versus Sr content; B: Sr/Ca versus Mg/Ca.

Within the patch reefs, the $\delta^{13}\text{C}$ isotope composition of the fine-grained carbonate matrix (−8.9 to −3.6‰) is significantly different from the included shells or the occasional sparry zone in-between shell valves (−2.0 to +0.6‰). Thus, the matrix samples are markedly depleted in ^{13}C , while the shell and sparry shell-filling samples are closer to the values usually found in Late Jurassic seawater carbonates, which range from 0 to 2‰ (Veizer et al., 1999; Prokoph et al., 2008). The patch reefs are also diverging isotopically from the enclosing marls $\delta^{13}\text{C}$ values, ranging from −0.2‰ to +2.0‰. The depleted $\delta^{13}\text{C}$ values of the carbonate matrix of the patch reefs indicate the presence of (a proportion of) a carbon source that was ^{13}C -depleted compared to seawater dissolved inorganic

carbon (DIC). It was inferred that the patch-reef matrix was an authigenic carbonate incorporating a fraction of biogenic, $\delta^{13}\text{C}$ -depleted carbon derived from microbial organic-compound remineralization during early diagenesis. Hatem et al. (2014) interpreted the patch reefs as scattered spots where bacterial activity was fuelled by seepage of hydrocarbon-bearing fluids. However, no molecular biomarkers typical of the bacteria-archaea consortia responsible for anaerobic oxidation of methane was found, but specific sulfate-reducing bacteria may have processed the seeping hydrocarbons, as some of them are known to degrade n-alkanes and n-alkenes (see Grossi et al., 2008 and references therein). Further, activity of sulfate-reducing bacteria is evidenced by abundant pyrite framboids and their specific isotopically-depleted sulfur isotopes. As a consequence of these sulfate-reducer activity, a localized alkalinity increase must have led to authigenic carbonate precipitation, with a $\delta^{13}\text{C}$ signature different from the values found for the enclosing marls or bivalve shells (Fig. 8). The fact that the $\delta^{13}\text{C}$ signature of bivalve shells is close to seawater indicates that they were not feeding on the bacterial biomass. Indeed oysters are so far not known to feed on bacteria or live in chemosymbiosis. They most probably simply used the authigenic carbonate as a firm ground.

The vertical distribution of $\delta^{13}\text{C}$ values in the Bancs Jumeaux Fm. at Wimereux shows that carbonate beds differ significantly from their caging marlstones in that they show relatively depleted $\delta^{13}\text{C}$ values. The discrepancy between limestone beds and marlstones indicates contrasting origins: $\delta^{13}\text{C}$ values of marlstones are consistent with those expected for Late Jurassic seawater carbonates (ranging from 0 to 2‰; Fig. 8). It means that the bulk of the marl carbonate fraction presents no detectable influence of diagenetic cement that would impact significantly the isotopic signature. In clear contrast, all the $\delta^{13}\text{C}$ values of the three limestone beds are slightly yet significantly lower than the marine carbonate values. It indicates that a significant fraction of the limestone beds carbonate content is of diagenetic origin, which lowers their $\delta^{13}\text{C}$ signature. The beds do not show $\delta^{18}\text{O}$ values strikingly different from those of the marls but they all appear to be less depleted in ^{18}O , or in other words they are closer to marine carbonate values, indicating very early diagenesis.

Both patch reefs and carbonate beds of the Bancs Jumeaux Fm. show $\delta^{13}\text{C}$ values that are significantly (although not strongly) depleted, suggesting that the carbonate of the patch reef matrix and the limestone beds resulted from two mixing sources: 1) a light DIC source such as produced by remineralization of organic compounds (e.g., hydrocarbon and/or sedimentary organic matter oxidation) and, 2) a seawater DIC source. Consequently, it is inferred that all limestone beds were impacted by diagenesis (remineralization of organic compounds) during deposition (influence of seawater on the isotopic signature of C and O). Thus the formation of the carbonate objects (reefs and beds) occurred during what we may call synsedimentary early diagenesis, in response to local alkalinity rises; most probably induced by the activity of sulfate reducers (e.g., De Craen, 1999; Burdige, 2006; Sotaert et al., 2007, and references therein).

This conclusion (sulfate reaction operating at the sediment-water interface or in its closest vicinity) is corroborated by the isotopic transect carried out through the basal bed of the Bancs Jumeaux at Wimereux-North. From base to top of the carbonate bed, the $\delta^{13}\text{C}$ values are less and less ^{13}C -depleted and thus closer and closer to caging-marls and seawater carbonate values. This observation alone also strongly suggests that the conditions leading to carbonate supersaturation and CaCO_3 precipitation were met at the boundary between the sulfate reducing zone and the water column, namely at or close to the sediment water interface. The interpretation was that the carbonate precipitation started at the sediment-water interface with the incorporation of light C isotopes released by organic-compound degradation and then the bed grew upward, incorporating less and less organic-derived C, hence more and more seawater-derived C. This scenario accounts for the fact that the base of the bed, where the carbonate began to precipitate, is impregnated with the terrigenous material and the carbonate becomes purer and purer upward. The upper part of the bed is almost devoid of terrigenous material because growth must have been quick and the sedimentation rate was probably low.

4 – Analytical methods

For the present study, we characterized the carbonate beds applying petrographical and geochemical methods, including the C, O and S isotopic composition of carbonate and pyrite, respectively. Thin sections of rocks were observed using a cathodoluminescence-equipped microscope (Olympus BX41 with a Citl 8200 MK4 cold-cathode cathodoluminescence device operating at 20 kV) and a scanning electron microscope (FEI Quanta 200 Environmental) equipped with a backscattered electron device and an energy dispersive spectroscopy-probe (X-Flash 3001 Brucker + Quantax 400 software). The carbonate content was determined with a Bernard-type calcimeter (acid digestion followed by CO₂ volume determination; accuracy < 5%). The grainsize of the HCl-insoluble fraction of the marls and limestone beds was determined using a Malvern Mastersizer Hydro 2000-G apparatus following the protocol described in Trentesaux et al. (2001). The decarbonated fraction of the sediment was sieved at 2 mm prior to grain-size analysis.

For stable isotope analysis (C and O), the samples were grounded in an agate mortar and sieved so as to ensure a grain size lower than 140 µm. Part of the samples were analyzed in the Institut de Physique du Globe de Paris. CO₂ was extracted by calcite dissolution with 100% H₃PO₄ (McCrea, 1950) at 25°C for 12 h in helium flushed Labco Exetainer® vials. Stable carbon and oxygen isotopic compositions of the evolved CO₂ were measured using a gas chromatograph coupled to an isotope ratio mass spectrometer (GC-IRMS; Analytical Precision 2003, today entitled GV 2003, provided by GV Instruments), with helium as carrier gas. Three internal standards were used to calibrate the $\delta^{13}\text{C}_{\text{sample}/\text{ref}}$ data provided by the GC-IRMS relative to the V-PDB scale. These standards have been calibrated relative to V-PDB using two international standards, NBS19 and IAEACO1 (IAEA catalogue). Results are given in the usual δ -notation relative to the international Standards PDB for the $\delta^{13}\text{C}$ and for the $\delta^{18}\text{O}$. The external reproducibility for $\delta^{13}\text{C}$ and $\delta^{18}\text{O}$ measurements is of 0.1‰ and 0.2‰, respectively (1σ). Each sample was measured twice and the average of two analyses is reported in the figures. Part of the sample were studied at the Pôle Spectrométrie Océan (PSO) in

Brest, using the same in-house and international standards, but using a Gas Bench 2 connected to Delta V Plus Thermo Fisher.

To determine the stable sulfur isotope composition $\delta^{34}\text{S}$) of pyrite, bulk rock samples were decarbonated through HCl digestion to concentrate pyrite. The decarbonated samples were oxidized with O_2 at 1050°C to produce SO_2 that was analyzed using a VG Sira mass spectrometer. The results were expressed in δ conventional notation, relative to the standard V-CDT (Vienna Canon Diablo Troilite). The standard used is a Ag_2S MERCK with $\delta^{34}\text{S} = +3\text{\textperthousand}$ vs. V-CDT. Each sample was measured in duplicate and the average values are reported. The analytical precision of measurements is $\pm 0.3\text{\textperthousand}$; the reproducibility is of $\pm 1\text{\textperthousand}$.

The mineralogical nature of the carbonate was determined following usual X-ray diffraction (XRD) procedures on micro-pulverized samples. To that end, a Bruker D4 Endeavour apparatus was used together with the Macdiff software (Bout-Roumazeilles et al., 1999).

Major and trace element concentrations were determined by X-ray fluorescence spectrometry (XRFS) using a PANalytical PW2400 spectrometer at the University of Lausanne. Major elements were determined on fused lithium tetraborate glass disc. For this purpose, samples were first heated to 1050°C in an oven in order to calculate the loss of ignition (LOI). Then, 1.2000 ± 0.0002 g of ignited sample was mixed with 6.0000 ± 0.0002 g of lithium tetraborate ($\text{Li}_2\text{B}_4\text{O}_7$) and placed in a Bead machine Perlx'3 at 1250°C to obtain the fused tablet. The obtained concentrations are given in weight percentages (wt.%). Trace element analyses were performed on pressed tablets after mixing 15% of the powdered samples with Mowiol 2%. The pressed tablets were then placed in an oven at 110°C for at least 6 hours before analysis by XRFS. The trace element concentrations are given in parts per million (ppm). Twenty samples of marlstones from the Calcaires du Moulin Wibert Fm. were analyzed by the SARM-CRPG spectrochemical laboratory of the Centre de Recherches en Pétrographie et Géochimie of Vandœuvre-lès-Nancy (geochemistry facility laboratory of the French Centre National de la Recherche Scientifique - CNRS). The determination of the major- and trace-element contents was carried out by ICP-OES and ICP-MS; the samples were prepared by fusion with

LiBO_2 and HNO_3 dissolution. Precision and accuracy were both better than 1% (mean 0.5%) for major-minor elements and 5% for trace metals, as checked by international standards and analysis of replicate samples (Carignan et al., 2001).

5. Results

5.1. Microfacies - For the Calcaires du Moulin Wibert Fm., the microfacies of the limestone beds were compared to the grainsize of the clastic fraction (HCl-insoluble) of the marlstone interbeds (Fig. 9). The grainsize distribution of the marlstone interbeds shows a two-peak distribution for most of the samples (8/11; Fig. 9). The main mode corresponds to silts and the accessory mode to sand-sized quartz grains. Thin rock section observations in the limestone beds also illustrate the presence of relatively large quartz grains. The samples of the middle part of the formation (beds B7 & B8 and interbeds A7 & A8) are devoid of quartz grains (mudstone texture of carbonate beds and silt-composed clastic fraction of marlstone interbeds). The stratigraphic distribution of the clastic fraction grainsize in the Calcaires du Moulin Wibert Fm. is therefore not depending on the facies. Hence, in spite of their mud- wacke-stone textures, which commonly suggest quiet depositional environments, the limestone beds (mud- to wackestone textures) do not correspond to quieter depositional conditions than those recorded by marlstones. The energy level was the same, whatever the facies.

5.2. Ca, Mg, Mn and Sr of carbonate objects - All the so-called carbonate objects at stake in the study (namely, carbonate beds and carbonate matrix of oyster patch reefs) were analyzed for their major and trace element concentrations, and more particularly focused to those usually associated to carbonate (Ca, Mg, Sr and Mn). Manganese distribution shows no special feature. In contrast, Mg and Sr yield striking features. Compared to the caging marlstones, all the carbonate objects studied fall in a separate area in a Ca vs Sr crossplot (Fig. 10). The same is true for Ca vs. Mg and the situation may be summarized in a Sr/Ca vs. Mg/Ca diagram (Fig. 10) indicating that all the carbonate objects

fall close to the end member of the sample distribution corresponding to relative depletion in both Sr and Mg.

5.3. Redox proxies - Twenty samples of the marlstone interbeds of the Calcaires du Moulin Wibert Fm. were analyzed for their redox-proxying trace metals. As far as the more diagnostic tracers are concerned, Mo is close to the analytical detection limit or below it (for 7 samples); U and V are positively correlated to Al (with $R^2 = 0.65$ and 0.96, respectively. In other words no authigenic enrichment could be detected in the sediments of the background, marly accumulation.

5.4. Stable isotopes – Twenty-seven analyses of C and O stable isotopes were performed on the carbonate beds of the Bancs Jumeaux Fm. cropping out at Cap Gris-Nez. Their $\delta^{13}\text{C}$ values fall in the $-4.2\text{\textperthousand}$ to $+0.4\text{\textperthousand}$ range; the $\delta^{18}\text{O}$ range from $-4.7\text{\textperthousand}$ to $-1.7\text{\textperthousand}$ (Fig. 11). Thus the ranges of values are similar to those of the carbonate beds of the Bancs Jumeaux Fm. of Wimereux (Tribouillard et al., 2012), summarized above. The Boundary bed separating the Grès de Châtillon Fm. from the overlying Argiles de Châtillon Fm. show $\delta^{13}\text{C}$ values ranging between $-11.5\text{\textperthousand}$ and $-0.4\text{\textperthousand}$, and $\delta^{18}\text{O}$ values ranging between $-4.3\text{\textperthousand}$ and $-1.8\text{\textperthousand}$ (6 samples; Fig. 11). To sum up, two samples among the six analyzed are as depleted in ^{13}C as the most depleted matrix samples of patch reefs (Fig. 8). The other four samples are in the same range as that of the Banc Jumeaux or Calcaires du Moulin Wibert. The nodular bed of the topmost part of the Argiles de Châtillon shows $\delta^{13}\text{C}$ and $\delta^{18}\text{O}$ ranging between $-5.9\text{\textperthousand}$ and $-3.6\text{\textperthousand}$, and $-5.7\text{\textperthousand}$ and $-2.7\text{\textperthousand}$, respectively. These values are quite similar to those observed for the carbonate beds of the Bancs Jumeaux Fm. Lastly, the limestone beds of the Calcaires du Moulin Wibert Fm. show $\delta^{13}\text{C}$ values comprised between $-1.8\text{\textperthousand}$ and $+0.3\text{\textperthousand}$, and $\delta^{18}\text{O}$ values comprised between $-3.6\text{\textperthousand}$ and $-1.9\text{\textperthousand}$. The five samples of hosting marlstones show $\delta^{13}\text{C}$ and $\delta^{18}\text{O}$ values comprised between $+0.9\text{\textperthousand}$ and $+1.5\text{\textperthousand}$, and $-4.9\text{\textperthousand}$ and $-3.1\text{\textperthousand}$, respectively. In other words, the carbonate beds of the Calcaires du Moulin Wibert Fm. show values comparable to those of the carbonate beds of the Bancs Jumeaux Fm the least depleted in ^{13}C (either from

Wimereux or Cap Gris-Nez). The same contrast between beds and hosting marlstones is observed for the Bancs Jumeaux Fm. and the Calcaires du Moulin Wibert Fm. (Fig. 11 and 11).

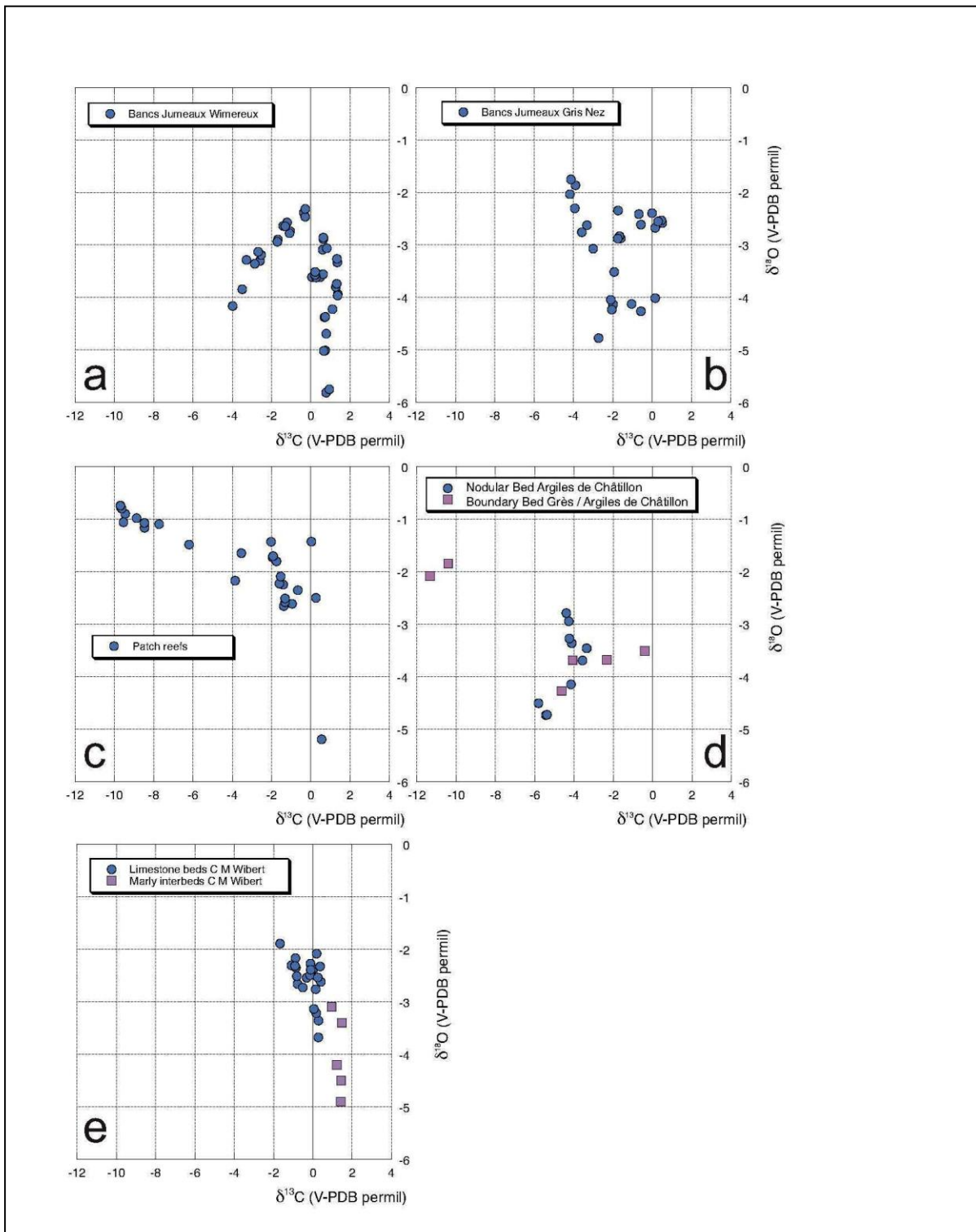


Fig. 11. Carbon and oxygen stable isotope composition of the various carbonate objects studied here.

6. Interpretations of analytical results

6.1. Facies/microfacies – All the carbonate objects studied are characterized by common features:

1 - a microsparitic texture of the fine-grained carbonate matrix is systematically observed, with a fringe of spar crystals surrounding most of the grains, clasts and bioclasts (pyrite, shells, quartz grains). Mavromatis et al. (2014) observed the same features in cold-seep related carbonate concretions offshore Costa Rica. In our samples, the carbonate consists always of calcite; no aragonite is observed and dolomite rhombs are quite rare.

2 - All the observed microfacies show the same homogeneous cathodoluminescence color, thus suggesting a single-step formation of the microsparite.

Microsparite may result from neomorphic replacement of a micritic matrix or from precipitation as cement, or even from a direct precipitation under bacterial control (see discussion in, e.g., Folk and Chafetz, 2000; Munnecke et al., 1997, 2001). In the present case, our geochemical analyses indicate that the microsparite is strongly depleted in both Sr and Mg, relative to the carbonate fraction of the hosting marls. In present/recent marine sediments, carbonate concretions induced by cold seep-related processes are usually made of Sr-rich aragonite and/or Mg-rich calcite (plus possible dolomite) (Torres et al., 2002; Bayon et al., 2007). However, with increasing age and burial, but also possibly on a short time scale, the original carbonates tend to recrystallize into Sr- and Mg-poor calcite, (Rodriguez et al., 2000; Kazmierczak et al., 2015 and references therein). Here, the homogeneous microsparite fabric and the marked depletion in both Sr and Mg strongly suggest that the original matrix was recrystallized into calcite. Because recrystallization usually induces increases in crystal size, the observed microsparite first indicates that the original matrix was made of micrite, and suggests that the recrystallization processes ended rapidly, preventing formation of larger spar crystals. We have no idea if the original carbonate matrix was made of aragonite or calcite; in addition, it is unclear whether the Late Jurassic oceans were prone to aragonite or calcite precipitation (Taylor, 2007), but these considerations have no implication for our interpretations.

6.2. Redox proxies - The studied carbonate levels are present in three different formations. The redox conditions prevailing during the deposition of the Bancs Jumeaux and Argiles de Châtillon formations have already been extensively described by Tribouillard et al., (2008, 2015) and references therein). For the Bancs Jumeaux Fm., the water column was oxygenated during deposition similarly to the Argiles de Châtillon, except for some episodes of laminated black shale deposition, characterized by dysaerobic conditions. Up to now, no trace element-grounding redox data were published for the Calcaires du Moulin Wibert Fm. Our results show that no detectable enrichment in redox tracers can be observed for the background sedimentary setting (hosting marlstones), which indicates that the water column and the sediment-water interface were oxygenated during the deposition of the marlstone interbeds.

6.3. Stable isotope composition - The samples analyzed in the present study show similar $\delta^{13}\text{C}$ values to those measured in the already-studied samples of the Bancs Jumeaux Fm. and the matrix of the patch reefs. All the carbonate bodies (either beds, nodular beds or patch reefs) show a consistent $\delta^{13}\text{C}$ dataset, clearly yielding depleted values. This homogeneous dataset indicates that all the carbonate levels are of diagenetic origin and impacted by a source of ^{12}C -enriched DIC mixing with seawater DIC. We may thus extend the interpretations formulated for the Bancs Jumeaux Fm. and patch reefs to all the other carbonate objects we examined. Interpreting all the carbonate beds, either continuous or nodular, as diagenetic in origin simplifies the sedimentological interpretations of the Late Jurassic of the Boulonnais. This explains the repeated intercalations of fine-grained limestones within a series of terrigenous deposits on a clastic-dominated ramp. In addition, it may account for the occurrence of numerous quartz grains within mudstone-wackestone limestones (Calcaires du Moulin Wibert Fm.), which is puzzling from a sedimentological point of view (coarse quartz grains suggesting a relatively high energy to be opposed to mud- wackestone textures suggesting quiet depositional environments). O'Reilly et al. (2014) observed such quartz inclusion

within early-diagenetic carbonate at shallow marine seep sites. Incidentally, these early forming carbonates are colonized by polychaetes and hydroids that probably benefit indirectly from available hard substrates as hypothesized for the oysters patch reefs of the Boulonnais.

Regarding oxygen isotopes, carbonate beds of Bancs Jumeaux and Calcaires du Moulin Wibert formations present $\delta^{18}\text{O}$ values similar to those of shells in the patch reef and tempestites, which are closer to the seawater signature than the $\delta^{18}\text{O}$ of the hosting marlstones (Figs. 8 and 11e). This indicates that during later diagenesis the original $\delta^{18}\text{O}$ was less altered by oxygen isotope reequilibration between pore water and carbonates in the carbonate objects (including shells) than in the hosting marlstones. This is fully compatible with the idea of a very early lithification of the limestone beds reducing their vulnerability to ulterior recrystallisation episodes, which would have altered their $\delta^{18}\text{O}$.

6.4. Early carbonate precipitation - The carbonate beds studied herein appear to be of diagenetic origin. In addition, some observations and analytical results suggest that the carbonate precipitation occurred close to (or even at) the sediment-water interface.

- The carbonate beds are commonly bioturbated and, in the case of the Bancs Jumeaux Fm., implying that carbonate was already firm by the time it was burrowed, as far as the intermediate bed is concerned (Fig.3D).
- The nodular bed (top of the Argiles de Châtillon Fm.) frequently shows a coquina layer in the center. The presence of a fossil or a fossil accumulation is a common feature in many diagenetic nodules; in the present case, many nodules of the bed do not contain shell-bed inclusions. Their presence is thus not a pre-requisite for the formation of the nodule. Furthermore, when present, the coquina has an erosional sole, irregularly grooving the underlying carbonate, and a flat top. This feature suggests that the storm-induced coquina was spilled over the seabed and incorporated during the diagenetic precipitation of the bed.

- The lower bed of the Bancs Jumeaux Fm. (at Wimereux) shows $\delta^{13}\text{C}$ values evolving from depleted values at the base toward seawater values at the top, suggesting a carbonate growth at the sediment-water interface. The $\delta^{18}\text{O}$ signature of the Bancs Jumeaux beds indicates carbonate precipitation and lithification close to the seawater reservoir.
- The $\delta^{34}\text{S}$ values of pyrites included in the carbonate (Bancs Jumeaux Fm.) are strongly depleted (Fig. 8), which suggests that bacterially-mediated sulfate reduction occurred in an "infinite" sulfate reservoir, i.e., seawater, in contrast to pyrite included in hosting marlstones. The less-depleted pyrite precipitated from a limited reservoir, i.e. from deeper pore waters where sulfate supply is limited. It is concluded that sulfate reduction, inducing authigenic carbonate precipitation, occurred very close to the sediment-water interface (if not just on the seabed), during the limestone bed authigenic precipitation.

6.5. Origin of the carbonate bodies - Our observations and analytical results demonstrates that the oyster reefs and carbonate beds (continuous or nodular) are of earliest diagenetic origin. The carbonate saturation and authigenic precipitation must have been induced by bacterially-mediated sulfate reduction reactions, fueled by fluids containing ^{12}C -enriched carbon of organic origin, mixing with seawater (De Craen et al., 1999). Such fluids can be methane-bearing ones in which case methane oxidation by bacterially-mediated sulfate reduction is named anaerobic oxidation of methane (AOM), but hydrocarbon-bearing fluids are also commonly mentioned (e.g., Jonk et al., 2003). Pore water fluids enriched in DIC produced by the sedimentary organic matter in the caging marlstone could also be envisaged. Carbonate precipitation must have occurred, at least for some of the limestone beds, very close to the sediment-water interface (as observed by Gontharet et al. (2007, 2009), in the Eastern Mediterranean). The fluids responsible for the formation of the carbonate objects must have circulated 1) either along individualized drains as is the case in pockmark fields (e.g., Gay et al., 2003, 2006) inducing the development of patch reefs, or, 2) more diffusively through sediments, leading to laterally extending impregnation of the seabed and

triggering authigenic precipitations of limestone beds over an extent of several kilometers. The redox-sensitive trace elements indicates that the water column was oxygenated (even if limited dysaerobic episodes — not recorded by trace-element distribution — cannot be ruled out). Thus, the sulfate-reducing reactions that went on at the sediment-water interface or very close beneath it, were not favored by water mass conditions but, instead, by upward-diffusing, oxygen-lean, dissolved organic carbon-bearing ascending fluids. Cold seep-related processes inducing diagenetic carbonate precipitation are quite common, involving either archaea + sulfate-reducing bacteria consortia in the case of AOM, or sulfate-reducing bacteria alone. The usual carbonate objects thus produced are concretions, nodules, chimneys or pavements. What is quite peculiar with the case at stake here is that true carbonate beds were created, in addition to more usual nodular beds and patch reefs.

Our understanding of the origin of the carbonate objects involves upward-circulating fluids containing isotopically-light carbon. Such fluids may have several possible origins: the underlying Devonian, Carboniferous or Jurassic (Callovian-Eraly Oxfordian) shale-rich formations (Mansy et al., 2007). In addition, our genetic scheme also involves increases in alkalinity, most probably induced by bacterial sulfate reduction reactions (pyrite is always quite abundant in the studied levels containing carbonate bodies or beds). As far as patch reefs are concerned, i.e., individualized seepages, such localized raises in alkalinity are commonly observed or admitted for present-day or ancients situations. However, the alkalinity increases must have been occasionally spatially extended in order to induce the diagenetic formation of beds of relatively developed lateral extent. Two antagonist factors must then be reconciled: bacterial sulfate reduction operates under oxygen-poor conditions but, according to trace-element geochemistry, the water masses were generally oxygenated during the Late Jurassic in the Boulonnais (except for some episodes of laminated black shale deposition under suboxic conditions; Tribouillard et al., 2015). To account for extended bacterial sulfate reduction at or to the sediment water interface, one can envision spills of oxygen-poor, DOC/DIC-bearing water over the sea floor; such spills would have been induced by synsedimentary fault movements (see discussion in Tribouillard et al., 2012). Another possible scenario is a spatially-

extended impregnation of the sediment (up to the sediment-water interface) by these fluids as evoked herein above. The ascending fluids would mix with pore waters that were enriched in isotopically-light dissolved C, released through organic-matter decay. The ascending fluids could also have simply pushed or flushed pore waters upward, without reaching the seafloor themselves. In any case, the ascending fluids, if alkaline enough, would have been ready to react with dissolved calcium ions, if available. In the case of the carbonate beds studied here, dissolved Ca^{2+} was present in too low proportions within pore waters to induce significant amounts of CaCO_3 within the sediment, but, close to or at the sediment-water interface, seawater DIC and Ca^{2+} being present in unlimited abundance, CaCO_3 precipitation would have occurred at or close to the sediment-water interface; hence the formation of limestone beds (continuous or nodular).

7. A tectonics context prone to synsedimentary fluid circulations

7.1. General setting - The Kimmeridgian-Tithonian series exposed along the Boulonnais cliffs are part of the northern margin of the Weald-Boulonnais basin (sometimes called also Weald-Boulonnais anticline due to its present structure). This margin, alike the adjacent North Sea and Wessex basin, was affected by a major Late Jurassic- Early Cretaceous rifting event (Butler and Pullan, 1990; Underhill and Paterson, 1998; Beeley and Norton, 1998; Newell, 2000; Taylor and Sellwood, 2002; Hansen et al, 2002; Mansy et al., 2003; Minguely et al., 2010) coeval with the general propagation of the Atlantic rift zone, north of the Gibraltar-Newfoundland fracture zone (e.g., Crosby et al, 2008; Bronner et al, 2011). The related pattern of subsidence and uplift induced the preservation of shallow marine Upper Jurassic and continental Lower Cretaceous (Wealdian) deposits in a restricted fault-bounded Boulonnais embayment upon which the present-day exposure is molded (Fig. 1A). This peculiar situation results directly from the Cenozoic (Late Eocene-Oligocene) tectonic inversion of the previous basin geometry (Mansy et al, 2003; Minguely et al, 2010) as emphasized by the complex compressive deformations and folding of Late Jurassic layers affecting the Cap Gris-Nez fault zone (Fig 1C; Pruvost, 1925; Lamarche et al., 1996; Averbuch, 2009).

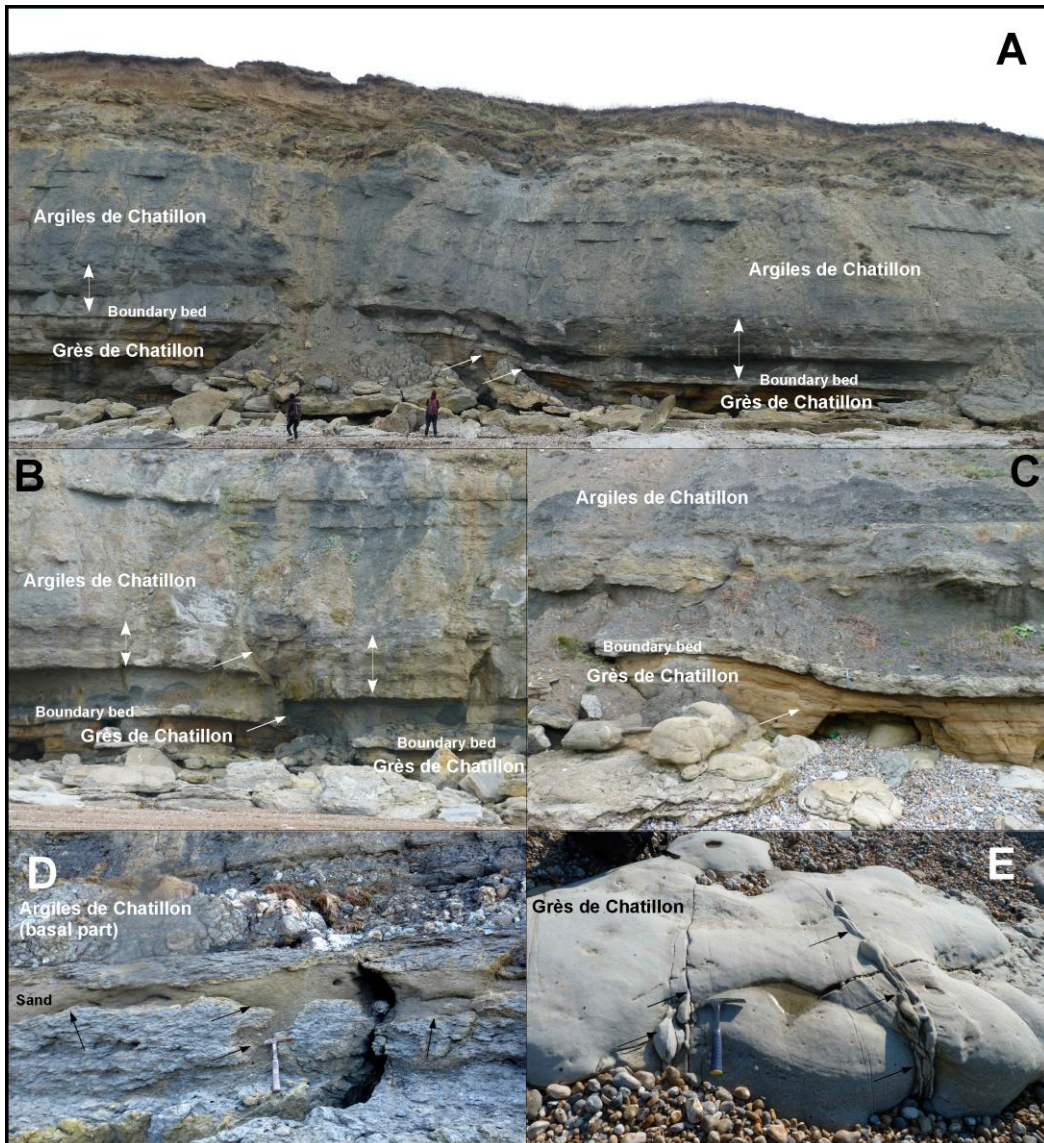


Fig. 12. Photographs of outcrops exposed along the section from Audresselles to Cran aux oeufs (see Fig. 1 for location)

illustrating the synsedimentary tectonic movements that affected the Boulonnais area during the Late Jurassic. A, B, C: synsedimentary south-dipping normal faults inducing lateral thickness variations of deposits at the transition between the Grès and Argiles de Châtillon formations (Late Kimmeridgian). Note the presence of the Boundary bed that forms the substrate of the disseminated oyster patch reefs. See Fig. 4 for a more detailed view of the normal faults exposed in C. D: heterogeneous sand body affecting the basal part of the Argiles de Châtillon Fm. in the Cran aux oeufs area (presumably due to fluidized sand injection from the underlying Grès de Châtillon). E: sand injectites into the Grès de Châtillon sandstones, forming the direct footwall of a normal fault at the Cran du Noirda (see Hatem et al, 2014 for a more detailed description).

The cross-section along the cliffs from the Cap Gris-Nez to Boulogne-sur-mer of Figure 1C illustrates perfectly well such geological evolution with a primary structuration of the basin by antithetic S- and N- dipping normal faults and their compressional reactivation within localized corridors (mostly S-dipping faults along the northern border of the basin). Such primary block-faulting geometry had a significant imprint on the subsidence pattern within the basin and, hence, on the lateral variability of the deposits. At a regional scale, this variability can be mostly assessed in the vicinity of the major fault zone bordering the basin to the north, i.e., the inverted South-dipping Cap Gris-Nez fault zone, with significant lateral facies changes expressed in both shallow marine (the Grès de Châtillon sandstone unit fading out north of the Cran aux Œufs area; see the cross section Fig. 1C) and deeper depositional sequences (for example, the Argiles de Châtillon Fm. with more numerous proximal tempestite levels towards the Cap Gris-Nez; see Fig. 2 and Hatem et al, 2014). On another hand, the rapid disappearance of Jurassic levels onshore, north of the Cap Gris-Nez & Landrethun fault zone (Fig. 1A), reveals a significant step in the subsidence intensity along the northern border fault zone in connection with the general half-graben structure of the basin (Butler and Pullan, 1990; Mansy et al, 2003) and the related gentle northward tilt of the underlying substratum before the Cenozoic inversion event. At a more local scale, such tectonic activity can be assessed by metric syn-sedimentary normal faults and soft-sediment deformations that can be observed in a recurrent manner throughout the Late Jurassic sequence exposed along the Boulonnais cliffs. Seismic-induced soft-sediment deformations and tsunami deposits have been described, in between the Slack-Epitre and Wimereux-Belle normal faults (Fig. 1), in the topmost Upper Jurassic sequence, i.e., the Late Tithonian series of the Pointe-aux-Oies Cape (Schnyder et al, 2005; Montenat et al, 2012). Along the Cap Gris-Nez shore, the transition between the Grès de Connincthun and Calcaires du Moulin Wibert formations displays also nice examples of soft-sediment deformations in the vicinity of a minor N-dipping normal fault (Hatem et al, 2014). The most extensive and demonstrative examples of the syn-sedimentary tectonic activity are, however, associated with the first-order increase of the relative sea-level at the transition between the Upper Kimmeridgian Grès de Châtillon sandstone unit

and the overlying Late Kimmeridgian-Lower Tithonian Argiles de Châtillon Fm. Along the cliffs from Audresselles to the Cran aux Œufs (Fig. 1C), the general rifted structure of the layers is accompanied by a set of minor S-dipping normal faults exposing recurrent arguments for differential subsidence and deposition during the sedimentation of the basal part of the Argiles de Châtillon Fm. (Figs. 12A & 12B) and the upper part of the Grès de Châtillon sandstones (Fig. 12C).

A major point to be emphasized is that such obvious tectonic instability appears to be associated with the release of fluids under pressure as suggested by the existence in these levels of different types of heterogeneous sand bodies featuring possible injectite structures (Fig. 12 D and E). Such structures are still under study but preliminary observations suggest that they could be related to the expulsion of fluidized sands from the Grès de Châtillon Fm. either upward into the basal Argiles de Châtillon layers (Fig. 12D) or laterally into the adjacent Grès de Châtillon layers in the footwall of the syn-sedimentary Cran-du-Noirda normal fault (Fig. 12E; see also Hatem et al, 2014 for a more detailed description of this structure). At a more regional scale, this period of instability corresponds to the deposition of a highly heterogeneous sequence with bioturbated sandy limestone levels such as the Boundary bed, on top of the Grès de Châtillon Fm. (Fig. 12) that supports the largely distributed oyster patch reefs observed from Audresselles to the Cap Gris-Nez area.

7.2. A model for the development of early diagenetic cold-seep-induced carbonates in the Late Jurassic series of the Boulonnais Basin - These field observations strongly support a primary tectonic origin for the release of dissolved organic carbon-bearing fluids involved in the early diagenetic carbonate cementation evidenced both in limestone beds and oyster patch reefs throughout the Late Jurassic sequence. The dissemination of patch reefs over a large area covering the northern border of the basin suggests that the fluid seeps formed a sort of micro-pockmark field. Such pattern of distributed fluids seepage at the sea floor was also recognized in the Porcupine Basin by Van Rensbergen et al. (2007) who showed, based on 3D seismic data and wells, a change of fluid/gas migration evolving from focused circulation along fault zones at depth to diffuse migration in the

shallow, unconsolidated deposits. Following this view, we propose a model (Fig. 13) considering fluids migration pathways dominantly focused at depth along the main fault zones of the northern margin of the basin, and evolving to a more diffuse mode in the unconsolidated syn-rift sedimentary layer. Such process would as well account for the localization of large oysters reefs (pseudo-bioherms) above the main Cap Gris-Nez fault zone and the general random distribution of isolated oyster patch reefs over the northern margin of the basin at times of massive release of fluids, i.e., the main phases of sea floor instability due to pulses of tectonic activity. On a more recurrent manner and at the basin scale (at least from Boulogne to Cap Gris-Nez), the diffuse release of dissolved organic-carbon bearing fluids through the unconsolidated depositional sequence would promote the impregnation of the sediment, possibly up to the sediment-water interface or very close to it, fueling bacterial sulfate reduction. These chemical reactions would have induced the alkalinity rise triggering in turn the authigenic carbonate precipitation, thereby generating limestone beds. The beds are laterally continuous, or more or less nodular limestone beds. Such a situation would have occurred episodically in the basin during the deposition of the Kimmeridgian-Tithonian marlstone sequences involved in the Calcaires du Moulin Wibert, Argiles de Châtillon and Banc Jumeaux formations.

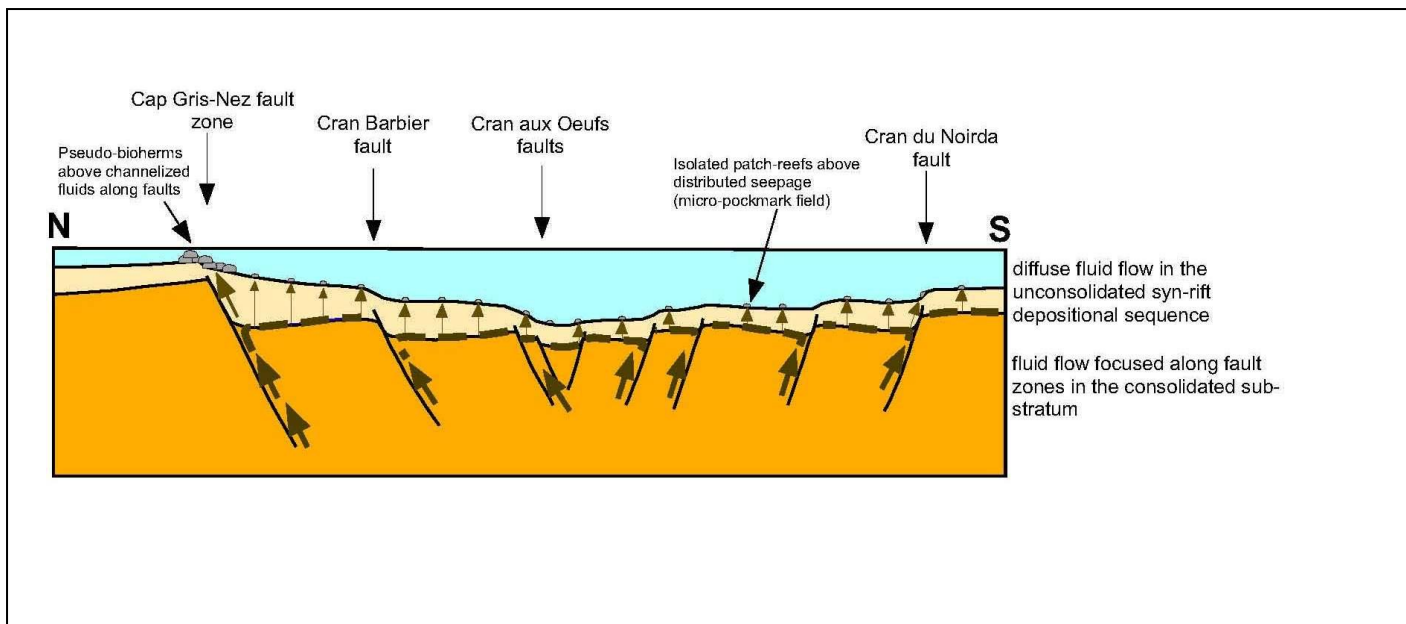


Fig. 13 . Schematic model (based on Van Rensbergen et al., 2007) illustrating the dynamics of organic carbon-rich fluids migration and the proposed effects on the localization of carbonate bodies (oyster patch reefs and pseudo-bioherms, diagenetic beds or nodules) within the general frame of the tectonic instability of the northern rifted margin of the Boulonnais Basin in Late Jurassic times.

Lastly, it is most probable that major fluid circulations also followed the network of sand levels still *pro-partे* uncemented today. Therefore, long-distance (hundreds of meters) lateral fluid connections along horizontal conduits certainly acted together with the vertical, fault-induced, ones that presumably operated at shorter ranges (a few meters?).

8. Conclusion

The model presented here relates the early-diagenetic formation of carbonate beds or oyster patch reefs to fluid circulations, induced by extensional tectonic movements, active during the Late Jurassic in the Boulonnais. These dissolved organic carbon-bearing fluids would have migrated to the water column, either at individualized spots, or through diffuse impregnation of the sediments up to, or close to, the sediment-water interface. The latter situation has induced the precipitation of fine-grained limestone beds over a relatively large extent (km-scale). Later during the basin history, such early-forming beds may have acted as localized shields or permeability barrier hampering further fluid circulation, which deserves consideration in a petroleum system.

Lastly, the beds thus induced are quite similar to common sedimentary, fine-grained limestone beds. In the absence of C, O or S isotope data, the diagenetic origin of the beds cannot be suspected, except based on the presence of microsparite and the unusual occurrence of floating quartz grains. Cold seep-related, diagenetic carbonate bodies are usually not described as continuous beds, and the results of this work suggest that the origin of fine-grained limestone beds interspersed through clastic-dominated series must be re-evaluated taking into account possible diagenetic effects induced by circulations of organic carbon-bearing fluids.

Acknowledgement. We thank the members of the technical staff of the laboratory, namely, Marion Delattre, Monique Gentric, Sylvie Regnier, Sandra Ventalon, Romain Abraham and Philippe Recourt, Thanks to Germain Bayon for his kind support.

Age	Ammonite zone	Formation	Short description
Tithonian	Pallassioides	Argiles de Wimereux	Grey claystones showing some sandy glauconitic beds, ending with a third phosphatic level (P3). Thickness 10 m
Tithonian	Pectinatus Wheatleyensis	Bancs Jumeaux	A group of 2/3 carbonate beds (Twins Beds), included within a marlstone matrix that is bounded by two phosphate levels (P1 and P2) containing pebbles of quartz and phtanite (chert). Thickness 1.8 m
Tithonian	Wheatleyensis Scitulus	Argiles de la Crèche	The formation consists of claystone and marlstone accumulations with some intervals of laminated black shales. Storm beds showing hummocky cross stratifications are numerous, notably at the top of the formation. Thickness 8
Tithonian	Gigas/Elegans	Grès de la Crèche	The formation consists of brown- to orange-colored sandstones and sandy marlstones with common cross-bedding and wave ripples, and intense bioturbation (especially U-shaped and Rhizocorallium burrows). Thickness 20 m
Encompassing the Kimmeridgian-Tithonian boundary	Autissiodorensis to Gigas/Elegans zones	Argiles de Châtillon	The formation consists of claystone and marlstone accumulations with two intervals of laminated black shales and a laterally variable number of occasional intercalated limestone beds. The marlstones show a gradual enrichment in silt in the upper part of the formation. Storm beds (coquina and/or sandstone seams with hummocky cross stratifications) are numerous, notably at the top of the formation. Thickness 10 m
Kimmeridgian	Eudoxus Zone, Contejeani subzone	Grès de Châtillon	The formation consists of brown- to orange-colored sandstones and sandy marlstones with common cross-bedding and wave ripples, and intense bioturbation (especially U-shaped and Rhizocorallium burrows). Thickness 5 m
Kimmeridgian	Eudoxus Zone, Contejeani subzone	Calcaires du Moulin Wibert	Irregular alternation of grey clay, more or less clear, and argillaceous limestones small beds (dm) and thicker beds (0,5-0,8 m). Thickness 10-
Kimmeridgian	Eudoxus Zone, Caletanum-Contejeani sub-zones	Grès de Conninchun	The formation is made up with a few sandstone beds that are rich in glauconite and large quartz grains. Abundant bivalves (Trigonia) and occasional echinoids are observed. Thickness 5-

Table 1 - Brief description of the geological formations evoked in this study (from Mansy et al., 2007).

References

- Al-Ramadan, K., Morad, S., Proust, J.-N., Al-Aasm, I., 2005. Distribution of diagenetic alterations in siliciclastic shoreface deposits within a sequence stratigraphic Framework: evidence from the upper Jurassic Boulonnais, NW France. *Journal of Sedimentary Research*, 75, 943-959.
- Averbuch O., 2009. Le Cap Gris-Nez: déformations à la limite septentrionale du bassin jurassique supérieur du Boulonnais. In: Des roches aux paysages dans le Nord-Pas de Calais. Richesse de notre patrimoine géologique. F. Robaszynski, G. Guyetant coord., Société géologique du Nord- Conservatoire des Sites du Nord et du Pas de Calais eds., 58-59.
- Bayon, G., Pierre, C., Etoubleau, J., Voisset, M., Cauquil, E., Marsset, T., Sultan, N., Le Drezen, E., Fouquet, Y., 2007. Sr/Ca and Mg/Ca ratios in Niger Delta sediments: Implications for authigenic carbonate genesis in cold seep environments. *Marine Geology*, 241, 93-109.
- Bayon, G., Pierre, C., Etoubleau, J., Voisset, M., Cauquil, E., Marsset, T., Sultan, N., Le Drezen, E., Fouquet, Y., 2007. Sr/Ca and Mg/Ca ratios in Niger Delta sediments: Implications for authigenic carbonate genesis in cold seep environments. *Marine Geology*, 241, 93-109.
- Beeley, H.S., Norton, M.G., 1998. The structural development of the Central English Channel High — constraints from section restoration. In: Underhill, J.R. (Ed.) *Development, Evolution and Petroleum Geology of the Wessex Basin*. Geological Society, London, Special Publications 133, 283-298.
- Bout-Roumazeilles, V., Cortijo, E., Labeyrie, L., Debrabant, P., 1999. Clay-mineral evidence of nepheloid layer contribution to the Heinrich layers in the Northwest Atlantic. *Palaeogeography, Palaeoclimatology, Palaeoecology*, 146, 211-228.
- Bronner, A., Sauter, D., Manatschal, G., Peron-Pinvidic G., Munsch M., 2011. Magmatic breakup as an explanation for magnetic anomalies at magma-poor rifted margins. *Nature geoscience* 4, 549-553.
- Burdige, D.J., 2006. *Geochemistry of marine sediments*. Princeton University Press, 609 p.
- Butler , M., Pullan, C.P. 1990. Tertiary structures and hydrocarbon entrapment in the Weald Basin of southern England. In: Hardman, R.F.P. & Brooks, J. (Eds.), *Tectonic Events Responsible for Britain's Oil and Gas Reserves*, Geological Society, London, Special Publications 55, 371-391.
- Carignan, J., Hild, P., Morel J., Yeghicheyan, D., 2001. Routine analysis of trace elements in geochemical samples using flow injection and low-pressure on-line liquid chromatography

- coupled to ICP-MS: a study of geochemical references materials BR, DR-N, UB-N, AN-G and GH. *Geostandard Newsletter*, 25, 187-198.
- Crosby, A., White, N., Edwards, G., Shillington, D.J., 2008 Evolution of the Newfoundland-Iberia conjugate rifted margins. *Earth and Planetary Science Letters* 273, 214-226.
- De Craen, M., Swennen, R., Keppens, E.M., Macaulay, C.I., Kiriakoulakis, K. 1999. Bacterially mediated formation of carbonate concretions in the Oligocene Boom Clay of Northern Belgium. *Journal Sedimentary Research*, 69, 1098-1106.
- Deconinck, J.-F., Geyssant, J.R., Proust, J.-N., Vidier, J.P., 1996. Sédimentologie et biostratigraphie des dépôts kimméridgiens et tithoniens du Boulonnais. *Annales de la Société Géologique du Nord*, 4, 157-170.
- Folk, R.L., Chafetz, H.S., 2000. Bacterially induced microscale and nanoscale carbonate precipitates. In R.E. Riding and S.M. Awramik (eds.) *Microbial Sediments*, Springer, pp. 40-49.
- Fürsich, F., Oschmann, W. 1986. Storm shell beds of *Nanogyra virgula* in the upper Jurassic of France. *Neues Jahrbuch für Geologie und Paläontologie Abhandlung*, 172, 141-161.
- Gay, A., Lopez, M., Cochonat, P., Sultan, N., Cauquil, E., Brigaud, F., 2003. Sinuous pockmark belt as indicator of a shallow buried turbiditic channel on the lower slope of the Congo Basin, West African Margin. In: Van Rensbergen, P., Hillis, R.R., Maltman, A.J., Morley, C.K. (Eds.), *Subsurface Sediment Mobilization*, Geological Society of London, Special Publications, 216, 173–189.
- Gay, A., Lopez, M., Ondreas, H., Charlou, J.L., Sermondadaz, G., Cochonat, P., 2006. Seafloor facies related to upward methane flux within a Giant Pockmark of the Lower Congo Basin. *Marine Geology*, 226, 81–95.
- Geyssant, J.R., Vidier, J.-P., Herbin, J.-P., Proust, J.N., Deconinck, J.-F., 1993. Biostratigraphie et paléoenvironnement des couches de passage Kimméridgien/Tithonien du Boulonnais (Pas de Calais): nouvelles données paléontologiques (ammonites), organisation séquentielle et contenu en matière organique. *Géologie de la France*, 4, 11-24.
- Gontharet, S., Pierre, C., Blanc-Valleron, M.-M., Rouchy, J.M., Fouquet, Y., Bayon, G., Foucher, J.P., Woodside, J., Mascle, J., The Nautinil Scientific Party, 2007. Nature and origin of diagenetic carbonate crusts and concretions from mud volcanoes and pockmarks of the Nile deep-sea fan

- (eastern Mediterranean Sea). Deep Sea Research Part II: Topical Studies in Oceanography, 54, 1292-1311.
- Gontharet, S., Stadnitskaia, A., Bouloubassi, I., Pierre, C., Sinnighe Damsté, J.S., 2009. Palaeo methane-seepage history traced by biomarker patterns in a carbonate crust, Nile deep-sea fan (Eastern Mediterranean Sea). Marine Geology, 261, 105-113.
- Grossi, V., Cravo-Laureau, C., Guyoneaud, R., Ranchou-Peyruse, A., Hirschler-Réa, A., 2008. Metabolism of n-alkanes and n-alkanides by anaerobic bacteria: A summary. Organic Geochemistry, 39, 1197-1203.
- Hansen, D.L., Blundell, D.J., Nielsen, S.B. 2002. A model for the evolution of the Weal Basin. Bulletin of the Geological Society of Denmark, 49, 109-118.
- Hatem, E., Tribouillard, N., Averbuch, O., Vidier, D., Sansjofre, P., Birgel, D., Guillot, F., 2014. Oyster patch reefs as indicators of fossil hydrocarbon seeps induced by synsedimentary faults. Marine and Petroleum Geology, 55, 176-185.
- Jonk, R., Mazzini, A., Duranti, D., Parnell, J., Cronin, B., Hurst, A., 2003. Fluid escape from réservoirs: implications from cold seeps, fractures and injected sands Part II. The fluids involved. Journal of Geochemical Exploration, 78-79, 297-300.
- Kaźmierczak, J., Fenchel, T., Kühl, M., Kempe, S., Kremer, B., Łącka, B., Małkowski, K., 2015. CaCO_3 precipitation in multilayered cyanobacterial mats: clues to explain the alternation of micrite and sparite layers in calcareous stromatolites. Life, 5, 744-769.
- Lamarche, J., Bergerat, F., Mansy, J.-L., 1996. Tectoniques plicatives et cassantes dans le Jurassique du Boulonnais : une histoire méso-cénozoïque polyphasée. Ann. Soc. Géol. Nord IV (2nd série), 171-179.
- Mansy, J.-L., Guennoc, P., Robaszynski, F., Amedro, F., Auffret, J.-P., Vidier, J.-P., Lamarche, J., Lefèvre, D., Sommé, J., Brice, D., Mistiaen, B., Prud'homme, A., Rohart, J.-C., Vachard, D., 2007. Notice explicative, carte géologique de la France (1/50 000), feuille Marquise (seconde édition), Orléans. BRGM, 213 p.
- Mansy, J.-L., Manby, G.M., Averbuch, O., Everaerts, M., Bergerat, F., Van Vliet-Lanoe, B., Lamarche, J., Vandycke, S., 2003. Dynamics and inversion of the Mesozoic Basin of the Weald-Boulonnais area: role of basement reactivation. Tectonophysics, 373, 161-179.

- Minguey, B., Averbuch, O., Patin, M., Rolin, D., Hanot, F., Bergerat, F., 2010. Inversion tectonics at the northern margin of the Paris basin (Northern France) : new evidence from seismic profiles and boreholes interpolation in the Artois area. *Bulletin de la Société Géologique de France*, 181 (5), 429-442.
- Montenat, C., Barrier, P., Fovez, H., Jolivalt, M., 2012. Déformations précoce d'origine séismique dans les dépôts du Tithonien supérieur du Boulonnais (Pointe aux Oies, Pas de Calais). *Bulletin inf. Géol. Bass. Paris* 49, 4, 5-20.
- Munnecke, A., Westphal, H., Elrick, M., Reijmer, J.J.G., 2001. The mineralogical composition of precursor sediment of calcareous rhythmites: a new approach. *International Journal of Earth Sciences*, 90, 795-812.
- Munnecke, A., Westphal, H., Reijmer, J.J.G., Samtleben, C., 1997. Microspar development during early marine burial diagenesis: a comparison of Pliocene carbonates from the Bahamas with Silurian limestones from Gotland (Sweden). *Sedimentology*, 44, 977-990.
- Newell, A.J., 2000. Fault activity and sedimentation in a marine rift basin (Upper Jurassic, Wessex Basin, UK). *Journal of the Geological Society*, 157, 83-92.
- O'Reilly, S. S., Hryniewicz, K., Little, C.T.S., Monteys, X., Szpak, M.T., Murphy, B.T., Jordan, S.F., Allen, C.C.R., Kelleher, B.P., 2014. Shallow water methane-derived authigenic carbonate mounds at the Codling Fault Zone, western Irish Sea. *Marine Geology*, 357, 139-150.
- Prokoph, A., Shields, G.A., Veizer, J., 2008. Compilation and time-series analysis of a marine carbonate $\delta^{18}\text{O}$, $\delta^{13}\text{C}$, $^{87}\text{Sr}/^{86}\text{Sr}$ and $\delta^{34}\text{S}$ database through Earth history *Earth-Science Reviews*, 87, 113-133.
- Proust J.-N., Deconinck J.-F., Geyssant J.R., Herbin J.-P., Vidier J.-P., 1995. Sequence analytical approach to the Upper Kimmeridgian-Lower Tithonian storm-dominated ramp deposits of the Boulonnais (Northern France). - A landward time-equivalent to offshore marine source rocks. *Geologisches Rundschau*, 84, 255-271.
- Pruvost, P., 1925. Observations sur la structure du Cap Gris-Nez et sur les mouvements qui ont affecté le pays boulonnais après le dépôt du Jurassique. *Bull. Serv. Carte géol. France* 156, XXVIII, 71p.
- Rodriguez, N.M., Paull, C.K., Borowski, W.S., 2000. Zonation of authigenic carbonates within gas hydrate-bearing sedimentary sections of the Blake Ridge: offshore southeastern North America.

- In: Paull, C.K., Matsumoto, R., Wallace, P.J., and Dillon, W.P. (Eds.), Proceedings of the Ocean Drilling Program, Scientific Results, Vol. 164, 301-312.
- Schnyder, J., Baudin, F., Deconick, J-F., 2005. A possible tsunami deposit around the Jurassic-Cretaceous boundary in the Boulonnais area (northern France). *Sedimentary Geology* 177, 209-227.
- Soetaert, K., Hofmann, A.F., Middelburg, J.J., Meysman, F.J.R., Greenwood, J., 2007. The effect of biogeochemical processes on pH. *Marine Chemistry*, 105, 30-51.
- Taylor, P.D., 2007. Seawater chemistry, biomineralization and the fossil record of calcareous organisms. in: Okada, H., Mawatari, S.F., Suzuki, N. and Gautam, P. (eds.), *Origin and Evolution of Natural Diversity*, Proceedings of International Symposium "The Origin and Evolution of Natural Diversity", 1–5 October 2007, Sapporo, pp. 21–29.
- Taylor, S.P., Sellwood, B.W., 2002. The context of lowstand events in the Kimmeridgian (Late Jurassic) sequence stratigraphic evolution of the Wessex–Weald Basin, Southern England. *Sedimentary Geology*, 151, 89-106.
- Torres, M.E., McManus, J., Huh, C.A., 2002. Fluid seepage along the San Clemente Fault scarp: basin-wide impact on barium cycling. *Earth Planetary Science Letters*, 203, 181–194.
- Trentesaux, A., Recourt, P., Bout-Roumazeilles, V., Tribouillard, N., 2001. Carbonate grain-size distribution in hemipelagic sediments from a laser particle sizer. *Journal of Sedimentary Research*, 71, 858-862.
- Tribouillard N., Ramdani A., Trentesaux A., 2005. Controls on organic accumulation in Late Jurassic shales of Northwestern Europe as inferred from trace-metal geochemistry. In: Harris N., ed., *The Deposition of Organic-Carbon-Rich Sediments: Models, Mechanisms, and Consequences*. SEPM Special Publication, 82, 145-164.
- Tribouillard, N., Bialkowski, A., Tyson, R.V., Vergès, E., Deconinck, J.-F., 2001. Organic facies and sea level variation in the Late Kimmeridgian of the Boulonnais area (northernmost France). *Marine Petroleum Geology*, 18, 371-389.
- Tribouillard, N., Lyons, T.W., Riboulleau, A., Bout-Roumazeilles, V., 2008. A possible capture of molybdenum during early diagenesis of dysoxic sediments. *Bulletin de la Société géologique de France*, 179, 3–12.

- Tribovillard, N., Sansjofre, P., Ader M., Trentesaux, A., Averbuch, O., Barbecot, F., 2012. Early diagenetic carbonate bed formation at the sediment-water interface triggered by synsedimentary faults. *Chemical Geology*, 300/301, 1-13.
- Tribovillard, N., Trentesaux, A., Ramdani, A., Baudin, F., Ribouleau, A., 2004. Contrôles de l'accumulation de matière organique dans la Kimmeridge Clay Formation (Jurassique supérieur, Yorkshire, G.B.) et son équivalent latéral du Boulonnais : l'apport des éléments traces métalliques. *Bulletin Société Géologique de France*, 175, 491-506.
- Tribovillard, N., Hatem, E., Averbuch, O., Barbecot, F., Bout-Roumazeilles, V., Trentesaux, A., 2015. Iron availability as a dominant control on the primary composition and diagenetic overprint of organic-matter-rich rocks. *Chemical Geology*, 401, 67-82.
- Underhill, J.R., Paterson, S. 1998. Genesis of Tectonic Inversion Structures: Seismic Evidence for the development of key structures along the Purbeck-Isle of Wight Monocline. *Journal of the Geological Society*, 155, 975-992.
- Vallone, J., 2014. Paleontology and morphology of the oyster domes from the Kimmeridgian of the Boulonnais (Nord-Pas-de-Calais, France). Unpublished Master Thesis, University of Lille.
- Van Rensbergen, P., Rabaute, A., Colpaert, A., St Ghislain, T., Mathijs, M., Bruggeman, A., 2007. Fluid migration and fluid seepage in the Connemara Field, Porcupine Basin interpreted from industrial 3D seismic and well data combined with High-resolution site Survey data. *International Journal of Earth Sciences*, 96, 185-197.
- Veizer, J., Ala, D., Azmy, K., Bruckschen, P., Buhl, D., Bruhn, F., Carden, G.A.F., Diener, A., Ebneth, S., Godderis, Y., Jasper, T., Korte, C., Pawellek, F., Podlaha, O.G., Strauss, H., 1999. $^{87}\text{Sr}/^{86}\text{Sr}$, ^{13}C and ^{18}O evolution of Phanerozoic seawater. *Chemical Geology*, 161, 59-88.
- Wignall, P.B., Newton, R., 2001. Black shales on the basin margin: a model based on examples from the Upper Jurassic of the Boulonnais, northern France. *Sedimentary Geology*, 144, 335-356.
- Williams, C.J., Hesselbo, S.P., Jenkyns, H.C., Morgans-Bell, H.S., 2001. Quartz silt in mudrocks as a key to sequence stratigraphy (Kimmeridge Clay Formation (Late Jurassic, Wessex Basin, UK). *Terra Nova*, 13, 449-455.

3.3 – Compléments

3.3.1- Calcaire du Moulin Wibert

Il s'agit d'une formation qui est visible dans plusieurs endroits dans la zone d'étude, notamment : 1- Cap Gris-nez (épaisseur 8 m), 2- Cap de la Crèche (épaisseur 10 m). Cette formation est constituée principalement d'alternances de bancs calcaires et d'argiles noires pyriteuses. Des bioturbations sont présentes, surtout au sommet de certains bancs calcaires. Les bancs carbonatés contiennent des coquilles de lamellibranches.

3.3.1.1 Calcaires du Moulin Wibert au Cap Gris-Nez : il s'agit de 12 bancs calcaires noduleux d'origine diagénétique précoce (Hatem et al. soumis) bien séparés par des niveaux argileux avec des épaisseurs de 20 – 50 cm.

3.3.1.2 Calcaires du Moulin Wibert au point de la Crèche : il s'agit de 10 bancs calcaires où on note l'absence de la régularité de l'alternance calcaire-marne dans le milieu de la formation, d'une part par l'épaisseur des bancs carbonatés, et d'autre part par le chevauchement bancs carbonatés avec des niveaux d'argile.

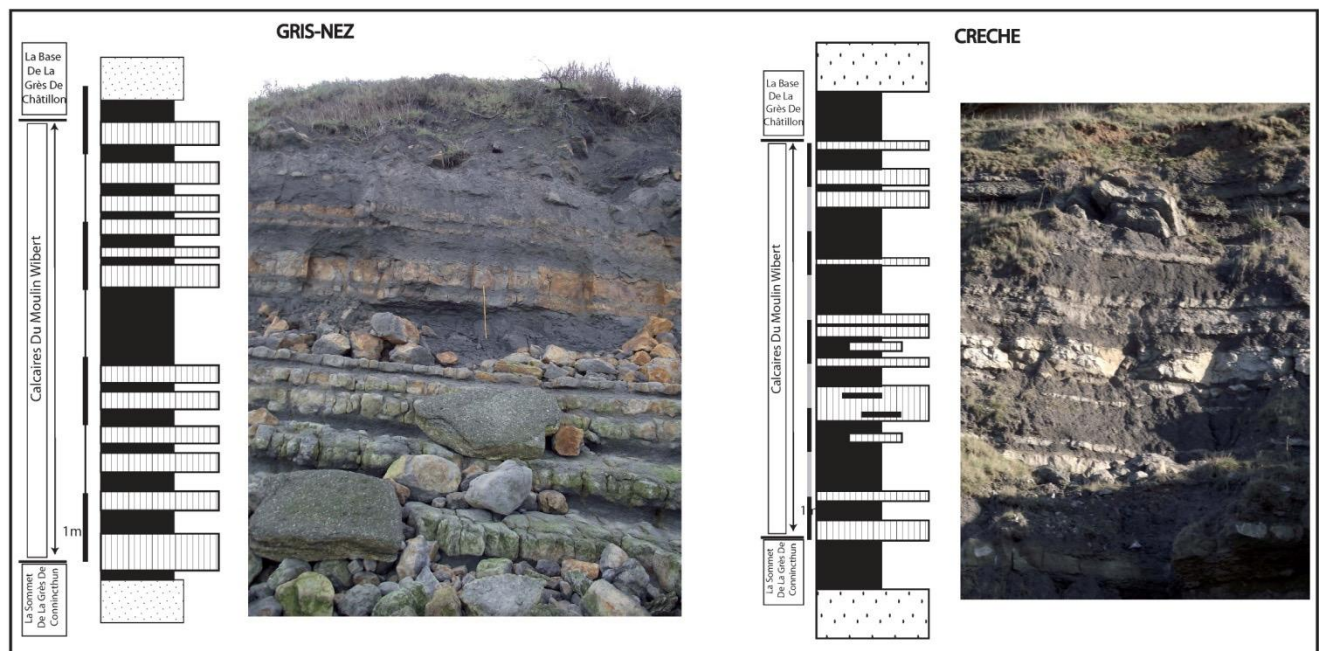


Figure 1. La formation des Calcaire du Moulin Wibert au Cap Gris-Nez et Cap de la Crèche.

Calcimétrie :

La teneur de CaCO₃ dans la MW Fig. 2, montre de contenus convergents dans toutes les échantillons, les changements sont progressifs et réguliers où elle augmente légèrement de la bas jusqu'au milieu, puis elle diminue légèrement vers le haut. Mais en général, il est homogène.

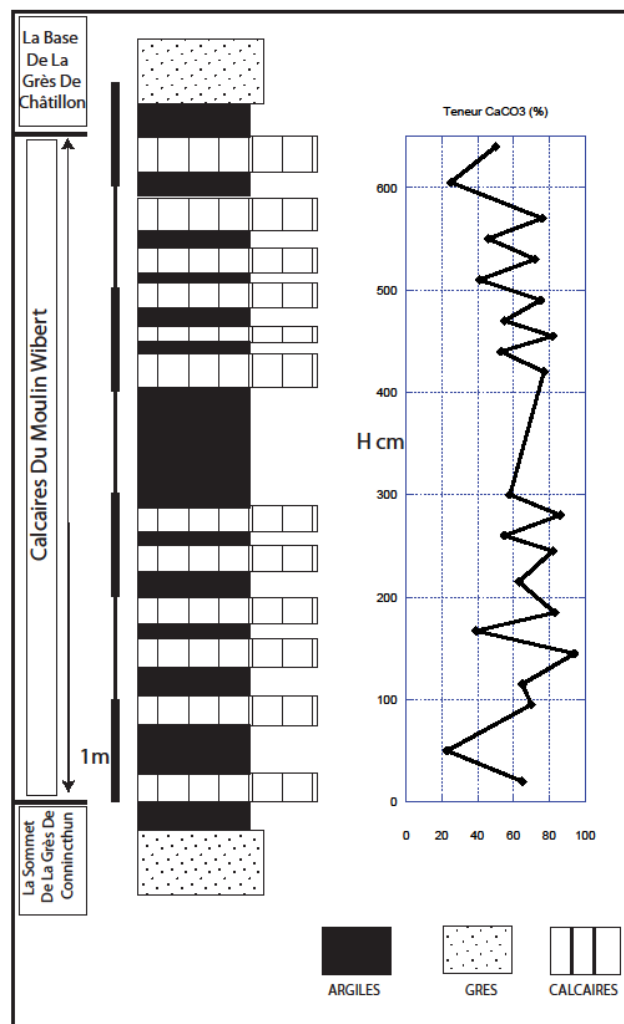


Figure 2. La teneur de CaCO₃ dans la formation du Calcaires du Moulin Wibert au Cap Gris-Nez

Granulométrie :

D'une part, pour les inter-bancs marneux concernant les CMW au Gris-Nez figure (3) dites « A1-A11 », on trouve que les courbes granulométriques marquent deux pics pour chaque niveau de marne sauf les niveaux (7et8) qui n'ont pas marqué qu'un pic.

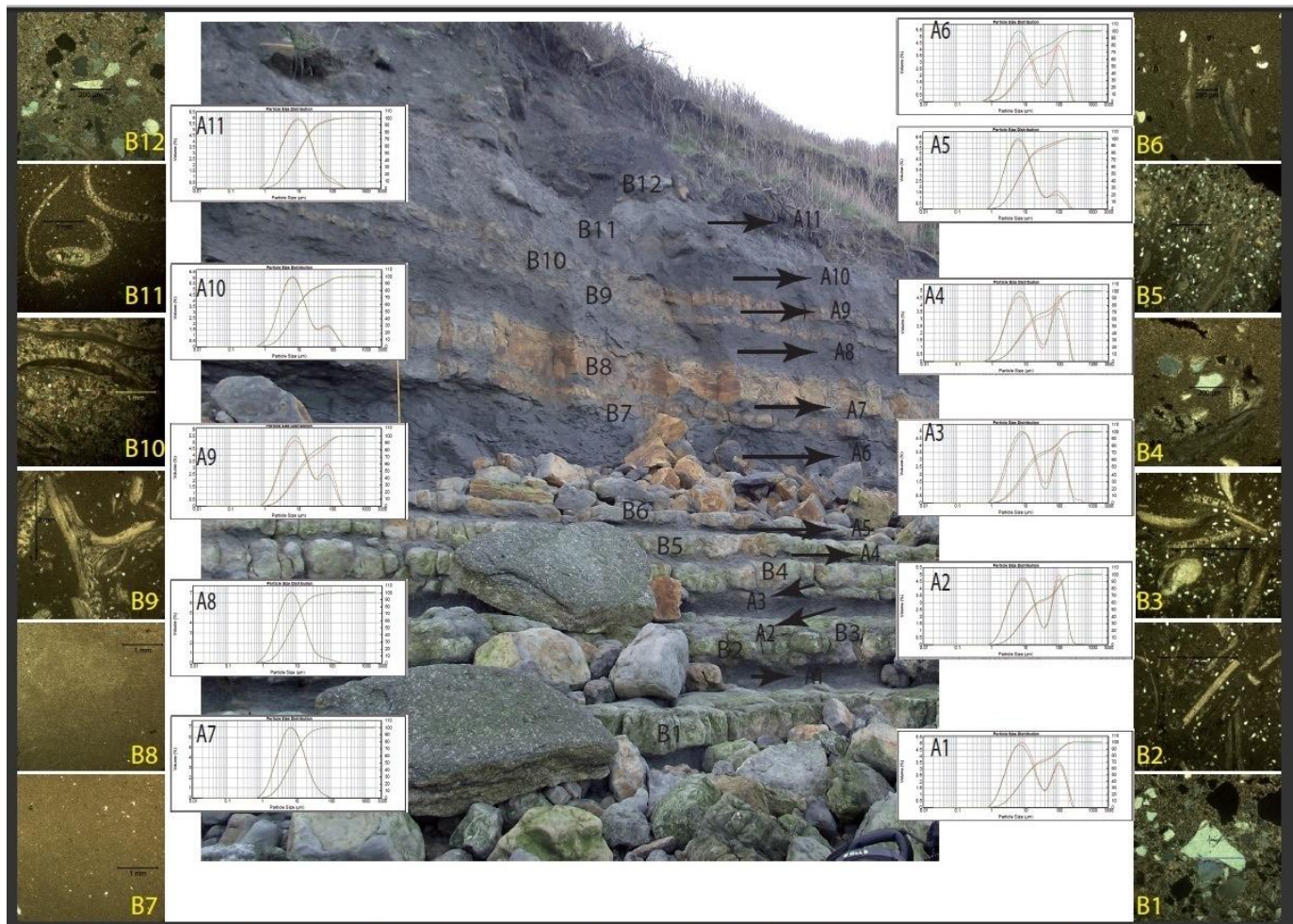


Figure 3. La graduation granulométrique des bancs (B1-B12) et des inter-bancs (A1-A11) du CMW au Gris-Nez.

D'autre part, la proportion de sable fin et le sable très fin mis en évidence par des analyses granulométriques au Gris-Nez est plus marquée que celles pour la coupe du Cap de la Crèche. Tandis que la proportion de la représentation du silt dans la Coupe de la Crèche est un peu plus forte que celle du Gris-Nez.

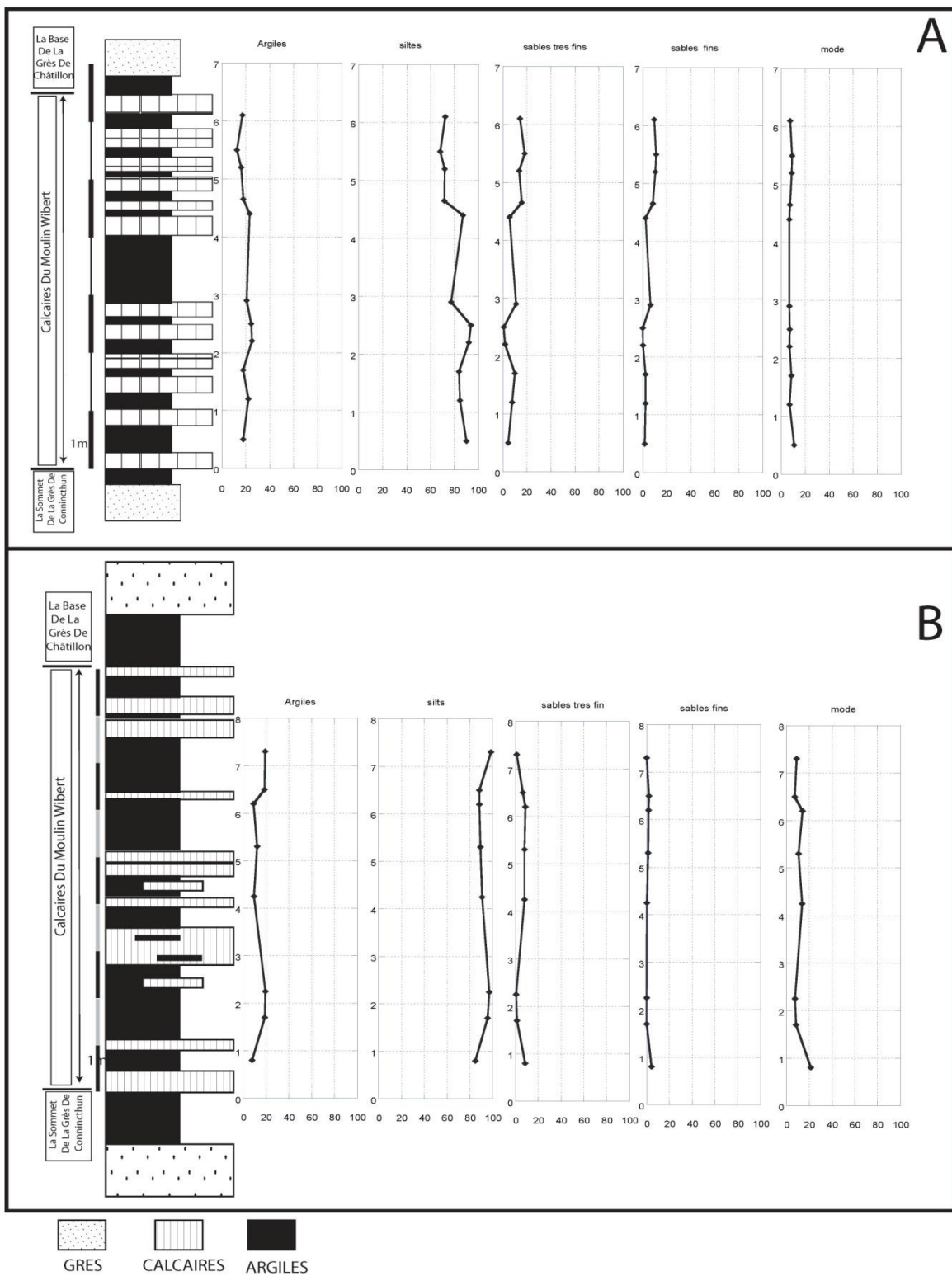


Figure 4. La granulométrie du CMW du Cap de Gris-Nez (A), et du Cap de la Crèche (B).

Rock-Eval :

Les deux gammes de la Formation CMW se tombent dans la zone d'immature (type3), mais, la gamme du Gris-Nez prend sa place dans le type 3 qui est plus haut par rapport de la gamme de la Crèche Fig.5.

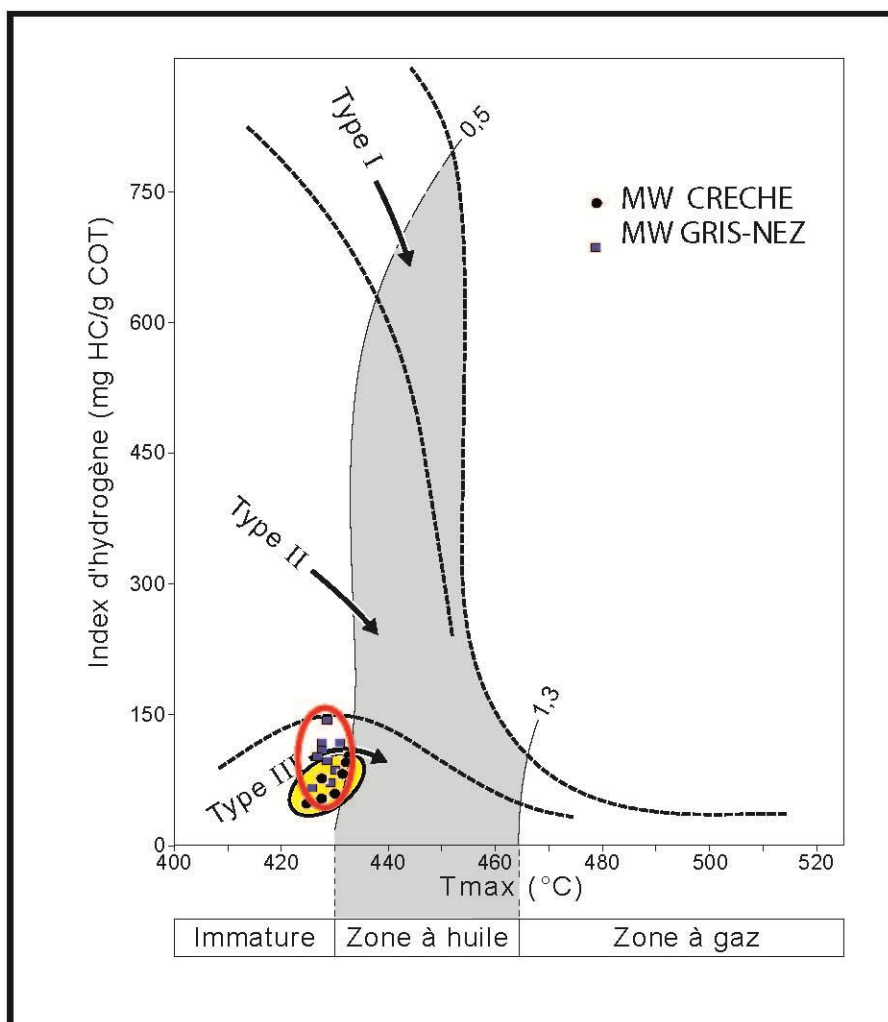


Figure 5. Les paramètres Rock-Eval pour CMW du Gris-Nez et De la Crèche.

Conclusion :

1. On voit que toutes les données (d'une part, les données granulométriques, et d'autre part la calcimétrie) montrent que l'environnement de sédimentation de cette formation CMW était plus stable dans le milieu que c'est vers le haut et en bas, où l'on note la rareté du quartz dans le milieu de la formation, en particulier dans les échantillons (7,8).

On peut noter également que la tendance croissante de la calcite à partir de la partie supérieure vers le centre avant de diminuer de nouveau vers le bas.

2. Les données qui viennent des deux paramètres : la granulométrie et le rock-Eval montrent qu'on est en face d'une formation proximale (Gris-Nez) et plus distale (Crèche), ce qui confirme les résultats de la formation Argiles de Châtillon, qui permet de mettre en évidence le même gradient.

3.3.2- Le banc noduleux de la partie supérieure de la Formation Argiles de Châtillon

Ce banc particulier se trouve dans la partie supérieure de la Formation des Argiles de Châtillon, intercalé entre plusieurs bancs de tempestites. Il apparaît sous la forme d'un banc carbonaté noduleux à grains fins observable sur environ 2 km (au moins) au nord d'Audresselles. Il est épais d'environ 25 cm et comporte souvent mais pas systématiquement en plein milieu, une lumachelle de coquilles d'huîtres (entières ou brisées) Fig. 1 & 2. Chaque nodule n'en contient donc pas. La base de la lumachelle est une semelle d'érosion irrégulière et le sommet est plat, et, il apparaît que ce banc est d'origine diagénétique (Hatem et al soumis).



Figure 1. Banc noduleux de la partie supérieure de la Formation Argiles de Châtillon, avec présence de tempestite, en coquilles d'huîtres ou de petite brisés de coquilles.

Quatre lames minces ont été réalisées afin d'étudier le développement du banc nodulaire (1, 2, 3, pour le vrai banc carbonatée, la 4^e pour le niveau de tempestite ; Fig. (2). Les résultats sont les suivants :

- 4 Le ciment en micro-sparite dans toutes les lames sauf le (3) qui donne un ciment de sparite dans sa partie supérieure.
- 5 Augmentation de la proportion de pyrite de 3 à 1 (du haut vers le bas).
- 6 Dans la lime mince 2, en utilisant la cathodoluminescence, on voit que les coquilles sont entourés par deux (ou plus) générations de recristallisation

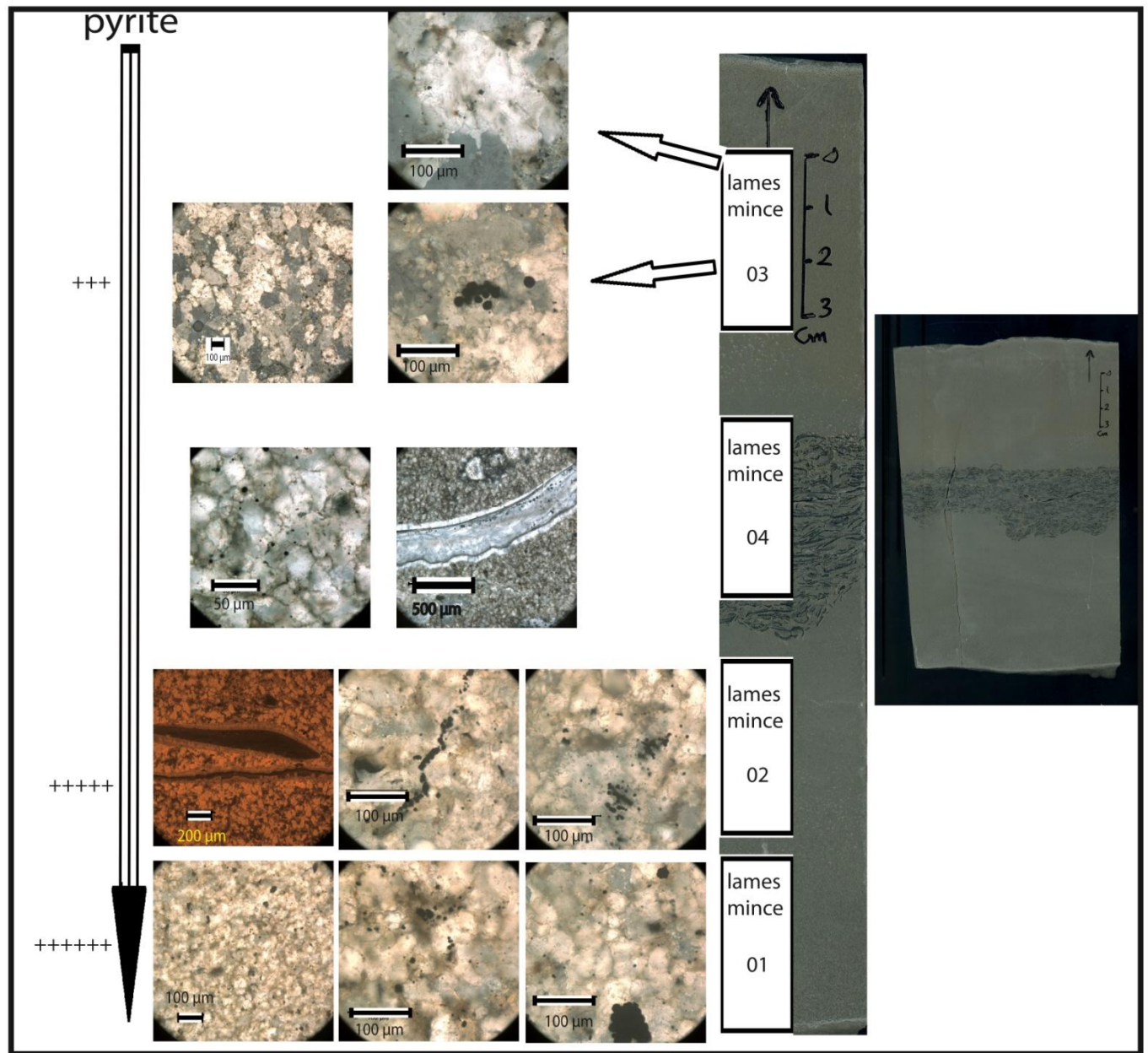


Figure 2. Développement du banc nodulaire (1, 2,3, pour le vrai banc carbonaté, la 4è pour le niveau de tempestite).

Chapitre 4 – Transect selon un gradient proximal-distal dans les Argiles de Châtillon.

4.1- Présentation

L'essentiel en quelques mots

Les marnes du Jurassique supérieur de la formation des Argiles de Châtillon sont bien exposées le long de falaises côtières du Boulonnais, cette formation d'argiles est un équivalent temporel latéral des sédiments riches en matière organique plus distaux de la Kimmeridge Clay Formation du Dorset (UK). Cette formation des Argiles de Châtillon est déposée dans un environnement (rampe terrigène) relativement peu profond, dominé par les apports clastiques (offshore sup/inf) ; elle est relativement riche en matière organique d'origine marine (MO) et est elle-même une potentielle roche mère de pétrole. Le long de cette rampe, les dépôts des Argiles de Châtillon ont enregistré un gradient proximal-distal, avec les conditions les moins profondes à proximité du Cap Gris-Nez, et les conditions plus distales à proximité des villes de Wimereux et Boulogne-sur-mer (Cap de la Crèche).

Le but de cette étude est d'examiner l'évolution latérale des conditions de dépôt de cette roche mère potentielle, afin de mieux comprendre l'accumulation de la MO sur les plateformes continentales. Plus précisément, l'accent sera mis sur les rôles de fer et de la composition des assemblages de minéraux argileux dans les processus de conservation de la MO.

Cet article est en partie une synthèse de nombreux articles publiés au cours de deux décennies, traitant des dépôts du Jurassique supérieur du Boulonnais, il présente également de nouveaux résultats sur la fraction clastiques de la formation des Argiles de Châtillon.

Pour étudier le transect traversant la zone du Boulonnais, nous avons examiné trois coupes dans les Argiles de Châtillon

1-) Cap de la Crèche « coupe distale », 2-) Cran du Noirda, 3-) Cap Gris-Nez « coupe proximale ».

Dans les trois coupes, les différences principales comportent quelques variations latérales :

1. d'épaisseur ; soit pour les coupes complètes, ou soit pour certains horizons qui sont présents dans les trois coupes, comme, à titre exemple, les argiles grises.
2. la variation latérale du nombre des tempestites. Les bancs de lumachelles sont dominants dans le cadre proximal du « cap Gris-Nez », tandis que des niveaux d'HCS (hummocky cross stratifications) sont plus abondants dans les coupes les plus distales du Cran du Noirda et beaucoup plus dans celle du Cap de la Crèche.

Les analyses granulométriques : la fraction dominant dans les trois coupes est le silt ce qui est en cohérence avec l'existence du gradient évoqué ci-dessus : variabilité de la taille des grains en domaine proximal au Gris-Nez, homogénéité moyenne au Cran du Noirda, et homogénéité plus marquée dans la coupe de la Crèche (domaine plus distal). La même signification se retrouve pour la fraction de taille des argiles qui donne relativement une importante proportion (moins ou égale 20%) à la coupe de la Crèche, tandis que la coupe du Gris-Nez (la plus proximale) montre en revanche une

fraction de taille de sable-fin relativement importante (inférieure ou égale à 20%). Le classement granulométrique montre la même tendance en cohérence avec le gradient.

Assemblage de minéraux argileux : la chlorite est le minéral argileux le moins abondant compris généralement entre 0 et 10 %. La répartition de la smectite est opposée à celle d'illite et d'illite+kaolinite. Cela concorde également avec le cas plus largement observé à l'échelle régionale du Jurassique supérieur (J-S) dans le Boulonnais. Sur les coupes du Noirda et Gris-nez : la smectite commence à augmenter à partir de la limite K/T vers le haut, alors que l'augmentation n'est établie que dans les trois derniers mètres de la formation au Cap de la Crèche. On indique là que la baisse du niveau de la mer a été accompagnée par la libération de smectite de la partie émergée du massif de Londres-Brabant. La fourniture de smectite a été enregistrée initialement par la coupe proximale (Cap Gris-Nez) et progressivement par la coupe la plus distale (coupe du Cran Noirda et, à la fin, par le Cap de la Crèche). Ceci est similaire à ce que rapportent plusieurs études publiées antérieurement sur une grande échelle, mais la différence ici est qu'un tel gradient dans la distribution de la smectite est observée sur une échelle d'environ 20 km.

Paramètres Rock-Eval : la MO est présente dans les trois coupes avec des valeurs (0.5-7%), tous les échantillons sauf 3 entrent dans la zone immature dans un diagramme de type Van Krevelen ou HI vs. Tmax. On voit aussi que tous les échantillons des trois coupes se chevauchent dans les zones de répartition des kérogènes de type II et III, indiquant d'un mélange de MO marine avec des MO terrestres. Malgré ce chevauchement, on voit qu'il s'observe également le gradient proximal-distal parce que les échantillons de Gris-Nez n'atteignent pas la valeur des échantillons du Noirda, qui à leur tour n'atteignent pas la valeur des échantillons de la Crèche.

Les métaux traces : Un sous-ensemble de l'échantillon a été analysé pour la composition élémentaire, les échantillons ont été pris au-dessous, à l'intérieur et au-dessus, respectivement, des niveaux des argiles laminés, afin de couvrir un très large éventail de valeurs de contenu organique.

Pour la coupe de la Crèche, Le vanadium montre une corrélation linéaire assez claire pour la teneur en aluminium (Al), ce qui indique une origine terrigène. En revanche, Mo et U montrent une faible corrélation avec Al. Aucun enrichissement authigène n'est visible pour la coupe distale (Crèche). Les échantillons des coupes plus proximales (Cap Gris-Nez et du Cran du Noirda) montrent des enrichissements modestes en U et Mo. Les conditions redox pourraient avoir été un peu plus dysoxiques dans la partie proximale du bassin que dans sa partie distale.

Le fer et l'assemblage des minéraux argileux :

On sait que la smectite est une phase porteuse potentielle pour le fer réactif (adsorption et incorporation interfoliaire). Le fer du réseau cristallin est abondant relativement dans l'Illite, mais il ne peut pas être considéré comme de fer réactif dans la mesure où il fait une partie de réseau cristallin. Concernant du Cap de la Crèche, la fraction décarbonatée de roche totale contient entre 7-25% de fraction de la taille des argiles, et dans la fraction argileuse elle-même, on voit que la smectite ne présente que moins de 25% au tout long de la formation sauf les trois mètres sommitaux. On en déduit la smectite qui représente entre 1 et 4% de la fraction clastique de la roche totale, ce qui est négligeable. En revanche, dans la coupe du Cran Noirda avec la fraction d'argiles est 5-17%, et 0-93% de smectite dans l'assemblage de l'argile, la smectite représente entre 0 et 11% de la fraction clastique de la composition de la roche totale. Dans la coupe la plus proximale (Cap Gris-

Nez), la fraction d'argile est 5-25%, dont 0-93% de smectite dans l'assemblage de l'argile, la smectite représente entre 0 et 7% de la fraction clastiques de la composition de la roche totale.

Dans la coupe du Noirda, une relation négative se dessine entre la smectite et le COT. Dans le cas de la coupe de Cap Gris-Nez, une corrélation négative assez claire a été trouvée entre la smectite et le COT. Avec ces résultats trop fragmentaires, nous ne pouvons pas être ambitieux dans nos interprétations, mais nous suggérons que, premièrement, la smectite pourrait être associée avec le fer réactif et, en second : le fer réactif pourrait être associé à une réduction de la préservation de la MO.

Donc, on peut dire tout d'abord, si elle est vraie, qu'une corrélation entre le fer réactif et la smectite indique que la quantité d'argile, même quand il est présent dans des proportions relativement faibles dans les sédiments de roches » peuvent avoir un impact significatif sur la composition chimique en roche totale. Deuxièmement, il est possible que la corrélation indique que la smectite puisse gouverner (au moins partiellement) la quantité de fer réactif des sédiments, ce qui à son tour affecte la préservation de la MO. Une plus grande abondance du fer réactif provoque la capture de sulfure libre et donc entrave la sulfuration de la MO, ce qui peut limiter la préservation da la MO. Il est donc suggéré que la quantité de smectite puisse avoir une empreinte négative sur la préservation et l'accumulation de la matière organique.

Conclusions :

- Le premier enseignement de ce travail est que la MO peut être accumulée jusqu'à quelques pourcents en poids de carbone organique dans les roches largement dominées par du silt et avec <20% de minéraux de la taille des argiles, et présentant des signes de la bioturbation et déposés dans des conditions de la productivité modérée. On peut donc trouver de la MO abondante même quand les conditions de dépôts ne s'y prêtaient pas particulièrement.
- Le deuxième enseignement est que nos résultats suggèrent que les assemblages des minéraux argileux pourraient avoir un impact significatif sur l'abondance de fer réactif même lorsque la fraction argileuse est présente dans des proportions modestes par rapport au silt.
- Le troisième message est que la smectite, généralement, considérée comme ayant une influence positive sur l'adsorption et la préservation de la MO, peut également avoir un impact négatif lorsque ce minéral peut transporter et libérer le fer réactif. Ce fer peut à son tour réagir avec des ions sulfure libérés par la décomposition de la OM par des bactéries de la sulfato-réduction, ce qui empêche le sulfure libre de réagir avec la MO. La sulfuration de la MO étant limitée par la capture de sulfure libre par le fer réactif, la préservation et l'accumulation de la MO en seront entravées.
- Enfin, cette étude montre qu'un gradient dans la distribution de la smectite (minéral réputé comme ayant une bonne flottabilité) peut être observé sur une échelle plus petite que 20 km, résultant de la façon dont les variations du niveau de la mer remobilise les stocks de minéraux argileux sur les terres émergées.

4.2- Small-scaled lateral variations of an organic-rich formation in a ramp-type depositional environment (the Late Jurassic of the Boulonnais, France): impact of the clastic supply

1. Introduction

The Late Jurassic marlstones of the Argiles de Châtillon Formation (Fm.) are well exposed along the coastal cliffs of the Boulonnais area (northernmost France), between the Cap Gris-Nez (or Gris-Nez Cape) and Equihen (south of Boulogne-sur-Mer; Fig. 1). These shelf sediments are lateral time equivalents of the distal organic-rich sediments of the Kimmeridge Clay Fm. deposited in the Wessex Basin (Dorset, UK). The Argiles de Châtillon Formation, though deposited in a clastic-dominated, relatively shallow (sometimes above the storm wave base) ramp environment, is relatively rich in marine organic matter (OM) and is a potential petroleum source rock. Along this ramp, the Argiles de Châtillon deposits recorded a proximal-distal gradient, with the shallowest conditions close to the Cap Gris-Nez, and the more distal conditions close to the cities of Wimereux and Boulogne-sur-mer (Cap de la Crèche section, Fig. 1; Mansy et al., 2007). The Boulonnais area has been experiencing an extensional tectonics regime during the Late Jurassic, expressed through synsedimentary faulting (Mansy et al., 2007; Hatem et al., 2014, submitted). The aim of the paper is to examine the lateral evolution of the depositional conditions of this potential source rock, in order to derive some general force-lines for better understanding OM accumulation on continental platforms. More specifically, emphasis will be set on the roles of iron and the composition of clay-mineral assemblages in the processes of OM preservation. The present paper is partly grounding upon a synthesis of many papers published during two decades, dealing with the Late Jurassic deposits of the Boulonnais (see below); it also presents new results on the clastic fraction of the Argiles de Châtillon Fm. This work tries to draw some guidelines about OM accumulation that can be transposed from the formation at stake here to other similar platform settings of any age or location.

2. Geological framework and previous results

Extensive studies of the Boulonnais sections have provided a depositional and sequence stratigraphical framework that may be used to help interpret variations in OM content and composition in response to fluctuations in relative sea-level (e.g., Proust et al., 1995; Herbin et al., 1995; Deconinck et al., 1996; Wignall and Newton, 2001; Tribouillard et al., 2001; Bialkowski et al., 2000; Schliif, 2003; Al-Ramadan et al., 2005; Braaksma et al., 2006). The most-studied section is exposed at the Cap de la Crèche, between Wimereux and Boulogne-sur-mer (Fig. 1). There, the 29 m-thick Argiles de Châtillon Fm. (*autissiodorensis* and *elegans* ammonite zones) is well visible, being bracketed between the upper part of the Grès de Châtillon Fm. below (shoreface sandstone formation, *eudoxus* zone), and the base of the Grès de la Crèche Fm. above (another shoreface sandstone formation, *scitulus* zone; Geyssant et al., 1993; Herbin et al., 1995; Deconinck et al., 1996; Wignall et al., 1996). The mudstones, siltstones and shales of the Argiles de Châtillon Fm. represent a low-energy shelf facies deposited below wave base, but revealing some storm influence with some shelly limestone beds (Fürsich & Oschmann, 1986) and levels showing hummocky cross stratifications. Like the more distal time equivalent shales and mudstones exposed at Kimmeridge on the Dorset coast (Cox & Gallois, 1981; Waterhouse, 1999), these sediments are also organic-rich in

part (Dunn, 1972; Herbin et al. 1991; Herbin & Geyssant, 1993; Geyssant et al. 1993; Proust et al., 1993, 1995; Proust, 1994; Deconinck et al., 1996), but their OM has a more mixed origin (El Albani et al., 1993; Herbin & Geyssant, 1993; Herbin et al., 1995). The higher pyrite contents, and the depauperate *in situ* macro and microbenthos and reduced bioturbation have long been used to suggest reducing and “stagnant”, but not persistently anoxic, conditions (Ager & Wallace, 1966, 1970; Barnard & Shipp, 1981). Several orders of cyclicity are recorded within the Argiles de Châtillon; the most prominent are:

- the Milankovitch-type (climatic) primary cycles (ca. 20 ky, Herbin et al., 1995),
- the superimposed longer-term cycles observed here (ca. 500 ky; Herbin et al., 1995; Waterhouse, 1999).

Sequence stratigraphical studies of the Wimereux section (Proust, 1994, Proust et al., 1993, 1995; Herbin et al., 1995; Al-Ramadan et al., 2005; Braaksma et al., 2006) allow us to relate observed

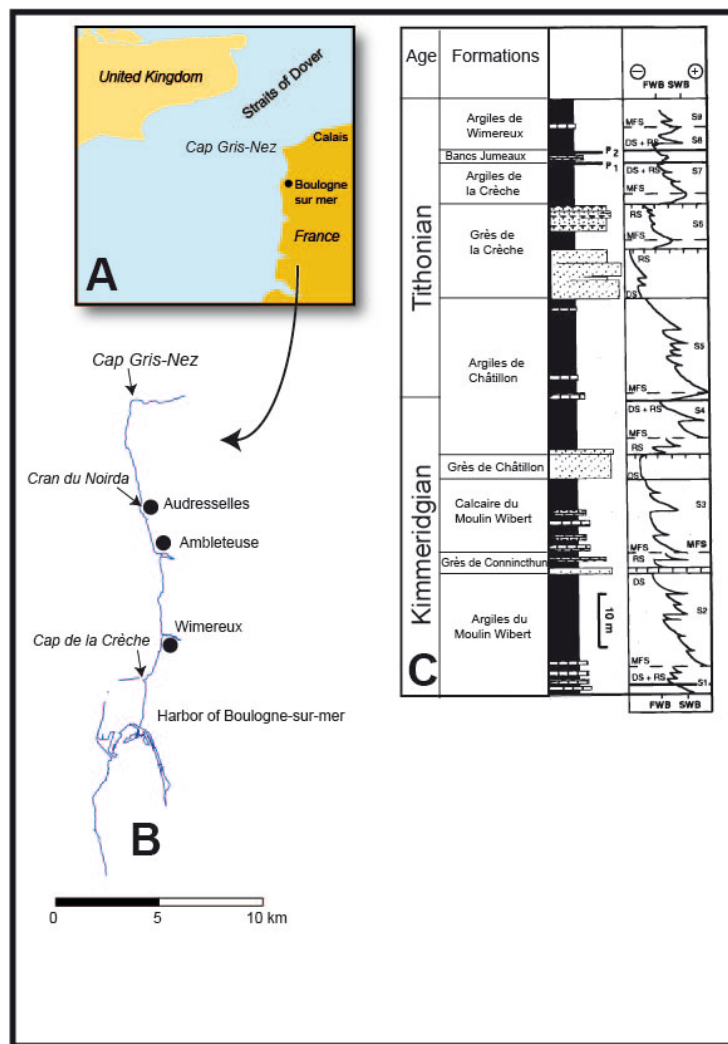


Fig. 1 – Maps showing the location of the study area, between the Gris Nez Cape and the city of Wimereux. Right-hand side: simplified lithostratigraphic log of the Late Jurassic formations cropping alongshore the Boulonnais (after Deconinck et al., 1996). FWB and SWB stand for fair-weather wave base and storm-weather wave base, respectively. P1 and P2 stand for the two horizons rich in phosphatized shells.

variations in organic facies to changes in relative sea level. Herbin et al. (1995) pointed out that relative sea-level rise was not the single cause for OM accumulation. Instead, these authors suggest that three parameters must act in conjunction:

- 1 - physiography (concerning the shape of the basin and the volume of sediments available),
- 2 - transgression (influencing the size of the area producing the organic material and the water depth),
- 3 - climate (governing the quality of the OM and the variation of primary productivity). Note that the climate of this period is reputed to have been warm (Brigaud et al., 2008; Dera et al., 2011).

As detailed descriptions of the lithofacies and stratigraphy of the "reference" section of the Cap de la Crèche have been given previously in Proust (1994), Proust et al. (1995), Herbin et al. (1995), Deconinck et al. (1996) and Wignall and Newton (2001), only a summary needs be offered here. The Grès de Châtillon consists of brown- to orange- coloured sandstones and sandy marlstones with common cross-bedding and wave ripples, and intense bioturbation (especially U-shaped and *rhizocorallium*, *ophiomorpha* and *thallasonoides* burrows). The formation ends with bioturbated limestone beds that mark the transition to the overlying Argiles de Châtillon Fm. that consists of claystone and siltstone accumulations with some intervals of laminated paper shales (Fig. 2), and a laterally variable number of local intercalated limestone beds, some of which are diagenetic in origin (Hatem et al., submitted). The marlstones show a gradual enrichment in silt in the upper part of the formation. Storm beds are numerous, notably around the Kimmeridgian-Tithonian (*autissiodorensis-elegans* zone) boundary and more particularly at the Cran du Noirda section.

The organic content of the Argiles de Châtillon Fm. (observed from the Cap de la Crèche section) is dominated by amorphous organic matter (AOM; Tyson, 1995). AOM represents the part of the kerogens the origin and nature of which cannot be determined through palynofacies observation alone (Tyson, 1995). Here, AOM is itself dominated by two main varieties distinguished on the basis of their color: orange or brown (see description and microphotographs in Tribouillard et al., 2001). Orange AOM exhibits distinct (and in some cases, almost angular) edges, and has a gel-like texture. Brown AOM has a more heterogeneous "flock" texture, less distinct "fuzzy" outlines, and tends to be less lustrous; in untreated kerogen slides it exhibits a more granular texture and the presence of pyrite crystallites and tiny framboids. It is also associated with lower fluorescence intensities (Tribouillard et al., 2001; Bialkowski et al., 2000).

In previous studies of the Kimmeridge Clay, orange AOM has been found to be nanoscopically amorphous, while brown AOM shows an ultralamina ultrastructure which is thought to represent selectively preserved cell walls of microplankton (Boussafir et al., 1994, 1995a, 1995b; Gelin et al., 1995, 1999). The ratio of the two types of AOM changes with the total organic carbon content (TOC) of the sediments, the proportion of orange AOM increases rapidly as TOC increases from 2 to 7% (Bialkowski et al., 2000; Tribouillard et al., 2001). The orange AOM is interpreted as resulting from natural vulcanization a.k.a. sulfurization (reaction with sulfides and polysulfides, see below), whereas brown AOM is interpreted to result from selective preservation of resistant biopolymers (selective oxidation of metabolisable constituents; Boussafir et al., 1994, 1995a, 1995b; Largeau et al., 1990; Derenne et al., 1991; Mongenot et al., 1997). Natural sulfurization is an early diagenetic process leading to the inter- or intramolecular incorporation of reduced inorganic sulfur species into low-

molecular-weight functionalized lipids resulting in the formation of resistant high molecular weight abiogenic “geopolymers” (Tegelaar et al., 1989).

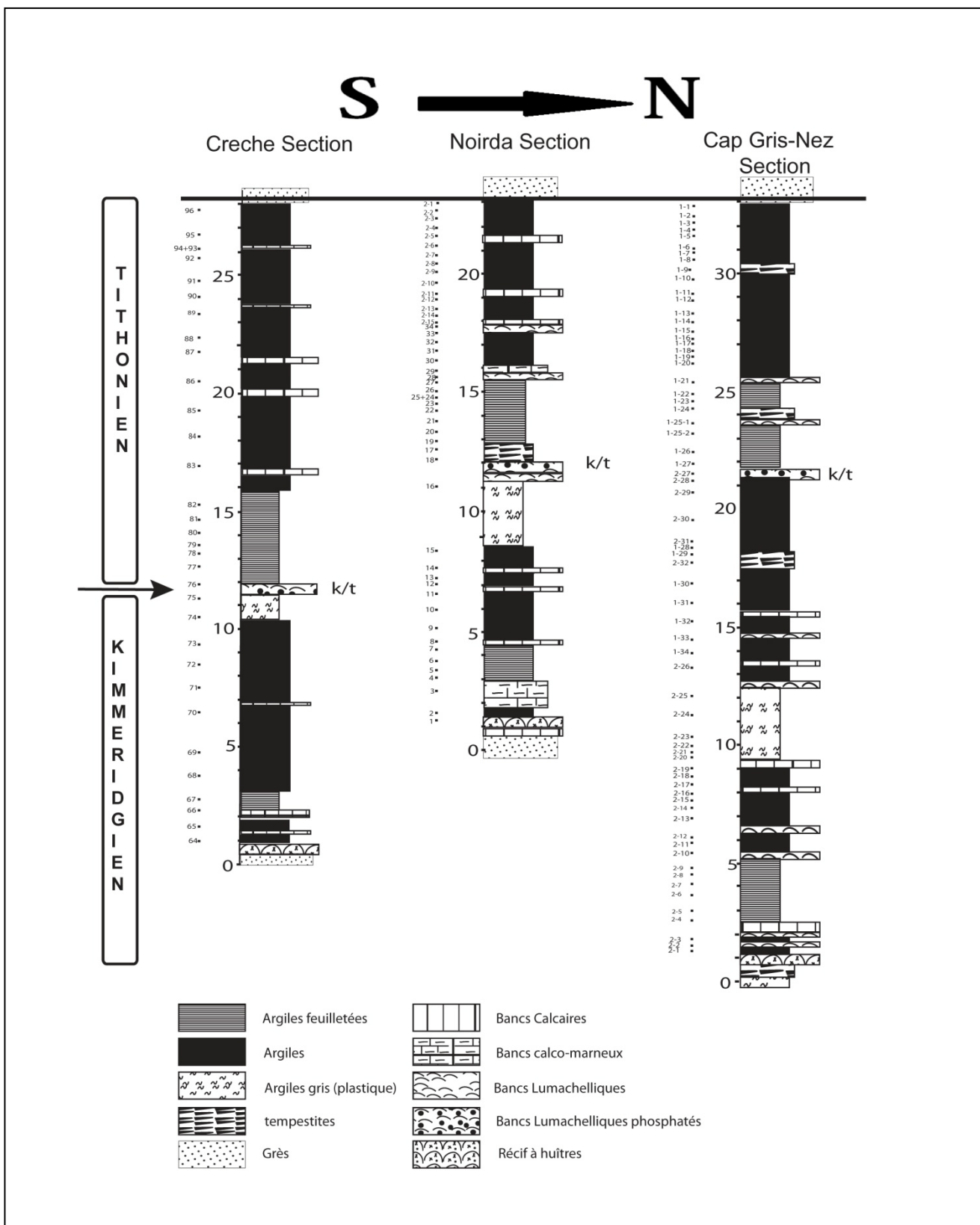


Fig. 2 – Simplified logs of the studied three sections.

3. Material and methods

To study a transect through the area of the Boulonnais where Jurassic formations crop out, namely from Cap Gris-Nez to Boulogne-sur-Mer, we examined three sections of the Argiles de Châtillon Fm. located, respectively, at Cap Gris-Nez (proximal setting), Cran du Noirda (intermediate setting, north end of Audresselles Village) and Cap de la Crèche (distal setting). The proximal-distal gradient is thus observed over a distance of about 15 km and is not sharp: the facies variations from one section to one another are not strong. Figure 2 illustrates the lithologies observed in the three sections and sampling steps. The same basic facies successions can be observed in the three sections. The main differences consist of some variations in thickness and a laterally variable number of storm-induced coquina beds (Fig. 2). These tempestites are dominantly made of small oysters (*Nanogyra nana*) and thin levels of sandstones showing hummocky cross stratifications (HCS). The oyster shell beds are dominant in the proximal setting of Cap Gris-Nez and the HCS levels are more abundant in the more distal settings of Cran du Noirda (they are not observed in the Cap de la Crèche section, the most distal part of the studied transect). In these sections, we could identify the level that is considered to correspond to the Kimmeridgian-Tithonian boundary (Geyssant et al., 1993). This level is rich in phosphatic debris and shells, and lies on top of a thick, shell-rich carbonate bed in the Cran du Noirda section (Proust et al., 1995). Notably, two laminated shale horizons are observed in each section; they are interpreted as deposited during marked elevation of sea level and begin with a maximum flooding surface. Both laminated shale horizons have a high organic carbon content (up to 9%) and, in the Cap de la Crèche section, are rich in orange-color AOM (Tribouillard et al., 2001).

For the three sections, grain-size distribution of the decarbonated fraction (HCl digestion) was analyzed using a laser-equipped Malvern Mastersizer apparatus, following the protocole of Trentesaux et al. (2001). The decarbonated fraction is considered to be representative of the clastic, land-derived component of the sediment, to which the authigenic fractions may be added (mainly pyrite frambooids or crystals), as well as organic flocs. Tempestite beds were not taken into consideration for grain-size study. The limit between silt and clay is 4 µm in the present paper.

For all samples, the carbonate content was measured using a Bernard calcimeter (acid digestion followed by CO₂ volume determination; accuracy < 5%). The Rock Eval pyrolysis parameters were determined with a Rock Eval VI apparatus: total organic carbon content (TOC, in wt.%), Tmax (°C), and Hydrogen Index (HI, in mg hydrocarbon per g TOC; see all details about Rock Eval pyrolysis and parameters in Espitalié et al., 1986; Lafargue et al., 1998; Behar et al., 2001).

The determination of the major- and trace-element contents was carried out by ICP-OES and ICP-MS by the spectrochemical laboratory of the *Centre de Recherches en Pétrographie et Géochimie* of Vandœuvre-les-Nancy (geochemistry laboratory of the French *Centre National de la Recherche Scientifique*). The samples were prepared by fusion with LiBO₂ and HNO₃ dissolution. Precision and accuracy were both better than 1% (mean 0.5%) for major-minor elements and 5% for trace metals, as checked by international standards and analysis of replicate samples (Carignan et al., 2001). Enrichment factors (EF) were calculated as: X_{EF} = [(X/Al)_{sample}/(X/Al)_{PAAS}], where X and Al represent the weight % concentrations of element X and Al, respectively. Samples were normalized using the average upper crust compositions of McLennan (2001). Aluminum normalization is commonly used to minimize the effects of variable dilution by carbonate or biogenic silica, although certain caveats apply to this approach (for a discussion, see Van der Weijden, 2002). The convenience of using

enrichment factors is that any value larger than 1.0 points to enrichment of an element relative to its average crustal abundance. In practical terms, EFs >3 represent a detectable enrichment of an element over average crustal concentrations, and EFs >10 represent a moderate to strong degree of enrichment (Algeo and Tribouillard, 2009).

The < 2 µm clay fraction was isolated and analyzed using the standard protocol for clay-mineral assemblage determination (a Bruker D4 Endeavour apparatus was used together with the Macdiff software; see detailed protocol in Bout-Roumazeilles et al., 1999).

Lastly, low-field magnetic susceptibility was measured on the dried samples, using a Kappabridge KLY 2 apparatus (three measures per sample) operating at an alternating magnetic field of 300 A/m (frequency 920 Hz). Low-field MS values were normalized with respect to sample mass to allow comparisons between samples of different density

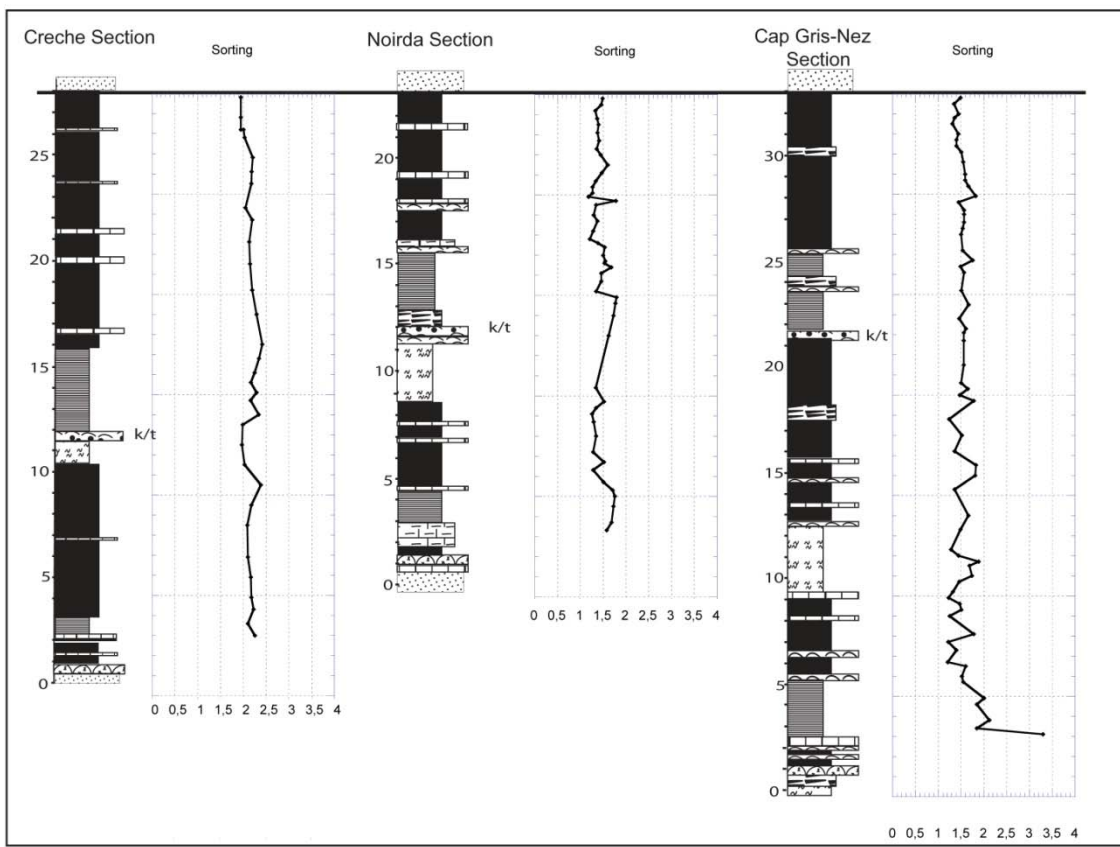


Fig. 3 – Compared stratigraphic evolution of the sorting index for the studied three sections.

4. Results

The analytical results are gathered in Tables 1 to 3.

4.1. Grainsize analysis

The dominant size fraction is that of silt for the three sections. Consistently with the existence of the proximal-distal gradient, the more remote site of Cap de la Crèche yields a relatively important clay-size fraction (up to 20%), while the more proximal Cap Gris-Nez site shows a relatively important fine-sand fraction (up to 20%). In addition sorting is smoother at Cap de la Crèche than at Cap Gris-Nez. Figure 3 and Tables 1 to 3 summarize the lateral evolution of grain-size distribution.

4.2. Clay-mineral assemblages

The assemblages contain illite, smectite, kaolinite and chlorite in variable proportions. Chlorite is the less abundant clay mineral, and shows smoothed stratigraphic distributions. Smectite distribution is largely opposed to that of illite + kaolinite, which is also the case at the scale of the entire late Jurassic in the Boulonnais (Deconinck et al., 1996). At the Cran du Noirda and Cap Gris-Nez sites, the smectite content starts increasing from the Kimeridgian-Tithonian boundary upward, whereas the increase is observed only in the top three meters at Cap de la Crèche (Fig. 4).

4.3. Rock Eval parameters

Organic matter is present in the three sections, with TOC values falling into the 0.5-7% range. Figure 5 illustrates the distribution of the Tmax and HI values for the three sections. All the samples (but 3) fall in the "immature" zone of the diagram, as determined by Tmax. The HI parameter shows that the samples of the three formations straddle the kerogen Types II and III, which indicates that a mixture of marine and terrestrial OM in variable proportions is present, for the three sites. The Cap de la Crèche samples are scattered between the lowest and highest ends of the sample sets. The Gris-Nez samples do not reach HI values as high as those of the other two sections. For the three sections, the highest TOC values are observed in the laminated shale levels. Lastly, a positive correlation is observed between TOC and HI, as already observed and discussed in Tribouillard et al. (2001).

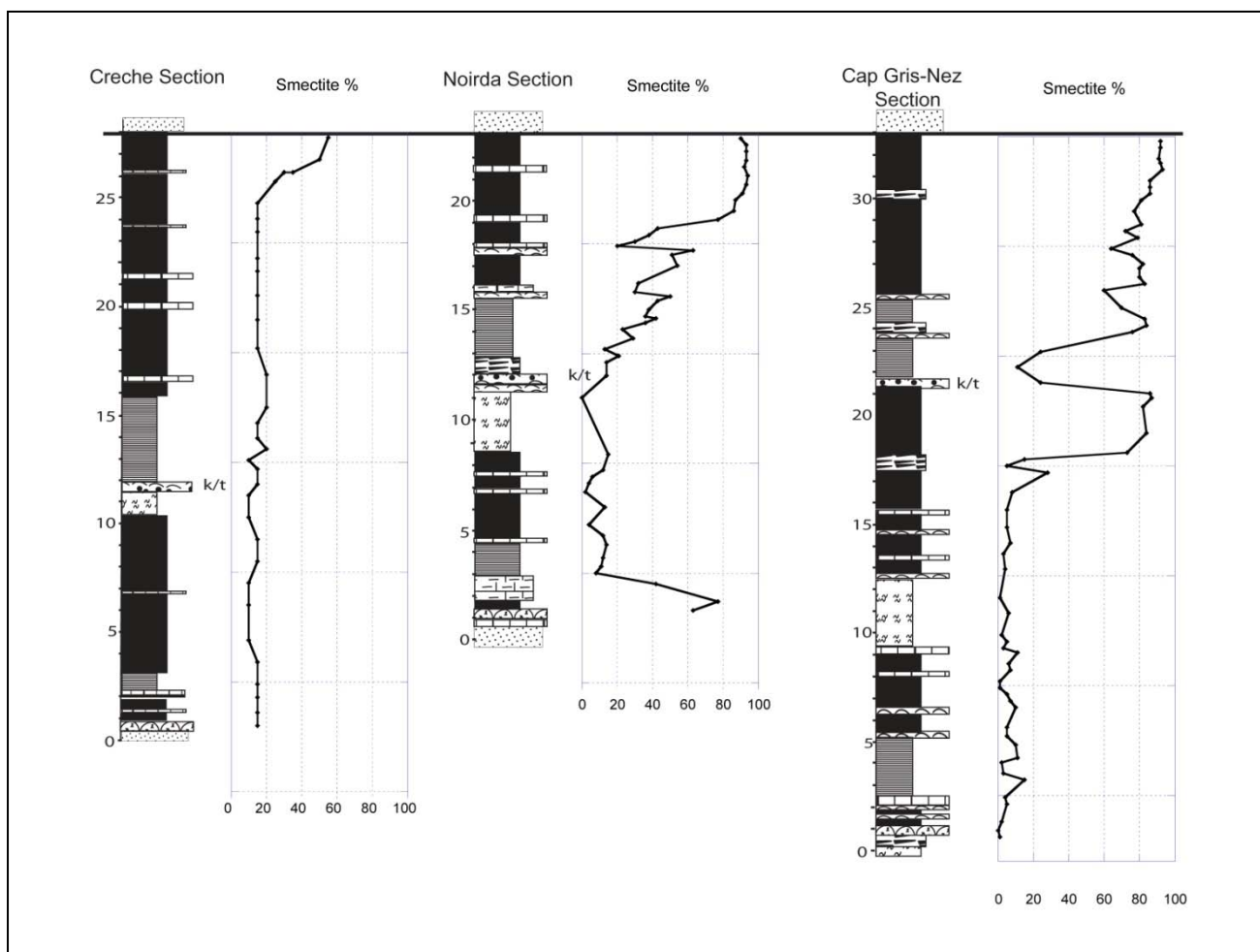


Fig. 4 - Compared stratigraphic evolution of the proportion of smectite within the clay-sized assemblages for the studied three sections.

4.4. Magnetic susceptibility and carbonate content

The stratigraphic distribution of magnetic susceptibility is, by and large, the same for the three sites, with a slight decrease upward in the section. Lastly, the vertical distribution of the carbonate content does not yield specific trends. At the Cap Gris-Nez, the high number of coquina beds induces more "noise" in the stratigraphic distribution.

4.5. Trace metals

A sample subset was analyzed for the elemental composition, 8 samples from the Cap Gris-Nez section, 19 samples from the Cran du Noirda section and 14 samples from the Cap de la Crèche section. The samples were taken below, within and above, respectively, the laminated shale levels, in order to cover a relatively wide array of TOC values. Focusing on the oxygen conditions of the depositional environment, the usual redox proxies, namely, uranium, vanadium and molybdenum (e.g., Brumsack, 2006; Tribouillard et al., 2006; Algeo and Rowe, 2012; Scott and Lyons, 2012) show no or modest enrichment. Vanadium shows a clear linear correlation to the aluminum content, which indicates a terrigenous origin. In contrast, Mo and U show poor correlation with Al. Considering enrichment factors (EF), Mo and U show EFs close to the value 1 for the Cap de la Crèche samples, which means that the elements are present in proportions identical to what is observed for the average upper crust of the Earth. In other words, no authigenic enrichment is visible for this distal section. The samples of the more proximal sections (Cap Gris-Nez and Cran du Noirda) show modest enrichments EF ranging from 1 to 6 for U and from 1 to 8 for Mo. A crossplot opposing the values of the enrichment factors of U and Mo, respectively, is drawn (Fig. 6) to decipher the oxygenation conditions of the depositional environments (see explanations of such diagrams in Algeo and Tribouillard, 2009; Tribouillard et al., 2012). All samples (mixing the three sections) fall in the "oxic to suboxic" area of the diagram, largely close to the "oxic" zone with both U and Mo keeping with enrichment-factor values below 10.

Regarding proxies for paleoproductivity (Tribouillard et al., 2006; Böning et al., 2015), nickel and copper show enrichment factors below or close to the value 1.

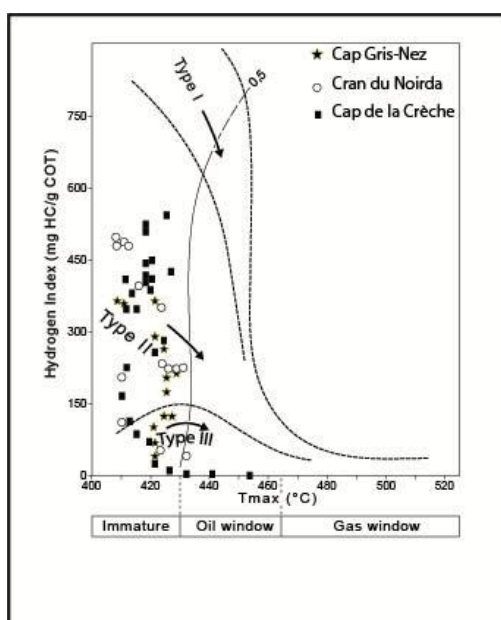


Fig. 5 – Rock Eval data .

5. Discussion

5.1. Smectite abundance and relative sea-level variations

The distribution of clay minerals along the proximal-distal transect at stake here shows that smectite is more present in the proximal environments than in the distal one. This observation is counter-intuition, in that differential settling of clays usually induces smectite prevalence in remote settings, in relation to its high floatability (Chamley, 1989). However, this observation was already expressed at least for the deposit range from the Oxfordian/Kimmeridgian Boundary to the end of the Tithonian of the Boulonnais (Schnyder et al., 2000; Hesselbo et al., 2009). These authors, grounding on their own results and those of published works, concluded that the landmass of the London-Brabant Massif was the likely source of detrital particles in the nearshore of the Boulonnais and that the low relief of this landmass would have been favorable to the steady-state erosion of smectite-rich soils. Hesselbo et al. (2009) observed the unusual occurrence of smectite in the shallowest environments throughout the Jurassic successions of the Boulonnais, whereas smectite is usually deposited in quiet offshore settings. Their interpretation is that during sea-level lowstand, the London-Brabant Massif was emerged and provided detrital smectite. Contrastingly, during sea-level highstand the massif was submerged and clay sedimentation was dominated by illite, kaolinite and I-S mixed-layer clays originating from more distant areas including Central, Armorican and Cornubian massifs. The same view may apply at the scale of the Argiles de Châtillon Fm. The formation recorded an initial sea-level rise followed by a gradual sea-level fall (Proust, 1994; Proust et al., 1993, 1995; Deconick et al., 1996). The sea-level fall was accompanied by the release of smectite from the emerged part of the London-Brabant Massif. The supply of smectite was recorded first by the proximal settings (Cap Gris-Nez) and gradually by the more distal settings (Cran du Noirda section and, in the end, Cap de la Crèche section).

What is noticeable here is that such a gradient in smectite distribution is observed on a scale of about 20 km, which is an interesting indication for all those using the composition of clay-mineral assemblages as a paleo-climatic or paleo-environmental tool. The more-or-less important abundance of smectite in an ancient sedimentary succession must be questioned in terms of sea-level variations, as well as in terms of evolution of on-land clay sources, even in small-dimension basins.

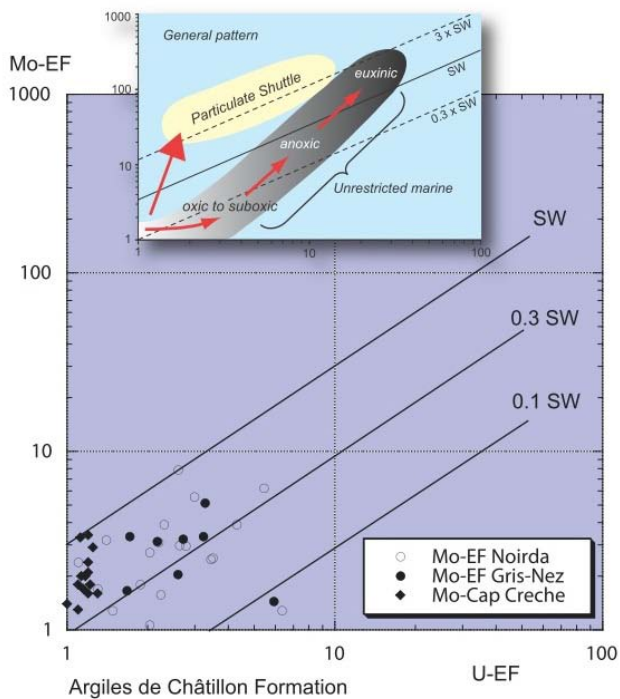


Fig. 6 - Crossplot opposing the respective enrichment factors of U and Mo for the three sections studied, as designed by Algeo and Tribovillard (2009) to derive paleoenvironmental information.

5.2. A potential oil source-rock despite lowly favorable conditions

The second point to comment is that the Argiles de Châtillon Fm. has some characteristics of a potential petroleum source rock, as well as its lateral, time-equivalent counterpart of the Kimmeridge Clay Fm. in UK (Herbin et al., 1995; Tribovillard et al., 2005). However, the Argiles de Châtillon Fm. was deposited above the storm wave base, where sediment accumulation was overwhelmed by silt-sized particles, and not clay-sized ones. The most-OM-rich levels, namely, the laminated shales, are unexpectedly not enriched in clay-sized fraction relatively to the other shales of the sections. In other words, the grain size of the clastic fraction of the sediment (clay vs. silt, which relates to pore water and dissolved-oxidant circulation and replenishment) did not preside over OM accumulation.

As far as redox conditions of deposition are concerned, the redox-proxying trace metals show that depositional conditions were not particularly prone to the development of oxygen limitation. The redox conditions may thus be termed "normal marine" for many of the samples, according to the seminal sense of the term defined by Raiswell and Berner (1985). "Normal marine" is used to refer to oxygenated conditions within the water column and at the sediment-water interface, with suboxic to anoxic conditions developing at shallow depth below this interface. Here, the relative enrichments in U and Mo observed for the proximal and intermediate sections (namely, Cap Gris-Nez and Cran du Noidra) indicate that the water column as well as the interface must have kept oxic, but for the samples yielding a detectable enrichment, reducing conditions must have got close to the sediment-water interface, inducing some diffusional capture of U and Mo (Algeo and Tribovillard, 2009; Scott and Lyons, 2012; Tribovillard et al., 2012). These redox conditions, inferred from trace metal concentrations, are corroborated by the presence of benthic foraminifers (A.Teresina, unpublished

Master thesis). Benthic foraminifer assemblages are observed in various facies of the Argiles de Châtillon Fm., including the laminated shales. The assemblages are dominated by the genus *Lenticulina* (Kandel, 1969). However, it is known that some benthic foraminifers may be present in oxygen-poor environments.

The trace elements referred to as proxies to paleoproductivity, i.e., Ni and Cu (see discussion in Tribovillard et al., 2008b; Böning et al., 2015), do not show any enrichment, thus suggesting that productivity was not high (we will not mention barium that cannot be used as a paleoproxy in the case of such relatively shallow environments). This conclusion is consistent with the one derived independently from organic parameters in the study by Tribovillard et al. (2001). The latter study concluded to productivity levels being of the same order of magnitude as that observed on today's marine platforms.

The predominance of silt over clay-sized minerals indicates that the depositional settings were not far away from shore, in turn suggesting that the sedimentation rate may have been relatively important, compared to common, clay-dominated, source rocks deposited in distal environments. In addition, the Argiles de Châtillon Fm. is (sometimes heavily) bioturbated (except for the laminated shales), which of course is not known to be a factor favorable to OM burial.

The distal-proximal gradient is observed within the Argiles de Châtillon Fm. and is best recorded by the lateral grain-size distribution. The organic content is only moderately impacted by the gradient. The land-derived, Type III, OM is expectedly a little more abundant at the Cap Gris-Nez as indicated by Rock Eval parameters (Fig. 5), but marine, Type II, OM is also present in the more proximal part of the basin. Lastly, Wignall and Newton (2001), basing on detailed facies observation, reported that oxygen levels were (at least episodically) lower in proximal settings of the Boulonnais than in more distal environments. An echo of this observation may be found in the redox-proxy distribution, since the Cran du Noirda and Cap Gris-Nez sections recorded slightly higher enrichment in Mo and U, compared to the Cap de la Crèche Section (but not reaching anoxic conditions (Fig. 6).

Thus the first conclusion is that one may encounter potential source rocks even in settings that are not a-priori prone to OM preservation and storage: relatively shallow environments dominated by deposition of silt-sized clastic particles, where sediment showing evidence of bioturbation and bio-irrigation were accumulated under normal-marine redox conditions. In addition, productivity was not high, but probably just comparable to what is observed on present platforms. The fact that the proximal-distal gradient did not impact significantly OM accumulation suggests that particle size distribution is not a first-order parameter for OM accumulation.

Despite environmental conditions that may be judged as unfavorable, or at least lowly favorable to OM preservation, the sediments studied here contain OM in noticeable abundance. The discrepancy must be explained.

5.3. Iron limitation, enhancing OM sulfurization, thence OM preservation

Within the Cap de la Crèche section, one can observe a marked enrichment in organic S-rich OM (sulfurized amorphous OM) in sediments deposited under normal marine conditions: the sediments accumulated up to several weight percents of vulcanized OM, whereas trace-metal distribution (together with the presence of benthic foraminifers and bioturbation) shows that bottom conditions were not reducing nor oxygen-deprived (except for the laminated intervals), reminding the Cap de la Crèche section has the lowest enrichment-factors values for U and Mo (see Tribovillard et al. 2001

for detail about the abundance of AOM in this section). The other two sections studied shows lower TOC values. In addition, the strong S-rich OM accumulation of the Cap de la Crèche took place under conditions of moderate productivity. This observation is not common, since accumulation of abundant, sulfurized OM has been attributed hitherto for paleo-environments characterized by high productivity and/or low terrigenous supply (review in Vandenbroucke and Largeau, 2007). In a few words, OM sulfurization takes place when sulfide ions can react with functionalized organic molecules, which implies that all the sulfide ions are not monopolized by Fe(II). An iron deficiency, either relative or absolute, will favor sulfide-OM interactions. If reactive iron is little or not supplied to the depositional environment, the iron deficiency will be termed as absolute. If reactive iron is actually supplied, but if a high organic flux is also present (in case of high productivity), the large pool of sulfide ions generated through bacterial sulfate reduction (at the expense of OM) will exhaust the reactive iron pool. As a consequence, sulfide will be available for sulfurization (Zaback et al., 1993; Tribouillard et al., 1994).

In the case of the Argiles de Châtillon, according to the information gathered from previous studies about the Cap de la Crèche section (Tribouillard et al., 2015), the Fe/Al ratio is most of the time close to the « stoichiometric » value of the averaged upper crust (0.44; McLennan, 2001) or slightly above it (mean Fe/Al = 0.53; n = 63). In the previous studies evoked above (Tribouillard et al., 2015), the part of the Fe content that is postulated to be in excess relative to the clastic fraction-associated part of the iron inventory (called Fe_{xs}) was calculated: taking into consideration the long diagenetic history of the sediments deposited about 152 millions years ago, as well as the detrital nature of the studied sedimentary rocks, it is considered that the chemically-inert fraction of the iron content was the part incorporated into the lattices of alumino-silicates; this non-reactive, or detrital part is calculated according to the following formula:

$$Fe_{detrital} = [Al]_{sample} \times [Fe]/[Al]_{upper\ crust}, \text{ with } [Fe]/[Al]_{upper\ crust} = 0.44 \text{ (McLennan, 2001).}$$

The iron content in excess to the detrital part then derived using the formula:

$$Fe_{xs} = Fe_{total} - Fe_{detrital}.$$

This fraction Fe_{xs} is considered to give a good estimate of the « paleo » reactive-iron proportion, regardless of its present mineralogical carrier phase, after the successive steps of long-term diagenesis (see Scholz et al., 2014). In the case of the Cap de la Crèche section, Fe_{xs} represents 16% on average of the total Fe inventory (Tribouillard et al., 2015). Thus it is inferred that the amount of reactive iron was relatively limited in the sediments of this section. It is concluded that sulfate-reducing reactions, induced by bacterially-mediated OM remineralization, operated with sediments rich in land-derived, clastic fractions, but limited in reactive iron (despite abundant silt and clay fractions). Consequently, OM could react with free ("unemployed") sulfide ions and accumulate organic sulfur. This sulfurization protected OM against further bacterial remineralization and permitted its accumulation in relatively large proportions. The important point is that reactive-iron limitation triggered OM sulfurization in spite of a relatively low supply of OM: remineralizing a large pool of OM producing enough sulfide to immobilize all the reactive iron ions was not required, since the reactive iron pool was limited. Consequently, although the OM flux must have been moderate (moderate surface productivity), OM was protected through sulfur incorporation and thence stored in relatively large amounts.

Excess iron is significantly more abundant in the other two sections that are more proximal than the Cap de la Crèche section. Fe_{xs} represents 32% on average of the total Fe inventory in the Noirda

section, and 30% in the Cap de la Crèche section (Table XX). For these two sections that are poorer in organic carbon than the Cap de la Crèche section, TOC values seem to be negatively correlated to the relative abundance of excess iron. The determination coefficient is of only 0.04 ($n = 12$) for the Gris Nez samples but is 0.61 ($n = 14$) for the Noirda samples. These results suggest that an increased amount of reactive iron may be associated to a decreased preservation of OM, but our data set does not allow us evidencing any clear-cut linear relation.

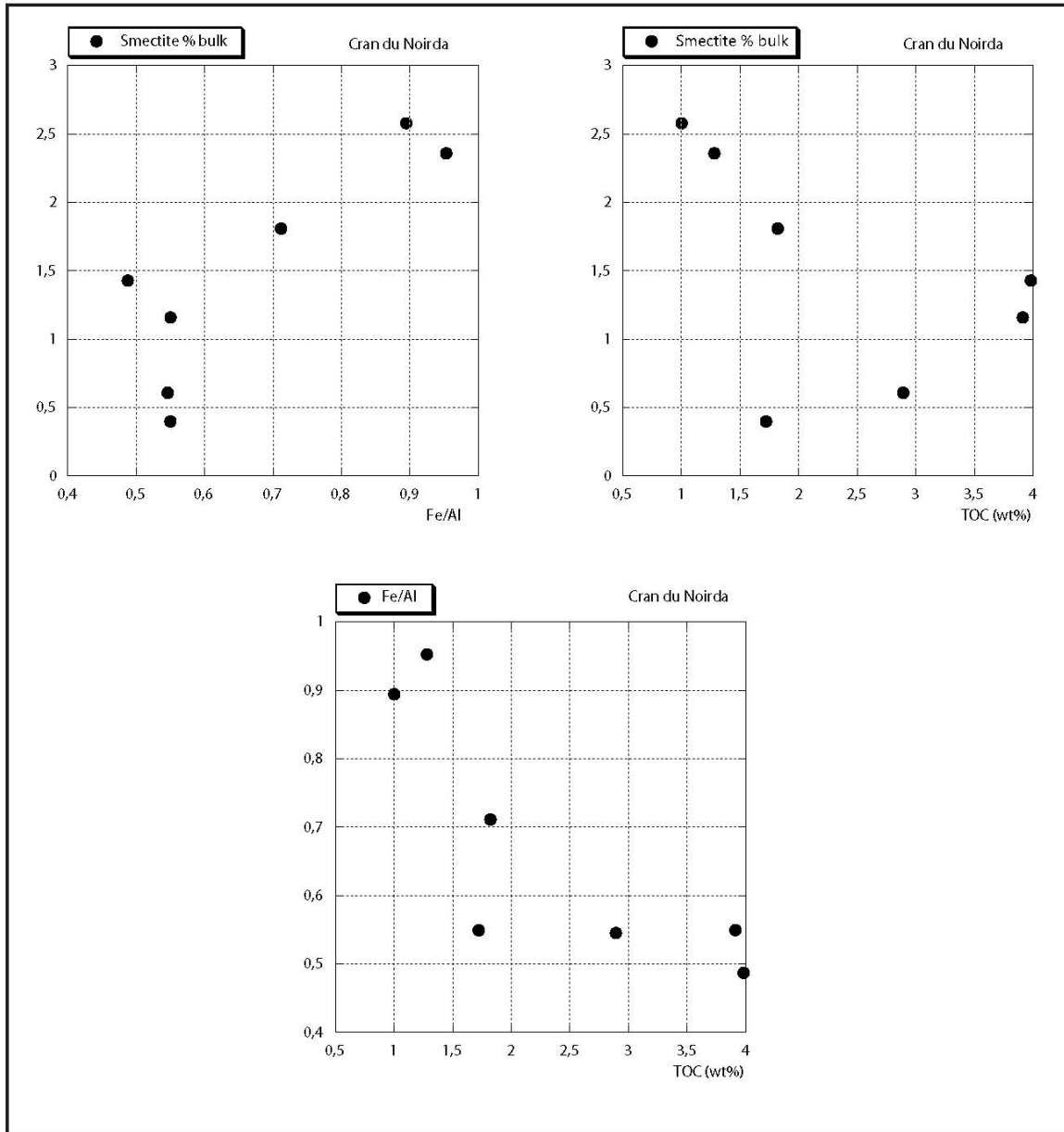


Fig. 7 – Crossplots illustrating the relationships between the Fe/Al ratio, TOC values and the proportion of smectite within the carbonate-free fraction of the bulk rock.

Iron, as an agent favoring OM remineralization was extensively discussed by Meyers et al. (2005) and Meyers (2007). For these authors, a relatively abundant flux of reactive iron will allow buffering dissolved sulfide via iron sulfidization (Canfield et al., 1992; Raiswell and Canfield, 1996). Dissolved sulfide is thus put "harmless", which will stop preventing the presence of infauna. The possible

presence of in-fauna will increase bioturbation and bio-irrigation, required to maintain oxidants such as dissolved oxygen and nitrate in pore waters, and hence enhance OM remineralization. Furthermore, active bioturbation and bio-irrigation can expand the thickness of the zone of aerobic OM degradation, thus increasing the exposure time of OM to dissolved oxygen. Reversely, these factors fostering OM degradation will be much tempered in case of reactive-iron limitation (Meyers, 2007). Our work adds one positive effect of iron limitation regarding OM accumulation: the sulfide ions, maintained at relatively high concentration in the dissolved state (if no iron-induced buffering takes place), as is the case for the Cap de la Crèche samples, will induce OM sulfurization, thus fostering OM preservation and hence, its burial. This OM accumulation is possible even in the case when OM is not particularly abundant, as is the case here.

Now an additional question is about the reason(s) why a relative iron deficiency may be observed in the case of the Cap de la Crèche, because the sediments are rich in fine-grained particles (silts and clays), which is a priori favorable to the presence of adsorbed iron ions (Burdige, 2006).

5.4. The causes of the reactive-iron deficiency or presence

The Argiles de Châtillon Fm. was deposited under relatively distal conditions accompanied by occasionally-reduced sedimentation rates, in a general context of sea-level rise (see Proust et al., 1995 or Wignall and Newton, 2001 for a detailed sequence stratigraphy description). Generally speaking, the reactive-iron supply to a basin may be conditioned by several factors.

- 1) The relative width of the platform being flooded during sea-level rise. The larger the transgression, the larger the volume of reworked and remobilized sediments, which will impact the possible release of iron being coating fine particles.
- 2) The flux of river-borne (Severmann et al., 2010) or air-borne (e.g., Baddock et al., 2013; Buck et al., 2013) iron-coated particles;
- 3) The flux of OM possibly associated with reactive iron (e.g., Krachler et al., 2012; Shigemitsu et al., 2013; Bressac and Huie, 2013; Barber et al., 2014). Notably, Krachler et al. (2012) indicated that peatland-derived iron-bearing lignin particles may have a sufficiently long half-life in ocean water to sustain iron concentration in extended regions of the ocean.

In parallel, iron may be redistributed with the marine environment itself. The current model (Poulton and Raiswell, 2002; Poulton and Canfield, 2005; Anderson and Raiswell, 2004; Lyons and Severmann, 2006; Owen et al., 2012; Rickard, 2012; Raiswell and Canfield, 2012; Scholz et al., 2013, 2014) explains how detrital iron deposited on the shelf may undergo suboxic diagenesis, thus releasing dissolved Fe (II). This aqueous iron may diffuse out of the sediment through the sediment-water interface where it is mainly oxidized and trapped as reprecipitated Fe(III) oxyhydroxides. Nevertheless a fraction of the dissolved iron thus released may be transported to the deeper (possibly euxinic) parts of the basin where it will be sequestered as iron sulfide (see discussion in Little et al., 2015).

Discussing these factors is rather hypothetical in the case of the Argiles de Châtillon, even if each of them can apply to the situation. That is why the attention will be instead focused on the composition of clay-mineral assemblages.

5.4.1. Iron and clay-mineral assemblages

The clay-mineral assemblages observed in the Boulonnais are composed of illite and kaolinite

opposed in abundance to smectite, plus illite-smectite mixed-layer minerals and chlorite, the latter being negligible (Deconinck et al., 1982, 1996). Smectite is a potential carrier phase for reactive iron, whereas illite and kaolinite are less prone to be coated by reactive iron (Chamley, 1989; Canfield et al., 1992; 1996). Structural iron, relatively abundant in illite, cannot be considered to be reactive as long as it is part of the mineral lattice. Thus, attention must be paid to the relations between smectite abundance and iron proportions. Concerning the Cap de la Crèche Section, the decarbonated fraction of the rocks of the entire section contain between 7 and 25% of clay-sized fraction ($<4\mu\text{m}$), and within the clay fraction itself, smectite amounts to less than 25% all along the section but the top three meters, inducing that smectite represents between 1 and 4% of the clastic fraction of the rock, which is negligible. Contrastingly, in the Cran du Noirda section with 5-17% clay fraction, and with 0-93% of smectite in the clay assemblage, smectite represents between 0 and 11% of the clastic fraction of the rock composition. In the proximal Cap Gris-Nez section with 5-25% clay fraction, and with 0-93% of smectite in the clay assemblage, smectite represents between 0 and 7% of the clastic fraction of the rock composition. For the sample subsets for which data about both the clay-mineral assemblages and geochemical composition, one can observe a positive correlation between the proportion of smectite within the bulk decarbonated fraction of the rock and the relative reactive-iron abundance, as well as a negative relationship between bulk smectite and TOC in the case of the Noirda section (Fig. 7). In the case of the Cap Gris-Nez section, a clear negative correlation is drawn between bulk smectite and TOC.

With this small sample set, we cannot be ambitious in our interpretations, but we suggest that first, smectite could be associated with reactive iron and, second reactive iron could be associated with reduced OM preservation.

The inference is twofold. First, if true, a correlation between reactive iron and smectite indicates that the amount of clay, even when present in relatively low proportions in the sediments of rocks, may have a significant impact on bulk-rock chemical composition. Second, and maybe more crucial, the correlation indicates that smectite may govern (at least partly) the amount of reactive iron of the sediment, which in turn impacts OM preservation. A higher abundance of reactive iron, capturing free sulfide and hence hampering OM sulfuration, may limit OM preservation. It is thus suggested that the amount of smectite may have a negative imprint on OM preservation and accumulation.

This interpretation is in partial contradiction with usual interpretations. Clay minerals, especially smectite, are considered to have a positive effect regarding OM accumulation (Zhang et al., 2014, and references therein): OM is frequently associated with fine-grained clay minerals, due to their high surface area and strong adsorption capacity. In clay-rich sediments, OM abundance is commonly correlated with smectite abundance). This correlation suggests that the expandable internal surface of smectite (i.e., interlayer region) can sequester large amounts of organic matter (Kennedy and Wagner, 2011). Indeed, it has been suggested that enhanced organic matter preservation in sediments is largely due to increased smectite abundance in sedimentary record through geological time (Kennedy et al., 2006): organic matter, once associated with smectite-rich sediments, would be physically protected against microbial oxidation (see details in Zhang et al., 2014).

Our preliminary results bring new and complementary views about what is currently known regarding the role of smectite played in OM accumulation. However our results are obviously too fragmentary and need further testing on other geological formations.

6. Conclusions

This work, synthesizing several previously published results and bringing new data on the detrital fraction of the rocks belonging to the Argiles de Châtillon Fm., allows us having a consistent, multi-parameter, view of the depositional conditions that favored OM accumulation. Some of our conclusions are neither restricted to the Argiles de Châtillon Fm., nor to the Boulonnais Region, but may be extended to many other clastic-dominated, relatively shallow, platform environments where black shales or even possible oil source-rocks were accumulated. The first “take-home” message is that OM may be accumulated up to a few weight percents of organic carbon in rocks largely dominated by silt and with only < 20% clay-sized minerals, and showing evidence of bioturbation and deposited under conditions of moderate productivity. The second teaching is that our results suggest that the clay-mineral assemblages may have a significant impact on reactive iron abundance even when the clay fraction is present in modest proportions compared to silt. The third message is that smectite, usually considered to have a positive influence on OM adsorption and preservation, may also have a negative impact when this mineral can carry and release reactive iron. This iron may in turn react with sulfide ions released from OM decay mediated by sulfate-reducing bacteria, which prevents free sulfide to react with OM. OM sulfurization being limited by the capture of free sulfide by reactive iron, OM preservation and accumulation will be hampered. However, this third message is suggested by our (quite simplistic) observations but still needs to be tested with other geological settings. Furthermore, even if our hypothesis is further confirmed, the exact mechanism is still to be determined: is reactive iron release by desorption from clay-mineral surface or by structural iron being reduced and solubilized through bacterial activity or diagenesis? Lastly, this study shows that a gradient in smectite distribution may be observed on a scale even as small as about 20 km, resulting from the way sea-level variations (re-) mobilize the on-land clay-mineral inventories. The more-or-less important abundance of smectite in an ancient sedimentary succession must be questioned in terms of sea-level variations, as well as in terms of evolution of on-land clay sources, even in small-dimension basins.

References

- Ager, D. & Wallace, P. (1966). The environmental history of the Boulonnais, France. Proc. Geol. Assoc., 77, 385-417.
- Ager, D. & Wallace, P. (1970). The distribution and significance of trace fossils in the uppermost Jurassic rocks of the Boulonnais, Northern France. In Crimes, T.P. & Harper, C. (eds) Trace fossils, Geol. Journ., spec. issue 3, 1-17.
- Al-Ramadan, K., Morad, S., Proust, J.-N., Al-Aasm, I., 2005. Distribution of diagenetic alterations in siliciclastic shoreface deposits within a sequence stratigraphic Framework: evidence from the upper Jurassic Boulonnais, NW France. Journal of Sedimentary Research, 75, 943-959.
- Algeo, T.J., Rowe, H., 2012. Paleoceanographic applications of trace-metal concentration data. Chemical Geology, 324–325, 6-18.
- Algeo, T.J., Tribouillard, N., 2009. Environmental analysis of paleoceanographic systems based on molybdenum-uranium covariation. Chemical Geology, 268, 211-225.
- Anderson, T.F., Raiswell, R., 2004. Sources and mechanisms for the enrichment of highly reactive iron in euxinic Black Sea sediments. American Journal of Science, 304, 203–233.

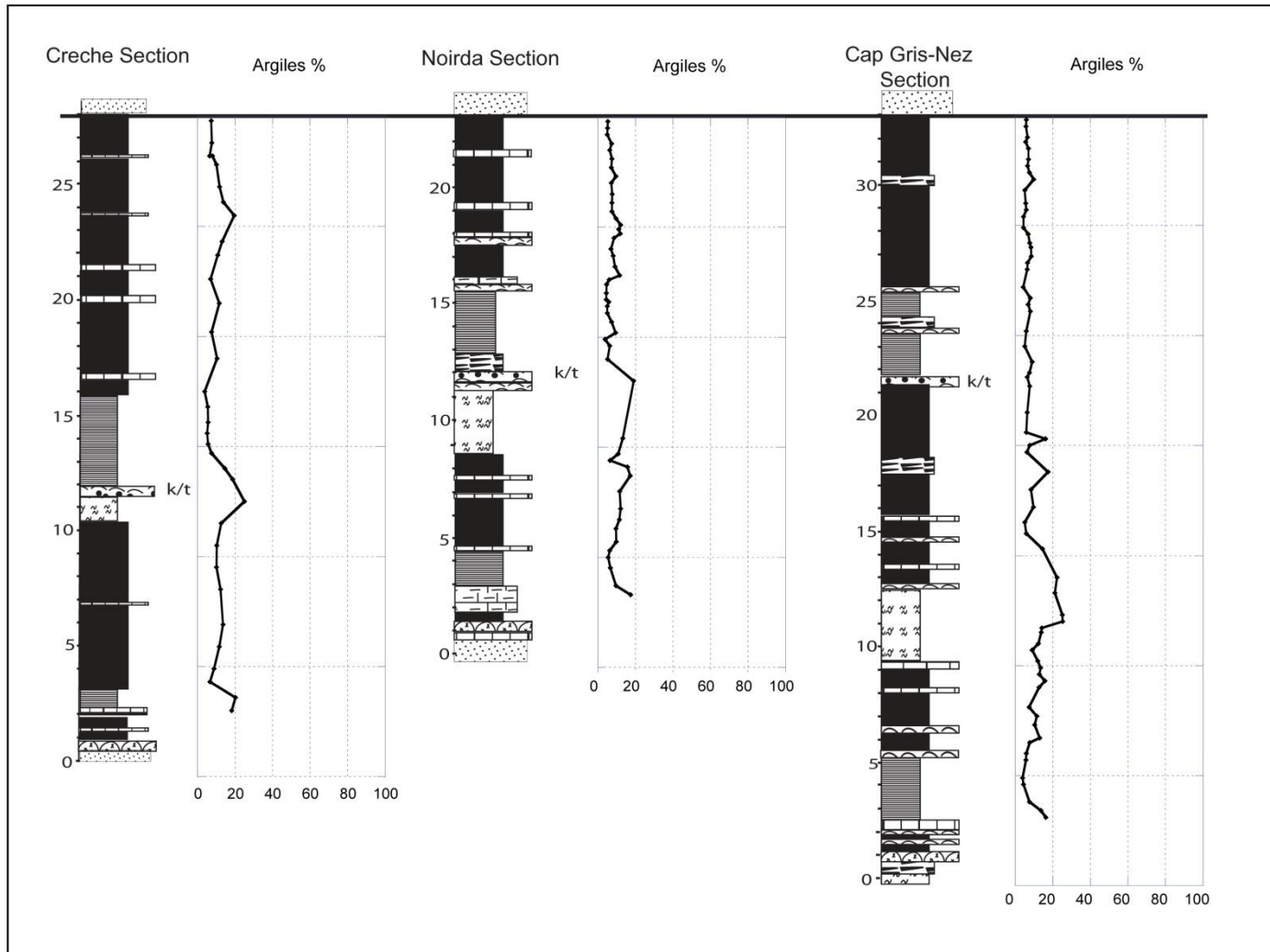
- Baddock, M., Boskovic, L., Strong, C., McTainsh, G., Bullard, J., Agranovski, I., Cropp, R., 2013. Iron-rich nanoparticles formed by aeolian abrasion of desert dune sand. *Geochemistry, Geophysics, Geosystems*, 14, 3720–3729.
- Barber, A., Lalonde, K., Mucci, A., Gélinas, Y., 2014. The role of iron in the diagenesis of organic carbon and nitrogen in sediments: a long-term incubation experiment. *Marine Chemistry*, 162, 1-9.
- Barnard, T. & Shipp, D.J. (1981). Kimmeridgian foraminifera from the Boulonnais. *Revue de Micropaléontologie*, 24, 3-26.
- Behar, F., Beaumont, V., De B. Penteado, H.L., 2001. Technologie Rock-Eval 6 : performances et développements. *Oil Gas Sci. Technol. Rev. Inst. Français Pétrole* 56, 111–134.
- Bialkowski, A., Tribouillard, N., Vergès, E., Deconinck, J.-F., 2000. Etude haute résolution de la distribution et de la granulométrie des constituants organiques sédimentaires. Corrélations avec les variations du niveau marin. *Kimméridgien/Tithonien du Boulonnais (Nord de la France)*. *Comptes Rendus Académie des Sciences, Paris*, II, 331, 451-458.
- Böning, P. Shaw, T., Pahnke, K., Brumsack, H.-J., 2015. Nickel as indicator of fresh organic matter in upwelling sediments. *Geochimica et Cosmochimica Acta*, 162, 99-108.
- Boussafir, M., Gelin, F., Lallier-Vergès, E., Derenne, S., Bertrand, Ph., Largeau, C., 1995a. Electron microscopy and pyrolysis of kerogens from the Kimmeridge Clay Fm., UK: source organisms, preservation processes and origin of microcycles. *Geochim. Cosmochim. Acta*, 59, 3731-3747.
- Boussafir, M., Lallier-Vergès, E., Bertrand, Ph., Badaut-Trauth, D., 1995b. SEM and STEM studies on isolated organic matter and rock microfacies from a short-term organic cycle of the Kimmeridge Clay Formation (Yorkshire, UK). In: Lallier-Vergès, E., Tribouillard, N.-P. & Bertrand, Ph. (eds.) *Organic matter accumulation. Lecture Notes in Earth Sciences*, 57, Springer, pp. 15-30.
- Boussafir, M., Lallier-Vergès, E., Bertrand, Ph., Badaut-Trauth, D., 1994. Structure ultrafine de la matière organique dans des roches mères du Kimméridgien du Yorkshire (UK). *Bulletin Société Géologique de France*, 165, 353-361.
- Bout-Roumazeilles, V., Cortijo, E., Labeyrie, L., Debrabant, P., 1999. Clay-mineral evidence of nepheloid layer contribution to the Heinrich layers in the Northwest Atlantic. *Palaeogeography, Palaeoclimatology, Palaeoecology*, 146, 211-228.
- Braaksma, H., Proust, J.-N., Kenter, J.A.M., Drijkonigen, G.G., Filippidou, N., 2006. Sedimentological, petrophysical, and seismic characterization of an upper Jurassic shoreface-dominated shelf margin (the Boulonnais, Northern France). *Journal of Sedimentary Research*, 76, 175–199.
- Bressac, M., Huie, C., 2013. Post-depositional processes: what really happens to new atmospheric iron in the ocean's surface? *Global Biogeochemical Cycles*, 27, 1-12, doi:10.1002/gbc.20076.
- Brigaud B., Pucéat E., Pellenard P., Vincent B. Joachimski M.M. Climatic fluctuations and seasonality during the Late Jurassic (Oxfordian-Early Kimmeridgian) inferred from delta O-18 of Paris Basin oyster shells. *EPSL*, 273, 1-2, 58-67.
- Brumsack H.-J., 2006. The trace metal content of recent organic carbon-rich sediments: Implications for Cretaceous black shale formation. *Palaeogeography, Palaeoclimatology, Palaeoecology*, 232, 344-361.
- Buck, C.S., Landing, W.M., Resing, J.A., 2013. Pacific Ocean aerosols: deposition and solubility of iron, aluminum, and other trace elements. *Marine Chemistry*, 157, 117-130.
- Burdige, D.J., 2006. *Geochemistry of marine sediments*. Princeton University Press, 609 p.
- Canfield D.E, Lyons, T.W., Raiswell, R., 1996. A model for iron deposition to euxinic Black Sea sediments. *American Journal of Science*, 296, 818-834.
- Canfield, D. E., Raiswell, R., Bottrell, S., 1992. The reactivity of sedimentary iron minerals toward sulfide. *American Journal of Science*, 292, 659–683.
- Carignan, J., Hild, P., Morel J., Yeghicheyan, D., 2001. Routine analysis of trace elements in geochemical samples using flow injection and low-pressure on-line liquid chromatography coupled to ICP-MS: a study of geochemical reference materials BR, DR-N, UB-N, AN-G and GH. *Geostandard Newsletter*, 25, 187-198.
- Chamley, H., 1989. *Clay Sedimentology*. Springer, Berlin, 623 p.
- Cox, B.M., Gallois, R.W, 1981. The stratigraphy of the Kimmeridge Clay of the Dorset type area and its correlation with some other Kimmeridgian sequences. *Rep. Instit. geol. Sci.* 80/4.
- Deconinck, J.-F., Chamley, H., Debrabant, P., Colbeaux, J.-P., 1982. Le Boulonnais au Jurassique supérieur : données de la minéralogie des argiles et de la géochimie. *Annales de la Société Géologique du Nord*, T. CII, p. 145-152.
- Deconinck, J.-F., Geyssant, J.R., Proust, J.-N., Vidier, J.P., 1996. Sédimentologie et biostratigraphie des dépôts kimméridgiens et tithoniens du Boulonnais. *Annales de la Société Géologique du Nord*, 4, 157-170.

- Derenne, S., Largeau, C., Casadevall, E., Berkaloff, C., Rousseau, B., 1991. Chemical evidence of kerogen formation in source rocks and oil shales via selective preservation of thin resistant outer walls of microalgae : origin of ultralaminae. *Geochimica et Cosmochimica Acta*, 55, 1041-1050.
- Dera G., Brigaud B., Monna F., Laffont R., Pucéat E., Deconinck J.F., Pellenard P., Joachimski M.M. & Durlet C. 2011. Climatic ups and downs in a disturbed Jurassic world. *Geology*, 39, 3, 215-218.
- Dunn, C.E., 1972. Trace Element Geochemistry of Kimmeridge Sediments in Dorset, North West France and Northern Spain. Ph.D. thesis, University of London.
- El Albani, A., Deconinck, J.-F., Herbin, J.-P. & Proust, J.-N., 1993. Caractérisation géochimique de la matière organique et minéralogie des argiles du Kimméridgien du Boulonnais. *Annales de la Société Géologique du Nord*, 2 (2ème série), 113-120.
- Espitalié, J., Deroo, G. and Marquis, F. (1986). La pyrolyse Rock Eval et ses applications. Part B Rev. Inst. Franç. Pétr., 40, 755-784.
- Fürsich, F.T & Oschmann, W. (1986). Storm shell beds of *Nanogyra virgula* in the Upper Jurassic of France. *Neues Jahrbuch Geologische Paläontologische Abhandlungen*, 172, 141-161.
- Gelin, F., Boussafir, M., Derenne, S., Largeau, C. and Bertrand, Ph., 1995. Study of qualitative and quantitative variations in kerogen chemical structure along a microcycle: correlation with ultrastructural features. in: Lallier-Vergès, E., Tribouillard, N.-P. and Bertrand, Ph. (eds.) *Organic matter accumulation. Lecture Notes in Earth Sciences*, 57, Springer, pp. 32-47.
- Gelin, F., Volkmann, J.K., Largeau, C., Derenne, S., Sinninghe Damsté, J.S. and de Leeuw, J.W., 1999, Distribution of aliphatic, non-hydrolyzable biopolymers in marine microalgae. *Org. Geochem.*, 30, 147-159.
- Geyssant, J.R., Vidier, J.-P., Herbin, J.-P., Proust, J.N., Deconinck, J.-F., 1993. Biostratigraphie et paléoenvironnement des couches de passage Kimméridgien/Tithonien du Boulonnais (Pas de Calais): nouvelles données paléontologiques (ammonites), organisation séquentielle et contenu en matière organique. *Géologie de la France*, 4, 11-24.
- Hatem, E., Tribouillard, N., Averbuch, O., Vidier, D., Sansjofre, P., Birgel, D., Guillot, F., 2014. Oyster patch reefs as indicators of fossil hydrocarbon seeps induced by synsedimentary faults. *Marine and Petroleum Geology*, 55, 176-185.
- Herbin J. P., Fernandez-Martinez J.L., Geyssant J.R., El Albani A., Deconinck J.-F. Proust J.-N., Colbeaux J.-P. & Vidier J.P. (1995). - Sequence stratigraphy of source rocks applied to the study of the Kimmeridgian/Tithonian in the Northwest European shelf (Dorset/UK, Yorkshire/UK and Boulonnais/France). - *Mar. Petrol. Geol.*, 12, 177-194.
- Herbin J.P., Müller C., Geyssant J., Mélières F. & Penn I.E. (1991) Hétérogénéité quantitative et qualitative de la matière organique dans les argiles du Val de Pickering (Yorkshire, U.K.) : cadre sédimentologique et stratigraphique, *Rev. Inst. Fr. Pétr.*, 46, 675-712.
- Herbin, J. P. & Geyssant, J.R., 1993. "Ceintures organique" au Kimméridgien/Tithonien en Angleterre (Yorkshire, Dorset) et en France (Boulonnais). *C. R. Acad. Sci. Paris*, 317 (II), 1309-1316.
- Herbin, J. P., Fernandez-Martinez, J.L., Geyssant, J.R., El Albani, A., Deconinck, J.-F., Proust, J.-N., Colbeaux, J.-P. & Vidier, J.P., 1995. Sequence stratigraphy of source rocks applied to the study of the Kimmeridgian/Tithonian in the north-west European shelf (Dorset/UK, Yorkshire/UK and Boulonnais/France). *Mar. Petrol. Geol.*, 12, 177-194.
- Hesselbo, S.P., Deconinck, J.-F., Huggett, J.M., Morgans-Bell, H.S., 2009. Late Jurassic palaeoclimatic change from clay mineralogy and gamma-ray spectrometry of the Kimmeridge Clay, Dorset, UK. *Journal of the Geological Society, London*, 166, 1123–1133.
- Kennedy, M., Droser, M., Mayer, M.L., Pevear, D., Mrofka, D., 2006. Late Precambrian oxygenation; Inception of the clay mineral factory. *Science*, 311, 1446–1449.
- Kennedy, M.J., Wagner, T., 2011. Clay mineral continental amplifier for marine carbon sequestration in a greenhouse ocean. *Proc. Natl. Acad. Sci. U. S. A.* 108, 9776–9781.
- Krachler, R., F. von der Kammer, F. Jirska, A. Süphandag, R. F. Krachler, C. Plessl, M. Vogt, B. K. Keppler, and T. Hofmann, 2012. Nanoscale lignin particles as source of dissolved iron to the ocean. *Global Biogeochemical Cycles*, 26, GB3024, doi:10.1029/2012GB004294.
- Lafargue, E., Marquis, F., Pillot, D., 1998. Les applications de Rock-Eval 6 dans l'exploration et la production des hydrocarbures, et dans les études de contamination des sols. *Oil Gas Sci. Technol. Rev. Inst. Français Pétrole* 53, 421–437.
- Largeau, C., Derenne, S., Casadevall, E., Berkaloff, C., Corolleur, M., Lugardon, Raynaud, J.F., Connan, J., 1990. Occurrence and origin of "ultralaminar" structures in "amorphous" kerogens of various source rocks and oil shales. *Advance in Organic Geochemistry* 89. *Org. Geochem.*, 16, 889-895.
- Little, S.H., Vance, D., Lyons, T.W., McManus, J., 2015. Controls on trace metal authigenic

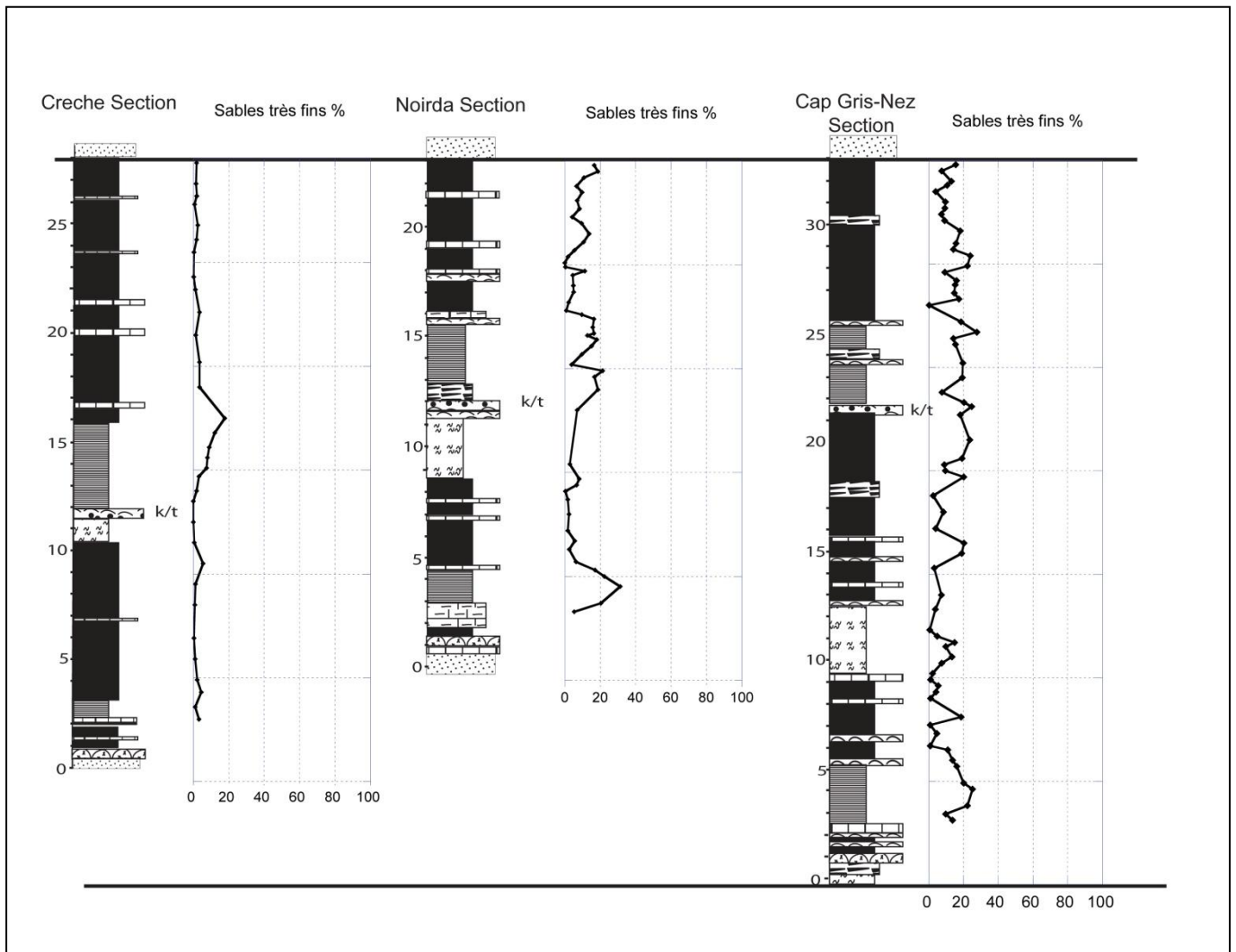
- enrichment in reducing sediments: insights from modern oxygen-deficient settings. *American Journal of Science*, 315, 77–119, DOI 10.2475/02.2015.01].
- Lyons, T.W., Severmann, S., 2006. A critical look at iron paleoredox proxies based on new insights from modern euxinic marine basins. *Geochimica et Cosmochimica Acta*, 70, 5698–5722.
- Mansy, J.-L., Guennoc, P., Robaszynski, F., Amedro, F., Auffret, J.-P., Vidier, J.-P. Lamarche, J., Lefèvre, D., Sommé, J., Brice, D., Mistiaen, B., Prud'homme, A., Rohart, J.-C., Vachard, D., 2007. Notice explicative, carte géologique de la France (1/50 000), feuille Marquise, second ed. BRGM, Orléans, p. 213.
- McLennan, S.M., 2001. Relationships between the trace element composition of sedimentary rocks and upper continental crust. *Geochemistry, Geophysics, Geosystems*, 2, 2000GC000109.
- Meyers, S.R., 2007. Production and preservation of organic matter: the significance of iron. *Paleoceanography*, 22, PA4211. doi:10.1029/2006PA001332.
- Meyers, S.R., Sageman, B.B., Lyons, T.W., 2005. Organic carbon burial rate and the molybdenum proxy: theroretical framework and the application to Cenomanian-Turonian oceanic anoxic event 2. *Paleoceanography*, 20, PA2002, doi: 10.1029/2004PA001068.
- Mongenot, T., Boussafir, M., Derenne S., Lallier-Vergès, E., Largeau, C., Tribouillard, N., 1997. Sulphur-rich organic matter from Bituminous Laminites of Orbagnoux (France, upper Kimmeridgian) - the role of early vulcanization. *Bulletin de la Société géologique de France*, 168 (3), 331-341.
- Owens, J.D., Lyons, T.W., Li , X., Macleod, K.G., Gordon, G., Kuypers, M.M.M., Anbar, A., Kuhnt, W., Severmann, S., 2012. Iron isotope and trace metal records of iron cycling in the proto-North Atlantic during the Cenomanian-Turonian oceanic anoxic event (OAE-2). *Paleoceanography*, 27, PA3223, doi:10.1029/2012PA002328.
- Poulton, S.W., Canfield, D.E., 2005. Development of a sequential extraction procedure for iron: implications for iron partitioning in continentally derived particulates. *Chemical Geology*, 214, 209–221.
- Poulton, S.W., Raiswell, R., 2002. The low-temperature geochemical cycle of iron: from continental fluxes to marine sediment deposition. *American Journal of Science*, 302, 774-805.
- Proust, J.-N., 1994. Notions élémentaires de stratigraphie séquentielle illustrées par un exemple. *Ann. Soc. Géol. du Nord*, 3 (II), 5-25.
- Proust, J.-N., Deconinck, J.-F., Geyssant, J.R., Herbin, J.-P., Vidier, J.-P., 1993. Nouvelles données sédimentologiques dans le Kimmérigien et le Tithonien du Boulonnais (France). *C. R. Acad. Sci. Paris*, 316, (II), 363-369.
- Proust, J.-N., Deconinck, J.-F., Geyssant, J.R., Herbin, J.-P., Vidier, J.P., 1995. Sequence analytical approach to the Upper Kimmeridgian-Lower Tithonian storm-dominated ramp deposits of the Boulonnais (Northern France). A landward time-equivalent to offshore marine source rocks. *Geologische Rundschau*, 84, 255-271.
- Raiswell, R., Berner, R.A., 1985. Pyrite formation in euxinic and semi-euxinic sediments. *Amer. J. Sci.*, 285, 710-724.
- Raiswell, R., Canfield, D.E., 1996. Rates of reaction between silicate iron and dissolved sulfide in Peru Margin sediments. *Geochimica et Cosmochimica Acta*, 60, 2777-2787.
- Raiswell, R., Canfield, D.E., 2012. The iron biogeochemical cycle past and present. *Geochemical Perspective*, 1, 1-186.
- Rickard, D., 2012. Sulfidic sediments and sedimentary rock. *Developments in Sedimentology*, 65, Elsevier, 801 p.
- Schlirf, M., 2003. Palaeoecologic significance of Late Jurassic trace fossils from the Boulonnais, N France. *Acta Geologica Polonica*, 53, 123-142.
- Schnyder, J., Baudin, F., Deconinck, J.F., Durlet, C., Jan du Chêne, R., Lathuilière, B., 2000. Stratigraphie et analyse sédimentologique du passage Oxfordien/Kimmérigien dans le Boulonnais. *Géologie de la France*, 4, 21 – 37.
- Scholz, F., McManus, J., Sommer, S., 2013. The manganese and iron shuttle in a modern euxinic basin and implications for molybdenum cycling at euxinic ocean margins. *Chemical Geology*, 335, 56-68.
- Scholz, F., Severmann, S., McManus, J., Hensen, C., 2014. Beyond the Black Sea paradigm: The sedimentary fingerprint of an open-marine iron shuttle. *Geochimica et Cosmochimica Acta*, 127, 368–380.
- Scott, C., Lyons, T.W., 2012. Contrasting molybdenum cycling and isotopic properties in euxinic versus non-euxinic sediments and sedimentary: refining the paleoproxies. *Chemical Geology*, 324-325, 19-27.
- Severmann, S., McManus, J., Berelson, W.M., Hammond, D.E., 2010. The continental shelf benthic

- iron flux and its isotope composition. *Geochimica et Cosmochimica Acta*, 74, 3984-4004.
- Shigemitsu, M., Nishioka, J., Watanabe, Y.W., Yamanaka, Y., Nakatsuka, T., Volkov, Y.N., 2013. Fe/Al ratios of suspended particulate matter from intermediate water in the Okhotsk Sea: Implications for long-distance lateral transport of particulate Fe. *Marine Chemistry*, 157, 41-48.
- Tegelaar, E.W., de Leeuw, J.W., Derenne, S., Largeau, C., 1989. A reappraisal of kerogen formation. *Geochim. Cosmochim. Acta*, 53, 3103-3106.
- Trentesaux, A., Récourt, P., Bout-Roumazeilles, V., Tribouillard, N., 2001. Carbonate grain-size distribution in hemipelagic sediments from a laser particle sizer. *Journal of Sedimentary Research*, 71, 858-862.
- Tribouillard, N., Hatem, E., Averbuch, O., Barbécot, F., Bout-Roumazeilles, V., Trentesaux, A., 2015. Iron availability as a dominant control on the primary composition and diagenetic overprint of organic-matter-rich rocks. *Chemical Geology* 401 (2015) 67–82.
- Tribouillard, N., Lyons, T.W., Riboulleau, A., Bout-Roumazeilles, V., 2008b. A possible capture of molybdenum during early diagenesis of dysoxic sediments. *Bulletin de la Société Géologique de France* 179 (1), 3–12.
- Tribouillard, N., Algeo, T.J., Baudin, F., Riboulleau, A., 2012. Analysis of marine environmental conditions based on molybdenum–uranium covariation—Applications to Mesozoic paleoceanography. *Chemical Geology*, 324-325, 46-58.
- Tribouillard, N., Bialkowski, A., Tyson, R.V., Vergès, E., Deconinck, J.-F., 2001. Organic facies and sea level variation in the Late Kimmeridgian of the Boulonnais area (northernmost France). *Marine Petroleum Geology*, 18, 371-389.
- Tribouillard, N., Desprairies, A., Lallier-Vergès, L., Bertrand, P., 1994. Sulfur incorporation of lipidic organic matter in reactive-iron deficient environments: a possible enhancement for the storage of hydrogen-rich organic matter. *Comptes Rendus Académie des Sciences, Paris*, 319, 1199-1206.
- Tribouillard, N., Ramdani, A., Trentesaux, A., 2005. Controls on organic accumulation in Late Jurassic shales of Northwestern Europe as inferred from trace-metal geochemistry. In: Harris N., ed., *The Deposition of Organic-Carbon-Rich Sediments: Models, Mechanisms, and Consequences*. SEPM Special Publication, 82, 145-164.
- Tyson, R.V., 1995. Sedimentary organic matter: organic facies and palynofacies. Chapman & Hall, London, 615 p.
- Van der Weijden, C.H., 2002. Pitfalls of normalization of marine geochemical data using a common divisor. *Marine Geology*, 184, 167–187.
- Vandenbroucke, M., Largeau, C., 2007. Kerogen origin, evolution and structure. *Organic Geochemistry*, 38, 719-833.
- Waterhouse, H.K., 1999. Orbital forcing of palynofacies in the Jurassic of France and the United Kingdom. *Geology*, 27, 511-514.
- Wignall, P.B., Sutcliffe, O.E., Clemson, J. and Young, E., 1996. Unusual shoreface sedimentology in the upper Jurassic of the Boulonnais, Northern France. *J. Sedim. Res.*, 3, 577-586.
- Wignall, P.B., Newton, R., 2001. Black shales on the basin margin: a model based on examples from the Upper Jurassic of the Boulonnais, northern France. *Sedimentary Geology*, 144, 335-356.
- Williams, C.J., Hesselbo, S.P., Jenkyns, H.C., Morgans-Bell, H.S., 2001. Quartz silt in mudrocks as a key to sequence stratigraphy (Kimmeridge Clay Formation (Late Jurassic, Wessex Basin, UK). *Terra Nova*, 13, 449-455.
- Zaback, D.A., Pratt, L.M., Hayes J.M., 1993. Transport and reduction of sulphate and immobilisation of sulphide in marine black shales. *Geology*, 21, 141-144.
- Zhang, J., Dong, H., Zebg, Q., Agrawal, A., 2014. The role of Fe(III) bioreduction by methanogens in the preservation of organic matter in smectite. *Chemical Geology*, 389, 16-28.

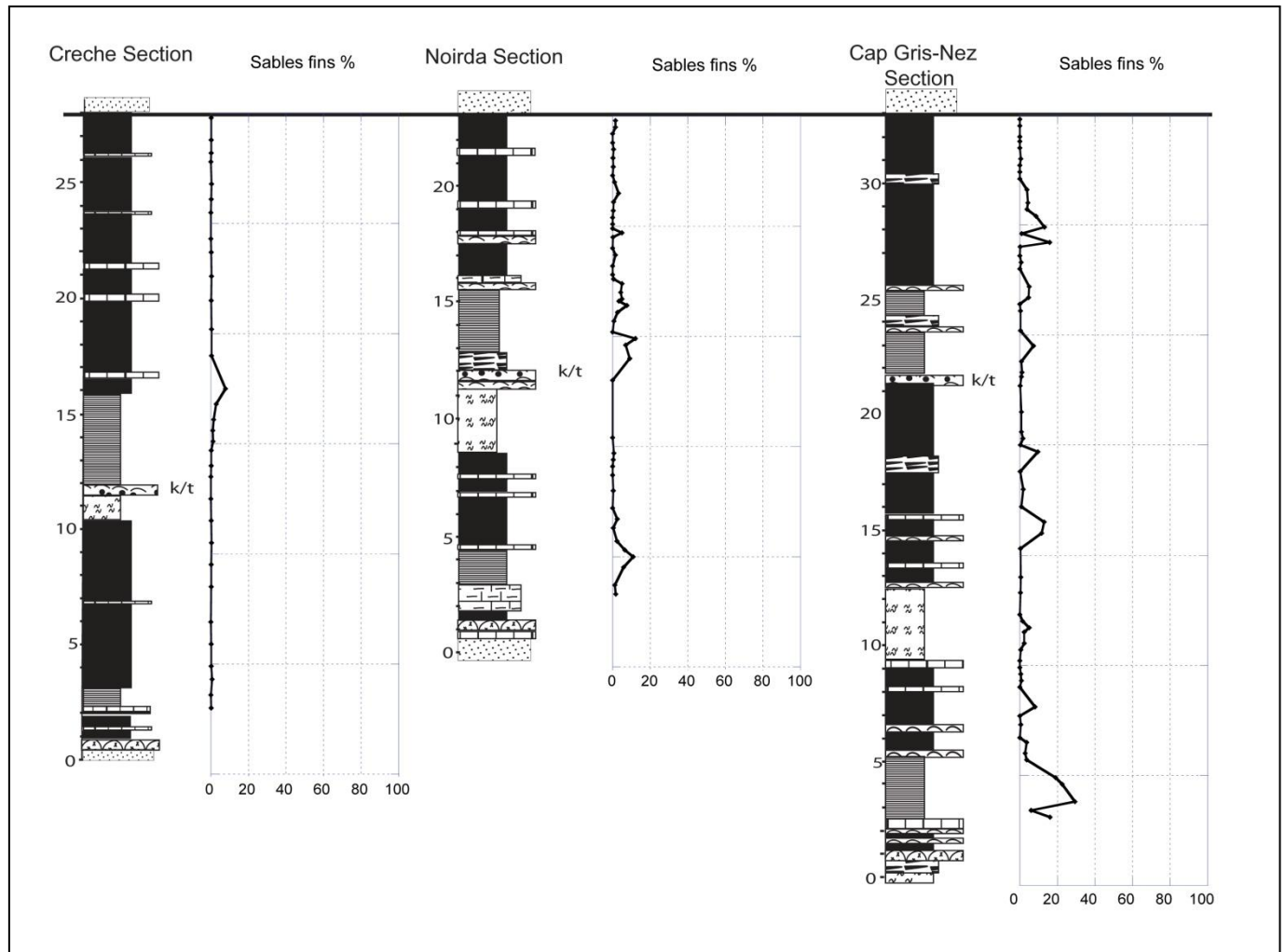
4.3 – Compléments



- Comparaison d'évolution stratigraphique de la proportion des argiles dans l'assemblage de roche totale décarbonatée pour les trois coupes étudiées.



- Comparaison d'évolution stratigraphique de la proportion des sables très fins dans l'assemblage de roche totale décarbonatée pour les trois coupes étudiées.



- Comparaison d'évolution stratigraphique de la proportion des sables fins dans l'assemblage de roche totale décarbonatée pour les trois coupes étudiées.

Chapitre 5 – Quelques observations importantes au cours du terrain

1- Les Grès de Châtillon (Kimméridgien supérieur) au lieu-dit "Cran aux œufs" :

Il s'agit d'ordinaire de sables et grès légèrement glauconieux peu fossilifères et montrant des rides de vagues et figures de houle ou de courant (rides, stratification entrecroisées et laminations planes). Cette formation apparaît en général sans argiles dans tous les sites où elle est présente. La seule exception est au Cran aux œufs (Figure 1).

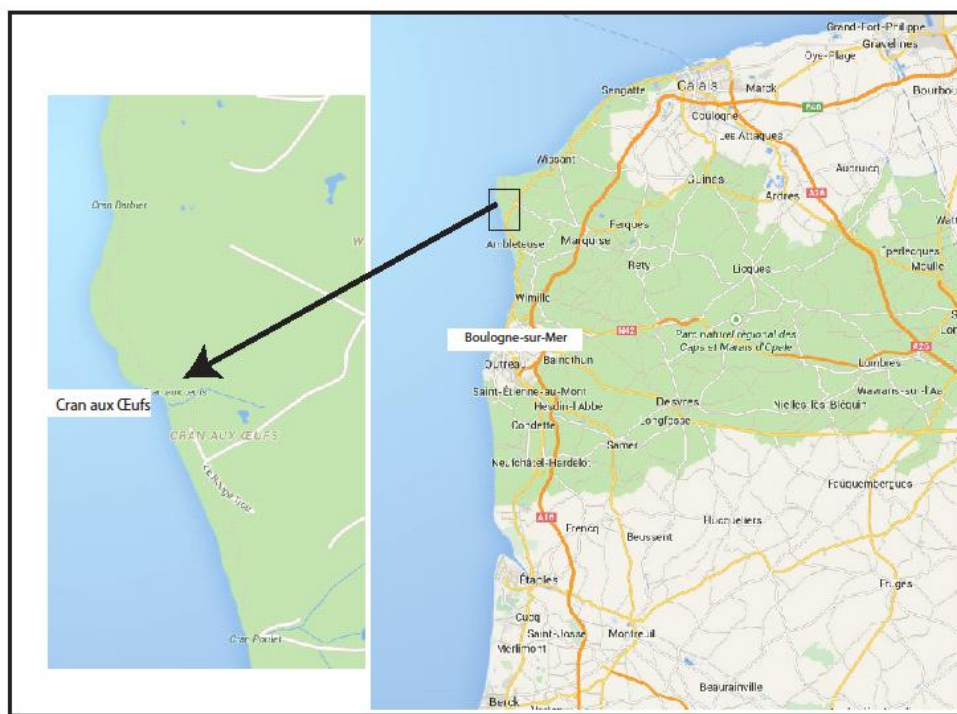


Figure 1. Cran aux œufs, Entre le *Cap Gris Nez* et *Audresselles* (au nord de *Boulogne*).

La transition entre les Grès et les Argiles de Châtillon est particulière par l'épaisseur des dépôts et le mélange entre récurrences argileuses et gréseuses qu'on observe que là. A titre d'exemple, les Grès de Châtillon se présentent localement comme une formation de grès mélangée avec des argiles montrant un niveau principal argilo-sableux avec quelques niveaux secondaires et avec un réseau de veines d'argiles connectées (Figure 2).

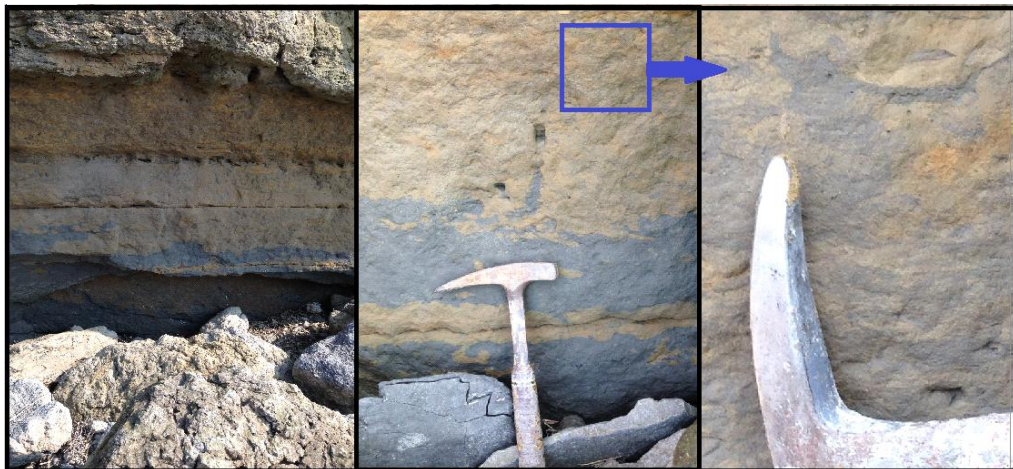


Figure 2. le mélange de sable et d'argiles dans la Grès de Châtillon au Cran aux œufs.

Dans ce cas, nous suggérons que la source d'argile provienne de l'un des cas suivants :

- Des figures de charge éventuellement associées à des mouvements sismiques (Figure (4-A) .



Figure 3. Faille normale au cran aux œufs.

- Des injections de fluides chargés en particules argileuses mis en mouvement lors du jeu de failles synsédimentaires (Figure 4B).

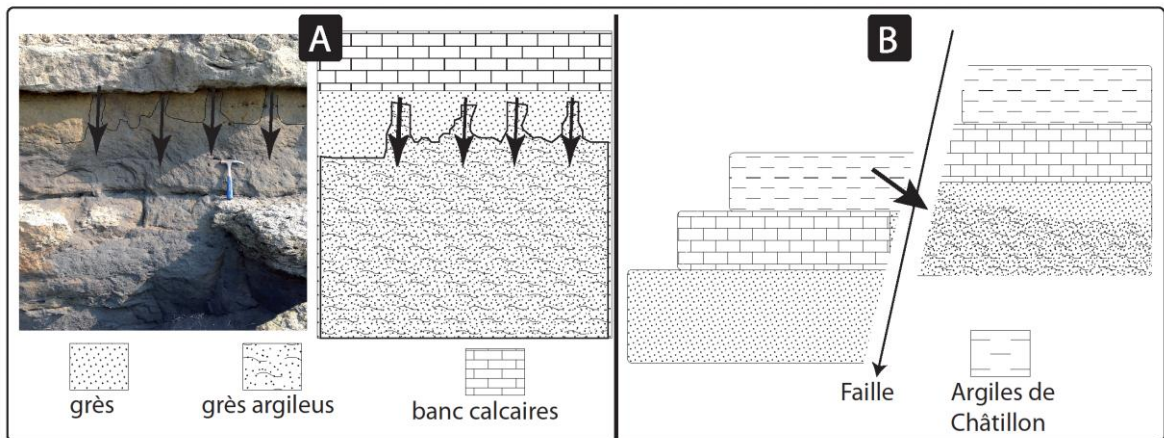


Figure 4. Modèle analytique du cas particulière de chevauchement d'argile avec du grès au Cran aux œufs ;A : figures de charges, B : Injectites associée à une faille synsédimentaire.

2- Absence des récifs d'huîtres et leur remplacement par un niveau de coquilles au Cran aux Œufs :

Nous avons parlé précédemment des constructions nommées récifs à huîtres, qui étaient comme des blocs isolés de différentes tailles, qui se trouvent majoritairement à la limite entre les deux formations des Grès de Chatillon et des Argiles de Châtillon.

Au Cran aux Œufs, l'exception est que ces dômes sont absents, et au lieu de cela il y a un niveau très riche en coquilles qui s'étendent latéralement dans l'argile (Figure 5).

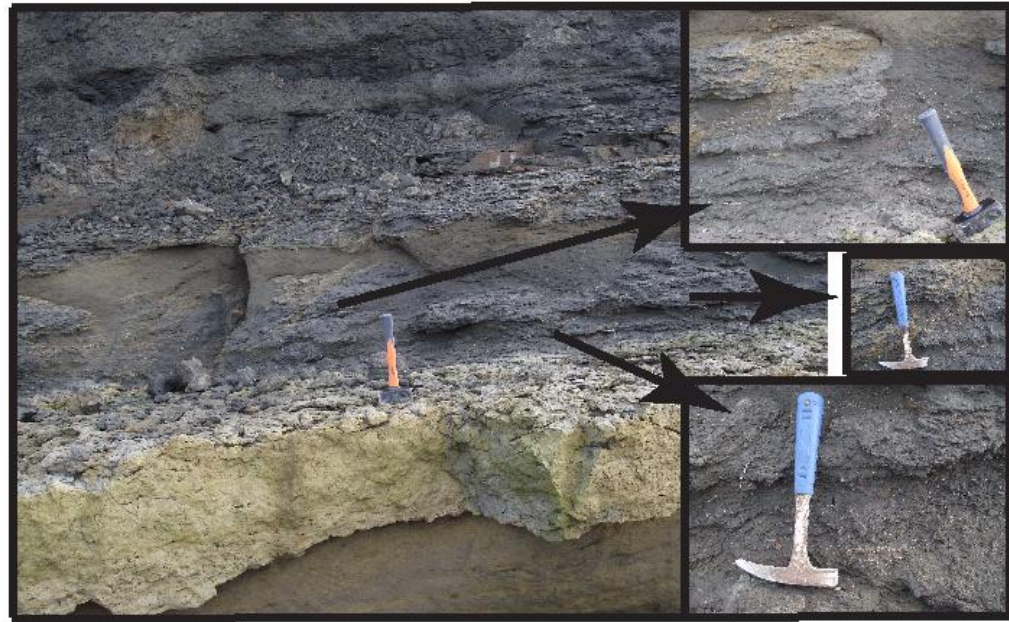


Figure 5. Illustration du niveau argileux existant au lieu des dômes à huîtres au Cran aux œufs.

Donc, la différence sera sous la forme de positionnement. Ce positionnement nous conduit à imaginer qu'il y avait un cas particulier de la nature de dépôts, qui est peut être un résultat de la sortie des fluides de densité relativement élevée, et riche en éléments nutritifs. Ces fluides auraient stimulé l'activité bactérienne et une sorte de gel carbonaté aurait pu se former en réponse à l'augmentation locale d'alcalinité. Les huîtres auraient pu trouver alors une base sur laquelle la population a pu se développer, dans un contexte plutôt favorable à l'accumulation de silts et argiles (Figure 6).

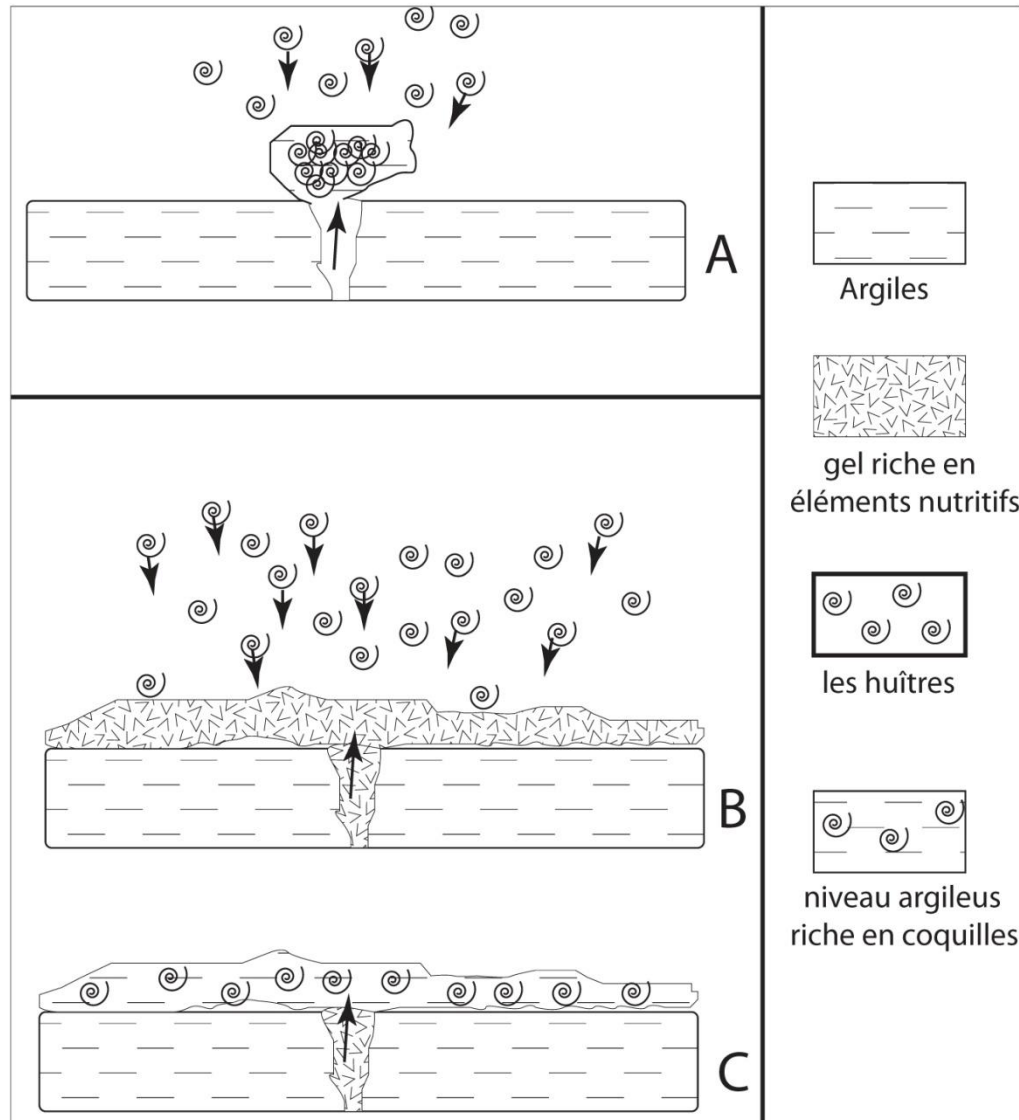


Figure 6. A : Ils représentent la situation générale pour former les dômes à huîtres, qui sont le résultat de sortie de « gaz ou liquide » riches en éléments nutritifs. B : Le cas particulier du sortie de gel riche en nutriments et son expansion en raison de sa viscosité et puis l'arrivée des huîtres.

3- BANCS JUMEAUX

Cette formation présente une transition entre les Argiles de la Crèche et les Argiles de Wimereux, elle représente un faciès de plate-forme de basse énergie (offshore sup/inf) mais avec une certaine influence des tempêtes exprimées par de minces intercalations de calcaires coquilliers (lumachelles). Il s'agit de trois bancs calcaires (b1, b2, b3) entre les deux niveaux phosphatées P1, P2 (Figure 7) : au Nord de Wimereux (A), et au Cap Gris-Nez (B), alors qu'elle montre seulement deux bancs calcaires au Sud de Wimereux (C).

La question ici est : quel est le banc carbonatée dans les trois qui a disparu au Wimereux sud ??

- En mesurant la distance entre les bancs carbonatés supérieure et inférieure dans les deux formations contenant trois bancs « figure (7) A, B », on trouve que cette distance est environ 75-80 cm, ce qui est la même distance entre les bancs carbonatées de Wimereux sud qui ne contient que deux bancs.
- Le banc de milieu dit b2 dans les deux formations qui comprennent des trois bancs calcaires «au Nord de Wimereux, et au Cap Gris-Nez » est comme un banc noduleuse, tandis qu'il est absent au sud de Wimereux (où il n'y a que deux bancs calcaires).
- Les bancs calcaires sont en sandwich entre les deux niveaux phosphatés P1 – P2, et donc l'absence du banc supérieure ou inférieure va augmenter la distance entre le banc moyen et le niveau de phosphate le plus proche de lui, ce qui est inexistant, où nous constatons que la distance est resté presque constant entre les niveaux de phosphate P1, P2 et les deux bancs carbonatées dans les trois sites. Ce qui indique que le banc qui est disparu au Wimereux est très probablement le banc b2.

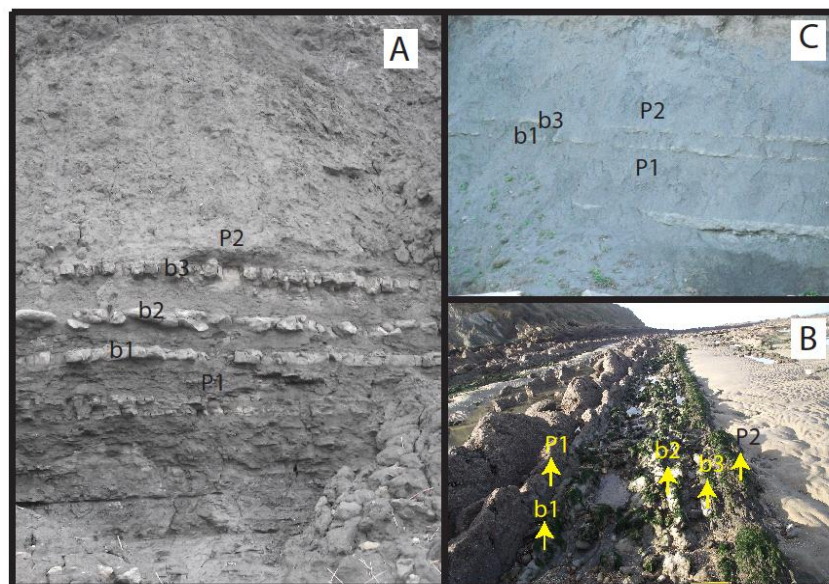


Figure 7. La formation des Bancs Jumeaux en trois sites différents, A : au nord de Wimereux, B : au Cap Gris-Nez, C : au sud de Wimereux.

Conclusion générale :

Les objectifs de ce mémoire étaient de répondre à des questions liées les unes aux autres, dans un cadre général qui était : les relations entre tectonique, remplissage des bassins, et conditions paléoenvironnementales de dépôt. Le chantier retenu est le Jurassique supérieur du Boulonnais, qui permet d'apporter un certain nombre de réponses.

- 1- L'objectif initial était de chercher l'origine de structures biologiques carbonatées, qui sont très différentes des dépôts terrigènes dominants dans le Jurassique supérieur. Ces objets carbonatés sont d'une part des petits biohermes à huîtres, aussi appelés récifs ou patches à huîtres, et d'autre part, des bancs calcaires à grain fin, d'aspect parfois noduleux (Bancs Jumeaux, Calcaires du Moulin Wibert, ...).

Nos travaux montrent que les carbonates constituant ces bancs calcaires ou la matrice des récifs à huîtres ont une origine diagénétique précoce. La précipitation du carbonate diagénétique résulte d'une augmentation locale de l'alcalinité, en réponse à l'activité de bactéries (notamment les bactéries sulfato-réductrices). Ces bactéries ont pu se développer grâce à des fluides riches en matière organique dissoute (voire en hydrocarbures) dont le mouvement ascendant fut permis par le jeu de failles synsédimentaires. Cette tectonique active durant le dépôt des sédiments du Jurassique supérieur a donc abouti, par une chaîne de réactions, à la formation de bancs calcaires dans un environnement où les conditions de dépôt ne se prêtaient pas à une sédimentation carbonatée. Cette interprétation permet d'expliquer la présence quelque peu énigmatique de bancs d'allure micritique au milieu de dépôts traduisant une certaine énergie. Elle n'a pu être formulée que grâce à la disponibilité d'analyses des isotopes stables du C, O et S. Cette interprétation est sans doute transposable à d'autres environnements de dépôt, quel que soit leur âge, si des remontées de fluides "nutritifs" atteignent des fonds marins propices à l'augmentation d'alcalinité. L'aspect novateur est que dans notre cas, la diagénèse a pu faire apparaître de véritables bancs (et pas seulement des alignements noduleux ou rognoneux) soit à l'interface eau-sédiment, soit à très courte distance sous cette interface, puisque nos approches isotopiques montrent que les réactions se sont produites au contact, ou presque, du "réservoir chimique infini" que constitue l'eau de mer.

Nos résultats montrent en outre que des horizons diagénétiques, plus ou moins continus latéralement peuvent se mettre en place rapidement au cours du dépôt. Cette information est importante dans une perspective de recherche de circulations de fluides, et donc utile pour la prospection pétrolière.

- 2- Un second objectif était de cerner les facteurs paléoenvironnementaux influençant les dépôts du Jurassique supérieur du Boulonnais, en particulier, pour évaluer l'impact direct et indirect de la tectonique synsédimentaire sur les conditions de dépôts au sens large.

Nous avons donc étudié la formation des Argiles de Châtillon le long d'un transect allant du Cap Gris-Nez au Cap de la Crèche. En effet, nos travaux suggèrent que les failles synsédimentaires aient pu localement créer des dépressions dans les fonds marins, sans négliger bien sûr les variations eustatiques du niveau marin. Le transect évoqué ci-dessus va donc des zones proximales du Gris-Nez vers des environnements plus profonds (offshore sup/inf) au Cap de la Crèche.

Nos résultats mettent en évidence ce gradient, notamment par l'analyse de la granulométrie des sédiments, voire, par l'étude de la matière organique, également. Le résultat le plus inattendu concerne la répartition stratigraphique de la smectite. Nous aurions pensé que sa bonne flottabilité aurait conduit à la trouver en plus grandes proportions dans les zones distales, comparées aux zones proximales. C'est l'inverse qui est observé et nous interprétons ceci comme le résultats de mélanges de sources de minéraux argileux. Les smectites sont très vraisemblablement issues des terres émergées bordant le bassin marin boulonnais au Jurassique supérieur. Elles ont pu être remobilisées et redistribuées au moment de la diminution du niveau marin et la reprise d'érosion des terres émergées. Les relativement courtes distances séparant nos coupes géologiques montrent que la dispersion de la smectite ne fut pas efficace, puisque l'on trouve des gradients très marqués sur des distances kilométriques seulement (moins de 20 km).

Cette information est utile si l'on souhaite étudier l'évolution de la composition des assemblages de minéraux argileux pour des reconstitutions des sources d'apports terrigènes, ou des conditions paléoclimatiques régnant sur les continents anciens.

L'étude de la distribution et de l'abondance de la matière organique (MO) nous a conduits à nous interroger sur le rôle du fer dans la préservation de la MO. En effet, selon la disponibilité du fer réactif, la MO a pu, en cas de limitation du fer, être mise en contact suffisamment prolongé avec des ions sulfures, ce qui a provoqué sa sulfuration et lui a conféré son caractère réfractaire (et donc sa préservation). Si au contraire le fer réactif est relativement abondant, alors les sulfures libérés par l'activité des bactéries hétérotrophes sulfato-réductrices ont pu former de la pyrite, du fait de la forte affinité des ions sulfures pour les atomes de fer réduits. Dans ce cas, la sulfuration ne peut pas opérer de manière significative. Le fer réactif conditionne donc certains aspects de la préservation et donc l'accumulation de MO.

Le fer sera plus ou moins abondant en réponse à de nombreux facteurs évoqués dans cette thèse. En particulier, il apparaît qu'un (très) faible taux de sédimentation puisse favoriser les apports en fer (à l'image des hard grounds). Ceci explique la plus grande richesse en fer et donc la plus grande pauvreté en MO des Bancs Jumeaux, comparés aux Argiles de Châtillon. De plus, nos travaux suggèrent que la smectite puisse être un vecteur de fer réactif (par adsorption), et donc un agent susceptible d'apporter les ions qu'utiliseront les bactéries réductrices du fer pour consommer la MO. La smectite pourrait donc ainsi concourir à la reminéralisation de la MO. Pourtant la smectite est classiquement considérée comme un véhicule potentiel de MO (de nouveau par adsorption ou agglomération). Nos résultats permettent d'apporter un éclairage nouveau sur le rôle de la smectite vis-à-vis de la préservation de la MO.

Toutefois, ces interprétations reposent sur des données trop limitées. Nous suggérons donc de pousser les investigations plus loin concernant ce nouveau rôle attribué à la smectite : celui de porteur de "munitions" (le fer) pour les bactéries mangeuses de MO !

Pour clore ce mémoire, nous constatons à quel point les conditions de dépôt (*sensu lato*) peuvent être variables de façon brutale ou subtile même dans des domaines de sédimentation aussi limités en taille que pouvait l'être le Boulonnais au Jurassique supérieur.

ANNEXE

La disponibilité du fer : un contrôle de la composition chimique et de l'empreinte diagénétique des roches riches en matière organique

Présentation

L'essentiel en quelques mots

Le fer est connu pour stimuler la productivité de surface de l'océan, ainsi que d'intervenir dans les processus de médiation bactérienne de la reminéralisation de matière organique, au cours de la diagenèse précoce. Dans cet article, nous examinons l'influence des apports en fer sur la géochimie (éléments majeurs et traces, $\delta^{34}\text{S}$, matière organique) de roches sédimentaires déposées dans un environnement de rampe marine dominée par des apports clastiques.

À cette fin, nous avons étudié deux formations du Jurassique supérieur de la zone d'étude du Boulonnais : (a)- la formation des Argiles de Châtillon, (b)- la formation des Bancs Jumeaux. Les deux formations ont été déposées dans des conditions assez similaires, mais elles diffèrent dans l'approvisionnement en fer réactif qu'elles ont reçu. Un seul des deux formations a été affectée par le processus de "shuttle" (navette) de particules de fer (oxydes et hydroxydes).

Dans cet article, nous explorons les différences entre ces formations, notamment à travers l'examen des métaux trace et la composition isotopique des isotopes stables, et nous insistons sur le rôle joué au cours de l'authigenèse/diagenèse. Notre objectif est de déterminer si la disponibilité de fer réactif pourrait être un facteur important dans le contrôle de stockage de matière organique.

Les deux formations contiennent de la matière organique (MO) sédimentaire; le contenu organique total (COT, en % en poids) est plus élevé dans l'Argiles de Châtillon que dans les Bancs Jumeaux.

On rappelle ici le fait que si le fer réactif était suffisamment disponible pour amortir entièrement la formation des ions sulfure par sulfato-réduction bactérienne, des sulfures de fer pourraient se former en abondance et les ions sulfure ne pourraient pas réagir avec la matière organique. Inversement, si le fer réactif n'a pas immobilisé par tous les ions sulfures formés, une partie de la masse d'ions sulfure pourrait réagir avec la MO, induisant la formation de matière organique sulfurisée (peu dégradable par les bactéries). Dans ce scénario ; le fer joue un rôle central, en ce que son abondance, par rapport à celle d'ions sulfure, contrôlent la diagenèse précoce de la MO et conduit à la formation de la matière organique amorphe (sulfurisée).

Pour cette étude, il est important de faire la distinction entre la partie de fer réactif qui peut être impliqué dans des réactions chimiques, et le fer "inerte" (lié solidement au sein de réseaux cristallins) qui est peu ou non réactif, lors du début de la diagenèse des sédiments.

Le processus de navette de fer peut être amélioré là où l'approvisionnement en fer est lui-même renforcé. En particulier, ces améliorations peuvent être observées dans deux contextes:

1) Dissolution de fer réactif à partir des sédiments dans des conditions sub-oxiques, suivi par le transport dans la partie oxique de la colonne d'eau et précipitation des oxy-hydroxydes de Fer.

2) sous des conditions oxiques, des procédés purement physiques peuvent causer la remise en suspension de particules fines de Fe-oxyhydroxydes et les transporter plus au large et les déposer au fond de la mer.

Pour la formation des Bancs Jumeaux, nous avons étudié 16 échantillons de l'affleurement à l'extrême nord de Wimereux, le pas de l'échantillonnage était de 10 cm.

Pour la formation de l'Argiles de Châtillon., Les échantillons ont été prélevés à partir de l'affleurement du Cap de la Crèche. Dans cette étude, nous avons utilisé l'ensemble de 55 échantillons qui ont été déjà échantillonnées et utilisées en 2001, plus de 22 échantillons supplémentaires couvrant le large éventail de contenus en matière organique de cette formation. Nous avons échantillonné seulement des faciès marneux, qu'ils soient riches ou pauvres en matière à l'exclusion des autres faciès rencontrés dans la formation de l'Argiles de Châtillon, comme les bancs de lumachelles (= tempestites en accumulation des argiles de *Nanogyra*) et des bancs carbonatées / gréseux, car ceux-ci autres faciès représentent d'autres conditions de dépôt.

La pyrite est couramment observée dans les deux coupes étudiées. Nous avons analysé la composition isotopique (^{34}S) de la pyrite qui est présente sous forme de framboïdes ou de cristaux minuscules inclus à l'intérieur ou associés avec la MO.

D'un point de vue de faciès, les deux formations sont assez semblables, montrant des roches constituées d'un mélange dominé par le silt et d'argile d'une part, et le carbonate biogénique de l'autre part.

Les assemblages de minéraux argileux dans la formation de Bancs Jumeaux sont quelque peu différents en ce que les échantillons de la formation des Argiles de Châtillon, sont dominés par l'illite + kaolinite, tandis que ceux des Bancs Jumeaux sont plus riches en smectite.

Nous avons aussi déterminé les concentrations des éléments majeurs / mineurs pour les échantillons de l'Argiles de Châtillon.

Le fer réactif est un peu plus abondant dans les Bancs Jumeaux que dans les Argiles de Châtillon.

Les échantillons des Bancs Jumeaux montrent une corrélation positive, au dessus de la ligne théorique de la pyrite dans un diagramme Fe vs. S. Aucune corrélation n'est observée pour les échantillons des Argiles de Châtillon.

Les principales conclusions de cette étude sont d'intérêt sur deux fronts:

1 - Reconstitutions paléoenvironnementales. Le processus de navette de fer particulaire peut causer des enrichissements en Mo, P, As et Sb dans les sédiments marins. Réciproquement, un co-enrichissement en Mo, P, As et Sb peut être utilisé pour identifier un effet "paléo-navette" si les enrichissements en U font défaut.

2 - Préservations Matière Organique (OM). Une limitation en fer réactif pendant le dépôt peut conduire à la préservation de ma MO en induisant la vulcanisation ou sulfuration, même dans les milieux marins montrant une productivité modeste.

En résumé, nous suggérons que la limitation de fer soit un facteur clé conditionnant à la fois la géochimie organique et inorganique de sédiments de marge.



Iron availability as a dominant control on the primary composition and diagenetic overprint of organic-matter-rich rocks



Nicolas Tribouillard ^{a,*}, Ebraheem Hatem ^a, Olivier Averbuch ^a, Florent Barbacot ^b, Viviane Bout-Roumazeilles ^a, Alain Trentesaux ^a

^a Université Lille 1 & CNRS UMR LOG 8187, Bâtiment SN5, 59655 Villeneuve d'Ascq Cedex, France

^b GEOTOP—Université du Québec à Montréal, Montréal, Canada

ARTICLE INFO

Article history:

Received 25 April 2014

Received in revised form 13 February 2015

Accepted 19 February 2015

Available online 27 February 2015

Edited by Michael E. Böttcher

Keywords:

Geochemistry

Organic matter preservation

Iron shuttle

Arsenic

Molybdenum

Antimony

ABSTRACT

Iron is known to stimulate surface ocean productivity, as well as intervene with bacterially-mediated processes of organic matter remineralization, during early diagenesis. In this paper, we examine the influence of iron supply on the geochemistry (trace metals, $\delta^{34}\text{S}$, organic matter) of sedimentary rocks deposited in a clastic-dominated marine ramp environment. To this end, we studied two Late Jurassic formations of the Boulonnais area (North-France). Both formations were deposited under quite similar conditions, but they differ in the reactive-iron supply they received. Only one of the two formations was affected by the particulate iron shuttle process. Our results indicate that 1) the iron shuttle may be recorded through concomitant enrichments in P, Mo, As and Sb; 2) a limited reactive-iron supply will allow the sulfurization of organic matter, even in a context of moderate productivity. Thus sulfurization can be a factor favoring a noticeable accumulation of organic matter: iron may thus be an important agent in the C cycle.

© 2015 Elsevier B.V. All rights reserved.

1. Introduction

The geological rocks of the Late Jurassic times (Kimmeridgian-Tithonian), cropping out along the Boulonnais shore (Strait of Dover, Northern France; Fig. 1), represent a proximal, lateral equivalent of the Kimmeridge Clay Formation (when used with a proper name, the word Formation will be abbreviated as Fm.), famous as a major petroleum source rock. These formations accumulated in a clastic-dominated ramp environment where the sedimentary succession is made up of an alternation of marlstone-dominated formations (called “Argiles”) and sandstone-dominated formations (termed “Grès”) reflecting a range of water depths from lower offshore to shoreface settings, respectively (e.g., Wignall, 1991; Ramanampisoa et al., 1992; Proust et al., 1995; Deconinck et al., 1996; Wignall and Newton, 2001; Williams et al., 2001; Al-Ramadan et al., 2005). In the present paper we compare two formations, namely the Argiles de Châtillon Fm. and the Bancs Jumeaux Fm. that accumulated in similar conditions: a relatively rapidly rising sea level (Taylor et al., 2001; Williams et al., 2001) and “normal” marine productivity in the sense that it was calculated that surface-water productivity was in the range of present-day open shelves (Tribouillard et al., 2001). Both formations show a comparable

marly facies with relatively abundant marine organic matter (OM), but they also yield marked differences. Horizons within the Argiles de Châtillon Fm. contain abundant OM that is rich in sulfur (sulfurized OM), whereas the Bancs Jumeaux Fm. does not yield such S-rich OM, but is instead rich in phosphatized biogenic clasts, typically bivalve shells. The two formations show contrasting magnetic parameters. In this paper, we further explore the differences between these formations, notably through the examination of the trace-metal and S-isotope composition, and emphasize the role played during authigenesis/diagenesis. Our focus is on determining whether reactive-iron availability could be an important factor controlling OM storage.

2. Geological framework and previous results

The shoreface sandstones and offshore mudrocks of the Kimmeridgian-Tithonian times are located along the Boulonnais coast of the Dover Strait (Fig. 1) and were deposited on the northwest European epicratonic platform, forming an embayment into the shoreline. The mudstones and shales of the Argiles de Châtillon (*autissiodorensis* + *gigas-elegans* ammonite zones, straddling the Kimmeridgian-Tithonian boundary), and the transition between the Argiles de la Crèche Fm. and Argiles de Wimereux Fm. (the so-called Bancs Jumeaux Fm., *wheatleyensis* + *pectinatus* ammonite zones,

* Corresponding author.

E-mail address: Nicolas.Tribouillard@univ-lille1.fr (N. Tribouillard).

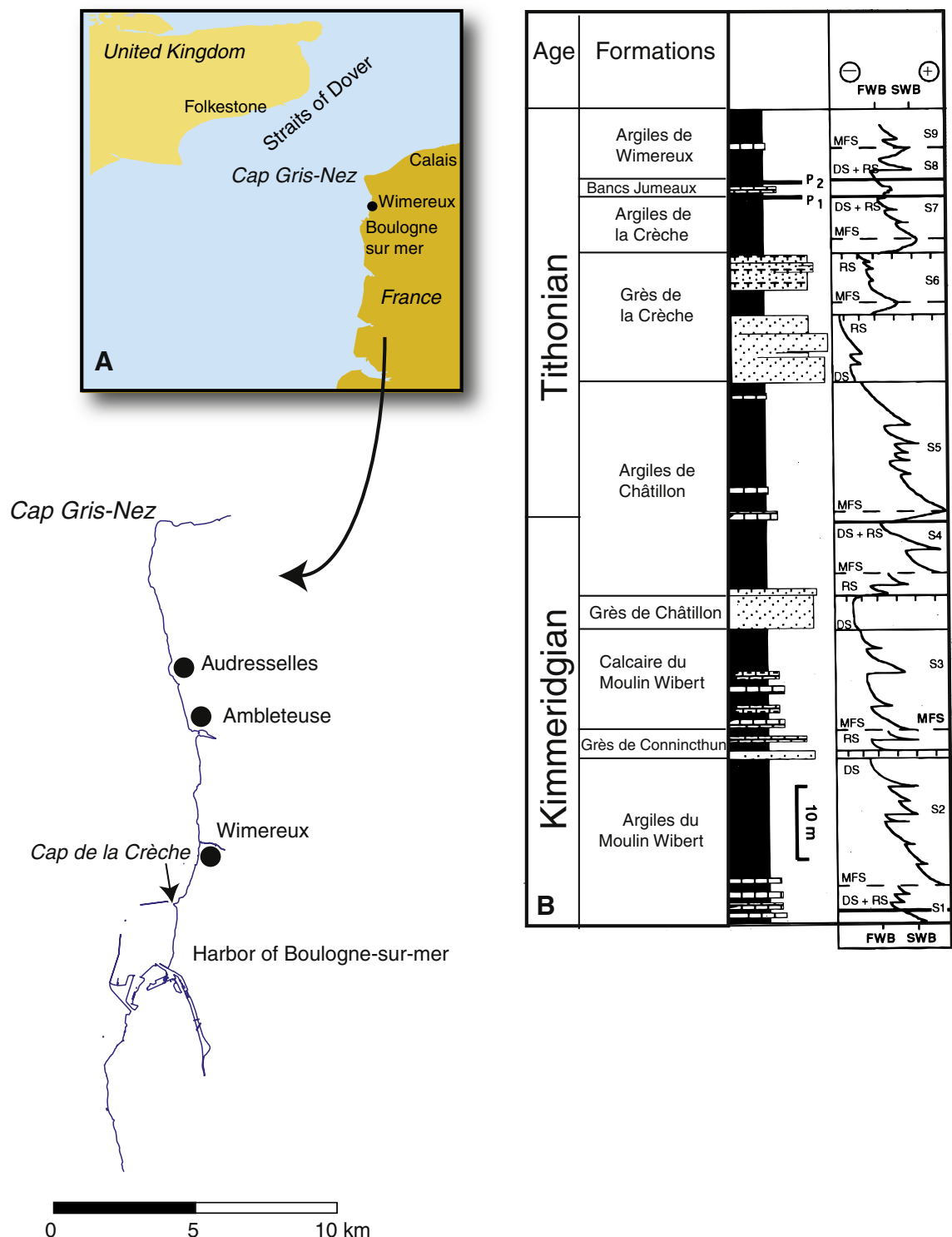


Fig. 1. Maps showing the location of the study area, between the Gris Nez Cape and the city of Wimereux. Right-hand side: simplified lithostratigraphic log of the Late Jurassic formations cropping alongshore the Boulonnais (after Deconinck et al., 1996). FWB and SWB stand for fair-weather wave base and storm-weather wave base, respectively. P1 and P2 stand for the two horizons rich in phosphatized shells.

Tithonian) represent a low-energy shelf facies deposited below fair-weather wave base, but with some storm influence expressed as thin shelly limestone interbeds and coquina beds (Wignall, 1991; Proust et al., 1995; Deconinck et al., 1996; Wignall and Newton, 2001; Williams et al., 2001). Similar to the more distal, time-equivalent, shales and mudstones of the Kimmeridge Clay Fm., exposed on the Dorset

(UK) coast, these sediments are also organic-rich (Tribovillard et al., 2001). Detailed descriptions of the lithofacies and stratigraphy (including sequence stratigraphy) can be found in Proust (1994), Proust et al. (1993, 1995), Herbin et al. (1995); Deconinck et al. (1996); Wignall (1991); Wignall and Newton (2001); Williams et al. (2001), Al-Ramadan et al. (2005) and Braaksma et al. (2006).

2.1. The Argiles de Châtillon Formation

The Argiles de Châtillon Formation is well exposed at the Cap de la Crèche (Crèche Cape), between Wimereux and Boulogne, where its thickness is about 30 m. The formation consists of claystone and marlstone (referred to mudstones in what follows) accumulations with some intervals of laminated black shales and a laterally variable number of coquina beds (tempestites made of accumulations of *Nanogryra* shell beds; Fürsich and Oschmann, 1986). These storm beds are numerous at the Kimmeridgian–Tithonian boundary. In contrast to the mudstones, the laminated, small pyrite frambooid-rich, organic-rich, black shales with an impoverished benthic fauna is a facies also typical of the Kimmeridge Clay Fm. classically interpreted as deposited under oxygen-restricted conditions (Wignall and Newton, 2001). Within the Argiles de Châtillon Fm., the clay mineral assemblage is very homogeneous, being made of illite (>50%), kaolinite (ca. 30%), smectite + illite/smectite mixed layers (<20%), plus < 10% chlorite (Proust et al., 1995; Deconinck et al., 1996). At the uppermost part of the formation, the assemblage evolves towards dominating smectite + illite/smectite mixed layers (>70%).

2.2. The Bancs Jumeaux Fm.

The Bancs Jumeaux Fm. is located at the boundary between the Argiles de la Crèche Fm. and the Argiles de Wimereux Fm. This interval (about 1.20 m thick) is sometimes referred to as the La Rochette Nodule Beds or the Bancs Jumeaux Fm. (Proust et al., 1995; Williams et al., 2001). It is bound at its base and top by two sharp erosional surfaces overlain by accumulations of phosphatic fossils and nodules, and quartz pebbles. Both levels correspond to condensed sedimentation plus erosion. These lower and upper P-rich levels are named P1 and P2, respectively. The top of the Argiles de la Crèche Fm. (i.e., the P1 horizon) is dated as belonging to the *wheatleyensis* zone, and the base of the Argiles de Wimereux Fm. (P2 horizon) to the *Pallasiodoides* zone (Geyssant et al., 1993; Herbin et al., 1995). The *pectinatus* zone has been recently documented in the upper part of the Bancs Jumeaux Fm. (Williams et al., 2001). At Wimereux, the Bancs Jumeaux Fm. consists of marlstones with three intercalated micritic mudstones containing occasional reworked thin pelecypod shell horizons. Only two of these beds are present at the Cap de la Crèche. These carbonate beds are interpreted as being of diagenetic origin (Tribouillard et al., 2012a). The marlstones of the Bancs Jumeaux Fm. do not show strong sedimentological evidences of condensed sedimentation, contrary to the P1 and P2 levels that bound the formation. However, reduced sedimentation rates are possibly shown by the presence of scattered glauconite grains. The Bancs Jumeaux Fm. has been interpreted as a transgressive systems tract (Proust et al., 1995; Deconinck et al., 1996; Williams et al., 2001). The Bancs Jumeaux Fm. is placed within the general evolution observed between the uppermost Argiles de la Crèche Fm. and lowermost Argiles de Wimereux Fm., with an increase in the illite + kaolinite abundance (from 30 to 50%, and 15 to 30%, respectively) at the expense of illite-smectite mixed-layers + smectite (from 50 to 15%; Proust et al., 1995).

2.3. Organic matter

Both formations contain sedimentary organic matter (OM); the total organic content (TOC, in weight %) is higher in the Argiles de Châtillon

than in the Bancs Jumeaux. Rock Eval data for the studied two formations are compared in Table 1. See Espitalié (1993) for the meaning and interpretations of the Rock Eval-pyrolysis parameters.

2.4. The organic content of the Argiles de Châtillon Fm.

The organic content of the Argiles de Châtillon Fm. is dominated by amorphous organic matter (AOM; Tyson, 1995). AOM represents the part of the kerogens, the origin and nature of which cannot be determined through palynofacies observation alone (Tyson, 1995). Here, AOM is itself dominated by two main varieties distinguished by their colors: orange or brown (see description and microphotographs in Tribouillard et al., 2001). Orange AOM exhibits distinct (and in some cases, almost angular) edges, and has a gel-like texture. Brown AOM has a more heterogeneous “flock” texture, less distinct “fuzzy” outlines, and tends to be less lustrous; in untreated kerogen slides it exhibits a more granular texture and the presence of pyrite crystallites and tiny frambooids. It is also associated with lower fluorescence intensities. In previous studies on the Kimmeridge Clay, orange AOM has been found to be nanoscopically amorphous, while brown AOM shows an ultralamina ultrastructure which is thought to represent selectively preserved cell walls of microplankton (Boussafir et al., 1994, 1995a, 1995b; Gelin et al., 1995, 1999). The ratio of the two types of AOM changes with the TOC of the sediments, the proportion of orange AOM increases rapidly as TOC increases from 2 to 7% (Bialkowski et al., 2000; Tribouillard et al., 2001). The orange AOM is interpreted as resulting from natural vulcanization or sulfurization (reaction with sulfides and polysulfide, see below), whereas brown AOM is interpreted to result from selective preservation of resistant biopolymers (selective oxidation of metabolizable constituents; Boussafir et al., 1994, 1995a, 1995b; Largeau et al., 1990; Derenne et al., 1991). Natural sulfurization is an early diagenetic process leading to the inter- or intramolecular incorporation of reduced inorganic sulfur species into low-molecular-weight functionalized lipids resulting in the formation of resistant high molecular weight abiogenic “geopolymers” (Tegelaar et al., 1989).

2.4.1. The Bancs Jumeaux Formation

The Bancs Jumeaux Formation has TOC values ≤2% (Table 1); the organic content is largely dominated by brown AOM. For both formations, the palynofacies also contain minor amounts of gelified and black opaque terrestrial debris, together with algal debris and algae (Tribouillard et al., 2004a).

2.5. Magnetic parameters and initial consideration about the role of iron

Various magnetic parameters, namely, magnetic susceptibility (MS), SIRM and S ratio, were measured for the Argiles de Châtillon Fm. (Tribouillard et al., 2002) and the Bancs Jumeaux Fm. (Tribouillard et al., 2004a). The results indicate that the MS signal of the rocks of these formations was governed by the clay-mineral content, but also tuned to the variable presence of iron sulfides. This second factor was linked to the type of AOM present, either orange (sulfurized) or brown (non-sulfurized). The initial interpretation was that the type of AOM (orange vs. brown) resulted from the reaction of sulfide ions with organic molecules during the sulfate-reduction stage of OM diagenesis. If sufficient reactive iron (defined as iron phases that readily react with hydrogen sulfide; Poulton and Raiswell, 2002) was available to fully buffer the sulfide ions formation, iron sulfides could form in abundance (which impacted the MS of the sediments) and sulfide ions could not react with OM (no sulfurization, hence the presence of brown AOM). Conversely, if reactive iron did not immobilize all the sulfide ions formed by sulfate-reduction, part of the sulfide ion pool could react with OM, inducing the formation of orange AOM but blurring the relationship between OM abundance and MS signal. In this scenario (Tribouillard et al., 2001, 2004a), iron plays a central role, in that its abundance, compared to that of sulfide ions, will control OM early

Table 1

Rock Eval data of the two formations studied (from Tribouillard et al., 2008a).

	TOC (wt.%)	HI (mg HC per g TOC)	Tmax (°C)
Argiles de Châtillon Fm.	1–8	80–556	411–453 (mean 423)
Bancs Jumeaux Fm.	1–2	150–360	420–430

diagenesis and lead to the formation of either brown or orange AOM. However, in this scenario, the emphasis was not set on the variations in the reactive-iron supply but instead on the amount (or flux) of OM subject to sulfate reduction (i.e., surface productivity) and on the reactivity of OM (e.g., its nature more or less labile, hence its propensity to undergo sulfate reduction). In the present paper, the emphasis is placed on the fluctuation of the reactive-iron supply and its impact, upon trace metal and S stable isotope content in the rocks.

3. Iron and the particulate shuttle effect

Iron has been the focal point of many studies about sediment geochemistry, notably regarding authigenesis and early diagenesis of sediments deposited under reducing conditions. Such conditions are propitious to the formation of iron sulfides and they involve OM. Within the huge literature, see notably the seminal papers of Berner (1970, 1984) as well as recent syntheses about iron written by Raiswell and Canfield (2012) and Rickard (2012) or edited by Taylor and Konhauser (2011); (see more specifically Poulton and Canfield, 2011; Taylor and Macquaker, 2011). For this kind of study, it is important to distinguish between the part of reactive iron that can be involved in chemical reactions, and “inert” iron (firmly bound within crystal lattices) that is poorly or not reactive during sediment early diagenesis (e.g., Canfield et al., 1992, 1996). To this end, numerous works were dedicated to iron speciation, with a recent, renewed approach (Wijsman et al., 2001; Poulton and Raiswell, 2002; Poulton and Canfield, 2005; Lyons and Severmann, 2006; Raiswell and Canfield, 2012), to selectively extract and distinguish between mineralogical forms of the iron-carrying phases of sediments and sedimentary rocks. In the present work, taking into consideration the long diagenetic history of the sediments deposited about 152 millions years ago, as well as the shaly nature of the studied sedimentary rocks, we considered that the chemically-inert fraction of the iron content was the part incorporated into the lattices of alumino-silicates; the relative amount of this non-reactive, or detrital, iron is calculated according to the following formula:

$$\text{Fe}_{\text{detrital}} = [\text{Al}]_{\text{sample}} \times [\text{Fe}] / [\text{Al}]_{\text{upper crust}}, \text{ with } [\text{Fe}] / [\text{Al}]_{\text{upper crust}} = 0.44$$

(McLennan, 2001).

The iron content in excess to the detrital part is then derived using the formula:

$$\text{Fe}_{\text{xs}} = \text{Fe}_{\text{total}} - \text{Fe}_{\text{detrital}}.$$

We consider that this Fe_{xs} fraction provides a good estimate of the initial reactive iron proportion during deposition of its mineralogical carrier phase, after the successive steps of long-term diagenesis (see Scholz et al., 2014).

In addition, a series of recent studies focused upon the so-called particulate shuttle effect (Crusius et al., 1996; Algeo and Lyons, 2006; Chappaz et al., 2008; Goldberg et al., 2009; Dellwig et al., 2010; Owens et al., 2012; Scott and Lyons, 2012; Jilbert and Slomp, 2013; Scholz et al., 2013). In a few words, the oxy-hydroxides of Fe and Mn easily bind to dissolved chemical species present in the oxidizing part of the water column. During settling, Fe- and Mn-oxy-hydroxides can thus adsorb significant amounts of Mo (Crusius et al., 1996; Chappaz et al., 2008; Algeo and Tribouillard, 2009; Helz et al., 2011; Kashiwabara et al., 2011; Martin et al., 2013) and iron oxy-hydroxides can incorporate P and As (see Section 6.3). The oxy-hydroxides in turn bind to settling particles or flocs of OM, or stick onto clay minerals. Once deposited, they can be chemically reduced and thus can release the ions they scavenged. These ions can in turn get solubilized at the sediment-water interface or into pore waters. In the latter case, they can be incorporated into diagenetic mineral phases (sulfides, carbonates, silicates, etc.; see Section 6.3). Emphasis is usually set on the role of iron in the particulate

shuttle, but the phenomenon may also be important for manganese (März et al., 2011a).

In addition, the iron shuttle process may be enhanced where iron supply is itself enhanced. In particular, such enhancements may be observed in two contexts: 1) Dissolution of reactive iron from sediments under suboxic conditions, followed by transport to oxic parts of the water column and Fe oxy-hydroxidesre-precipitation. Such a situation requires the presence of an oxygen minimum zone impinging on the continental margin above the depositional setting studied. In addition, redox conditions cannot be too severely reducing, as otherwise the diagenetically released iron will be fixed in situ as iron sulfides, preventing its diffusion back into the water column. 2) Under fully oxic conditions, purely physical processes can cause re-suspension of fine Fe oxy-hydroxides particles at the sea floor (e.g., through wave and/or current activity on a continental shelf), and re-depositional deeper on the continental slope. These points are discussed below.

The Bancs Jumeaux Fm. has been much studied recently and the depositional conditions are rather well constrained (Tribouillard et al., 2004a, 2008a, 2012a, 2012b). Notably, the sediments of the formation are interpreted as deposited under normally oxygenated, marine conditions prone to the operating of the iron particulate shuttle (Tribouillard et al., 2012b). The iron shuttle hypothesis explains why the Bancs Jumeaux sediments are enriched in Mo and not in U as visualized in a Mo vs. U diagram as defined in Algeo and Tribouillard (2009).

4. Methods

4.1. Sampling

For the Bancs Jumeaux Fm., we studied 16 samples from the outcrop at the North end of Wimereux, at the so-called Pointe de la Rochette. The sampling step was 10 cm. The geochemical composition (organic and inorganic data) has been partly published in Tribouillard et al. (2011, 2012a, 2012b). Here, additional results are given regarding trace metal, P and Fe contents.

For the Argiles de Châtillon Fm., the samples were picked from the outcrop of the so-called Cap de la Crèche. The initial study of 2001 (Tribouillard et al., 2001) was grounded on the examination of the organic content of 55 samples. Twenty-one samples were also analyzed for major element concentrations but the results had not been published yet. In this study, we used the same set of 55 samples plus an additional 22 samples spanning the wide range of OM content of this formation. We only sampled organic-rich facies and organic-poorer mudstones at the exclusion of the other facies encountered in the Argiles de Châtillon Fm., namely, coquina beds (= tempestites made of *Nanogyra* shell accumulation) and some carbonate/sandstone beds, because these other facies represent other deposition conditions. The rationale for the sampling was to consider only facies of the same type (fine-grained, clastic-dominated mudstones and shales) but covering a large range of organic content, because one of the goals of the paper is to study factors favoring OM preservation and accumulation. Thus we studied samples containing abundant OM dominated by orange AOM, or dominant brown AOM and samples yielding a medium to low organic content. For this second sample set, major and trace element contents were determined. Lastly, some additional analyses (sample set #3) were collected from Ramdani (1996).

4.2. Analytical procedures

The carbonate content was determined with a Bernard-type calcimeter (acid digestion followed by CO_2 volume determination; accuracy <5%). The mineralogical nature of the carbonate was determined following usual X-ray diffraction (XRD) procedures on micro-pulverized samples. Concerning the determination of clay mineral assemblages, in addition to the results published by Deconinck et al. (1996) for the entire late Jurassic of the Boulonnais, we analyzed the

samples chosen for geochemical analysis. The clay fraction was isolated and analyzed using the standard protocol for clay-mineral assemblage determination (XRD analyses of both carbonates and clays was performed using a Bruker D4 Endeavour apparatus together with the MacDiff software; see detailed protocols in Bout-Roumazeilles et al., 1999).

We observed and analyzed three phosphatized shells and their infilling, as well as ten indurated marlstone fragments (Bancs Jumeaux Fm.) using a FEI Quanta 200 scanning electronic microscope equipped with a Rontec energy-dispersive-spectroscopy (EDS) microprobe, looking for P concentrations.

For the analysis of the second sample set of the Argiles de Châtillon Fm., the determination of the major- and trace-element contents was carried out by ICP-OES and ICP-MS by the spectrochemical laboratory of the *Centre de Recherches en Pétrographie et Géochimie* of Vandoeuvre-les-Nancy (geochemistry laboratory of the French *Centre National de la Recherche Scientifique*). The samples were prepared by fusion with LiBO₂ and HNO₃ dissolution. Precision and accuracy were both better than 1% (mean 0.5%) for major–minor elements and 5% for trace metals, as checked by international standards and analysis of replicate samples (Carignan et al., 2001). Enrichment factors (EFs) were calculated as: $X_{\text{EF}} = [(X/\text{Al})_{\text{sample}} / (X/\text{Al})_{\text{PAAS}}]$, where X and Al represent the weight % concentrations of elements X and Al, respectively. Samples were normalized using the post-Archean average shale (PAAS) compositions of Taylor and McLennan (1985). Aluminum normalization is commonly used to minimize the effects of variable dilution by carbonate or biogenic silica, although certain caveats apply to this approach (for a discussion, see Van der Weijden, 2002). The convenience of using enrichment factors is that any value larger than 1.0 points to enrichment of an element is relative to its average crustal abundance. In practical terms, EFs > 3 represent a detectable enrichment of an element over average crustal concentrations, and EFs > 10 represent a moderate to strong degree of enrichment (Algeo and Tribouillard, 2009).

Pyrite is commonly observed in both studied sections. We analyzed the S isotopic composition of pyrite that is present as framboids or tiny crystals included within or associated with OM, notably AOM. Isolating small pyrite crystallites from OM and AOM is quite challenging. Consequently, determining the S isotopic composition of these small pyrite grains is facing the difficulty that the isotopic signature would be impacted by the presence of organically-bound S. Thus, we focused upon the larger pyrite particulates (see poly-framboids in Fig. 5) that can easily be extracted from the sediments. For such large pyrite extraction, 11 samples of the Bancs Jumeaux and 6 samples of the Argiles de Châtillon were crushed to centimeter-size lumps that were decarbonated using HCl. Once deflocculated after several rinsings, the suspended clay minerals were removed from the beakers by removing the supernatant (the operation must be repeated several times). The residue was then treated with HF to solubilize quartz grains and residual aluminosilicate grains. After these operations, only clean pyrite particles and some heavy minerals were still present. To determine the sulfur isotope composition ($\delta^{34}\text{S}$), the pyrite samples were oxidized with O₂ at 1050 °C to produce SO₂ that was analyzed using a VG Sira mass spectrometer (Institute of Earth Sciences, Paris XI-Orsay University). The results were expressed in δ conventional notation, relative to the standard V-CDT (Vienna Canon Diablo Troilite). The standard used is a Ag₂S MERCK with $\delta^{34}\text{S} = +3\%$ vs. V-CDT. Each sample was measured in duplicate and the average values are reported. The analytical precision of measurements is $\pm 0.3\%$; the reproducibility is of $\pm 1\%$.

5. Results

From a facies point of view, the two formations are quite similar, showing rocks made of a mixture of dominating silt and clays from one part, and biogenic carbonate from the other part, with CaCO₃ concentrations ranging between 10% and 31% for the Argiles de Châtillon

and between 18% and 50% for the Bancs Jumeaux, excluding the diagenetic carbonate beds >90% CaCO₃. The clay mineral assemblages are somewhat different in that the samples of the Argiles de Châtillon Fm. are dominated by illite + kaolinite, whereas those of the Bancs Jumeaux Fm. are richer in smectite (Table 2).

The major/minor/trace-element concentrations determined for the Argiles de Châtillon samples are reported in Tables 3 and 4. For major/minor elements, the Al-normalized distribution is quite smooth, except for Ca/Al that depends on the amount of calcium carbonate present in the rock, and Si/Al that is linked to variable proportions of silt-sized quartz particles (Table 5).

For trace elements, chromium, germanium, nickel, lead, thorium, and vanadium (Cr, Ge, Ni, Pb, Th and V, respectively) show linear correlations to the Al content with even a determination coefficient R² equal to 0.83 in the case of V, a trace metal reputed to be redox-sensitive (Table 6). In contrast, molybdenum, arsenic and antimony, uranium, zinc and zirconium (Mo, As, Sb, Zn, and Zr, respectively) show poor correlation with Al. Uranium is in an intermediate position (Table 6). Considering enrichment factors (EFs; Table 5), V, Cr, Ni, Cu, Zn, Zr, U, and Th show enrichment factors close to the value 1, which means that the elements are present in proportions identical to the average upper crust with no apparent authigenic enrichment. The samples with the highest Si/Al have the highest EF in Zr, and to a lesser degree, Cr and Th, which is attributed to the presence of heavy minerals in association with the silt-size fraction of these four samples. In addition, the samples with the highest organic contents yield the highest enrichment factors in U and Mo (samples N1, N2, NN2 & NN3); nevertheless, even in this case, the enrichment factors keep at low values. Compared to the other trace elements, the metalloids As and Sb show relatively high enrichment factors; however in contrast to what is observed for the Bancs Jumeaux, no correlation is observed with iron or phosphorus, and, furthermore, Sb-EF is correlated to Th-EF ($R^2 = 0.71$), which is not true for As. Arsenic is correlated to no other element and shows relatively constant proportions (mean concentrations 8.3 ppm with standard deviation 1.7).

Iron is slightly more abundant in the Bancs Jumeaux than in the Argiles de Châtillon (Fig. 2; Table 3). In the latter formation, the Fe/Al is most of the time close to the average upper crust value (0.44; McLennan, 2001) or slightly above it (mean Fe/Al = 0.53; n = 63), whereas Fe/Al is consistently above this value in the Bancs Jumeaux Fm. (mean Fe/Al = 0.85; n = 17). In the Bancs Jumeaux Fm., Fe vs. Al relationship shows a determination coefficient $R^2 = 0.62$. For the Argiles de Châtillon Fm., $R^2 = 0.68$ for the sample set #1 and 0.72 for the sample set #2. In a Fe_{total} vs. S_{total} crossplot (Lückge et al., 1996), the samples of the Bancs Jumeaux Fm. show a positive correlation, plotting above the theoretical pyrite line (Fig. 3). No such correlation is observed for the Argiles de Châtillon samples.

We calculated Fe_{xs}, namely, the part of the Fe content that is postulated to be in excess relative to the clastic fraction-associated part of the iron inventory (see Section 3). If we calculate the proportion of Fe_{xs} relative to the total Fe content of the sample, we observe that, on average, Fe_{xs} represents 38% of total Fe inventory in the Bancs Jumeaux samples, and 16% only in the Argiles de Châtillon samples (Fig. 2). In the case of the Bancs Jumeaux Fm., Fe_{xs} shows correlations with phosphorus concentration and the following trace metals: Mo, As and Sb when the latter three elements are considered either as concentrations or enrichment factors. Noteworthily, the correlation between P from one side

Table 2
Compared clay-mineral contents of the two formations studied.

Clay minerals	Bancs Jumeaux Fm.	Argiles de Châtillon Fm.
Illite-smectite mixed-layers	30–84% (mean 67%)	30–50% (mean 37%)
Illite	14–50% (mean 27%)	30–47% (mean 41%)
Chlorite	0–2% (mean 1%)	4–6% (mean 5%)
Kaolinite	1–19% (mean 5%)	15–19% (mean 17%)

Table 3

Iron data for the two formations studied: Fe/Al ratio and proportion of Fe_{xs} within total Fe content of the samples.

Bancs Jumeaux Fm.		Argiles de Châtillon Formation					
Fe/Al	% $\text{Fe}_{\text{xs}}/\text{Fe}_{\text{total}}$	Sample set 1		Sample set 2		Sample set 3	
		Fe/Al	% $\text{Fe}_{\text{xs}}/\text{Fe}_{\text{total}}$	Fe/Al	% $\text{Fe}_{\text{xs}}/\text{Fe}_{\text{total}}$	Fe/Al	% $\text{Fe}_{\text{xs}}/\text{Fe}_{\text{total}}$
0.59	26	0.84	48	0.74	40.8	0.43	0
0.80	46	0.90	52	0.65	32.8	0.42	0
1.14	62	0.51	14	0.59	25.9	0.37	0
1.03	58	0.52	16	0.87	50.3	0.46	5
0.61	29	0.58	24	0.53	18.5	0.44	1
0.60	27	0.60	28	0.57	23.8	0.34	0
0.68	36	0.84	48	0.55	20.5	0.40	0
0.57	24	0.48	9	0.61	28.5	0.41	0
0.58	25	0.48	9	0.64	31.7	0.41	0
0.49	12	0.51	14	0.59	25.9	0.44	1
0.63	31	0.46	6	0.52	15.8	0.40	0
0.80	46	0.67	35	0.58	24.4	0.47	8
0.64	32	0.43	0	0.57	23.7	0.46	6
0.67	35	0.50	12	0.57	23.7	0.46	6
0.66	34	0.50	14	0.60	27.8	0.49	12
0.66	34	0.53	18	0.48	9.3	0.45	3
3.22	86	0.45	3	0.55	21.2	0.41	0
		0.47	7	0.49	11.7	0.42	0
		0.42	0	1.15	62.3	0.48	9
		0.49	11	0.54	19.8	0.19	0
		0.54	20			0.33	0
		0.56	22				

and As or Sb from the other side is even better than the correlation Fe_{xs} vs. As or Sb (Table 7; Fig. 4). However, the Fe_{xs} vs. Mo correlation is better than the P vs. Mo correlation. Lastly, Mo and As enrichment factors are correlated. No such correlations are observed with the Argiles de Châtillon samples (Table 7); what is described above is specific to the samples of the Bancs Jumeaux Fm.

EDS analyses and elemental mapping using SEM show that the phosphatic shells are made of oxygen, phosphorus, calcium, fluorine, sulfur and sodium. The composition of the various samples analyzed shows the following concentration ranges: oxygen 34.3–43.9 wt.%; fluorine 10.6–12.5 wt.%; phosphorus 8.5–11.8 wt.%; calcium 29.5–35.2 wt.%; sodium 0.5–0.6 wt.% and sulfur 1.1–5.6 wt.%. This chemical composition suggests that the P-rich shells are made of francolite. SEM elemental mapping shows that the sediments contain abundant, scattered, tiny P concentrations.

The studied samples of the two formations yielded large pyrite grains (poly-fraiboids), frequently measuring several tens of micrometers (Fig. 56 and see also details and pictures in Tribouillard et al., 2008a). The $\delta^{34}\text{S}$ values of pyrite poly-fraiboids are ranging between -42.0 and -26.9‰ CDT for the Bancs Jumeaux Fm., and between -9.9 and 0.2‰ CDT for the Argiles de Châtillon Fm. (Fig. 5).

6. Interpretation

6.1. Bottom water redox conditions

Concerning the Bancs Jumeaux Fm., it is already known that these sediments accumulated under dominant oxic-possibly suboxic conditions, and that they must have experienced the particulate shuttle process. The peculiar point regarding the trace metal content is an enrichment in Mo but not in any other element (Tribouillard et al., 2008a, 2012a, 2012b).

In the case of the Argiles de Châtillon Fm., we observe no significant enrichments in redox-sensitive and/or sulfide-forming elements in the mudstone samples, while the four samples of laminated black shales indicate some enrichment in both U and Mo. It is inferred that sediment accumulation took place dominantly under normal, oxic conditions in the water column (mudstones), except for the episodes of laminated

black shale deposition that corresponded to dysaerobic conditions. This interpretation finds some confirmation with the presence of benthic foraminifiers (dominating *Lenticulina*, also present in the laminated black shales; unpublished Master thesis of T. Adesina).

Nickel and copper can be used as paleoproduction proxies (see discussion in Calvert and Pedersen, 1993; Sageman and Lyons, 2003; Brumsack, 2006; Tribouillard et al., 2008b; Böning et al., 2009). No strong productivity was recorded by the Argiles de Châtillon rocks, as indicated by the absence of enrichments in Ni and Cu. These conclusions are consistent with those of a modeling by Tribouillard et al. (2001) pointing to a productivity level comparable to what is currently observed on marine platforms.

Regarding the redox proxies of the Argiles de Châtillon samples, the clear correlation between V and Al shows that bottom conditions did not lead to authigenic enrichments in V. In addition, except for the four OM-richest samples, no significant enrichment is observed in Mo and U (Table 4 and Fig. 6), which suggest that bottom-water conditions were not oxygen-restricted or reducing during deposition of the mudstone facies. For the four OM-richest samples (laminated black shale facies), U-enrichment is weak, which suggests dysaerobic conditions developing at the sediment water interface; Mo-EFs are only modestly higher. In the absence of marked V enrichment, this modest Mo enrichment is ascribed to the easy capture of Mo by organic S-rich OM (Tribouillard et al., 2004b).

The correlation between Sb and Th suggests that Sb has been supplied with some clastic, land derived, sediment fraction; the moderate and constant As enrichment cannot be accounted for by any correlation with other major or trace elements and remain unexplained here. A possible explanation is that a specific, As-rich lithology would have been eroded in the hinterland supplying the Boulonnais area with clastic fractions.

To sum up, the distribution of the redox-sensitive elements indicates that the Argiles de Châtillon Fm. accumulated under largely normal marine, oxic conditions, with possible short shifts to dysaerobic conditions during episodes of high OM-accumulation (laminated black shales). These conclusions match with what has been previously concluded for the Bancs Jumeaux Fm., with the only difference that the latter formation benefited from the particulate shuttle effect.

Table 4

Geochemical data (major and trace elements) of the sample set from the Argiles de Châtillon Fm. <LD. means below limit of detection. See calculation of excess iron (Fe_{xs}) in text.

Samples	Si %	Al %	Fe %	Mn %	Mg %	Ca %	Na %	K %	Ti %	P %	Fe_{xs} %		
N1	28.14	2.09	1.75	0.01	0.34	11.21	0.29	0.84	0.17	0.32	0.84		
N2	25.60	2.97	2.68	0.02	0.66	11.36	0.39	1.08	0.22	0.23	1.39		
N3	21.29	7.26	3.68	0.02	1.41	4.56	0.73	2.27	0.39	0.24	0.53		
N4	24.26	6.42	3.32	0.02	1.45	4.54	0.77	2.10	0.40	0.23	0.53		
N5	24.44	5.65	3.25	0.02	1.53	4.32	0.56	1.99	0.37	0.38	0.80		
NN1	29.87	4.05	2.44	0.01	0.61	6.42	0.28	1.17	0.37	0.06	0.68		
NN2	31.43	1.22	1.02	0.01	0.23	10.30	0.10	0.40	0.10	0.06	0.49		
NN3	22.29	7.34	3.52	0.02	1.39	3.56	0.24	2.27	0.41	0.24	0.33		
CC 1	21.52	6.45	3.09	<LD.	1.51	5.45	0.23	2.21	0.35	0.20	0.29		
CC 2	18.72	5.99	3.03	<LD.	1.46	7.32	0.30	2.04	0.33	0.22	0.42		
CC 3	20.05	6.81	3.16	<LD.	1.45	4.80	0.30	2.22	0.35	0.22	0.20		
CC 4	17.75	4.93	3.30	<LD.	1.01	9.55	0.21	1.66	0.27	0.14	1.16		
CC 5	17.37	6.03	2.57	<LD.	1.13	9.11	0.20	1.94	0.29	0.12	0.00		
CC 6	20.83	6.19	3.07	<LD.	1.36	6.29	0.25	2.09	0.35	0.17	0.38		
CC 7	19.28	5.70	2.87	<LD.	1.16	7.61	0.21	1.87	0.32	0.18	0.40		
CC 8	19.64	5.84	3.08	<LD.	1.21	7.47	0.24	1.99	0.31	0.18	0.55		
CC 9	15.40	4.95	2.22	<LD.	1.00	10.11	0.15	1.60	0.27	0.10	0.06		
CC 10	16.70	5.51	2.59	<LD.	1.07	9.45	0.20	1.83	0.29	0.15	0.19		
CC 11	18.42	5.84	2.45	<LD.	1.13	8.93	0.22	1.87	0.32	0.13	0.00		
CC 12	21.10	6.44	3.16	<LD.	1.34	6.93	0.23	2.17	0.35	0.21	0.36		
CC 13	23.04	5.47	2.97	<LD.	1.21	6.49	0.33	1.89	0.35	0.15	0.59		
CC 14	19.03	5.32	2.97	<LD.	1.12	10.85	0.19	1.83	0.29	0.12	0.65		
Samples	As ppm	Ba ppm	Co ppm	Cr ppm	Cu ppm	Mo ppm	Ni ppm	Sb ppm	Th ppm	U ppm	V ppm	Zn ppm	Zr ppm
N1	8.9	127.4	3.0	37.3	5.5	1.5	12.5	0.3	5.3	3.1	29.7	<LD.	336.7
N2	11.6	165.4	4.4	43.3	7.2	1.7	17.6	0.4	6.0	2.3	43.7	43.8	284.2
N3	8.1	234.7	9.2	97.5	22.5	3.3	46.2	0.4	8.5	2.7	96.3	56.2	147.9
N4	7.9	240.0	8.7	96.7	18.3	2.1	48.8	0.4	9.6	2.8	85.7	56.6	196.4
N5	8.5	223.5	8.1	89.4	20.0	3.3	42.1	0.4	8.8	2.8	75.8	58.5	228.8
NN1	3.9	144.4	5.7	77.6	7.3	0.6	13.1	0.3	6.3	2.0	54.0	37.0	522.2
NN2	3.0	59.1	1.9	24.8	<LD.	1.8	7.8	<LD.	2.3	1.1	21.1	<LD.	113.9
NN3	9.3	260.9	9.8	110.7	28.9	5.4	62.6	0.5	10.4	5.8	107.9	66.2	168.7
CC 1	8.1	233.9	9.3	94.6	22.2	2.5	49.2	0.6	10.0	2.7	91.2	64.2	201.1
CC 2	8.8	211.2	8.7	86.0	20.7	2.2	48.5	0.4	9.0	2.4	84.1	58.0	158.7
CC 3	8.1	231.5	8.4	91.3	23.6	4.2	48.8	0.5	9.7	2.7	87.5	55.7	160.7
CC 4	8.7	186.1	7.8	72.4	16.5	3.1	40.7	0.4	7.4	2.1	67.3	62.4	154.7
CC 5	8.7	240.4	10.1	81.2	17.6	1.6	41.8	0.4	8.6	2.2	79.8	96.1	131.3
CC 6	8.7	228.7	9.2	91.1	20.6	2.7	46.1	0.5	9.6	2.5	84.5	63.3	183.5
CC 7	9.2	205.3	9.2	88.1	20.9	3.0	49.1	0.5	8.6	2.4	79.9	103.5	182.8
CC 8	9.8	214.2	9.2	86.5	20.4	1.9	46.8	0.5	8.9	2.3	83.8	79.1	171.7
CC 9	7.7	196.8	11.1	76.8	18.9	1.6	42.6	0.5	7.4	1.9	73.3	52.3	133.6
CC 10	8.4	193.5	9.7	80.6	18.2	2.1	43.9	0.4	7.9	2.1	78.7	51.0	141.0
CC 11	8.7	220.8	10.0	87.9	18.9	1.4	42.9	0.5	8.4	2.2	82.8	55.5	157.0
CC 12	9.5	231.6	9.0	99.2	21.2	2.1	50.6	0.5	10.0	2.7	93.7	68.5	207.5
CC 13	8.4	223.6	7.7	85.3	17.3	1.6	40.4	0.5	9.2	2.5	73.5	60.5	239.8
CC 14	8.0	196.9	7.9	80.6	16.4	1.6	39.7	0.4	8.1	2.2	73.0	53.8	182.6

6.2. Reactive iron availability

A striking feature of our results is the relationship linking Fe, P and the trace metals Mo, As and Sb in the case of the Bancs Jumeaux Fm. The first point is about the relative abundance of iron in excess to the fraction linked to the detrital content of the samples (Fe_{xs}), which can be observed for the Bancs Jumeaux Fm. Fe_{xs} is considered to be a good estimate of the reactive-iron supply to the sediments. Fe_{xs} can be supplied mainly through the rain of settling Fe oxy-hydroxides when the water column is under oxidizing conditions or through the rain of iron sulfides (FeS or FeS_2) when the lower part of the water column is sulfidic (in case of euxinic conditions). The Bancs Jumeaux Fm. shows trace-metal abundances indicating that their sediments did not accumulate under reducing, oxygen-restricted conditions. Consequently, the syngenetic formation of iron sulfides within the water column may be ruled out for the Bancs Jumeaux. Thus the Fe_{xs} supply is inferred to result from Fe-oxy-hydroxides settling in a 'normal marine' seawater mass. The Bancs Jumeaux Fm. is already known to have experienced the

particulate shuttle effect as evidenced from the differences between Mo- and U-enrichment factors (Tribouillard et al., 2012b). Our results about U and Mo show that the Argiles de Châtillon did not experience such shuttle process. It comes out that, with no particulate shuttle, the iron content of the Argiles de Châtillon is expectedly closer to the average crustal content than in the case of the Bancs Jumeaux Fm. that has an additional source of iron through particulate shuttle. This is corroborated by the fact that, contrary to the Argiles de Châtillon that shows no correlation between Fe and S, the Bancs Jumeaux samples plot above the theoretical pyrite line, which indicates that sulfur must have been completely fixed into pyrite, leaving an excess fraction of reactive unsulfidized iron (Lückge et al., 1996).

6.3. Reactive iron as a cause of enrichment in P, Mo, As and Sb

In the case of the Bancs Jumeaux Fm., Fe_{xs} is correlated to P, As, and, to a lesser degree, Sb, while such correlations are not apparent in the Argiles de Châtillon Fm.

Table 5

Geochemical data (Al-normalized concentrations and enrichment factors) of the sample set from the Argiles de Châtillon Fm. EF stands for enrichment factor (see text). <LD. means below limit of detection.

Samples	Si/Al %:%	Fe/Al %:%	Mn/Al %:%	Mg/Al %:%	Ca/Al %:%	Na/Al %:%	K/Al %:%	Ti/Al %:%	P/Al %:%	Ba/Al ppm:%	Ni/Al ppm:%	Cu/Al ppm:%	Zn/Al ppm:%
N1	13.46	0.84	0.01	0.16	5.36	0.14	0.40	0.08	0.15	60.9	6.0	2.6	<LD.
N2	8.61	0.90	0.01	0.22	3.82	0.13	0.36	0.07	0.08	55.7	5.9	2.4	14.8
N3	2.93	0.51	0.00	0.19	0.63	0.10	0.31	0.05	0.03	32.3	6.4	3.1	7.7
N4	3.78	0.52	0.00	0.23	0.71	0.12	0.33	0.06	0.04	37.4	7.6	2.8	8.8
N5	4.33	0.58	0.00	0.27	0.76	0.10	0.35	0.07	0.07	39.6	7.5	3.5	10.4
NN1	7.37	0.60	0.00	0.15	1.58	0.07	0.29	0.09	0.01	35.6	3.2	1.8	9.1
NN2	25.72	0.84	0.01	0.19	8.43	0.08	0.33	0.08	0.05	48.4	6.3	<LD.	<LD.
NN3	3.04	0.48	0.00	0.19	0.49	0.03	0.31	0.06	0.03	35.6	8.5	3.9	9.0
CC 1	3.34	0.48	<LD.	0.23	0.84	0.04	0.34	0.05	0.03	36.3	7.6	3.4	9.9
CC 2	3.13	0.51	<LD.	0.24	1.22	0.05	0.34	0.06	0.04	35.3	8.1	3.5	9.7
CC 3	2.95	0.46	<LD.	0.21	0.70	0.04	0.33	0.05	0.03	34.0	7.2	3.5	8.2
CC 4	3.60	0.67	<LD.	0.21	1.94	0.04	0.34	0.05	0.03	37.8	8.3	3.3	12.7
CC 5	2.88	0.43	<LD.	0.19	1.51	0.03	0.32	0.05	0.02	39.9	6.9	2.9	15.9
CC 6	3.36	0.50	<LD.	0.22	1.02	0.04	0.34	0.06	0.03	36.9	7.4	3.3	10.2
CC 7	3.38	0.50	<LD.	0.20	1.34	0.04	0.33	0.06	0.03	36.0	8.6	3.7	18.2
CC 8	3.36	0.53	<LD.	0.21	1.28	0.04	0.34	0.05	0.03	36.7	8.0	3.5	13.5
CC 9	3.11	0.45	<LD.	0.20	2.04	0.03	0.32	0.05	0.02	39.7	8.6	3.8	10.6
CC 10	3.03	0.47	<LD.	0.19	1.71	0.04	0.33	0.05	0.03	35.1	8.0	3.3	9.3
CC 11	3.15	0.42	<LD.	0.19	1.53	0.04	0.32	0.05	0.02	37.8	7.3	3.2	9.5
CC 12	3.28	0.49	<LD.	0.21	1.08	0.04	0.34	0.05	0.03	36.0	7.9	3.3	10.6
CC 13	4.21	0.54	<LD.	0.22	1.19	0.06	0.35	0.06	0.03	40.9	7.4	3.2	11.1
CC 14	3.58	0.56	<LD.	0.21	2.04	0.03	0.34	0.05	0.02	37.0	7.5	3.1	10.1
Samples	Sr/Al ppm:%	V/Al ppm:%	Cr/Al ppm:%	Co/Al ppm:%	Zr/Al ppm:%	Mo/Al ppm:%	U/Al ppm:%	Th/Al ppm:%	Cd/Al ppm:%	As/Al ppm:%	Sb/Al ppm:%	Ge/Al ppm:%	Pb/Al ppm:%
N1	137.1	14.2	17.8	1.4	161.1	0.7	1.5	2.5	0.1	4.3	0.2	0.4	3.1
N2	107.3	14.7	14.6	1.5	95.6	0.6	0.8	2.0	0.2	3.9	0.1	0.3	3.1
N3	27.2	13.3	13.4	1.3	20.4	0.5	0.4	1.2	0.0	1.1	0.1	0.2	2.2
N4	28.7	13.4	15.1	1.4	30.6	0.3	0.4	1.5	0.0	1.2	0.1	0.2	2.3
N5	34.8	13.4	15.8	1.4	40.5	0.6	0.5	1.6	0.1	1.5	0.1	0.2	2.4
NN1	64.3	13.3	19.2	1.4	128.9	0.1	0.5	1.6	0.0	1.0	0.1	0.5	2.7
NN2	###	17.2	20.3	1.6	93.2	1.5	0.9	1.9	<LD.	2.5	<LD.	0.6	3.8
NN3	24.6	14.7	15.1	1.3	23.0	0.7	0.8	1.4	0.0	1.3	0.1	0.2	2.7
CC 1	41.4	14.1	14.7	1.4	31.2	0.4	0.4	1.5	0.1	1.2	0.1	0.2	4.3
CC 2	54.3	14.0	14.4	1.5	26.5	0.4	0.4	1.5	0.1	1.5	0.1	0.2	2.8
CC 3	38.6	12.9	13.4	1.2	23.6	0.6	0.4	1.4	0.1	1.2	0.1	0.2	3.6
CC 4	83.1	13.6	14.7	1.6	31.4	0.6	0.4	1.5	0.1	1.8	0.1	0.2	3.2
CC 5	66.6	13.2	13.5	1.7	21.8	0.3	0.4	1.4	0.1	1.4	0.1	0.2	2.7
CC 6	50.1	13.7	14.7	1.5	29.6	0.4	0.4	1.5	0.1	1.4	0.1	0.2	2.7
CC 7	61.5	14.0	15.4	1.6	32.1	0.5	0.4	1.5	0.1	1.6	0.1	0.2	3.1
CC 8	57.3	14.4	14.8	1.6	29.4	0.3	0.4	1.5	0.0	1.7	0.1	0.2	2.9
CC 9	91.6	14.8	15.5	2.2	27.0	0.3	0.4	1.5	0.0	1.6	0.1	0.2	4.2
CC 10	74.5	14.3	14.6	1.8	25.6	0.4	0.4	1.4	0.0	1.5	0.1	0.2	2.7
CC 11	64.8	14.2	15.1	1.7	26.9	0.2	0.4	1.4	0.0	1.5	0.1	0.2	3.8
CC 12	51.7	14.5	15.4	1.4	32.2	0.3	0.4	1.6	0.0	1.5	0.1	0.2	2.9
CC 13	52.3	13.4	15.6	1.4	43.8	0.3	0.5	1.7	0.0	1.5	0.1	0.2	3.1
CC 14	63.1	13.7	15.2	1.5	34.3	0.3	0.4	1.5	0.0	1.5	0.1	0.2	2.8
Samples	As EF	Co EF	Cr EF	Cu EF	Mo EF	Ni EF	Sb EF	U EF	V EF	Zn EF	Zr EF		
N1	22.8	0.7	1.7	0.8	3.9	1.1	6.6	4.3	1.1	0.0	6.8		
N2	20.8	0.7	1.4	0.8	3.1	1.1	5.3	2.2	1.1	1.7	4.0		
N3	6.0	0.6	1.3	1.0	2.4	1.2	2.1	1.1	1.0	0.9	0.9		
N4	6.6	0.6	1.5	0.9	1.7	1.4	2.4	1.3	1.0	1.0	1.3		
N5	8.0	0.7	1.5	1.1	3.2	1.4	2.8	1.4	1.0	1.2	1.7		
NN1	5.1	0.7	1.9	0.6	0.8	0.6	2.9	1.4	1.0	1.0	5.5		
NN2	13.2	0.7	2.0	0.0	7.9	1.2	3.3	2.6	1.3	0.0	3.9		
NN3	6.7	0.6	1.5	1.3	3.9	1.6	2.7	2.3	1.1	1.0	1.0		
CC 1	6.7	0.7	1.4	1.1	2.1	1.4	3.5	1.2	1.1	1.1	1.3		
CC 2	7.8	0.7	1.4	1.1	2.0	1.5	2.8	1.1	1.1	1.1	1.1		
CC 3	6.3	0.6	1.3	1.1	3.3	1.3	2.9	1.1	1.0	0.9	1.0		
CC 4	9.5	0.7	1.4	1.1	3.4	1.5	3.4	1.2	1.0	1.4	1.3		
CC 5	7.7	0.8	1.3	0.9	1.4	1.3	2.8	1.0	1.0	1.8	0.9		
CC 6	7.5	0.7	1.4	1.1	2.4	1.4	3.2	1.2	1.0	1.2	1.3		
CC 7	8.6	0.8	1.5	1.2	2.9	1.6	3.4	1.2	1.1	2.1	1.4		
CC 8	9.0	0.7	1.4	1.1	1.7	1.5	3.2	1.1	1.1	1.5	1.2		
CC 9	8.4	1.1	1.5	1.2	1.8	1.6	4.1	1.1	1.1	1.2	1.1		
CC 10	8.1	0.8	1.4	1.1	2.0	1.5	3.1	1.1	1.1	1.0	1.1		
CC 11	8.0	0.8	1.5	1.0	1.3	1.3	3.2	1.1	1.1	1.1	1.1		
CC 12	7.9	0.7	1.5	1.1	1.8	1.4	3.1	1.2	1.1	1.2	1.4		
CC 13	8.2	0.7	1.5	1.0	1.6	1.3	3.3	1.3	1.0	1.3	1.9		
CC 14	8.1	0.7	1.5	1.0	1.6	1.4	3.0	1.2	1.0	1.1	1.5		

Table 6
Coefficient of determination R^2 for the Element-Al₂O₃ relationships.

Element vs. Al ₂ O ₃ correlation	Determination coefficient R^2
As	0.04
Cr	0.74
Cu	0.66
Ge	0.74
Mo	0.17
Ni	0.55
Sb	0.23
Th	0.78
U	0.68
V	0.83
Zn	0.02
Zr	0.05

6.3.1. Phosphorus

Phosphorus can be supplied to the sediments through OM inputs; subsequent OM decomposition would release P to pore waters, making it available for diagenetic relocation or return to the water column. Phosphorus can lastly be provided by phosphate-rich particles such as

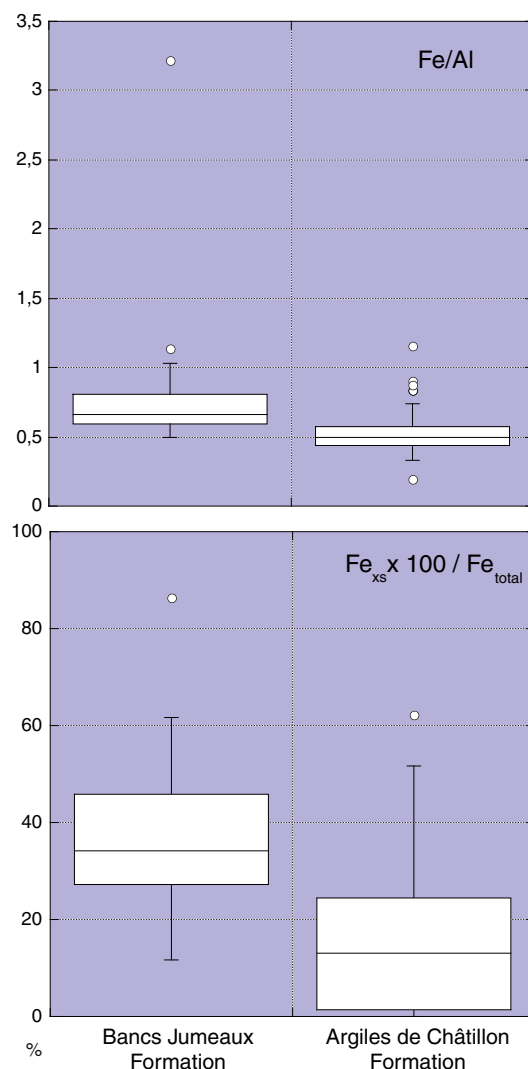


Fig. 2. Iron data for the two formations studied: Fe/Al ratio and proportion of Fe_{xs} within total Fe content of the samples. Fe_{xs} is an approximation of the authigenic Fe content. $Fe_{xs} = Fe_{total} - Fe_{detrital}$. $Fe_{detrital} = [Al]_{sample} \times [Fe]/[Al]_{upper\ crust}$, with $[Fe]/[Al]_{upper\ crust} = 0.44$ (McLennan, 2001).

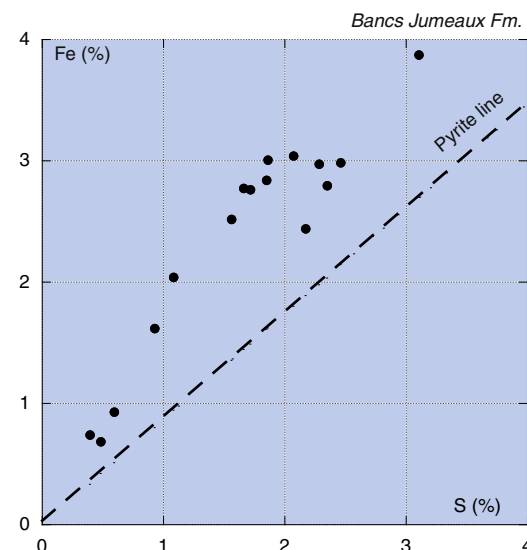


Fig. 3. Total sulfur concentration opposed to total iron concentrations, showing the stoichiometric line for pyrite, for the Bancs Jumeaux samples. The fact that iron plots above the pyrite line suggests that pyrite formation was limited by sulfate abundance, which left iron in excess.

fish bones and scales, and in association (adsorption + co-precipitation) with the settling flux of Fe oxy-hydroxides (Ingall and Van Cappellen, 1990; Ingall et al., 1993; van Cappellen and Ingall, 1994; Föllmi, 1996; Slomp et al., 1996; Anderson and Raiswell, 2004; März et al., 2008, 2014; Breier et al., 2012). After deposition, the transfer of P from the labile P-carrying phases (OM, Fe oxy-hydroxides, hydroxyapatite) into authigenic apatite is the dominant and ultimate P sink with increasing sediment age and burial depth (Delaney, 1998; Anderson et al., 2001; Slomp and Van Cappellen, 2007; März et al., 2008; Piper and Perkins, 2014).

In the present work, the facts that 1) Fe_{xs} and P are correlated in the Bancs Jumeaux sample set and not in that of the Argiles de Châtillon, and 2) the Argiles de Châtillon Fm. though richer in OM than the Bancs Jumeaux Fm., is poorer in P, strongly suggest that the main supplier of P to the sediment of the Bancs Jumeaux was the iron shuttle, which does not exclude a possible additional supply by biogenic fractions. For the Argiles de Châtillon Fm. with no shuttle effect, the iron oxyhydroxides could not be an important carrier of P (no Fe_{xs}-P correlation are observed) and biogenic phases must have been the main suppliers (TOC and P are correlated, Table 7). For these two formations, the

Table 7
Comparison of the coefficient of determination R^2 calculated for the two formations studied.

	Determination coefficient R^2	
	Bancs Jumeaux Fm.	Argiles de Châtillon Fm.
Fe vs. Al	0.62	Sample set 1: 0.62 Sample set 2: 0.72
P vs. As	0.62	0.28
P vs. As-EF	0.90	0.07
P vs. SB-EF	0.90	0.04
P vs. TOC	0.05	0.46
P vs. Fe _{xs}	0.79	0.08
Fe _{xs} vs. Mo	0.73	0.04
Fe _{xs} vs. Mo-EF	0.57	0.05
Fe _{xs} vs. As	0.72	0.03
Fe _{xs} vs. As-EF	0.57	0.32
Fe _{xs} vs. Sb	0.40	0.11
Fe _{xs} vs. Sb-EF	0.58	0.17
Mo-EF vs. As-EF	0.87	0.19

Bancs Jumeaux Formation

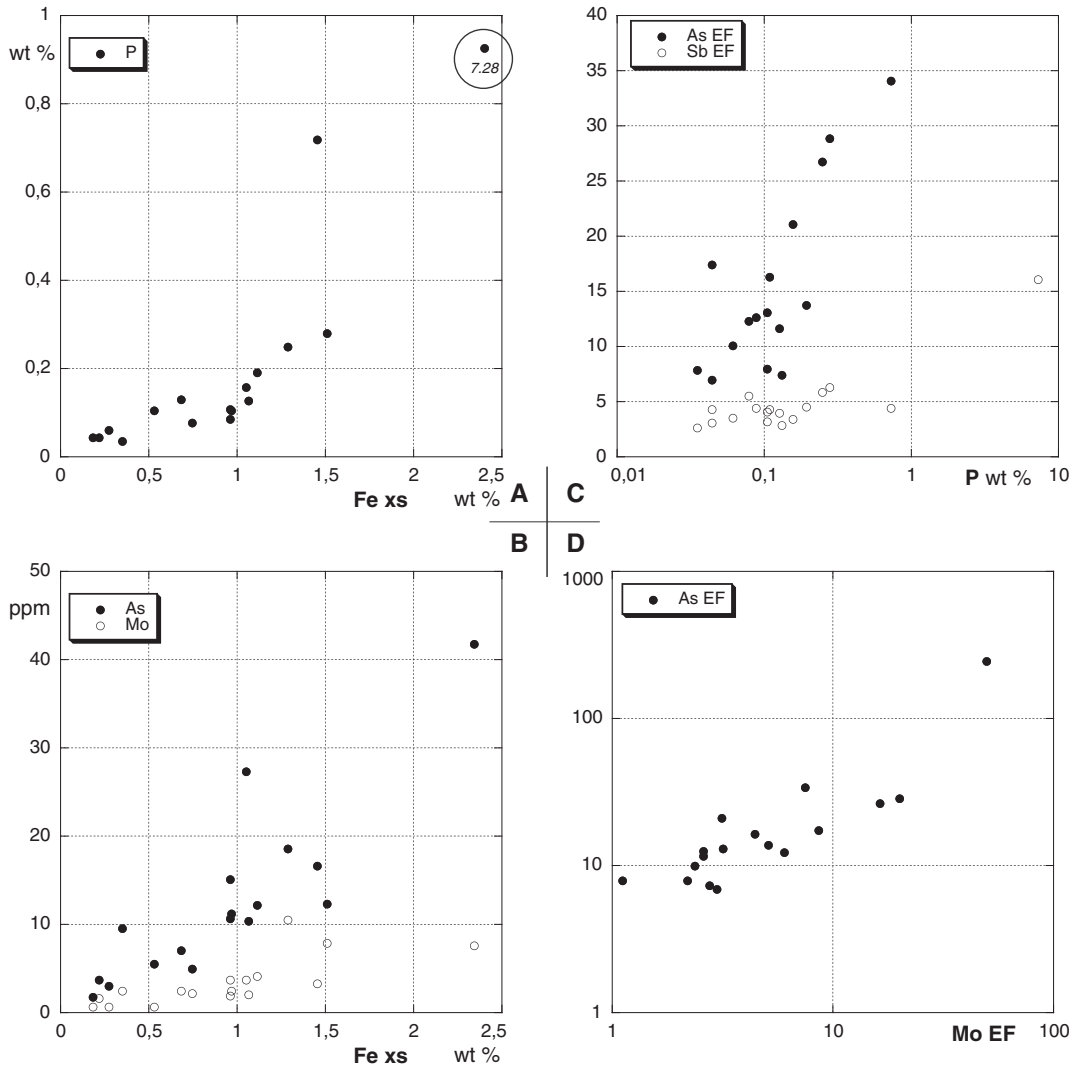


Fig. 4. Various crossplots illustrating the correlations between element abundance for the Bancs Jumeaux samples. EF stands for enrichment factor. A: Fe_{xs} vs. P; B: Fe_{xs} vs. As and Mo; C: P vs. As-EF and Sb-EF; D: and Mo-EF vs. As-EF.

absence of strongly reducing conditions during deposition (except for the laminated black shales) allows us ruling out any significant, early-diagenetic, loss of P (e.g., Jarvis et al., 1994; Föllmi, 1996; Filippelli, 2001; Algeo and Ingall, 2007; Reed et al., 2011). In addition, both formations have been interpreted to have experienced relatively low productivity (close to present open shelves, see above) and Schenau et al. (2005) discussed how, during periods of reduced productivity, a limited supply of OM would increase oxygen penetration depth into sediments, and thus the sorption capacity of the iron oxides for phosphate. Furthermore, bioturbation may play a role: downward mixing of solid-phase reactive P may be essential to prevent direct loss of phosphate to the bottom waters (Schenau et al., 2005; Meyers, 2007).

In the Bancs Jumeaux Fm., P appears both as francolite replacing carbonate in bivalve shells, as well as in tiny P-rich particles densely scattered within the sediment matrix. It is not easy deciphering whether phosphate precipitation took place during the earliest stages of diagenesis or during further steps. Francolite precipitation is conditioned by alkalinity, pH, Eh and bacterial activity (Reimers et al., 1996; Benítez-Nelson, 2000). Francolite can precipitate either rapidly (most probably replacing a short-lived and poorly crystallized precursor (Föllmi, 1996)) or slowly (usually replacing calcite but possibly directly also; Föllmi, 1996; Jarvis et al., 1994; Piper and Perkins, 2004, 2014;

Trappe, 1998). The P concentration must be high enough to support francolite supersaturation. This enrichment may result from a high organic matter supply in highly productive marine environments such as upwelling areas (Arning et al., 2009a, 2009b), but high productivity is not always a prerequisite. In low-productivity portions of the seas, it is often considered that P enrichment can be effectuated by redox cycling of iron, with P sorption onto iron-oxy-hydroxide coatings and Fe-P coprecipitation (e.g., Jarvis et al., 1994; Piper and Perkins, 2004; Dellwig et al., 2010; n.b., manganese also can be involved in P enrichment; Wang and van Cappellen, 1996).

The degree to which remineralized organic P is retained as a reactive fraction in sediments depends on the redox conditions of the depositional system (Slomp et al., 1996). In environments with at least intermittently oxic bottom waters, redox cycling of Fe within the sediment limits the diffusive flux of remineralized P to the overlying water column: Fe oxy-hydroxides that scavenge phosphate from sediment pore waters are precipitated above the oxic/anoxic interface and dissolved below it, leading to retention of P for a period sufficient to permit slow growth of authigenic phosphate phases. In permanently anoxic environments with sulfidic bottom waters, Fe-oxy-hydroxides do not precipitate within the sediment, reducing the potential for adsorption and complexation of remineralized organic P. Lastly, sulfate-reducing

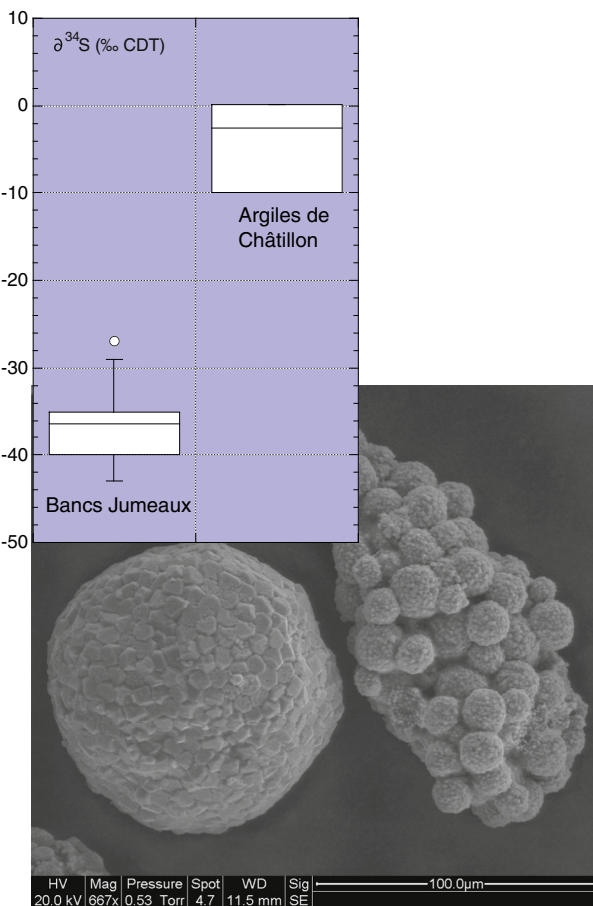


Fig. 5. Stable sulfur isotope data ($\delta^{34}\text{S}$ % CDT) for the two formations compared in this study. Inserted electronic image illustrates the two pyrite-framboid morphologies most frequently observed in the samples.

conditions are generally considered to prevent francolite formation because the correlative rise in alkalinity increases francolite solubility and prevents supersaturation to be reached and thus precipitation to take place (Cha et al., 2005; Soudry, 2000; Trappe, 1998; and references therein). Consequently, francolite is generally presented as precipitating under suboxic conditions and not anoxic-sulfidic conditions (Froelich et al., 1988; Jarvis et al., 1994; Föllmi, 1996; Piper and Perkins, 2014). However, some recent works challenged this view (Goldhammer et al., 2010).

6.3.2. Mo, As and Sb

In the Bancs Jumeaux sample set, correlations are observed between Fe_{xs} on one hand, and Mo, As and Sb on the other hand. The relationship between Fe_{xs} and Mo can clearly be attributed to the role of iron (and manganese) oxy-hydroxides through particulate shuttle processes, as detailed in Algeo and Tribouillard (2009), Helz et al. (2011), Scholz et al. (2011, 2013), and Scott and Lyons (2012). The relationship between Fe_{xs} and As can be attributed to the same phenomenon, because the role of iron oxy-hydroxides in the transfer of As from the water column to the sediments has been well explored (Sullivan and Aller, 1996; Minami and Kato, 1997; Cutter et al., 2001; Chaillou et al., 2003; O'Day, 2006; Vaughan, 2006; Breier et al., 2012; Berner et al., 2013; Neumann et al., 2013). The same is true for Sb, because Sb and As are considered to have similar geochemical properties in marine and also river systems (e.g., Cutter et al., 2001; Asaoka et al., 2012). Here, if we except the most phosphate-rich sample, a mean 4.2 enrichment factor is observed for Sb in the Bancs Jumeaux, which is a relatively high value for sedimentary rocks. No such relationships can be observed for the Argiles de Châtillon samples, whatever their organic content, in agreement with the absence of iron shuttle.

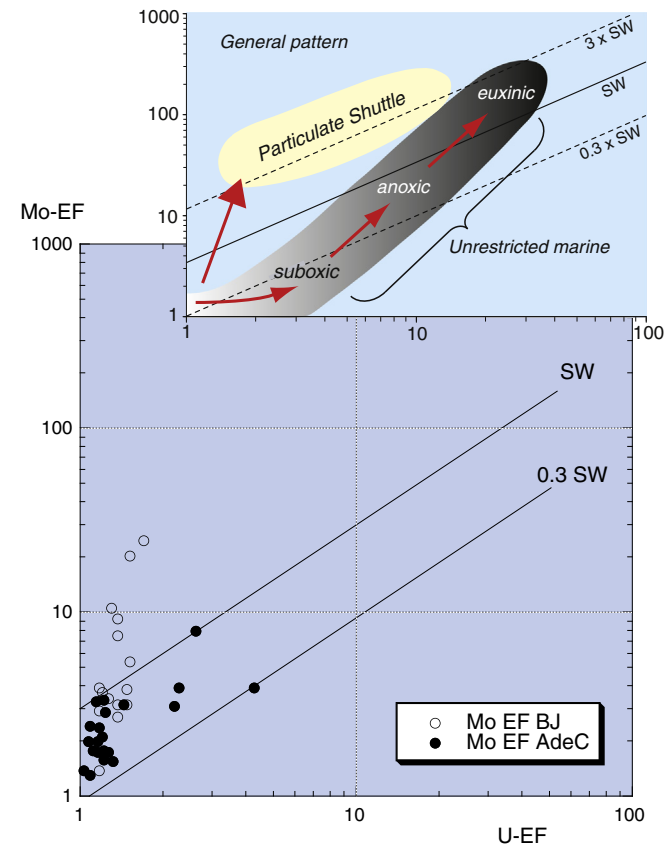


Fig. 6. Crossplot opposing the respective enrichment factors of U and Mo for the two formations studied, as designed by Algeo and Tribouillard (2009) to derive paleoenvironmental information. BJ stands for Bancs Jumeaux Fm., AdeC stands for Argiles de Châtillon Fm.

de Châtillon samples, whatever their organic content, in agreement with the absence of iron shuttle.

In total, we can consider that Mo, As and Sb have been brought to the sediments of the Bancs Jumeaux Fm. together with iron oxy-hydroxides. During diagenesis, the trace metals must have been incorporated into pyrite, taking into account the high degree of trace-metal pyritization known for Mo, As and Sb (Huerta-Díaz and Morse, 1992; Bostick and Fendorf, 2003; Couture et al., 2010; Berner et al., 2013).

6.4. $\delta^{34}\text{S}$ of pyrite

The isotopic signatures of the large pyrite (poly-) framboids show contrasting value ranges between the two formations, with significantly lower $\delta^{34}\text{S}$ for the Bancs Jumeaux Fm. (Fig. 5). By and large, lower $\delta^{34}\text{S}$ values are often associated with early diagenetic pyrite relative to later diagenetic phases (e.g., Canfield et al., 1992) because of progressive isotopic evolution of the sulfate reservoir as isotopically light sulfur is preferentially reduced during bacterial sulfate reduction. Under these later burial stages, far removed from the overlying seawater reservoir, there would be less light S availability in the pore waters and thus less incorporation into later pyrite (see Chappaz et al., 2014). In the present case, we compare two populations of framboids, i.e., a type of pyrite morphology that is considered to form during early diagenesis. Regarding the Bancs Jumeaux Fm., where pyrite framboids yield more isotopic fractionation, we may infer that sulfate availability was not a limiting factor. It means that the redox front was at close distance below the sediment-water interface, which allowed sulfate diffusion from the seawater reservoir down to the bacterial sulfate-reduction zone. In parallel, such a setting is consistent with the Mo enrichment as discussed in Tribouillard et al. (2008a). In the case of the Argiles de Châtillon Fm.,

within the mudstone facies, the redox front would have been lying deeper below the sediment-water interface, hampering sulfate diffusion down to the sulfate-reduction zone and leading to less fractionation. This interpretation of the isotope data is consistent with trace-metal distribution for the mudstone facies.

Alternatively, contrasting conditions of initial sediment porosity could be invoked to account for contrasting isotope fractionation, but we have no indication that such initial differences might have existed. Lastly, it might also be suggested that these frambooids formed from an iron pool that was released shortly after deposition, e.g., through the alteration of Fe-rich minerals (smectites, for instance; Canfield et al., 1992).

7. Discussion

7.1. Co-enrichment in Fe, P, Mo, As and Sb as a proxy for the particulate shuttle process

The Bancs Jumeaux sediments experienced deposition under conditions promoting particulate shuttling of trace elements by Fe- (and possibly Mn-) oxy-hydroxides. The shuttle process is already known to favor Mo enrichment (Dale et al., 2012; Berelson et al., 2013), but from the present study, we conclude that the shuttle process may also cause some enrichment in P and As, as well as Sb, though to a lesser degree in the latter case. Such a co-enrichment in Fe, Mo, As and Sb was already observed in some particular settings: cold hydrocarbon seepages in Southeastern France (Jurassic Terres Noires Fm.; Tribouillard et al., 2013) and in the pockmark field of the Congo Fan and Gulf of Mexico (Hu et al., 2014; see also Bayon et al., 2011). Reciprocally, we suggest that a correlation between iron (Fe_{xs}) and Mo, P, As (and Sb) could indicate that an iron shuttle process was operated by the time of sediment settling. However, caution must be taken, because syngenetic pyrite (i.e., formed directly with the water column of euxinic environments) may also incorporate Mo, As and Sb present in seawater (Berner et al., 2013). However, in the latter case, the development of euxinic conditions induces pronounced enrichments in Mo and U, in particular. Consequently, to conclude that Mo, P, As and Sb are enriched via the iron shuttle process, U concentrations cannot be markedly enriched.

7.2. Lack of reactive iron favored early natural sulfurization of OM

A second important finding of this work is that one can observe a marked enrichment in organic S-richOM (or sulfurized OM) in the Argiles de Châtillon that could occasionally accumulate several weight percents of vulcanized OM. This unusual S-richOM accumulation took place under conditions of modest productivity. Such an observation is quite unusual inasmuch as accumulation of abundant, sulfurized OM has been reported hitherto for (paleo-) environments characterized by high productivity and/or low terrigenous supply (carrier phase for reactive iron). See review in Vandenbroucke and Largeau (2007). In brief, OM sulfurization takes place when sulfide ions ($\text{HS}^-/\text{H}_2\text{S}$) can react with functionalized organic molecules, which implies that all the sulfide ions are not monopolized by Fe(II). In other words, there must be an iron deficiency, either relative or absolute. If little or no reactive iron is supplied to the depositional environment, the iron deficiency will be absolute. If reactive iron is supplied, but if a marked organic flux is also present (high productivity), the large amount of sulfide ions generated through sulfate reduction linked to bacterially-mediatedOM decay will exhaust the reactive iron pool, and sulfide will be available for sulfurization (Zaback et al., 1993; Tribouillard et al., 1994). Here, in the case of the Argiles de Châtillon, sulfate-reducing reactions, induced by bacterially-mediatedOM remineralization, operated with sediments rich in land-derived, clastic fractions, but limited in reactive iron (despite abundant silt and clay fractions). Consequently, OM could react with "unemployed" or excess sulfide ions and incorporate S. This so-called natural vulcanization protected OM against further

degradation and permitted its accumulation in noticeable amounts. The conspicuous point is that the reactive-iron limitation triggered OM sulfurization with relatively little OM present. The remineralization of a large pool of MO was not required to produce enough sulfide to immobilize reactive iron. Consequently, although the OM flux must have been moderate (moderate surface productivity), OM was protected through sulfur incorporation and stored in relatively large amounts.

The role of iron as a factor favoring OM remineralization was discussed by Meyers et al. (2005) and Meyers (2007). In the arguments of the authors, a relatively abundant flux of reactive iron will allow buffering of dissolved sulfide via iron sulfidization (see also Canfield et al., 1992; Raiswell and Canfield, 1996). Dissolved sulfide is thus made "harmless", allowing for the presence of infauna. This, in turn, will increase bioturbation and bio-irrigation, required to maintain oxidants such as dissolved oxygen and nitrate in pore waters, and hence enhance OM remineralization. Furthermore, active bioturbation and bio-irrigation can expand the zone of aerobic OM degradation, thus increasing the exposure time of OM to dissolved oxygen. Conversely, these factors fostering OM degradation will be much tempered in case of reactive-iron limitation (Meyers, 2007). Our work adds one positive effect of iron limitation: the sulfide ions, maintained at relatively high concentration in the dissolved state if iron-induced buffering cannot take place, will induce OM sulfurization, hence further promoting OM preservation and burial.

Carbonate rocks are often poor in reactive iron and, in some occasions, they may be strongly enriched in sulfured AOM. This is the case for some Late Jurassic formations deposited in shallow platform environments: e.g., the Akkuyu Fm. of Turkey(Baudin et al., 1999) and the "Laminites bitumineuses" of Orbagnoux in the French Jura Mountains (Mongenot et al., 1997, 1999; Sarret et al., 2002). For these formations, OM sulfurization was ascribed to reactive-iron limitation. In addition, carbonate rocks are sometimes good petroleum source rocks and their kerogens are most of the time of the type II-S, which means that the OM is enriched in organic S(Jones, 1984; Oehler, 1984; Palacas et al., 1984; Claypool and Mancini, 1989; Taguchi and Mori, 1992). Thus, even carbonate rocks can also contain OM that has been preserved by sulfurization processes induced by iron limitation. However, most carbonate rocks, even when poor in reactive iron, are not rich in S-containingOM, implying that reactive-iron shortage alone cannot account for OM preservation in any situation. It is an important factor that plays its full role when other factors operate in conjunction: a level of productivity that must remain above a minimum threshold, and anoxic conditions occurring at relatively shallow depth below the sediment-water interface. This latter point is required for sulfate-reducing reactions to be launched, thus producing sulfide that will sulfurize organic molecules (lipids and carbohydrates).

Moving from the general case to the particulars of this study, in the case of the Argiles de Châtillon and Bancs Jumeaux Fms., other local factors may have played a significant role. One factor favoring the preservation of OM was the shallow water conditions during deposition of both formations, which limited the exposure time to oxidizing conditions during OM settling. A second favoring factor is the sedimentation rate. Sedimentation rate was higher for the Argiles de Châtillon Fm. than for the Bancs Jumeaux Fm., which helped limit the exposure time of OM to dissolved oxygen-containing pore waters in the Argiles de Châtillon Fm.

7.3. Reactive iron supply

Now that the consequences of the presence or absence of a detectable reactive-iron supply to sediments have been discussed, the question arises why the Bancs Jumeaux experienced a higher iron supply compared to the Argiles de Châtillon showing a terrigenous supply with a "normal", average shale-type, concentration in iron. Usually, iron is supplied to the depositional environment on platforms in two ways: allochthonous supply by winds and rivers, and autochthonous

redistribution from proximal settings to distal ones (review in Raiswell and Canfield, 2012).

7.3.1. External inputs

The two formations studied were deposited during a large second-order sea-level rise (Tribouillard et al., 2005) and both correspond to periods of relatively distal conditions accompanied by occasionally-reduced sedimentation rates (see Proust et al., 1995 or Wignall and Newton, 2001 for a detailed sequence stratigraphy description). The reactive-iron supply to the basin may have been conditioned by several factors: 1) the relative width of the platform being flooded during sea-level rise; 2) the flux of river-borne (Severmann et al., 2010) or airborne (e.g., Baddock et al., 2013; Buck et al., 2013) iron-coated particles; and 3) the flux of OM possibly associated with reactive iron (e.g., Krachler et al., 2012; Bressac and Huie, 2013; Shigemitsu et al., 2013; Barber et al., 2014). Discussing these factors is rather conjectural in the case in point here, but it may be observed that the sediments of the Bancs Jumeaux are richer in smectite and poorer in kaolinite than those of the Argiles de Châtillon Fm. It is suggested that smectite could have been a Fe-carrying phase operating more efficiently in the case of the Bancs Jumeaux Fm. (see Canfield et al., 1992; 1996).

The scenario asking for the minimum hypotheses is basing upon contrasting sedimentation rates. As reminded above, Fe_{xs} can be supplied mainly through the rain of settling Fe oxy-hydroxides (particulate) when the water column is under oxidizing conditions. The sedimentation rate was probably lower during the deposition of the Bancs Jumeaux compared to the Argiles de Châtillon. A reduced sedimentation rate usually favors iron accumulation because the settling Fe-oxyhydroxides no longer “diluted” by the terrigenous supply nor by autochthonous biogenic particles (this process may cause the iron or manganese encrustation of hardgrounds in the case of extremely reduced sedimentation rates). In this view, the Bancs Jumeaux could have been enriched in iron simply as a result of a reduced sedimentation rate. In contrast, the Argiles de Châtillon experienced a relatively higher sedimentation rate due to a higher clastic supply and they accumulated iron in the same proportions as those of the so-called average shale.

7.3.2. Internal redistribution

Iron may have been redistributed with the marine environment itself. The current model (Poulton and Raiswell, 2002; Anderson and Raiswell, 2004; Lyons and Severmann, 2006) and further developments

in Owens et al., 2012; Rickard, 2012; Scholz et al., 2014) suggests that detrital iron deposited on the shelf undergoes suboxic diagenesis, which generates aqueous Fe (II). This iron diffuses from the sediment to the sediment-water interface where it is oxidized and precipitated as Fe (III) oxy-hydroxides. However a fraction appears to be transported to the deeper, euxinic parts of the basin where it is sequestered as iron sulfide. It is possible that, like the finer sediment fraction, these Fe (III) oxy-hydroxide particles accumulated slowly and are thus concentrated in the deeper parts of the basin with the siliciclastic clay fraction (Rickard, 2012). This scheme (normally applying to deeper environments) is all the more interesting for the present study in that it agrees with previous observations by Wignall and Newton (2001). These authors described a proximal-to-distal trend from the north of the Boulonnais (close to the Gris-Nez Cape) to the south (close to Boulogne city). Contrary to expectation, their work clearly indicates the development of oxygen-poor deposition in relatively shallow-water setting (N of the Boulonnais), passing down-dip into better oxygenated facies in the vicinity of the sections studied here. They conclude that “the salient point here is that black shale deposition on the Boulonnais Basin margin occurred above ‘normal’ storm wave base”. Wignall and Newton (2001) suggested that the transgressive, nearshore black shales recorded deposition beneath a small volume of sulfidic bottom water, trapped beneath an unusually shallow pycnocline developed during the initial phases of parasequence deposition. A point of cornerstone importance for the present paper is the development of euxinic conditions of deposition (long-lasting or intermittent) in the north of the Boulonnais “which would have decreased the importance of lateral Fe advection” (Wignall and Newton, 2001). This scheme explains why the deeper parts of the Boulonnais (i.e., the sections between Wimereux and Boulogne studied here) collected only limited amounts of reactive iron, during the deposition of the Argiles de Châtillon Fm.

It may be noted that the model of (very) shallow environments being submitted to anoxic-to-euxinic conditions has been illustrated recently: e.g., Bond et al. (2013) and Carmichael et al. (2014) for the Late Devonian events of Canada and Central Asia, respectively; Stein et al. (2012) for the Barremian–Aptian transition on the N-Tethyanplatform, and März et al. (2011b) for the Eocene Arctic Ocean. Such a model is somewhat counter-intuitive in that one might think that supra-thermocinal depositional conditions, as may be met in platform settings, must be oxygen-replenished through easy exchanges with atmosphere. To account for shallow, oxygen-restricted,

Table 8

Comparison of the depositional conditions of the two formations studied.

	Bancs Jumeaux Fm.	Argiles de Châtillon Fm.
Oxic water column	A flux of reactive iron (oxy-hydroxides) adsorbs P and trace metals that are soluble under oxidizing conditions (Mo, As, Sb), and transfers them to sediment. U unconcerned. So-called iron shuttle.	No such reactive-iron flux, no iron shuttle, therefore no such transfer.
Oxic sediment-water interface	Oxic conditions, hampering diffusion-induced enrichment of sediment in redox-sensitive trace metal. No additional Mo enrichment, no U enrichment.	Idem.
Reducing conditions within pore water and sediment	Allowing trace metal transferred by iron shuttle to be reduced and trapped within sediment. Sulfate-reducing reactions cause pyrite precipitation in large proportions.	Sulfate-reducing reactions cause pyrite formation, thus trapping and inerting reactive iron. During episodes of OM-rich, laminated, black shales, shoaling of the redox-cline that gets near to the sediment-water interface. It can cause a diffusion-induced U enrichment but no V enrichment. Relatively depleted reactive iron cannot buffer sulfide. Excess sulfide ions react with functionalized organic molecules and “vulcanize” them, inducing formation of sulfurized OM.
Dissolved sulfide ion abundance	Relatively abundant reactive iron buffers sulfide released through bacterial OM remineralization. Pyrite precipitation. Not enough dissolved sulfide to react with OM.	Sediment not enriched in trace metals, except for light U enrichment in OM-rich, laminated black shales. Presence of sulfurized AOM.
Sediment characteristics	Sediment enriched in iron shuttle-sensitive metals: P, Mo, As, Sb. No enrichment in other redox-sensitive elements (U, V, ...). No sulfurized AOM.	

depositional conditions, the authors invoke climate warming, that may contribute to the development of anoxic–dysoxic waters in shallow environments due to the decreased O₂-solubility in warmer water, as well as the greater metabolic demand for oxygen as temperature increases (Bond et al., 2013).

To conclude with this point, it is observed that seasonal hypoxia/anoxia may develop year after year in some present-time embayments that have dimensions comparable to those of what was the Boulonnais during the late Jurassic times (e.g., Li et al., 2014). In the same way, we may envision that such seasonal hypoxia/anoxia could develop in the proximal environment of the Jurassic Boulonnais, limiting lateral advection of iron, as mentioned by Wignall and Newton (2001).

8. Summary

The scenario presented here is summarized in Table 8. The main conclusions of this study are of interest on two fronts:

- 1 Paleoenvironmental reconstructions. The particulate iron shuttle may cause enrichments of Mo, P, As and Sb in marine sediments. Reciprocally, co-enrichments in Mo, P, As and Sb may be used to identify a paleo-shuttle effect if U enrichments are lacking.
- 2 OM preservation. A limitation in reactive iron during deposition may lead to vulcanization-induced preservation of OM, even in marine settings with only modest productivity.

In summary, we suggest that iron limitation is a key factor conditioning both the organic and inorganic geochemistry of margin sediments.

Acknowledgments

We thank Romain Abraham, Laurence Debeauvais, Marion Delattre, Philippe Recourt, and Sandra Ventalon for their technical assistance, and Monique Gentric for her administrative management. Thanks to Adewale Adesina for picking forams in some of our samples. Thanks to Magali Ader for her fruitful discussions. This paper was considerably improved thanks to suggestions by Christian März and two anonymous referees, as well as Michael E. Böttcher, co-editor of *Chemical Geology*. This work was partly funded by INSU, CNRS program SYSTER.

References

- Algeo, T.J., Ingall, E., 2007. Sedimentary Corg:P ratios, paleocean ventilation, and Phanerozoic atmospheric pO₂. *Palaeogeogr. Palaeoclimatol. Palaeoecol.* 256, 130–155.
- Algeo, T.J., Lyons, T.W., 2006. Mo-total organic carbon covariation in modern anoxic marine environments: implication for analysis of paleoredox and paleohydrographic conditions. *Paleoceanography* 21, PA1016. <http://dx.doi.org/10.1029/2004PA001112>.
- Algeo, T.J., Tribouillard, N., 2009. Environmental analysis of paleoceanographic systems based on molybdenum–uranium covariation. *Chem. Geol.* 268, 211–225.
- Al-Ramadan, K., Morad, S., Proust, J.-N., Al-Aasm, I., 2005. Distribution of diagenetic alterations in siliciclastic shoreface deposits within a sequence stratigraphic framework: evidence from the upper Jurassic Boulonnais, NW France. *J. Sediment. Res.* 75, 943–959.
- Anderson, T.F., Raiswell, R., 2004. Sources and mechanisms for the enrichment of highly reactive iron in euxinic Black Sea sediments. *Am. J. Sci.* 304, 203–233.
- Anderson, L.D., Delaney, M.L., Faul, K.L., 2001. Carbon to phosphorus ratios in sediments: implications for nutrient cycling. *Glob. Biogeochem. Cycles* 15, 65–79.
- Arning, E.T., Birgel, D., Brunner, B., Peckmann, J., 2009a. Bacterial formation of phosphatic laminites off Peru. *Geobiology* 7, 295–307.
- Arning, E.T., Lückge, A., Breuer, C., Gusone, N., Birgel, D., Peckmann, J., 2009b. Genesis of phosphorite crusts off Peru. *Mar. Geol.* 262, 68–81.
- Asaoka, S., Takahashi, Y., Araki, Y., Tanimizu, M., 2012. Comparison of antimony and arsenic behavior in an Ichinokawa river water-sediment system. *Chem. Geol.* 334, 1–8.
- Baddock, M., Boskovic, L., Strong, C., McTainsh, G., Bullard, J., Agronovski, I., Cropp, R., 2013. Iron-rich nanoparticles formed by aeolian abrasion of desert dune sand. *Geochem. Geophys. Geosyst.* 14, 3720–3729.
- Barber, A., Lalonde, K., Mucci, A., Gélinas, Y., 2014. The role of iron in the diagenesis of organic carbon and nitrogen in sediments: a long-term incubation experiment. *Mar. Chem.* 162, 1–9.
- Baudin, F., Tribouillard, N., Laggoun-Defarge, F., Lichtfouse, E., Monod, O., Gardin, S., 1999. Depositional environment of a Kimmeridgian carbonate “black band” (Akkuyu Fm., SW Turkey). *Sedimentology* 46, 589–602.
- Bayon, G., Birot, D., Ruffine, L., Caprais, J.-C., Ponzevera, E., Bollinger, C., Donval, J.-P., Charlou, J.-L., Voisset, M., Grimaud, S., 2011. Evidence for intense REE scavenging at cold seeps from the Niger Delta margin. *Earth Planet. Sci. Lett.* 312, 443–452.
- Benitez-Nelson, C.R., 2000. The biogeochemical cycling of phosphorus in marine systems. *Earth Sci. Rev.* 51, 109–135.
- Berelson, W.M., McManus, J., Severmann, S., Reimers, C.E., 2013. Benthic flux of oxygen and nutrients across Oregon/California shelf sediments. *Cont. Shelf Res.* 55, 66–75.
- Berner, R.A., 1970. Sedimentary pyrite formation. *Am. J. Sci.* 268, 1–23.
- Berner, R.A., 1984. Sedimentary pyrite formation: an update. *Geochim. Cosmochim. Acta* 48, 605–615.
- Berner, R.A., Puchelt, H., Nöltner, T., Kramar, U., 2013. Pyrite geochemistry in the Toarcian Posidonia Shale of south-west Germany: evidence for contrasting trace-element patterns of diagenetic and syngenetic pyrites. *Sedimentology* 60, 548–573.
- Bialkowski, A., Tribouillard, N., Vergès, E., Deconinck, J.-F., 2000. Etude haute résolution de la distribution et de la granulométrie des constituants organiques sédimentaires. Corrélations avec les variations du niveau marin. *Kimméridgien/Tithonien du Boulonnais (Nord de la France)*. CR Acad. Sci. Paris II 331, 451–458.
- Bond, D.P., Zaton, M., Wignall, P.B., Marynowski, L., 2013. Evidence for shallow-water ‘Upper Kellwasser’ anoxia in the Frasnian–Famennian reefs of Alberta, Canada. *Lethaia* 46, 355–368.
- Böning, P., Brumsack, H.-J., Schnetger, B., Grunwald, M., 2009. Trace element signatures of Chilean upwelling sediments at ~36°S. *Mar. Geol.* 259, 112–121.
- Bostick, B.C., Fendorf, S., 2003. Arsenite sorption on troilite (FeS) and pyrite (FeS₂). *Geochim. Cosmochim. Acta* 67, 909–921.
- Boussafir, M., Lallier-Vergès, E., Bertrand, Ph., Badaut-Trauth, D., 1994. Structure ultrafine de la matière organique dans des roches mères du Kimméridgien du Yorkshire (UK). *Bull. Soc. Géol. Fr.* 165, 353–361.
- Boussafir, M., Gelin, F., Lallier-Vergès, E., Derenne, S., Bertrand, Ph., Largeau, C., 1995a. Electron microscopy and pyrolysis of kerogens from the Kimmeridge Clay Fm., UK: source organisms, preservation processes and origin of microcycles. *Geochim. Cosmochim. Acta* 59, 3731–3747.
- Boussafir, M., Lallier-Vergès, E., Bertrand, Ph., Badaut-Trauth, D., 1995b. SEM and STEM studies on isolated organic matter and rock microfacies from a short-term organic cycle of the Kimmeridge Clay Formation (Yorkshire, UK). In: Lallier-Vergès, E., Tribouillard, N.-P., Bertrand, Ph. (Eds.), *Organic Matter Accumulation*. Lecture Notes in Earth Sciences 57. Springer, pp. 15–30.
- Bout-Roumazeilles, V., Cortijo, E., Labeyrie, L., Debrabant, P., 1999. Clay-mineral evidence of nepheloid layer contribution to the Heinrich layers in the Northwest Atlantic. *Palaeogeogr. Palaeoclimatol. Palaeoecol.* 146, 211–228.
- Braaksma, H., Proust, J.-N., Kenter, J.A.M., Drijkoningen, G.G., Filippidou, N., 2006. Sedimentological, petrophysical, and seismic characterization of an upper Jurassic shoreface-dominated shelf margin (the Boulonnais, Northern France). *J. Sediment. Res.* 76, 175–199.
- Breier, J.A., Toner, B.M., Fakra, S., Manganini, S.J., White, S.N., Thurnherr, A.M., German, C.R., 2012. Sulfur, sulfides, oxides, and organic matter aggregated in the deep-sea hydrothermal plumes 551 of 9° 50' N East Pacific Rise. *Geochim. Cosmochim. Acta* 88, 216–236.
- Bressac, M., Huie, C., 2013. Post-depositional processes: what really happens to new atmospheric iron in the ocean's surface? *Glob. Biogeochem. Cycles* 27, 1–12. <http://dx.doi.org/10.1002/gbc.20076>.
- Brumsack, H.-J., 2006. The trace metal content of recent organic carbon-rich sediments: implications for Cretaceous black shale formation. *Palaeogeogr. Palaeoclimatol. Palaeoecol.* 232, 344–361.
- Buck, C.S., Landing, W.M., Resing, J.A., 2013. Pacific Ocean aerosols: deposition and solubility of iron, aluminum, and other trace elements. *Mar. Chem.* 157, 117–130.
- Calvert, S.E., Pedersen, T.F., 1993. Geochemistry of recent oxic and anoxic sediments: implications for the geological record. *Mar. Geol.* 113, 67–88.
- Canfield, D.E., Raiswell, R., Bottrell, S., 1992. The reactivity of sedimentary iron minerals toward sulfide. *Am. J. Sci.* 292, 659–683.
- Canfield, D.E., Lyons, T.W., Raiswell, R., 1996. A model for iron deposition to euxinic Black Sea sediments. *Am. J. Sci.* 296, 818–834.
- Carignan, J., Hild, P., Morel, J., Yeghicheyan, D., 2001. Routine analysis of trace elements in geochemical samples using flow injection and low-pressure on-line liquid chromatography coupled to ICP-MS: a study of geochemical reference materials BR, DR-N, UB-N, AN-G and GH. *Geostand. Newslett.* 25, 187–198.
- Carmichael, S.K., Waters, J.A., Suttor, T.J., Kido, E., DeReuil, A., 2014. A new model for the Kellwasser Anoxia Events (Late Devonian): shallow water anoxia in an open oceanic setting in the Central Asian Orogenic Belt. *Palaeogeogr. Palaeoclimatol. Palaeoecol.* 399, 394–403.
- Cha, H.J., Lee, C.B., Kim, B.S., Choi, M.S., Ruttenberg, K.C., 2005. Early diagenetic redistribution and burial of phosphorus in the sediments of the southwestern East Sea (Japan Sea). *Mar. Geol.* 216, 127–143.
- Chailhou, G., Schäfer, J., Anschutz, P., Lavaux, G., Blanc, G., 2003. The behaviour of Arsenic in the muddy sediments of the Bay of Biscay (France). *Geochim. Cosmochim. Acta* 67, 2993–3003.
- Chappaz, A., Gobeil, C., Tessier, A., 2008. Geochemical and anthropogenic enrichments of Mo in sediments from perennially oxic and seasonally anoxic lakes in Eastern Canada. *Geochim. Cosmochim. Acta* 72, 170–184.
- Chappaz, A., Lyons, T.W., Gregory, D.D., Reinhard, C.T., Gill, B.C., LiC, Large, R.R., 2014. Does pyrite act as an important host for molybdenum in modern and ancient euxinic sediments? *Geochim. Cosmochim. Acta* 126, 112–122.
- Claypool, G.E., Mancini, E.A., 1989. Geochemical relationships of petroleum in Mesozoic reservoirs to carbonate source rocks of Jurassic Smackover Formation, southwestern Alabama. *AAPG Bull.* 73, 904–924.

- Couture, R.-M., Gobeil, C., Tessier, A., 2010. Arsenic, iron and sulfur co-diagenesis of in lake sediments. *Geochim. Cosmochim. Acta* 74, 1238–1255.
- Crusius, J., Calvert, S., Pedersen, T., Sage, D., 1996. Rhenium and molybdenum enrichments in sediments as indicators of oxic, suboxic and sulfidic conditions of deposition. *Earth Planet. Sci. Lett.* 145, 65–78.
- Cutter, G.A., Cutter, L.S., Featherstone, A.M., Lohrenz, S.E., 2001. Antimony and arsenic biogeochemistry in the western Atlantic Ocean. *Deep-Sea Res. II* 48, 2895–2915.
- Dale, A.W., Meyers, S.R., Aguilera, D.R., Arndt, S., Wallmann, K., 2012. Controls on organic carbon and molybdenum accumulation in Cretaceous marine sediments from the Cenomanian–Turonian interval including Oceanic Anoxic Event 2. *Chem. Geol.* 324–325, 28–45.
- Deconinck, J.-F., Geyssant, J.R., Proust, J.-N., Vidier, J.P., 1996. Sédimentologie et biostratigraphie des dépôts kimméridgiens et tithoniens du Boulonnais. *Ann. Soc. Géol. Nord* 4, 157–170.
- Delaney, M.L., 1998. Phosphorus accumulation in marine sediments and the oceanic phosphorus cycle. *Glob. Biogeochem. Cycles* 12, 563–572.
- Dellwig, O., Leipe, T., März, C., Glockzin, M., Pollehn, F., Schnetger, B., Yakushev, E.V., Böttcher, M.E., Brumsack, H.-J., 2010. A new particulate Mn–Fe–P-shuttle at the redoxcline of anoxic basins. *Geochim. Cosmochim. Acta* 74, 7100–7115.
- Derenne, S., Largeau, C., Casadevall, E., Berkloff, C., Rousseau, B., 1991. Chemical evidence of kerogen formation in source rocks and oil shales via selective preservation of thin resistant outer walls of microalgae: origin of ultralaminæ. *Geochim. Cosmochim. Acta* 55, 1041–1050.
- Esplatié, J., 1993. Rock Eval pyrolysis. In: Bordenave, M.L. (Ed.), *Applied Petroleum Geochemistry*. Technip, Paris, pp. 237–261.
- Filippelli, G., 2001. Carbon and phosphorus cycling in anoxic sediments of the Saanich Inlet, British Columbia. *Mar. Geol.* 174, 307–321.
- Föllmi, K.B., 1996. The phosphorus cycle, phosphogenesis and marine phosphate-rich deposits. *Earth Sci. Rev.* 40, 55–124.
- Froelich, P.N., Arthur, M.A., Burnett, W.C., Deakin, M., Hensley, V., Jahnke, R., Kaul, L., Kim, K.-H., Roe, K., Soutar, A., Vathakanon, C., 1988. Early diagenesis of organic matter in Peru continental margin sediments: phosphorite precipitation. *Mar. Geol.* 80, 309–343.
- Fürsch, F., Oschmann, W., 1986. Storm shell beds of *Nanogyra virgula* in the upper Jurassic of France. *N. Jb. Geol. Paläont. Abh.* 172, 141–161.
- Gelin, F., Boussafir, M., Derenne, S., Largeau, C., Bertrand, Ph., 1995. Study of qualitative and quantitative variations in kerogen chemical structure along a microcycle: correlation with ultrastructural features. In: Lallier-Vergès, E., Tribouillard, N.-P., Bertrand, Ph. (Eds.), *Organic Matter Accumulation*. Lecture Notes in Earth Sciences 57. Springer, pp. 32–47.
- Gelin, F., Volkmann, J.K., Largeau, C., Derenne, S., Sinninghe Damsté, J.S., de Leeuw, J.W., 1999. Distribution of aliphatic, non-hydrolyzable biopolymers in marine microalgae. *Org. Geochem.* 30, 147–159.
- Geyssant, J.R., Vidier, J.-P., Herbin, J.-P., Proust, J.N., Deconinck, J.-F., 1993. Biostratigraphie et paléoenvironnement des couches de passage Kimméridgien/Tithonien du Boulonnais (Pas de Calais): nouvelles données paléontologiques (ammonites), organisation séquentielle et contenu en matière organique. *Géol. Fr.* 4, 11–24.
- Goldberg, T., Archer, C., Vance, D., Poulton, S.W., 2009. Mo isotope fractionation during adsorption to Fe (oxyhydr)oxides. *Geochim. Cosmochim. Acta* 73, 6502–6516.
- Goldhammer, T., Brüchert, V., Ferdelman, T.G., Zabel, M., 2010. Microbial sequestration of phosphorus in anoxic upwelling sediments. *Nat. Geosci.* 3, 557–561. <http://dx.doi.org/10.1038/ngeo913>.
- Helz, G.R., Bura-Nakić, E., Mikac, N., Ciglenečki, I., 2011. New model for molybdenum behavior in euxinic waters. *Chem. Geol.* 284, 323–332.
- Herbin, J.-P., Fernandez-Martinez, J.L., Geyssant, J.R., El Albani, A., Deconinck, J.-F., Proust, J.-N., Colbeaux, J.-P., Vidier, J.P., 1995. Sequence stratigraphy of source rocks applied to the study of the Kimmeridgian/Tithonian in the Northwest European shelf (Dorset/UK, Yorkshire/UK and Boulonnais/France). *Mar. Pet. Geol.* 12, 177–194.
- Hu, Y., Feng, D., Peckmann, J., Roberts, H.H., Chen, D., 2014. New insights into cerium anomalies and mechanisms of trace metal enrichment in authigenic carbonate from hydrocarbon seeps. *Chem. Geol.* 381, 55–66.
- Huerta-Díaz, M.A., Morse, J.W., 1992. Pyritization of trace metals in anoxic marine sediments. *Geochim. Cosmochim. Acta* 56, 2681–2702.
- Ingall, E.D., Van Cappellen, P., 1990. Relation between sedimentation rate and burial of organic phosphorus and organic carbon in marine sediments. *Geochim. Cosmochim. Acta* 54, 373–386.
- Ingall, E., Bustin, R.M., Van Cappellen, P., 1993. Influence of water-column anoxia on the burial and preservation of carbon and phosphorus in marine shales. *Geochim. Cosmochim. Acta* 57, 303–316.
- Jarvis, I., Burnett, W.C., Nathan, Y., Almbaydin, F.S.M., Attia, A.K.M., Castro, L.N., Flicoteaux, R., Hilmy, M.E., Husain, V., Qutawnnah, A.A., Serjani, A., Zanin, Y.N., 1994. Phosphorite geochemistry: state of the art and environmental concerns. *Eclogae Geol. Helv.* 87, 643–700.
- Jilbert, T., Slomp, C.P., 2013. Iron and manganese shuttles control the formation of authigenic phosphorus minerals in the euxinic basins of the Baltic Sea. *Geochim. Cosmochim. Acta* 107, 155–169.
- Jones, R.W., 1984. Comparison of carbonate and shale source rocks. In: Palacas, G. (Ed.), *Petroleum Geochemistry and Source Rock Potential of Carbonate Rocks*. AAPG Studies in Geology 18, pp. 163–180.
- Kashiwabara, T., Takahashi, Y., Tanimizu, M., Usui, A., 2011. Molecular-scale mechanisms of distribution and isotopic fractionation of molybdenum between seawater and ferromanganese oxides. *Geochim. Cosmochim. Acta* 75, 5762–5784.
- Krachler, R., von der Kammer, F., Jirsa, F., Süphandag, A., Krachler, R.F., Plessl, C., Vogt, M., Keppler, B.K., Hofmann, T., 2012. Nanoscale lignin particles as source of dissolved iron to the ocean. *Glob. Biogeochem. Cycles* 26, GB3024. <http://dx.doi.org/10.1029/2012GB004294>.
- Largeau, C., Derenne, S., Casadevall, E., Berkloff, C., Corolleur, M., Lugardon, Raynaud, J.F., Connan, J., 1990. Occurrence and origin of “ultralaminar” structures in “amorphous” kerogens of various source rocks and oil shales. *Advance in Organic Geochemistry* 89Org. *Geochem.* 16, 889–895.
- Li, X.J., Shi, H.M., Xia, H.-Y., Zhou, Y.-P., Qiu, Y.W., 2014. Seasonal hypoxia and its potential forming mechanisms in the Mirs Bay, the Northern South China Sea. *Cont. Shelf Res.* 80, 1–7.
- Lückge, A., Boussafir, M., Lallier-Vergès, E., Littke, R., 1996. Comparative study of organic matter preservation in immature sediments along the continental margins of Peru and Oman. I: results of petrographical and bulk geochemical data. *Org. Geochem.* 24, 437–451.
- Lyons, T.W., Severmann, S., 2006. A critical look at iron paleoredox proxies based on new insights from modern euxinic marine basins. *Geochim. Cosmochim. Acta* 70, 5698–5722.
- Martin, P., van der Looff, M.R., Cassar, N., Vandromme, P., d’Ovidio, F., Stemmann, L., Rengarajan, R., Soares, M., González, H.E., Ebersbach, F., Lampitt, R.S., Sanders, R., Barnett, B.A., Smetacek, V., Naqvi, S.W.A., 2013. Iron fertilization enhanced net community production but not downward particle flux during the Southern Ocean iron fertilization experiment LOHALEX. *Glob. Biogeochem. Cycles* 27, 871–881. <http://dx.doi.org/10.1029/gbc.20077>.
- März, C., Poultion, S.W., Beckmann, B., Küster, K., Wagner, T., Kasten, S., 2008. Redox sensitivity of P cycling during marine black shale formation: Dynamics of sulfidic and anoxic, non-sulfidic bottom waters. *Geochim. Cosmochim. Acta* 72 (15), 3703–3717.
- März, C., Stratmann, A., Matthiessen, J., Meinhardt, A.-K., Eckert, S., Schnetger, B., Vogt, C., Stein, R., Brumsack, H.-J., 2011a. Manganese-rich brown layers in Arctic Ocean sediments: composition, formation mechanisms, and diagenetic overprint. *Geochim. Cosmochim. Acta* 75, 7668–7687.
- März, C., Vogt, C., Schnetger, B., Brumsack, H.-J., 2011b. Variable Eocene–Miocene sedimentation processes and bottom water redox conditions in the Central Arctic Ocean (IODP Expedition 302). *Earth Planet. Sci. Lett.* 310, 526–537.
- März, C., Poultion, S.W., Wagner, T., Schnetger, B., Brumsack, H.-J., 2014. Phosphorus burial and diagenesis in the central Bering Sea (Bowers Ridge, IODP Site U1341): perspectives on the marine P cycle. *Chem. Geol.* 363, 270–282.
- McLennan, S.M., 2001. Relationships between the trace element composition of sedimentary rocks and upper continental crust. *Geochem. Geophys. Geosyst.* 2 (2000GC000109).
- Meyers, S.R., 2007. Production and preservation of organic matter: the significance of iron. *Paleoceanography* 22, PA4211. <http://dx.doi.org/10.1029/2006PA001332>.
- Meyers, S.R., Sageman, B.B., Lyons, T.W., 2005. Organic carbon burial rate and the molybdenum proxy: theoretical framework and the application to Cenomanian–Turonian oceanic anoxic event 2. *Paleoceanography* 20, PA2002. <http://dx.doi.org/10.1029/2004PA001068>.
- Minami, H., Kato, Y., 1997. Remobilization of arsenic in sub-oxic sediments from seafloor of the continental margin. *J. Oceanogr.* 53, 553–562.
- Mongenot, T., Boussafir, M., Derenne, S., Lallier-Vergès, E., Largeau, C., Tribouillard, N., 1997. Sulphur-rich organic matter from Bituminous Laminates of Orbagnoux (France, upper Kimmeridgian) – the role of early vulcanization. *Bull. Soc. Geol. Fr.* 168 (3), 331–341.
- Mongenot, T., Derenne, S., Largeau, C., Tribouillard, N., Lallier-Vergès, E., Dessert, D., Connan, J., 1999. Spectroscopic, kinetic and pyrolytic studies of kerogen from the dark parallel laminae facies of the sulphur-rich Orbagnoux deposit (Upper Kimmeridgian, Jura). *Org. Geochem.* 30, 39–56.
- Neumann, T., Scholz, F., Kramar, U., Ostermaier, M., Rausch, N., Berner, Z., 2013. Arsenic in frambooidal pyrite from recent sediments of a shallow water lagoon of the Baltic Sea. *Sedimentology* <http://dx.doi.org/10.1111/sed.12031>.
- O'Day, P., 2006. Chemistry and mineralogy of arsenic. *Elements* 2, 77–83.
- Oehler, J.H., 1984. Carbonate source rock in the Jurassic Smackover trend of Mississippi, Alabama, and Florida. In: Palacas, G. (Ed.), *Petroleum Geochemistry and Source Rock Potential of Carbonate Rocks*. AAPG Studies in Geology 18, pp. 63–70.
- Owens, J.D., Lyons, T.W., Li, X., Macleod, K.G., Gordon, G., Kuyper, M.M.M., Anbar, A., Kuht, W., Severmann, S., 2012. Iron isotope and trace metal records of iron cycling in the proto-North Atlantic during the Cenomanian–Turonian oceanic anoxic event (OAE-2). *Paleoceanography* 27, PA3223. <http://dx.doi.org/10.1029/2012PA002328>.
- Palacas, G.J., Anders, D.E., King, J.D., 1984. South Florida basin. Prime example of carbonate source rock of petroleum. In: Palacas, G. (Ed.), *Petroleum Geochemistry and Source Rock Potential of Carbonate Rocks*. AAPG Studies in Geology 18, pp. 71–96.
- Piper, D.Z., Perkins, R.B., 2004. A modern vs. Permian black shale – the hydrography, primary productivity, and water-column chemistry of deposition. *Chem. Geol.* 206, 177–197.
- Piper, D.Z., Perkins, R.B., 2014. Geochemistry of a marine phosphate deposit: a signpost to phosphogenesis. In: Scott, S.D. (Ed.), *Geochemistry of Mineral Deposits*, second edition. Treatise on Geochemistry vol. 13, pp. 293–312.
- Poulton, S.W., Canfield, D.E., 2005. Development of a sequential extraction procedure for iron: implications for iron partitioning in continentally derived particulates. *Chem. Geol.* 214, 209–221.
- Poulton, S.W., Canfield, D.E., 2011. Ferruginous conditions: a dominant feature in the ocean through Earth's history. *Elements* 7, 107–112.
- Poulton, S.W., Raiswell, R., 2002. The low-temperature geochemical cycle of iron: from continental fluxes to marine sediment deposition. *Am. J. Sci.* 302, 774–805.
- Proust, J.-N., 1994. Notions élémentaires de stratigraphie séquentielle illustrées par un exemple. *Ann. Soc. Géol. Nord* 3 (II), 5–25.
- Proust, J.-N., Deconinck, J.-F., Geyssant, J.R., Herbin, J.-P., Vidier, J.P., 1993. Nouvelles données sédimentologiques dans le Kimméridgien et le Tithonien du Boulonnais (France). *CR Acad. Sci. Paris* 316 (II), 363–369.
- Proust, J.-N., Deconinck, J.-F., Geyssant, J.R., Herbin, J.-P., Vidier, J.P., 1995. Sequence analytical approach to the Upper Kimmeridgian–Lower Tithonian storm-dominated

- ramp deposits of the Boulonnais (Northern France). A landward time-equivalent to offshore marine source rocks. *Geol. Rundsch.* 84, 255–271.
- Raiswell, R., Canfield, D.E., 1996. Rates of reaction between silicate iron and dissolved sulfide in Peru Margin sediments. *Geochim. Cosmochim. Acta* 60, 2777–2787.
- Raiswell, R., Canfield, D.E., 2012. The iron biogeochemical cycle past and present. *Geochem. Perspect.* 1, 1–186.
- Ramanampisoa, L., Bertrand, P., Disnar, J.R., Lallier-Vergès, E., Pradier, B., Tribouillard, N.-P., 1992. *Etude à haute résolution d'un cycle du carbone organique des argiles du Kimméridgien du Yorkshire (G.-B.): résultats préliminaires de géochimie et de pétrographie organique.* CR Acad. Sci. Paris II 314, 1493–1498.
- Ramdani, A., 1996. Les paramètres qui contrôlent la sédimentation cyclique de la Kimmeridge Clay Formation dans le bassin de Clevelan (Yorkshire, Grande Bretagne) – comparaison avec le Boulonnais (France). PhD thesis, Paris XI-Orsay University, unpublished.
- Reed, D.C., Slomp, C.P., Gustafsson, B.G., 2011. Sedimentary phosphorus dynamics and the evolution of bottom-water hypoxia: a coupled benthic–pelagic model of a coastal system. *Limnol. Oceanogr.* 56, 1075–1092.
- Reimers, C.E., Ruttenberg, K.C., Canfield, D.E., Christiansen, M.B., Martin, J.B., 1996. Porewater pH and authigenic phases formed in the uppermost sediments of the Santa Barbara Basin. *Geochim. Cosmochim. Acta* 60, 4037–4057.
- Rickard, D., 2012. Sulfidic sediments and sedimentary rock. *Developments in Sedimentology* 65, Elsevier (801 p.).
- Sageman, B.B., Lyons, T.W., 2003. Geochemistry of fine-grained sediments and sedimentary rocks. In: Holland, H.D., Turekian, K.K. (Eds.), *Treatise on Geochemistry*. vol. 7. Elsevier, pp. 115–158.
- Sarret, G., Mongenot, T., Connan, J., Derenne, S., Kasrai, M., Bancroft, G.M., Largeau, C., 2002. Sulfur speciation in kerogens of the Orbagnoux deposit (Upper Kimmeridgian, Jura) by XANES spectroscopy and pyrolysis. *Org. Geochem.* 33, 877–895.
- Schenau, S.J., Reichart, G.J., de Lange, De Lange, G.J., 2005. Phosphorus burial as a function of paleoproductivity and redox conditions in Arabian Sea sediments. *Geochim. Cosmochim. Acta* 69, 919–931.
- Scholz, F., Hensen, C., Noffke, A., Rohde, A., Liebetrau, V., Wallmann, K., 2011. Early diagenesis of redox-sensitive trace metals in the Peru upwelling area – response to ENSO-related oxygen fluctuations in the water column. *Geochim. Cosmochim. Acta* 75, 7257–7276.
- Scholz, F., McManus, J., Sommer, S., 2013. The manganese and iron shuttle in a modern euxinic basin and implications for molybdenum cycling at euxinic ocean margins. *Chem. Geol.* 335, 56–68.
- Scholz, F., Severmann, S., McManus, J., Hensen, C., 2014. Beyond the Black Sea paradigm: the sedimentary fingerprint of an open-marine iron shuttle. *Geochim. Cosmochim. Acta* 127, 368–380.
- Scott, C., Lyons, T.W., 2012. Contrasting molybdenum cycling and isotopic properties in euxinic versus non-euxinic sediments and sedimentary: refining the paleoproxies. *Chem. Geol.* 324–325, 19–27.
- Severmann, S., McManus, J., Berelson, W.M., Hammond, D.E., 2010. The continental shelf benthic iron flux and its isotope composition. *Geochim. Cosmochim. Acta* 74, 3984–4004.
- Shigemitsu, M., Nishioka, J., Watanabe, Y.W., Yamanaka, Y., Nakatsuka, T., Volkov, Y.N., 2013. Fe/Al ratios of suspended particulate matter from intermediate water in the Okhotsk Sea: implications for long-distance lateral transport of particulate Fe. *Mar. Chem.* 157, 41–48.
- Slomp, C.P., Van Cappellen, P., 2007. The global marine phosphorus cycle: sensitivity to oceanic circulation. *Biogeosciences* 4, 155–171.
- Slomp, C.P., Van der Gaast, S.J., Van Raaphorst, W., 1996. Phosphorus binding by poorly crystalline iron oxides in North Sea sediments. *Mar. Chem.* 52, 55–73.
- Soudry, D., 2000. Carbonate–phosphate competition in the Negev phosphorites (southern Israel): a microstructural study. In: Glenn, C.R., Prévôt-Lucas, L., Lucas, J. (Eds.), *Marine authigenesis: from global to microbial*. SEPM Spec. Publ. 66, pp. 415–426.
- Stein, M., Arnaud-Vanneau, A., Adatte, T., Fleitmann, D., Spangenberg, J.E., Föllmi, K.B., 2012. Paleoenvironmental and paleoecological change on the northern Tethyan carbonate platform during the late Barremian–earliest Aptian. *Sedimentology* 59, 939–963.
- Sullivan, K.A., Aller, R.C., 1996. Diagenetic cycling of arsenic in Amazon shelf sediments. *Geochim. Cosmochim. Acta* 60, 1465–1477.
- Taguchi, K., Mori, K., 1992. The distribution and generation of hydrocarbons in carbonate source rocks. In: Whelan, J.K., Farrington, J.W. (Eds.), *Organic Matter Production, Accumulation and Preservation in Recent and Ancient Sediments*. Columbia University Press, New York, pp. 487–515.
- Taylor, K.G., Konhauser, K.O., 2011. Iron in Earth surface systems. *Elements* 7, 1–144.
- Taylor, K.G., Macquaker, J.H.S., 2011. Iron minerals in marine sediments record chemical environments. *Elements* 7, 113–118.
- Taylor, S.R., McLennan, S.M., 1985. *The Continental Crust: Its Composition and Evolution*. Blackwell, Oxford (312 pp.).
- Taylor, S.P., Sellwood, B.W., Gallois, R.W., Chambers, M.H., 2001. A sequence stratigraphy of the Kimmeridgian and Bolonian stages (Late Jurassic): Wessex–Weald Basin, southern England. *J. Geol. Soc.* 158, 179–192.
- Tegelaar, E.W., de Leeuw, J.W., Derenne, S., Largeau, C., 1989. A reappraisal of kerogen formation. *Geochim. Cosmochim. Acta* 53, 3103–3106.
- Trappe, J., 1998. *Phanerozoic phosphorite depositional systems*. Lecture Notes in Earth Sciences 76. Springer (316 p.).
- Tribouillard, N., Desprairies, A., Lallier-Vergès, L., Bertrand, P., 1994. Sulfur incorporation of lipidic organic matter in reactive-iron deficient environments: a possible enhancement for the storage of hydrogen-rich organic matter. *CR Acad. Sci. Paris* 319, 1199–1206.
- Tribouillard, N., Bialkowski, A., Tyson, R.V., Vergès, E., Deconinck, J.-F., 2001. Organic facies and sea level variation in the Late Kimmeridgian of the Boulonnais area (northernmost France). *Mar. Pet. Geol.* 18, 371–389.
- Tribouillard, N., Averbuch, O., Bialkowski, A., Deconninck, J.-F., 2002. The influence of the early diagenesis of marine organic matter on the magnetic-susceptibility signal of sedimentary rock. *Bull. Soc. Geol. Fr.* 173, 295–306.
- Tribouillard, N., Averbuch, O., Riboulleau, A., 2004a. Influence of marine organic-matter diagenesis on magnetic susceptibility of sedimentary rocks: the sulphide pathway. *Ann. Soc. Géol. Nord* t.11 (2^e série), 57–67.
- Tribouillard, N., Riboulleau, A., Lyons, T., Baudin, F., 2004b. Enhanced trapping of molybdenum by sulfurized organic matter of marine origin as recorded by various Mesozoic formations. *Chem. Geol.* 213, 385–401.
- Tribouillard, N., Ramdani, A., Trentesaux, A., 2005. Controls on organic accumulation in Late Jurassic shales of Northwestern Europe as inferred from trace-metal geochemistry. In: Harris, N. (Ed.), *The Deposition of Organic-Carbon-Rich Sediments: Models, Mechanisms, and Consequences*. SEPM Special Publication 82, pp. 145–164.
- Tribouillard, N., Bout-Roumazeilles, V., Algeo, T.J., Lyons, T.W., Sionneau, T., Montero-Serrano, J.C., Riboulleau, A., Baudin, F., 2008a. Paleodepositional conditions in the Orca Basin as inferred from organic matter and trace metal contents. *Mar. Geol.* 254, 62–72.
- Tribouillard, N., Lyons, T.W., Riboulleau, A., Bout-Roumazeilles, V., 2008b. A possible capture of molybdenum during early diagenesis of dysoxic sediments. *Bull. Soc. Geol. Fr.* 179, 3–12.
- Tribouillard, N., Bout-Roumazeilles, V., Riboulleau, A., Baudin, F., Danelian, T., Riquier, L., 2011. Transfer of germanium to marine sediments: insights from its accumulation in radiolarites and authigenic capture under reducing conditions. Some examples through geological ages. *Chem. Geol.* 282, 120–130.
- Tribouillard, N., Algeo, T.J., Baudin, F., Riboulleau, A., 2012a. Analysis of marine environmental conditions based on molybdenum–uranium covariation—applications to Mesozoic paleoceanography. *Chem. Geol.* 324–325, 46–58.
- Tribouillard, N., Sansjofre, P., Ader, M., Trentesaux, A., Averbuch, O., Barbicot, F., 2012b. Early diagenetic carbonate bed formation at the sediment–water interface triggered by synsedimentary faults. *Chem. Geol.* 300 (301), 1–13.
- Tribouillard, N., Armynot du Châtelet, E., Gay, A., Barbicot, F., Sansjofre, P., Potdevin, J.-L., 2013. Geochemistry of cold seepage-impacted sediments: Per-ascensum or per-descensum trace metal enrichment? *Chem. Geol.* 340, 1–12.
- Tyson, R.V., 1995. *Sedimentary Organic Matter: Organic Facies and Palynofacies*. Chapman & Hall, London (615 p.).
- Van Cappellen, P., Ingall, E.D., 1994. Benthic phosphorus regeneration, net primary production and ocean anoxia: a model of the coupled marine biogeochemical cycles of carbon and phosphorus. *Paleoceanography* 9, 677–692.
- Van der Weijden, C.H., 2002. Pitfalls of normalization of marine geochemical data using a common divisor. *Mar. Geol.* 184, 167–187.
- Vandenbroucke, M., Largeau, C., 2007. Kerogen origin, evolution and structure. *Org. Geochim.* 38, 719–833.
- Vaughan, D.J., 2006. *Arsenic. Elements* 2, 71–75.
- Wang, Y., van Cappellen, P., 1996. A multicomponent reactive transport model of early diagenesis: application to redox cycling in coastal marine sediments. *Geochim. Cosmochim. Acta* 60, 2993–3014.
- Wignall, P.B., 1991. Test of the concepts of sequence stratigraphy in the Kimmeridgian (Late Jurassic) of England and northern France. *Mar. Pet. Geol.* 8, 430–441.
- Wignall, P.B., Newton, R., 2001. Black shales on the basin margin: a model based on examples from the Upper Jurassic of the Boulonnais, northern France. *Sediment. Geol.* 144, 335–356.
- Wijsman, J.W.M., Middleburg, J.J., Heip, C.H.R., 2001. Reactive iron in Black Sea sediments: implications for iron cycling. *Mar. Geol.* 172, 167–180.
- Williams, C.J., Hesselbo, S.P., Jenkyns, H.C., Morgans-Bell, H.S., 2001. Quartz silt in mudrocks as a key to sequence stratigraphy (Kimmeridge Clay Formation, Late Jurassic, Wessex Basin, UK). *Terra Nova* 13, 449–455.
- Zaback, D.A., Pratt, L.M., Hayes, J.M., 1993. Transport and reduction of sulphate and immobilisation of sulphide in marine black shales. *Geology* 21, 141–144.

Tableau 1:

Données isotopiques des patchs reefs

Samples	Type	d ¹³ C	d ¹⁸ O	CaCO3 %	d ¹⁸ O matrix	d ¹⁸ O shell	d ¹⁸ O shell filling
ambleteuse 01	Carbonate matrix	-8,87	-0,98	85,79	-0,98		
ambleteuse 02	Carbonate matrix	-8,47	-1,07	87,16	-1,07		
ambleteuse 03	Carbonate matrix	-6,20	-1,48	82,67	-1,48		
ambleteuse 04	Carbonate matrix	-7,73	-1,09	89,07	-1,09		
ambleteuse 05	Carbonate matrix	0,03	-1,43	75,02	-1,43		
noirda 01	Carbonate matrix	-3,86	-2,17	45,44	-2,17		
cgn03	Carbonate matrix	-3,63	-3,44	76,15	-3,44		
noirda 02	Shell	0,26	-2,50	43,52		-2,50	
ambleteuse 06	Shell	-1,93	-1,70	69,88		-1,70	
Cap Gris-Nez 01	Shell	-0,40	-2,83	88,10		-2,83	
ambleteuse 07	Shell filling	-2,03	-1,43	73,39			-1,43
noirda 03	Shell filling	0,55	-5,19	86,02			-5,19
Cap Gris-Nez 02	Shell filling	-0,80	-4,75	92,53			-4,75

Tableau 2:

Toutes les données: Granulométrie, Diffraction des argiles et Calcimétrie pour les marnes intercalées au Calcaires du Moulin Wibert, Cap Gris-Nez													
échantillon	H strata (m)	Sceptibilité Magnétique m^3/kg	CaCO ₃	Argiles $<4\mu\text{m}$	Silts	Sables très fins	Sables fins	Sables moyens	Mode	Smectite %	Illite %	Chlorite %	Kaolinite %
1	6,1	3,867E-08	26	17	72	14	10	0	7,342	6	47	8	39
2	5,5	3,185E-08	42	13	68	18	11	1	9,102	5	48	10	37
3	5,2	3,426E-08	43	16	72	13	10	0	8,655	5	52	10	33
4	4,65	2,656E-08	52	18	71	16	8	0	7,213	11	47	10	32
5	4,4	2,787E-08	55	23	87	5	2	-	6,699	11	46	10	34
6	2,9	2,787E-08	61	21	77	11	6	0	6,725	10	49	9	32
7	2,5	3,448E-08	54	24	94	1	-	-	7,097	12	47	9	31
8	2,2	1,137E-08	63	25	92	2	0	-	6,946	8	51	10	32
9	1,7	3,477E-08	39	18	84	10	2	-	8,388	8	47	10	35
10	1,2	2,352E-08	65	22	84	8	2	-	6,838	11	51	8	30
11	0,5	5,001E-08	23	18	90	4	2	0	10,568	7	49	9	35

Tableau 3:

Toutes les données: Granulométrie, Diffraction des argiles et Calcimétrie pour les marnes intercalées au Calcaires du Moulin Wibert, Cap de la Crèche											
Echantillon	CaCO3 %	H strat (m)	Mode	Argiles	Silts	Sables très fins	Sables fins	Smectite %	Illite%	Chlorite%	Kaolinite%
CMW9	18	7,3	9,1	19	99	1	-	4	46	7	37
CMW8	24	6,5	7,42	19	88	7	2	4	43	6	35
CMW7	19	6,2	14,3	9	88	9	2	10	46	8	38
CMW6	17	5,3	10,87	12	89	8	1	6	47	9	36
CMW5	34	4,25	13,93	10	91	8	0	6	48	10	38
CMW3	63	2,25	7,72	20	97	1	-	10	43	9	36
CMV2	34	1,7	8,5	19	96	1	0	8	47	10	47
CMW1	45	0,8	21,5	8	85	9	4	12	43	8	43

Tableau 4:

	Rock Eval Calcaires du Moulin au Cap Gris Nez - Wibert, Bancs Jumeaux au Wimereux-Nord																					
information	Sample	Qty - (mg)	KFID	S1 - (mg/g)	S2 - (mg/g)	PI	Tmax(°C)	TpkS2(° C)	S3CO - (mg/g)	S3'CO - (mg/g)	S3 - (mg/g)	S3' - (mg/g)	PC(%)	RC(%)	TOC(%)	HI	OICO	OI	pyromINC(%)	oxiMINC(%)	MINC(%)	Eq. CaCO3
Calcaires du Moulin Wibert	AMW 2	52,1	1 253	0,05	0,80	0,06	428	467	0,08	0,4	0,83	15,9	0,11	0,54	0,65	123	12	128	0,44	4,62	5,06	42
	AMW 3	49,3	1 253	0,04	0,82	0,04	428	467	0,08	0,4	0,88	16,1	0,11	0,64	0,75	109	11	117	0,45	5,20	5,64	47
	AMW 4	50,7	1 253	0,03	0,69	0,04	428	467	0,08	0,3	0,77	14,6	0,09	0,50	0,59	117	14	131	0,40	6,60	7,00	58
	AMW 5	53,6	1 253	0,03	1,06	0,03	429	468	0,09	0,4	1,22	19,0	0,14	0,58	0,72	147	12	169	0,53	6,29	6,82	57
	AMW 6	56,6	1 253	0,02	0,53	0,04	427	466	0,04	0,3	0,94	16,2	0,08	0,42	0,50	106	8	188	0,45	7,12	7,57	63
(Marnes intercalées)	AMW 7	87,2	1 253	0,02	0,41	0,05	426	465	0,06	0,3	0,52	15,5	0,06	0,54	0,60	68	10	87	0,43	6,74	7,17	60
Cap Gris-Nez	AMW 9	87,3	1 253	0,02	0,86	0,02	430	469	0,15	0,4	0,62	13,3	0,10	0,76	0,86	100	17	72	0,37	4,50	4,87	41
	AMW 10	94,1	1 253	0,02	0,47	0,04	429	468	0,06	0,3	0,45	11,6	0,06	0,51	0,57	82	11	79	0,32	7,67	8,00	67
	AMW 10	94,3	1 253	0,02	0,49	0,05	429	468	0,07	0,3	0,44	11,6	0,06	0,53	0,59	83	12	75	0,32	7,59	7,92	66
	AMW 11	88,5	1 253	0,03	1,82	0,01	431	470	0,21	0,4	0,55	16,1	0,19	1,19	1,38	132	15	40	0,45	2,66	3,11	26
Calcaires du Moulin Wibert	CMW 01	94,4	1 253	0,02	0,58	0,03	428	467	0,06	0,2	0,33	7,9	0,07	0,29	0,36	161	17	92	0,22	7,02	7,24	60
	CMW 02	92,6	1 253	0,01	0,13	0,09	421	460	0,03	0,1	0,42	12,7	0,03	0,22	0,25	52	12	168	0,35	8,05	8,40	70
	CMW 03	96,0	1 253	0,01	0,34	0,04	430	469	0,04	0,2	0,39	8,5	0,05	0,31	0,36	94	11	108	0,24	7,86	8,09	67
	CMW 04	100,2	1 253	0,01	0,15	0,07	424	463	0,03	0,2	0,42	10,8	0,03	0,34	0,37	41	8	114	0,30	7,53	7,82	65
	CMW 05	96,1	1 253	0,02	0,11	0,12	420	459	0,02	0,1	0,28	8,4	0,02	0,15	0,17	65	12	165	0,23	7,75	7,99	67
	CMW 06	98,0	1 253	0,01	0,19	0,07	431	470	0,08	0,1	0,41	9,5	0,03	0,19	0,22	86	36	186	0,26	8,02	8,28	69
Bancs Carbonatées	CMW 07	98,2	1 253	0,01	0,17	0,06	429	468	0,03	0,2	0,38	10,1	0,03	0,32	0,35	49	9	109	0,28	7,84	8,12	68
Cap Gris-Nez	CMW 07	98,3	1 253	0,01	0,16	0,06	429	468	0,03	0,2	0,35	10,4	0,03	0,18	0,21	76	14	167	0,29	7,76	8,05	67
	CMW 08	87,2	1 253	0,03	0,19	0,13	427	466	0,03	0,2	0,72	13,1	0,04	0,26	0,30	63	10	240	0,36	8,70	9,06	75
	CMW 09	94,8	1 253	0,02	0,23	0,07	428	467	0,03	0,2	0,37	9,7	0,04	0,20	0,24	96	12	154	0,27	8,01	8,28	69
	CMW 10	93,9	1 253	0,04	0,17	0,19	424	463	0,03	0,2	0,43	7,5	0,03	0,12	0,15	113	20	287	0,21	8,44	8,65	72
	CMW 11	88,9	1 253	0,05	0,19	0,22	428	467	0,03	0,2	0,35	9,9	0,04	0,23	0,27	70	11	130	0,27	8,03	8,30	69
	CMW 12	99,5	1 253	0,01	0,15	0,08	426	465	0,02	0,2	0,38	9,0	0,03	0,17	0,20	75	10	190	0,25	7,43	7,68	64
Bancs Jumeaux	BJ-GN 01	90,6	1 253	0,06	0,63	0,09	425	464	0,07	0,4	0,55	12,2	0,08	0,48	0,56	112	12	98	0,34	3,39	3,73	31
	BJ-GN 02	91,3	1 253	0,02	0,32	0,07	429	468	0,02	0,2	0,29	4,9	0,04	0,15	0,19	168	11	153	0,14	7,85	7,98	66
	BJ-GN 03	84,8	1 253	0,03	1,11	0,02	425	464	0,07	0,4	0,49	12,7	0,12	0,48	0,60	185	12	82	0,35	6,24	6,60	55
	BJ-GN 03	84,0	1 253	0,02	1,04	0,02	425	464	0,05	0,3	0,43	10,4	0,11	0,40	0,51	204	10	84	0,29	5,59	5,88	49
	BJ-GN 04	99,8	1 253	0,05	6,08	0,01	424	463	0,27	0,5	0,90	19,6	0,56	1,43	1,99	306	14	45	1	0,58	1,13	9
	BJ-GN 05	93	1 253	0,02	0,23	0,08	426	465	0,02	0,1	0,32	6,7	0,03	0,18	0,21	110	10	152	0	8,40	8,58	71
	BJ-GN 06	94,1	1 253	0,03	4,11	0,01	426	465	0,19	0,5	0,98	21,0	0,39	1,16	1,55	265	12	63	1	3,69	4,27	36
	BJ-GN 07	98,8	1 253	0,03	3,12	0,01	427	466	0,16	0,5	1,01	22,6	0,31	1,07	1,38	226	12	73	1	3,12	3,75	31
	BJ-GN 08	95,9	1 253	0,03	2,78	0,01	427	466	0,15	0,5	1,17	29,2	0,28	0,98	1,26	221	12	93	1	3,09	3,90	32
(Nord Wimereux)	BJ-GN 09	86,4	1 253	0,01	0,26	0,05	426	465	0,01	0,2	0,31	7,4	0,04	0,13	0,17	153	6	182	0	8,50	8,70	72
	BJ-GN 10	99	1 253	0,01	0,29	0,05	427	466	0,03	0,1	0,34	8,5	0,04	0,24	0,28	104	11	121	0	7,86	8,10	67
	BJ-GN 11	99,6	1 253	0,02	0,66	0,03	426	465	0,05	0,2	0,66	18,1	0,08	0,58	0,66	100	8	100	1	5,52	6,02	50
	BJ-GN 11	99,4	1 253	0,03	0,71	0,04	426	465	0,06	0,3	0,70	17,7	0,09	0,59	0,68	104	9	103	0	5,48	5,97	50
	BJ-GN 12	95,4	1 253	0,01	0,33	0,04	427	466	0,02	0,1	0,29	5,5	0,04	0,11	0,15	220	13	193	0	7,96	8,12	68
	BJ-GN 13	95,2	1 253	0,01	0,98	0,01	424	463	0,06	0,3	0,42	12,8	0,10	0,43	0,53	185	11	79	0	4,02	4,37	36
	BJ-GN 14	98,2	1 253	0,02	0,90	0,02	425	464	0,06	0,3	0,47	13,3	0,10	0,39	0,49	184	12	96	0	3,79	4,16	35
	BJ-GN 15	91,7	1 253	0,02	0,80	0,03	426	465	0,05	0,3	0,51	15,3	0,09	0,47	0,56	143	9	91	0	3,10	3,52	29
	BJ-GN 16	92,6	1 253	0,02	1,49	0,01	429	468	0,12	0,4	0,74	14,8	0,16	0,91	1,07	139	11	69	0	2,55	2,97	25

Tableau 5:

Données concernant des RockEval: Calcaire du Moulin Wibert au Cap de la Crèche.												
sapmle	PC [%]	RC [%]	TOC [%]	MINC [%]	HI [mg HC/g]	OI [mg CO ₂ /g]	Tmax [°C]	S1 [mg HC/g]	S2a [mg HC/g]	S2b [mg HC/g]	S3	Quant
bancs 1	0,06	0,37	0,43	5,93	114	120	430	0,01	0,49	0,00	0,52	70,1
bancs 2	0,07	0,70	0,77	5,00	92	52	426	0,01	0,70	0,00	0,40	55,3
bancs 3	0,04	0,41	0,45	8,59	62	94	426	0,01	0,28	0,00	0,42	64,6
bancs 5	0,08	0,67	0,75	4,83	100	81	432	0,01	0,74	0,00	0,60	60,1
bancs 6	0,47	1,61	2,08	2,13	259	31	423	0,02	5,38	0,00	0,64	51,9
bancs 7	0,12	1,00	1,11	2,72	106	53	432	0,01	1,18	0,00	0,59	70,4
bancs 8	0,03	0,38	0,41	3,25	52	104	424	0,01	0,21	0,00	0,43	79,5
bancs 9	0,04	0,46	0,50	2,17	68	86	429	0,01	0,34	0,00	0,43	64,2
intercalé 1	0,06	0,93	0,99	3,31	55	65	426	0,01	0,55	0,00	0,64	86
intercalé 1 -BASE	0,14	0,87	1,01	2,31	149	38	426	0,01	1,50	0,00	0,38	78,5
intercalé 2	0,07	0,88	0,95	3,16	61	72	427	0,01	0,58	0,00	0,68	55,8
intercalé 2 -BASE	0,12	1,03	1,15	2,72	117	36	429	0,01	1,34	0,00	0,41	58,8
intercalé 3	0,12	1,07	1,19	1,67	100	59	429	0,02	1,18	0,00	0,70	42,1
intercalé 3 -BASE	0,06	0,58	0,65	5,78	97	57	424	0,01	0,63	0,00	0,37	66,2
intercalé 4	0,08	0,81	0,89	1,64	77	97	433	0,02	0,68	0,00	0,87	57
intercalé 5	0,03	0,42	0,45	3,30	56	88	431	0,01	0,25	0,00	0,39	72,4
intercalé 6	0,04	0,44	0,48	2,86	61	92	430	0,01	0,29	0,00	0,44	69,2
intercalé 7	0,04	0,51	0,55	1,90	53	79	427	0,01	0,29	0,00	0,44	67,2
intercalé 8	0,04	0,55	0,59	1,69	61	65	428	0,01	0,36	0,00	0,38	68,4
intercalé 9	0,04	0,51	0,55	1,13	55	80	429	0,01	0,30	0,00	0,44	66,5
intercalé 10	0,04	0,46	0,50	1,15	54	90	429	0,01	0,27	0,00	0,45	65,8

Tableau 6:

Données de composition de Carbone et oxygéné (isotope stable) pour les Lumachelles mises en place à l'occasion de tempêtes au sein des argiles de Châtillon				
la première série			la deuxième série	
Echantillons	d13C	d18O	CaCO3%	Echantillons
	0,1	0,2	10	
06 Lg lumachelle; gris-nez	1,2	-2,9	89	01 Lumachelle - falaise ; gris-nez
03 Lg lumachelle; gris-nez	-0,9	-2,2	88	0,7
05 Lg lumachelle; gris-nez	-0,1	-2,2	71	-0,5
01 Lg lumachelle; gris-nez	1,5	-5,1	82	01 Tempestite - falaise ; gris-nez
02 Lg lumachelle; gris-nez	1,4	-3,6	77	-1,0
t-01-g tempestite; gris-nez	-1,1	-2,2	64	B02 Banc calcaire; gris-nes
TN-01 Tempestite; Noirda	0,0	-4,8	41	-1,2
N01 Lumachelle Noirda	1,3	-3,4	84	-0,8
L1* lumachelle Noirda	-1,4	-3,9	85	BN-02- calcaire- Noirda
				BN-01- banc calcaire- Noirda
				-3,9
				-4,7
				-4,3
				77

Données de composition de Carbon Et oxygen (isotope stable) pour le banc sommital : qui représente la limite entre la Grès de Châtillon. et les Argiles de Châtillon.				
Echantillons	d13C	d18O	CaCO3%	
BSM01- 220m cran aux œufs bas	-0,8	-2,6	60	
BSM02 - 220m cran aux œufs haut	0,5	-5,1	32	
BSM 001- 150m cran aux œufs bas	-1,4	-2,9	60	
BSM002- 150m cran aux œufs haut	0,7	-7,5	34	
BSM1- 0m cran aux œufs bas	0,6	-4,8	38	

Tableau 7:

données de composition de Carbone et oxygène (isotope stable) au Calcaires du Moulin Wibert- Cap Gris-Nez		
Échantillon	δ13C	δ18O
CMW-1	0,75	-2,5
CMW-2	-1	-2,34
CMW-3	0,03	-2,52
CMW-4	-1,31	-2,29
CMW-5	0,31	-2,25
CMW-6	0,23	-2,29
CMW-7	0,15	-2,31
CMW-8	-0,33	-2,19
CMW-9	-0,38	-2,16
CMW-10	-0,6	-2,48
CMW-11	-1,42	-1,87
CMW-12	-1,06	-2,14
CMW-1-2	0,87	-2,3
CMW-2-2	-1,14	-2,31
CMW-3-2	-0,2	-2,42
CMW-4-2	0,02	-2,34
CMW-5-2	-1,17	-2,31
CMW-6-2	-0,49	-2,43
CMW-7-2	-0,57	-2,45
CMW-8-2	0,01	-2,47
CMW-9-2	-0,36	-2,45
CMW-11-2	-1,66	-1,93
CMW-12-2	-1,12	-2,25

Tableau 8:

données de composition de Carbone et oxygène (isotope stable) au Calcaires du Moulin Wibert-Cap Gris-Nez, pour 4 bancs calcaires			
échantillon	d13C	d18O	CaCO3%
cmw b01-1	-0,2	-2,2	75
cmw b01-2	-0,5	-1,9	80
cmw b01-3	-0,3	-2,1	94
cmw b01-4	-0,5	-1,9	81
cmw b01-5	-0,6	-2,0	88
cmw b04-1 bas	-0,6	-2,2	94
cmw b04-2	-0,3	-2,3	94
cmw b04-3	-1,0	-2,2	95
cmw b04-4	-0,9	-2,2	100
cmw b04-5	-0,7	-2,2	96
cmw b08-1	0,9	-2,4	99
cmw b08-2	-0,3	-2,2	102
cmw b08-3	-0,2	-2,6	103
cmw b08-4	0,0	-2,5	97
cmw b08-5	-0,3	-2,3	98
cmw b08-6	0,9	-3,1	92
cmw b11-1	-0,8	-2,2	79
cmw b11-2	-1,5	-1,9	84
cmw b11-3	-1,3	-1,7	83
cmw b11-4	-1,5	-2,0	80
cmw b11-5	-1,1	-2,2	75

Tableau 9:

Calcaires Du Molin Wibert/ Gris-Nez			
	Sample	H cm	Teneur CaCO3 (%) 02
(Marnes intercalées)	1	605	25
	2	550	46
	3	510	41
	4	470	55
	5	440	53
	6	300	58
	7	260	55
	8	215	63
	9	167	39
	10	115	65
	11	50	23
Bancs Calcaires	1	640	50
	2	570	76
	3	530	72
	4	490	75
	5	455	82
	6	420	77
	7	280	86
	8	245	82
	9	185	83
	10	145	94
	11	95	70
	12	20	65

Tableau 10:

Eléments majeurs % - bancs lumachelles et Tempestite-Argiles de Châtillon au Cap Gris-Nez et Noirda.

Eléments majeurs % - bancs lumachelles et Tempestite-Argiles de Châtillon au Cap Gris-Nez et Noirda.															
Echant.	SiO2	TiO2	Al2O3	Fe2O3	MnO	MgO	CaO	Na2O	K2O	P2O5	LOI	Cr2O3	NiO	Somme	
	wt-%	wt-%	wt-%	wt-%	wt-%	wt-%	wt-%	wt-%	wt-%	wt-%	wt-%	wt-%	wt-%	wt-%	
TS2	23,86	0,23	5,10	2,85	0,09	1,59	64,50	0,31	1,09	0,11	0,00	0,01	0,00	99,74	
01-lumachelle: gris-nez	6,20	0,07	1,09	1,96	0,03	0,35	51,10	0,16	0,16	0,07	37,97	0,00	0,00	99,17	
02-lumachelle: gris-nez	7,66	0,08	1,52	2,68	0,03	0,47	49,91	0,19	0,22	0,10	36,31	0,00	0,00	99,18	
03-lumachelle: gris-nez	7,53	0,12	2,51	2,03	0,06	0,95	47,77	0,13	0,35	0,05	37,80	0,01	0,00	99,30	
05-lumachelle: gris-nez	12,07	0,17	3,33	3,70	0,09	0,96	44,60	0,18	0,57	0,07	33,34	0,01	0,01	99,09	
06-lumachelle: gris-nez	3,77	0,05	0,93	1,52	0,02	0,44	51,93	0,12	0,11	0,11	40,23	0,00	0,00	99,23	
Tempestite - falaise ; gris-nez	21,62	0,25	3,86	1,92	0,05	1,37	38,30	0,30	0,75	0,13	31,30	0,01	0,00	99,86	
Tempestite; Noirda	45,20	0,10	1,40	3,20	0,03	0,33	27,11	0,10	0,39	0,24	21,08	0,00	0,00	99,17	
Lumachelle Noirda	2,93	0,05	0,75	5,94	0,03	0,37	53,62	0,13	0,10	0,10	35,14	0,00	0,00	99,16	
Lumachelle Noirda*	14,57	0,07	1,11	2,01	0,12	0,39	44,95	0,10	0,22	1,07	34,49	0,00	0,00	99,09	

Tableau 11:

Éléments traces %

Echantillon	Sc (ppm)	V (ppm)	Cr (ppm)	Mn (ppm)	Co (ppm)	Ni (ppm)	Cu (ppm)	Zn (ppm)	Ga (ppm)	Ge (ppm)	As (ppm)	Se (ppm)
Calcaires Moulin Wibert-Gris-Nez-01	<LLD	33	93	503	7	16	5	13	4	<LLD	4	<LLD
Calcaires Moulin Wibert-Gris-Nez-02	<LLD	27	26	338	7	11	4	20	4	<LLD	<LLD	<LLD
Calcaires Moulin Wibert-Gris-Nez-03	<LLD	23	19	245	5	9	4	12	3	<LLD	<LLD	<LLD
Calcaires Moulin Wibert-Gris-Nez-04	<LLD	25	24	231	5	7	4	12	3	<LLD	<LLD	<LLD
Calcaires Moulin Wibert-Gris-Nez-05	<LLD	14	16	161	3	5	3	8	2	<LLD	<LLD	<LLD
Calcaires Moulin Wibert-Gris-Nez-06	<LLD	23	17	210	4	8	4	12	3	<LLD	<LLD	<LLD
Calcaires Moulin Wibert-Gris-Nez-07	<LLD	25	20	261	4	9	4	15	4	<LLD	<LLD	<LLD
Calcaires Moulin Wibert-Gris-Nez-08	<LLD	23	21	286	5	7	4	13	4	<LLD	<LLD	<LLD
Calcaires Moulin Wibert-Gris-Nez-09	<LLD	30	22	234	5	9	4	13	4	<LLD	<LLD	<LLD
Calcaires Moulin Wibert-Gris-Nez-10	<LLD	23	18	273	6	8	4	11	3	<LLD	<LLD	<LLD
Calcaires Moulin Wibert-Gris-Nez-11	<LLD	40	33	433	8	12	6	23	6	<LLD	<LLD	<LLD
Calcaires Moulin Wibert-Gris-Nez-12	<LLD	25	33	296	6	9	4	12	4	<LLD	<LLD	<LLD
Banc carbonaté au sien de l'Argiles de Châtillon-NOIRDA-01		36	33	866	6	12	5	15	5	<LLD	<LLD	<LLD
Banc carbonaté au sien de l'Argiles de Châtillon-NOIRDA-02	<LLD	32	30	558	6	11	6	14	4	<LLD	<LLD	<LLD
Banc carbonaté au sien de l'Argiles de Châtillon-NOIRDA-03	<LLD	24	24	858	5	9	5	13	4	<LLD	<LLD	<LLD
Banc carbonaté au sien de l'Argiles de Châtillon-NOIRDA-04	<LLD	11	13	1094	3	5	4	8	1	<LLD	<LLD	<LLD
Banc carbonaté au sien de l'Argiles de Châtillon-NOIRDA-05	<LLD	26	25	728	4	9	5	12	4	<LLD	<LLD	<LLD
Banc carbonaté au sien de l'Argiles de Châtillon-NOIRDA-06	<LLD	28	26	695	5	9	5	13	4	<LLD	<LLD	<LLD
Bancs Jumeaux au Gris-Nez-05	<LLD	15	12	193	3	5	4	9	3	<LLD	<LLD	<LLD
Bancs Jumeaux au Gris-Nez-09	<LLD	17	17	332	4	6	4	10	3	<LLD	<LLD	<LLD
Bancs Jumeaux au Gris-Nez-10	<LLD	13	12	427	3	4	4	8	2	<LLD	<LLD	<LLD
Bancs Jumeaux au Gris-Nez-12	<LLD	7	7	449	3	3	3	5	1	<LLD	<LLD	<LLD

Éléments traces %

Echantillon	Br	Rb	Sr	Y	Zr	Nb	Mo	Ag	Cd	Sn	Sb	Te
	(ppm)											
Calcaires Moulin Wibert-Gris-Nez-01	2	28	235	12	132	4	2	<LLD	<LLD	<LLD	<LLD	<LLD
Calcaires Moulin Wibert-Gris-Nez-02	2	27	254	7	44	4	1	<LLD	<LLD	<LLD	<LLD	<LLD
Calcaires Moulin Wibert-Gris-Nez-03	2	23	262	6	43	4	2	<LLD	<LLD	<LLD	<LLD	<LLD
Calcaires Moulin Wibert-Gris-Nez-04	2	25	248	6	38	4	1	<LLD	<LLD	<LLD	<LLD	<LLD
Calcaires Moulin Wibert-Gris-Nez-05	1	15	281	4	27	3	1	<LLD	<LLD	<LLD	<LLD	<LLD
Calcaires Moulin Wibert-Gris-Nez-06	3	24	305	6	32	4	<LLD	<LLD	<LLD	<LLD	<LLD	<LLD
Calcaires Moulin Wibert-Gris-Nez-07	3	27	340	8	30	3	<LLD	<LLD	<LLD	<LLD	<LLD	<LLD
Calcaires Moulin Wibert-Gris-Nez-08	4	25	285	6	27	4	<LLD	4	<LLD	<LLD	<LLD	<LLD
Calcaires Moulin Wibert-Gris-Nez-09	2	29	300	7	37	4	1	<LLD	<LLD	<LLD	<LLD	<LLD
Calcaires Moulin Wibert-Gris-Nez-10	<LLD	23	314	5	30	3	<LLD	4	4	<LLD	<LLD	<LLD
Calcaires Moulin Wibert-Gris-Nez-11	2	43	269	12	76	6	<LLD	<LLD	3	<LLD	<LLD	<LLD
Calcaires Moulin Wibert-Gris-Nez-12	2	25	235	6	114	4	1	4	<LLD	<LLD	<LLD	<LLD
<hr/>												
Banc carbonaté au sien de l'Argiles de Châtillon-NOIRDA-01	1	31	192	8	45	4	<LLD	<LLD	<LLD	<LLD	<LLD	<LLD
Banc carbonaté au sien de l'Argiles de Châtillon-NOIRDA-02	1	32	182	8	46	5	<LLD	<LLD	<LLD	<LLD	<LLD	<LLD
Banc carbonaté au sien de l'Argiles de Châtillon-NOIRDA-03	1	29	183	9	67	5	<LLD	<LLD	<LLD	<LLD	<LLD	<LLD
Banc carbonaté au sien de l'Argiles de Châtillon-NOIRDA-04	<LLD	15	402	5	22	3	<LLD	<LLD	<LLD	<LLD	<LLD	<LLD
Banc carbonaté au sien de l'Argiles de Châtillon-NOIRDA-05	5	34	192	6	34	4	<LLD	<LLD	<LLD	<LLD	<LLD	<LLD
Banc carbonaté au sien de l'Argiles de Châtillon-NOIRDA-06	2	29	198	7	29	4	<LLD	<LLD	<LLD	<LLD	<LLD	<LLD
<hr/>												
Bancs Jumeaux au Gris-Nez-05	2	23	202	4	22	3	<LLD	<LLD	<LLD	<LLD	<LLD	<LLD
Bancs Jumeaux au Gris-Nez-09	3	22	212	8	29	3	3	<LLD	<LLD	<LLD	<LLD	<LLD
Bancs Jumeaux au Gris-Nez-10	5	18	174	5	29	3	1	<LLD	4	<LLD	<LLD	<LLD
Bancs Jumeaux au Gris-Nez-12	<LLD	12	184	3	15	2	<LLD	4	<LLD	<LLD	<LLD	<LLD

Éléments traces %

Echantillon	I	Cs	Ba	La	Ce	Nd	Sm	Yb	Hf	Ta	W	Hg	Tl
	(ppm)												
Calcaires Moulin Wibert-Gris-Nez-01	<LLD	8	78	31	27	18	<LLD	2	2	<LLD	1	<LLD	<LLD
Calcaires Moulin Wibert-Gris-Nez-02	5	3	62	18	22	11	<LLD	1	<LLD	<LLD	<LLD	<LLD	1
Calcaires Moulin Wibert-Gris-Nez-03	<LLD	6	52	27	11	6	<LLD	1	1	1	<LLD	<LLD	<LLD
Calcaires Moulin Wibert-Gris-Nez-04	5	6	53	20	13	5	<LLD	1	<LLD	<LLD	<LLD	<LLD	<LLD
Calcaires Moulin Wibert-Gris-Nez-05	4	10	40	20	6	7	6	<LLD	<LLD	<LLD	<LLD	<LLD	<LLD
Calcaires Moulin Wibert-Gris-Nez-06	7	5	54	14	19	11	<LLD	<LLD	1	1	<LLD	<LLD	<LLD
Calcaires Moulin Wibert-Gris-Nez-07	8	8	65	16	20	9	<LLD	<LLD	3	<LLD	<LLD	<LLD	<LLD
Calcaires Moulin Wibert-Gris-Nez-08	6	7	58	15	11	8	<LLD	1	1	<LLD	<LLD	<LLD	<LLD
Calcaires Moulin Wibert-Gris-Nez-09	4	9	70	23	18	14	4	<LLD	4	<LLD	<LLD	<LLD	<LLD
Calcaires Moulin Wibert-Gris-Nez-10	3	8	53	21	19	12	<LLD	<LLD	1	2	1	<LLD	<LLD
Calcaires Moulin Wibert-Gris-Nez-11	5	6	92	22	25	11	<LLD	1	<LLD	<LLD	<LLD	<LLD	<LLD
Calcaires Moulin Wibert-Gris-Nez-12	<LLD	7	61	11	16	7	<LLD	<LLD	4	1	<LLD	<LLD	<LLD
<hr/>													
Banc carbonaté au sien de l'Argiles de Châtillon-NOIRDA-01	3	9	114	24	22	13	<LLD	1	<LLD	<LLD	<LLD	<LLD	<LLD
Banc carbonaté au sien de l'Argiles de Châtillon-NOIRDA-02	<LLD	6	100	19	21	9	<LLD						
Banc carbonaté au sien de l'Argiles de Châtillon-NOIRDA-03	<LLD	8	89	19	17	10	4	1	<LLD	<LLD	<LLD	<LLD	<LLD
Banc carbonaté au sien de l'Argiles de Châtillon-NOIRDA-04	3	7	46	15	7	8	<LLD						
Banc carbonaté au sien de l'Argiles de Châtillon-NOIRDA-05	3	8	77	20	7	6	7	1	3	<LLD	<LLD	<LLD	<LLD
Banc carbonaté au sien de l'Argiles de Châtillon-NOIRDA-06	<LLD	11	87	21	18	11	<LLD						
<hr/>													
Bancs Jumeaux au Gris-Nez-05	5	10	43	15	6	5	3	<LLD	2	<LLD	<LLD	<LLD	<LLD
Bancs Jumeaux au Gris-Nez-09	9	9	43	17	14	5	<LLD	<LLD	1	<LLD	<LLD	<LLD	<LLD
Bancs Jumeaux au Gris-Nez-10	4	4	38	10	12	6	3	<LLD	1	<LLD	<LLD	<LLD	<LLD
Bancs Jumeaux au Gris-Nez-12	<LLD	8	25	9	8	7	<LLD	2	<LLD	<LLD	<LLD	<LLD	<LLD

Éléments traces %

Echantillon	Pb (ppm)	Bi (ppm)	Th (ppm)	U (ppm)
Calcaires Moulin Wibert-Gris-Nez-01	8	<LLD	4	<LLD
Calcaires Moulin Wibert-Gris-Nez-02	4	<LLD	5	<LLD
Calcaires Moulin Wibert-Gris-Nez-03	1	<LLD	5	<LLD
Calcaires Moulin Wibert-Gris-Nez-04	<LLD	<LLD	5	<LLD
Calcaires Moulin Wibert-Gris-Nez-05	<LLD	<LLD	4	<LLD
Calcaires Moulin Wibert-Gris-Nez-06	<LLD	<LLD	5	<LLD
Calcaires Moulin Wibert-Gris-Nez-07	2	<LLD	4	1
Calcaires Moulin Wibert-Gris-Nez-08	<LLD	<LLD	6	<LLD
Calcaires Moulin Wibert-Gris-Nez-09	2	<LLD	5	1
Calcaires Moulin Wibert-Gris-Nez-10	1	<LLD	4	1
Calcaires Moulin Wibert-Gris-Nez-11	3	<LLD	6	<LLD
Calcaires Moulin Wibert-Gris-Nez-12	3	<LLD	5	<LLD
<hr/>				
Banc carbonaté au sien de l'Argiles de Châtillon-NOIRDA-01	3	<LLD	6	<LLD
Banc carbonaté au sien de l'Argiles de Châtillon-NOIRDA-02	2	<LLD	7	<LLD
Banc carbonaté au sien de l'Argiles de Châtillon-NOIRDA-03	2	<LLD	6	<LLD
Banc carbonaté au sien de l'Argiles de Châtillon-NOIRDA-04	<LLD	<LLD	4	1
Banc carbonaté au sien de l'Argiles de Châtillon-NOIRDA-05	3	<LLD	5	<LLD
Banc carbonaté au sien de l'Argiles de Châtillon-NOIRDA-06	2	<LLD	6	<LLD
<hr/>				
Bancs Jumeaux au Gris-Nez-05	<LLD	<LLD	5	<LLD
Bancs Jumeaux au Gris-Nez-09	<LLD	<LLD	5	3
Bancs Jumeaux au Gris-Nez-10	<LLD	<LLD	5	<LLD
Bancs Jumeaux au Gris-Nez-12	<LLD	<LLD	4	<LLD

Tableau 12:

Éléments traces %

Echantillon	Sc	V	Cr	Mn	Co	Ni	Cu	Zn	Ga	Ge	As	Se
	(ppm)											
LLD	1	2	1	2	1	1	1	1	1	1	2	1
01-lumachelle: gris-nez	<LLD	15	16	103	5	5	4	7	2	<LLD	<LLD	<LLD
02-lumachelle: gris-nez	<LLD	23	31	128	6	8	5	21	2	<LLD	<LLD	<LLD
03-lumachelle: gris-nez	<LLD	24	21	379	6	9	5	14	3	<LLD	<LLD	<LLD
05-lumachelle: gris-nez	<LLD	34	40	613	8	17	6	31	5	<LLD	<LLD	<LLD
06-lumachelle: gris-nez	<LLD	11	15	122	4	5	4	6	1	<LLD	<LLD	<LLD
Tempestite - falaise ; gris-nez	<LLD	31	33	289	6	11	6	25	5	<LLD	<LLD	<LLD
Tempestite; Noirda	<LLD	13	19	140	4	7	4	10	2	<LLD	<LLD	<LLD
Lumachelle Noirda	<LLD	19	18	348	3	7	4	8	2	<LLD	<LLD	<LLD
Lumachelle Noirda*	<LLD	10	17	102	5	5	3	9	2	<LLD	<LLD	<LLD

Éléments traces %

Echantillon	Rb	Sr	Y	Zr	Nb	Mo	Ag	Cd	Sn	Sb	Te	I
	(ppm)											
LLD	1	1	1	1	1	1	3	3	2	3	2	3
01-lumachelle: gris-nez	14	571	3	20	2	2	<LLD	<LLD	4	<LLD	<LLD	<LLD
02-lumachelle: gris-nez	19	609	5	25	3	2	<LLD	<LLD	<LLD	<LLD	<LLD	<LLD
03-lumachelle: gris-nez	25	282	5	24	3	1	<LLD	<LLD	<LLD	<LLD	<LLD	<LLD
05-lumachelle: gris-nez	35	284	7	47	4	2	<LLD	<LLD	<LLD	<LLD	<LLD	5
06-lumachelle: gris-nez	12	568	3	15	2	1	<LLD	<LLD	<LLD	<LLD	<LLD	<LLD
Tempestite - falaise ; gris-nez	37	202	10	85	5	<LLD						
Tempestite; Noirda	16	248	8	53	3	1	<LLD	<LLD	<LLD	<LLD	<LLD	<LLD
Lumachelle Noirda	18	174	6	51	3	2	<LLD	<LLD	<LLD	<LLD	<LLD	<LLD
Lumachelle Noirda*	10	398	4	12	2	2	<LLD	<LLD	<LLD	<LLD	<LLD	4

Éléments traces %

Echantillon	Ba	La	Ce	Nd	Sm	Yb	Hf	Ta	W	Hg	Tl	Pb
	(ppm)											
LLD	5	7	5	3	3	1	1	1	1	1	1	1
01-lumachelle: gris-nez	48	14	10	7	<LLD							
02-lumachelle: gris-nez	69	16	12	10	<LLD							
03-lumachelle: gris-nez	57	15	12	8	<LLD	1	<LLD	<LLD	<LLD	<LLD	<LLD	<LLD
05-lumachelle: gris-nez	92	16	23	7	<LLD	<LLD	1	<LLD	<LLD	<LLD	<LLD	2
06-lumachelle: gris-nez	41	16	11	3	<LLD							
Tempestite - falaise ; gris-nez	100	12	26	11	4	<LLD	2	<LLD	1	<LLD	<LLD	3
Tempestite; Noirda	53	9	18	8	3	<LLD	3	<LLD	<LLD	<LLD	<LLD	<LLD
Lumachelle Noirda	51	16	<LLD	5	<LLD	2	<LLD	<LLD	<LLD	<LLD	<LLD	<LLD
Lumachelle Noirda*	35	17	9	7	<LLD	<LLD	4	<LLD	<LLD	<LLD	<LLD	<LLD

Éléments traces %

Echantillon	Bi	Th	U	Cs	Br
	(ppm)	(ppm)	(ppm)	(ppm)	(ppm)
LLD	1	1	1	2	1
01-lumachelle: gris-nez	<LLD	3	2	4	2
02-lumachelle: gris-nez	<LLD	4	3	4	3
03-lumachelle: gris-nez	<LLD	6	<LLD	9	3
05-lumachelle: gris-nez	<LLD	5	<LLD	7	3
06-lumachelle: gris-nez	<LLD	3	2	10	1
Tempestite - falaise ; gris-nez	<LLD	6	1	7	3
Tempestite; Noirda	<LLD	4	<LLD	2	<LLD
Lumachelle Noirda	<LLD	5	2	6	2
Lumachelle Noirda*	<LLD	4	<LLD	8	2

Tableau 13 -1.

Argiles de Châtillon - toutes les échantillon, Granulométrie, Diffraction des argiles, dans les trois sites étudiés , Cap de la Crèche.

échantillons La Crèche	Hstrat (m)	Kaolinite %	Illite %	Chlorite %	Smectite %	CaCO3 %	Grain Moyen	Mediane, Folk	Mediane
Ar-ch-96	0,2	10	25	10	55	16,72	18,87	18,34	16,52
Ar-ch-95	1,2	10	25	15	50	16,29	18,08	17,64	16,09
Ar-ch-94	1,8	20	35	10	35	23,87	19	18,54	16,64
Ar-ch-93	1,8	20	35	15	30	20,75	17,65	17,19	15,09
Ar-ch-92	2,2	25	40	10	25	16,44	13,55	13,16	11,37
Ar-ch-91	3,2	35	40	10	15	22,84	13,84	13,07	9,51
Ar-ch-90	3,9	35	40	10	15	11,66	11,33	10,59	7,23
Ar-ch-89	4,5	30	45	10	15	12,94	8,23	7,85	5,5
Ar-ch-88	5,7	25	50	10	15	20,71	11,31	11,01	9,5
Ar-ch-87	6,3	25	45	15	15	25,54	14,13	13,68	10,8
Ar-ch-86	7,4	25	45	15	15	20,16	19,04	18,48	14,97
Ar-ch-85	8,5	25	50	10	15	37,62	12,99	12,45	9,7
Ar-ch-84	9,8	30	45	10	15	15,53	18,69	18,14	14,2
Ar-ch-83	11	25	40	15	20	21,17	15,81	15,11	10,52
Ar-ch-82	12,5	20	45	15	20	10,8	43,13	41,46	29,81
Ar-ch-81	13,2	25	45	15	15	9,42	30,58	29,15	22,01
Ar-ch-80	13,9	25	45	15	15	12,5	26,1	25,01	19,28
Ar-ch-79	14,4	25	40	15	20	12,13	25,97	25,13	20,83
Ar-ch-78	14,9	30	50	10	10	17,25	23,87	22,99	17,45
Ar-ch-77	15,3	25	50	10	15	16,33	19,21	18,7	15,25
Ar-ch-76	16	25	50	10	15	35,38	12,91	12,31	8,67
Ar-ch-75	16,5	40	40	10	10	27,38	7,16	6,29	5,65
Ar-ch-74	17,5	40	40	10	10	14,13	5,45	5,23	4,23
Ar-ch-73	18,5	30	45	10	15	13,37	10,71	10,37	8,69
Ar-ch-72	19,5	30	45	10	15	19,1	17,5	17,08	10,03
Ar-ch-71	20,5	30	50	10	10	23,79	15,2	14,77	11,98
Ar-ch-70	21,5	30	45	15	10	40,31	11,87	11,41	9,23
Ar-ch-69	23,1	30	50	10	10	18,57	10,36	10,02	8,11
Ar-ch-68	24,1	30	45	10	15	12,99	13,14	12,71	10,21
Ar-ch-67	25,1	30	40	15	15	17,21	16,1	15,6	12,29
Ar-ch-66	25,7	30	45	10	15	16,96	18,92	18,17	13,45
Ar-ch-65	26,4	35	40	10	15	24,23	8,03	7,4	5,06
Ar-ch-64	27	30	45	10	15	38,87	10,99	9,76	6,13

Tableau 13 -1.

**Argiles de Châtillon - toutes les échantillon, Granulométrie, Diffraction des argiles, dans les trois sites étudiés ,
Cap de la Crèche.**

échantillons La Crèche	Argiles	Silt	Sable très fin	Sable fin	Mode	classement	assymétrie
Ar-ch-96	7,3	90,7	1,9	0,1	23,04	1,95	0,28
Ar-ch-95	7,7	90,6	1,6	0,1	22,42	1,95	0,26
Ar-ch-94	6,6	91,3	2	0,1	22,97	1,95	0,29
Ar-ch-93	8	90	1,9	0,1	20,68	2,01	0,32
Ar-ch-92	10,2	89,1	0,7	0	16,48	2,03	0,35
Ar-ch-91	11,9	85,1	2,6	0,3	12,02	2,21	0,55
Ar-ch-90	13,9	84	1,9	0,2	7,77	2,19	0,61
Ar-ch-89	19,6	80,1	0,3	0	5,46	2,18	0,58
Ar-ch-88	13,1	86,8	0,1	0	14,11	2,05	0,34
Ar-ch-87	10,7	88	1,2	0,1	16,74	2,2	0,45
Ar-ch-86	7	89,2	3,5	0,3	22,49	2,13	0,42
Ar-ch-85	11,6	86,8	1,4	0,2	14,68	2,15	0,48
Ar-ch-84	7,4	88,8	3,5	0,3	22,38	2,2	0,46
Ar-ch-83	10,5	85,7	3,5	0,4	12,44	2,29	0,57
Ar-ch-82	3,9	70,5	17,7	7,8	47,56	2,42	0,52
Ar-ch-81	5,4	79,9	12,1	2,9	37,72	2,35	0,5
Ar-ch-80	5,6	83,8	8,9	1,6	34,39	2,25	0,48
Ar-ch-79	5,2	85,7	8	1,1	35,22	2,17	0,4
Ar-ch-78	5,7	85,6	7,5	1,2	34,02	2,29	0,49
Ar-ch-77	7,4	89,1	3,3	0,2	23,5	2,16	0,41
Ar-ch-76	14,6	83,3	1,9	0,2	12,43	2,34	0,56
Ar-ch-75	18,8	81,1	0	0	7,53	1,99	0,43
Ar-ch-74	25	75	0	0	5,39	1,97	0,54
Ar-ch-73	12,6	86,8	0,6	0,1	12,83	2,03	0,4
Ar-ch-72	10,4	83,7	5,4	0,4	10,59	2,39	0,66
Ar-ch-71	10,1	88,5	1,3	0,1	18,4	2,18	0,41
Ar-ch-70	12,3	86,7	0,9	0,1	13,45	2,09	0,44
Ar-ch-69	13,7	86,6	0,4	0	12,4	2,1	0,43
Ar-ch-68	11,6	87,3	1	0,1	16,53	2,17	0,43
Ar-ch-67	8,8	88,8	2,2	0,2	17,61	2,18	0,45
Ar-ch-66	6,7	88	4,6	0,7	17,4	2,23	0,52
Ar-ch-65	20,3	78,7	1	0	5,31	2,1	0,63
Ar-ch-64	18,3	78,3	3,2	0,2	5,69	2,26	0,67

Tableau 13 -2.

Argiles de Châtillon - toutes les échantillon, Granulométrie, Diffraction des argiles, dans les trois sites étudiés , Noirda

échantillons Noirda	H,strat (m)	Smectite %	Illite %	Chlorite %	Kaolinite %	susceptibilité magnétique m³/kg	CaCO3%	Grain Moyen	Argiles <4µm
N2-01	0,2	90	9	1	0	1,68E-08	16	43	5,31
N2-02	0,5	93	6	1	0	1,69E-08	18	40	5,23
N2-03	0,8	93	6	1	0	2,21E-08	13	32	5,06
N2-04	1,2	93	6	1	0	2,20E-08	9	26	7,29
N2-05	1,5	92	7	1	0	2,17E-08	20	30	6,28
N2-06	1,9	94	5	1	0	2,25E-08	26	25	7,4
N2-07	2,3	93	6	1	0	2,24E-08	26	27	7,1
N2-08	2,7	91	8	1	0	2,48E-08	20	21	9,58
N2-09	3	87	11	2	1	3,26E-08	24	29	7,1
N210	3,5	86	11	1	1	2,55E-08	22	33	7,65
N2-11	3,9	77	16	3	5	3,16E-08	39	29	7,43
N2-12	4,3	43	34	6	18	4,11E-08	21	24	7,54
N2-13	4,6	38	38	5	18	3,85E-08	21	19	9,6
N2-14	4,9	30	43	7	21	3,66E-08	27	17	12,12
N2-15	5,1	20	47	9	24	4,23E-08	36	15	11,19
N34	5,3	63	25	4	9	2,65E-08	44	33	11,98
N33	5,5	51	31	5	13	4,45E-08	9	23	8,61
N32	6	54	26	4	15	3,61E-08	8	24	6,95
N31	6,3					3,99E-08	15	26	8,1
N30	6,8	32	44	7	18	4,16E-08	20	20	9,26
N29	7,2	30	41	7	21	3,96E-08	20	16	11,7
N28	7,4	50	29	6	14	3,44E-08	4	32	6,02
N27	7,6	43	34	7	17	3,67E-08	8	46	4,68
N26	8	38	38	7	17	3,95E-08	9	43	4,57
N25	8,3	36	37	8	19	3,71E-08	10	47	4,47
N24	8,4	42	34	6	18	3,79E-08	9	40	5,81
N23	8,6	36	40	7	18	4,21E-08	7	52	5,04
N22	8,9	23	46	8	23	3,83E-08	7	41	5
N21	9,3	29	43	5	23	3,69E-08	2	32	7,29
N20	9,8	13	48	10	29	3,68E-08	13	22	9,48
N19	10,1	21	48	7	24	3,31E-08	15	74	3,87
N17	10,4	14	51	10	25	3,76E-08	10	58	6,3
N18	11	14	47	8	31	3,52E-08	10	48	5,18
N16	12	0	53	10	36	3,86E-08	10	20	19,11
N15	14,6	15	51	9	25	4,65E-08	13	17	13,31
N14	15,3	12	51	9	28	3,45E-08	29	24	10,81
N13	15,6	6	55	12	27	5,35E-08	22	26	6,5
N12	15,9	4	54	9	32	5,99E-08	14	14	15,71
N11	16,3	2	51	11	35	5,46E-08	17	14	17,28
N10	17	13	48	9	30	5,12E-08	18	19	11,73
N9	17,8	4	58	10	28	5,64E-08	11	17	12,19
N8	18,3	12	50	9	30	4,52E-08	15	25	11,53
N7	18,7	14	47	9	29	5,67E-08	11	19	9,56
N6	19,3	12	44	8	35	5,67E-08	10	27	9,79
N5	19,7	11	50	9	30	4,88E-08	3	47	6,29
N4	20	8	50	7	35	4,69E-08	9	57	5,48
N3	20,5	42	35	6	16	2,23E-08	48	51	6,66
N2	21,3	77	16	1	6	2,98E-08	13	38	9,61
N1	21,7	63	24	2	11	3,52E-08	17	22	17,42

Tableau 13 -2.

**Argiles de Châtillon - toutes les échantillon, Granulométrie, Diffraction des argiles, dans les trois sites étudiés ,
Noirda**

échantillons Noirda	Silt	Sable très fin	Sable fin	Sables moyens	Mode	classement	assymétrie
N2-01	80,28	16,6	1,51	1,15	46,3	1,49E+00	0
N2-02	79,4	18,8	1,45	0	46,9	1,46E+00	0
N2-03	88,96	10,71	0,06	0	37,2	1,33E+00	0
N2-04	92,85	6,63	0	0	31,2	1,37E+00	0
N2-05	89,25	9,85	0,51	0	32,6	1,40E+00	0
N2-06	92,42	6,98	0,12	0	26,2	1,38E+00	0
N2-07	90,71	8,42	0,41	0	28,2	1,41E+00	0
N2-08	95,02	4,2	0,04	0	19,7	1,36E+00	0
N2-09	89,02	9,4	1,1	0	28,6	1,45E+00	0
N210	82,36	13,9	3,13	0	27,6	1,60E+00	0
N2-11	88,27	10,61	0,53	0	33,1	1,47E+00	0
N2-12	93,46	5,52	0,33	0,04	22,2	1,34E+00	0
N2-13	97,1	1,96	0	0	18,2	1,27E+00	0
N2-14	97,47	0	0	0	16,541	1,27E+00	0
N2-15	98,61	0,29	0	0	13,9	1,18E+00	0
N34	82,46	11,32	4,98	0,05	9	1,78E+00	- 0
N33	94,38	4,53	0,28	0,03	21	1,35E+00	0
N32	94,6	4,79	0	0	26	1,29E+00	0
N31	92,35	5	1,57	0,4	20	1,38E+00	0
N30	96,88	2,22	0	0	20	1,28E+00	0
N29	97,96	0,87	0	0	13	1,21E+00	0
N28	89,07	9,73	0,61	0,12	36	1,39E+00	0
N27	77,18	16,48	5,01	1,03	40	1,54E+00	0
N26	78,78	15,89	4,38	0,66	36	1,50E+00	0
N25	77,11	16,55	5,1	0,92	39	1,55E+00	0
N24	82,49	12,69	3,33	1,02	32	1,53E+00	0
N23	72,02	18,04	7,75	1,78	45	1,68E+00	0
N22	80,65	15,05	2,7	1,14	40	1,46E+00	0
N21	88,21	9,7	0,69	0,76	34	1,46E+00	0
N20	95,15	3,88	0	0	23	1,35E+00	0
N19	61,58	21,42	12,05	4,71	64	1,79E+00	0
N17	74,24	16,82	6,94	1,48	47	1,77E+00	0
N18	68,82	18,65	9,16	2,96	53	1,73E+00	0
N16	89,92	6,96	0,05	0	7	1,62E+00	- 0
N15	95,68	2,8	0,01	0	12	1,34E+00	- 0
N14	90,08	8,2	0,73	0	11	1,52E+00	- 0
N13	92,6	6,67	0,36	0	22	1,35E+00	0
N12	97,76	0,31	0	0	11	1,26E+00	0
N11	96,13	1,68	0	0	9	1,29E+00	- 0
N10	95,47	2,39	0,36	0,04	15	1,35E+00	0
N8	90,55	5,59	2,48	0,23	12	1,52E+00	- 0
N7	96,08	2,59	0,35	0,21	15	1,28E+00	0
N6	90,19	6,41	2,33	0,25	13	1,51E+00	- 0
N5	74,42	17,1	6,55	1,39	47	1,71E+00	0
N4	65,14	22,33	10,89	1,18	75	1,76E+00	0
N3	62,28	31,24	5,79	0	76	1,73E+00	0
N2	77,18	20,36	1,18	0	55	1,69E+00	0
N1	90,13	5,32	1,61	0,45	8	1,58E+00	- 0

Tableau 13 -3.

Argiles de Châtillon - toutes les échantillon, Granulométrie, Diffraction des argiles, dans le Cap Gris-Nez

échantillon Gris-Nez	H strat (m)	Smectite %	Illite %	Chlorite %	Kaolinite %	susceptibilité magnétique m ³ /kg	CaCO ₃ %
1--1	0,2	92	7	1	0	1,89E-08	29
1--2	0,5	92	7	1	0	1,88E-08	35
1--3	1	91	7	1	0	1,82E-08	40
1--4	1,2	92	7	1	0	2,32E-08	40
1--5	1,5	93	6	1	0	2,91E-08	26
1--6	2	86	9	2	3	3,55E-08	20
1--7	2,3	86	10	2	2	3,02E-08	18
1--8	2,6	86	9	2	3	2,73E-08	16
1--9	2,9	81	13	2	4	2,66E-08	14
1--10	3,4	77	15	2	6	3,31E-08	9
1--11	4	81	13	2	4	3,78E-08	15
1--12	4,3	72	17	4	6	3,92E-08	13
1--13	4,6	79	14	3	4	3,36E-08	12
1--14	5,1	64	22	5	9	3,25E-08	9
1--15	5,4	76	17	3	4	3,41E-08	22
1--16	5,8	82	11	2	5	2,56E-08	13
1--17	6	80	13	2	5	2,68E-08	8
1--18	6,4	80	10	3	7	2,51E-08	11
1--19	6,7	83	10	2	4	2,39E-08	24
1--20	7	60	22	6	11	2,29E-08	24
1--21	7,8	70	18	4	7	3,47E-08	8
1--22	8,3	83	12	2	4	2,18E-08	18
1--23	8,6	84	10	2	4	2,26E-08	25
1--24	8,9	76	16	3	5	2,41E-08	22
1--25-	9,8	24	40	10	26	3,25E-08	18
1--26	10,5	11	45	12	32	3,83E-08	10
1--27	11,2	24	40	11	26	3,46E-08	20
2--27	11,7	86	11	1	2	2,05E-08	13
2--28	11,9	87	10	1	2	2,35E-08	9
2--29	12,3	82	12	1	5	2,41E-08	9
2--30	13,5	84	11	1	4	2,76E-08	16
2--31	14,4	73	18	2	6	3,37E-08	9
1--28	14,7	15	49	10	26	4,02E-08	35
1--29	15	5	50	18	27	3,84E-08	44
2--32	15,3	28	41	8	23	4,17E-08	10
1--30	16,2	8	55	11	25	3,82E-08	78
1--31	17	5	52	10	32	3,55E-08	66
1--32	17,8	5	53	13	29	5,68E-08	11
1--33	18,5	7	47	13	34	4,75E-08	9
1--34	19	3	50	13	34	1,26E-08	31
2--26	19,7	4	53	12	31	3,37E-08	60
2--25	21	1	54	12	33	4,48E-08	12
2--24	21,7	6	56	10	28	4,97E-08	10
2--23	22,7	2	43	10	45	4,80E-08	8

Tableau 13 -3.

Argiles de Châtillon - toutes les échantillon, Granulométrie, Diffraction des argiles, dans le Cap Gris-Nez

echantillon Gris-Nez	H strat (m)	Smectite %	Illite %	Chlorite %	Kaolinite %	susceptibilité magnétique m ³ /kg	CaCO ₃ %
2--22	23	5	51	10	33	3,38E-08	11
2--21	23,3	3	49	10	37	4,33E-08	12
2--20	23,5	11	48	9	32	4,26E-08	13
2--19	24	6	56	10	28	3,25E-08	43
2--18	24,3	7	54	11	28	4,38E-08	34
2--17	24,8	1	56	9	33	5,61E-08	8
2--16	25,1	1	58	10	31	5,42E-08	23
2--15	25,4	5	56	9	31	5,24E-08	7
2--14	25,7	7	58	11	24	5,30E-08	15
2--13	26	10	51	9	31	5,62E-08	12
2--12	26,9	5	55	10	30	3,80E-08	16
2--11	27,3	5	55	9	31	5,63E-08	9
2--10	27,7	10	56	8	26	5,59E-08	15
2--9	28,3	11	58	8	23	5,52E-08	9
2--8	28,5	2	56	8	33	5,10E-08	10
2--7	29	3	54	10	32	5,53E-08	5
2--6	29,3	15	47	9	30	5,53E-08	7
2--5	30,1	4	53	10	33	5,07E-08	5
2--4	30,4	5	54	9	33	3,92E-08	9
2--3	31,2	2	59	7	33	1,16E-08	4
2--2	31,6	0	55	7	38	4,04E-08	12
2--1	31,9	1	53	6	40	1,80E-08	9

Tableau 13 -3.

Argiles de Châtillon - toutes les échantillon, Granulométrie, Diffraction des argiles, le Cap Gris-Nez

echantillon Gris-Nez	Mediane	Argiles <4µm	Silt	Sable très fin	Sable fin	assymétrie	Mode	classement	Sables moyens	Grain Moyen
1--1	29,3	6	84	16	0	0,32	49	1,49	-	34
1--2	23,1	6	92	7	-	0,24	38	1,35	-	28
1--3	29,9	7	86	13	-	0,36	44	1,45	-	33
1--4	29,2	5	89	11	-	0,36	41	1,36	-	32
1--5	19,8	7	96	4	-	0,21	31	1,31	-	24
1--6	20,8	7	89	10	1	0,12	30	1,44	-	30
1--7	21,8	7	90	9	0	0,17	34	1,4	-	28
1--8	18,9	7	92	7	0	0,11	28	1,4	-	26
1--9	17,1	10	90	9	0	0,05	39	1,51	-	26
1--10	29,9	5	77	18	4	0,17	50	1,55	1	43
1--11	27,7	5	79	16	4	0,12	40	1,59	1	43
1--12	25,1	6	81	14	4	0,09	35	1,59	1	40
1--13	41,4	4	66	24	9	0,24	68	1,66	1	57
1--14	46,5	4	60	22	13	0,19	76	1,82	4	72
1--15	20,9	7	89	9	1	0,1	29	1,45	1	31
1--16	25,8	8	83	16	16	0,23	51	1,57	0	34
1--17	24,1	8	84	15	0	0,21	50	1,57	-	32
1--18	26,9	9	85	15	0	0,3	48	1,57	-	33
1--19	29,8	7	82	17	1	0,3	49	1,54	-	36
1--20	29,8	6	82	0	-	0,3	49	1,5	-	36
1--21	32,2	4	75	19	5	0,15	50	1,54	1	47
1--22	39,2	8	67	28	5	0,38	72	1,76	-	47
1--23	27,4	7	85	14	0	0,29	47	1,49	-	33
1--24	24,1	8	84	15	0	0,2	51	1,57	-	33
1--25-	32,3	6	80	20	0	0,08	52	1,51	-	38
1--26	35,0	5	71	19	7	0,17	51	1,67	2	53
1--27	15,7	9	91	8	1	-0,01	15	1,46	-	25
2--27	30,8	8	78	20	1	0,3	57	1,61	-	38
2--28	39,8	6	74	25	1	0,44	57	1,56	-	43
2--29	31,1	8	81	18	0	0,35	49	1,56	-	36
2--30	38,0	6	75	24	1	0,41	56	1,56	-	42
2--31	32,6	6	80	19	1	0,32	49	1,5	-	38
1--28	10,5	16	87	9	2	-0,2	8	1,65	-	23
1--29	19,1	8	89	10	0	0,07	25	1,47	-	28
2--32	35,1	6	68	20	10	0,17	60	1,78	1	55
1--30	8,8	17	95	2	0	-0,08	8	1,24	-	14
1--31	16,5	8	89	8	2	-0,04	14	1,52	0	29
1--32	13,4	10	94	4	1	-0,04	13	1,36	0	22
1--33	40,7	5	64	20	13	0,14	70	1,83	3	67
1--34	30,0	6	68	19	12	0,05	95	1,81	1	54
2--26	10,0	15	95	3	0	-0,09	10	1,36	-	17
2--25	8,5	22	88	7	1	-0,23	6	1,66	-	19
2--24	8,7	21	92	4	0	-0,13	7	1,49	0	16
2--23	7,3	25	95	1	-	-0,08	6	1,28	-	11

Tableau 13 -3.

Argiles de Châtillon - toutes les échantillon, Granulométrie, Diffraction des argiles, dans le Cap Gris-Nez

echantillon Gris-Nez	Mediane	Argiles <4µm	Silt	Sable très fin	Sable fin	assymétri e	Mode	classemen t	Sables moyens	Grain Moyen
2--22	7,5	25	89	5	1	-0,21	6	1,45	0	17
2--21	13,0	14	78	15	5	-0,2	8	1,89	-	34
2--20	12,9	14	86	10	2	-0,13	10	1,69	-	27
2--19	12,7	12	82	13	2	-0,2	9	1,74	-	29
2--18	16,5	9	91	7	1	0,04	18	1,46	-	25
2--17	12,9	12	97	2	-	0,05	16	1,32	-	18
2--16	10,4	13	98	1	-	-0,02	10	1,23	-	15
2--15	13,1	13	93	5	0	-0,01	13	1,47	-	21
2--14	11,4	16	92	4	1	-0,06	11	1,51	1	24
2--13	11,7	13	98	1	-	0,05	13	1,25	-	16
2--12	23,5	7	72	19	8	0	15	1,78	-	44
2--11	12,1	11	98	1	-	0,06	14	1,22	-	16
2--10	14,4	10	94	5	1	0,02	16	1,4	0	22
2--9	10,9	13	98	1	-	0,03	12	1,21	-	15
2--8	19,2	8	85	11	4	-0,01	19	1,6	0	33
2--7	25,3	6	83	14	3	0,12	35	1,52	-	37
2--6	27,8	6	80	16	4	0,15	42	1,55	-	40
2--5	69,5	4	48	20	19	0,22	113	2,01	13	111
2--4	67,8	4	48	25	23	0,37	120	1,85	3	85
2--3	86,9	7	41	22	29	0,52	144	2,12	6	96
2--2	13,7	14	82	10	6	-0,17	9	1,85	1	34
2--1	16,4	16	63	14	16	-0,18	6	3,3	4	61

Tableau 14:

Summary_Table

	RockEval Argiles de Châtillon (Cap Gris-Nez, Noirda)						
	Echantillon	PC [%]	RC [%]	TOC [%]	MINC [%]	HI [mg HC/g TOC]	OI [mg CO2/g TOC]
Cap Gris-Nez	Gris-Nez 1-2	0,11	0,91	1,02	4,16	106	71
	Gris-Nez 2-14	0,32	1,35	1,66	1,94	208	61
	Gris-Nez 2-8	1,14	2,28	3,42	1,14	385	46
	Gris-Nez 1-31	0,17	0,77	0,93	7,66	188	77
	Gris-Nez 1-23	0,05	0,33	0,38	3,57	111	97
	Gris-Nez 2-25	0,03	0,37	0,40	1,35	44	137
	Gris-Nez 2-5	3,39	3,45	6,83	0,98	584	30
	Gris-Nez 1-19	0,05	0,28	0,34	3,23	143	117
	Gris-Nez 1-29	0,22	0,81	1,03	5,84	232	73
	Gris-Nez 1-25-1	0,27	0,78	1,06	3,73	287	69
	Gris-Nez 1-11	0,90	1,78	2,69	2,23	386	49
	Gris-Nez 1-25-2	0,25	0,69	0,95	2,48	299	57
	Gris-Nez 1-27	0,12	0,72	0,84	2,33	143	83
Noirda	Noirda 14	0,18	0,72	0,89	4,06	221	54
	Noirda 7	0,39	1,67	2,05	1,66	214	35
	Noirda 10	0,23	1,51	1,74	2,30	146	38
	Noirda 22	0,88	2,02	2,89	0,80	349	47
	Noirda 27	1,63	2,34	3,98	1,00	485	27
	Noirda 3	0,01	0,12	0,14	6,41	54	204
	Noirda 18	1,76	2,61	4,37	1,39	472	37
	Noirda 19	1,39	2,08	3,48	1,55	471	33
	Noirda 1	0,04	0,47	0,51	2,21	58	102
	Noirda 25	1,54	2,36	3,91	1,33	466	27
	Noirda Superieur -2	0,13	1,02	1,15	3,11	124	40
	Noirda Superieur -9	0,52	1,31	1,82	3,45	331	30
	Noirda Superieur -5	0,23	1,05	1,28	4,52	200	42
	Noirda Superieur -13	0,36	1,36	1,72	1,89	243	27

Tableau 14:

Summary_Table

	RockEval Argiles de Châtillon (Cap Gris-Nez, Noirda)					
	Echantillon	S2a [mg HC/g]	S2b [mg HC/g]	S3	Re6type	Quant
Cap Gris-Nez	Gris-Nez 1-2	1,09	0,00	0,73	Analysis	50,5
	Gris-Nez 2-14	3,47	0,00	1,02	Analysis	58,4
	Gris-Nez 2-8	13,16	0,00	1,56	Analysis	70,7
	Gris-Nez 1-31	1,76	0,00	0,72	Analysis	67,7
	Gris-Nez 1-23	0,42	0,00	0,37	Analysis	68,2
	Gris-Nez 2-25	0,18	0,00	0,55	Analysis	60,2
	Gris-Nez 2-5	39,94	0,00	2,05	Analysis	52,1
	Gris-Nez 1-19	0,48	0,00	0,39	Analysis	39,5
	Gris-Nez 1-29	2,39	0,00	0,75	Analysis	55,1
	Gris-Nez 1-25-1	3,03	0,00	0,73	Analysis	44,1
	Gris-Nez 1-11	10,38	0,00	1,32	Analysis	43,1
	Gris-Nez 1-25-2	2,83	0,00	0,54	Analysis	49,5
	Gris-Nez 1-27	1,21	0,00	0,70	Analysis	50,9
Noirda	Noirda 14	1,98	0,00	0,48	Analysis	63,1
	Noirda 7	4,41	0,00	0,72	Analysis	55,9
	Noirda 10	2,55	0,00	0,66	Analysis	62,4
	Noirda 22	10,09	0,00	1,36	Analysis	59,6
	Noirda 27	19,28	0,00	1,07	Analysis	51
	Noirda 3	0,07	0,00	0,28	Analysis	56,1
	Noirda 18	20,64	0,00	1,61	Analysis	62,1
	Noirda 19	16,38	0,00	1,15	Analysis	53
	Noirda 1	0,30	0,00	0,52	Analysis	55,4
	Noirda 25	18,22	0,00	1,06	Analysis	60,7
	Noirda Superieur -2	1,42	0,00	0,46	Analysis	57,1
	Noirda Superieur -9	6,03	0,00	0,55	Analysis	43,3
	Noirda Superieur -5	2,56	0,00	0,54	Analysis	43,2
	Noirda Superieur -13	4,18	0,00	0,47	Analysis	59,9

Tableau 15:

Eléments majeurs % - Argiles de Châtillon-Cap Gris Nez

Echant.	SiO2	Al2O3	Fe2O3	MnO	MgO	CaO	Na2O	K2O	LOI	Cr2O3	NiO
	wt-%	wt-%	wt-%	wt-%	wt-%	wt-%	wt-%	wt-%	wt-%	wt-%	wt-%
ARCH1-2	54,00	3,00	2,00	1,00	1	19,00	0,36	0,7	16,00	8,00	0,00
ARCH1-11	50,00	9,00	4,00	3,00	3,00	10,00	0,7	2,00	16,00	8,00	8,00
ARCH1-19	59,00	5,00	2,00	2,00	1,00	14,00	0,7	1,00	13,00	8,00	0,00
ARCH1-23	58,00	5,00	2,00	2,00	1,00	15,00	0,7	1,00	14,00	8,00	0,00
ARCH1-25	51,00	6,00	4,00	4,00	3,00	14,00	0,5	1,00	16,00	8,00	0,00
ARCH1-25A	65,00	6,00	2,00	2,00	1,00	9,00	0,7	1,00	10,00	8,00	0,00
ARCH1-27	57,00	6,00	4,00	2,00	1,00	13,00	0,5	1,00	12,00	8,00	0,00
ARCH1-29	40,00	7,00	4,00	4,00	2,00	21,00	0,4	1,00	21,00	8,00	8,00
ARCH1-31	17,00	5,00	2,00	2,00	1,00	39,00	0,3	1,00	31,00	6,00	6,00
ARCH2-5	45,00	13,00	5,00	3,00	2,00	4,00	0,6	2,00	21,00	1,00	7,00
ARCH2-14	48,00	12,00	5,00	2,00	2,00	11,00	0,5	2,00	14,00	1,00	8,00
ARCH2-25	61,00	14,00	3,00	2,00	1,00	5,00	0,6	2,00	9,00	1,00	9,00

Tableau 16:

Eléments majeurs % - Argiles de Châtillon-Cap Gris Nez

Echant.	SiO2	Al2O3	Fe2O3	MnO	MgO	CaO	Na2O	K2O	LOI	Cr2O3	NiO
	wt-%	wt-%	wt-%	wt-%	wt-%	wt-%	wt-%	wt-%	wt-%	wt-%	wt-%
ARCH1-2	54,00	3,00	2,00	1,00	1	19,00	0,36	0,7	16,00	8,00	0,00
ARCH1-11	50,00	9,00	4,00	3,00	3,00	10,00	0,7	2,00	16,00	8,00	8,00
ARCH1-19	59,00	5,00	2,00	2,00	1,00	14,00	0,7	1,00	13,00	8,00	0,00
ARCH1-23	58,00	5,00	2,00	2,00	1,00	15,00	0,7	1,00	14,00	8,00	0,00
ARCH1-25	51,00	6,00	4,00	4,00	3,00	14,00	0,5	1,00	16,00	8,00	0,00
ARCH1-25A	65,00	6,00	2,00	2,00	1,00	9,00	0,7	1,00	10,00	8,00	0,00
ARCH1-27	57,00	6,00	4,00	2,00	1,00	13,00	0,5	1,00	12,00	8,00	0,00
ARCH1-29	40,00	7,00	4,00	4,00	2,00	21,00	0,4	1,00	21,00	8,00	8,00
ARCH1-31	17,00	5,00	2,00	2,00	1,00	39,00	0,3	1,00	31,00	6,00	6,00
ARCH2-5	45,00	13,00	5,00	3,00	2,00	4,00	0,6	2,00	21,00	1,00	7,00
ARCH2-14	48,00	12,00	5,00	2,00	2,00	11,00	0,5	2,00	14,00	1,00	8,00
ARCH2-25	61,00	14,00	3,00	2,00	1,00	5,00	0,6	2,00	9,00	1,00	9,00

Tableau 17:

Eléments majeurs % - Argiles de Châtillon-Noirda

Eléments majeurs % - Argiles de Châtillon-Noirda														
Echant.	SiO ₂	TiO ₂	Al ₂ O ₃	Fe ₂ O ₃	MnO	MgO	CaO	Na ₂ O	K ₂ O	P ₂ O ₅	LOI	Cr ₂ O ₃	NiO	
	wt-%	wt-%	wt-%	wt-%	wt-%	wt-%	wt-%	wt-%	wt-%	wt-%	wt-%	wt-%	wt-%	wt-%
NOIRDA-1	61	0,6	7,9	4,3	0,0	1,1	10,2	0,2	1,5	0,2	11,9	0,0	-	
NOIRDA-3	45	0,3	2,6	1,7	0,0	0,4	26,3	0,2	0,5	0,1	21,8	0,0	-	
NOIRDA-7	49	0,7	14,2	5,6	0,0	2,6	7,8	0,3	2,8	0,3	16,0	0,0	0,0	
NOIRDA-10	42	0,6	11,0	6,0	0,0	2,1	16,5	0,2	2,2	0,6	17,5	0,0	0,0	
NOIRDA-14	49	0,5	6,5	3,8	0,0	1,9	18,1	0,2	1,4	0,5	17,8	0,0	-	
NOIRDA-18	54	0,6	9,6	4,2	0,0	1,8	10,2	0,4	2,1	0,6	15,6	0,0	0,0	
NOIRDA-19	56	0,6	10,4	4,2	0,0	1,2	7,2	0,5	2,3	0,9	16,0	0,0	0,0	
NOIRDA-22	59	0,7	10,9	4,5	0,0	1,3	6,2	0,6	2,4	0,7	12,6	0,0	0,0	
NOIRDA-25	55	0,7	11,0	4,6	0,0	2,1	6,8	0,5	2,4	0,7	15,5	0,0	0,0	
NOIRDA-27	58	0,7	10,4	3,8	0,0	1,7	6,8	0,6	2,3	0,6	14,4	0,0	0,0	
NOIRDA-SUP02	60	0,5	3,9	2,7	0,0	0,6	15,3	0,2	0,8	0,1	14,8	0,0	-	
NOIRDA-SUP05	41	0,4	5,7	4,1	0,0	0,9	24,3	0,2	1,0	0,2	21,7	0,0	-	
NOIRDA-SUP09	43	0,6	10,5	5,7	0,0	2,0	14,5	0,3	2,2	0,5	20,1	0,0	0,0	
NOIRDA-SUP13	51	0,7	12,0	5,0	0,0	2,5	9,1	0,4	2,5	0,3	15,8	0,0	0,0	

Tableau 18:

Concentrations en éléments traces ppm-Argiles de Châtillon- Cap Gris Nez

Echant.	Sc	V	Cr	Mn	Co	Ni	Cu	Zn	Ga	Ge	As	Se
	(ppm)											
LLD	1	2	1	2	2	1	1	1	1	1	3	1
ARCH1-2	4	34	52	130	3	11	6	26	4	<LLD	8	<LLD
ARCH1-11	8	67	70	221	8	33	14	43	12	<LLD	4	<LLD
ARCH1-19	6	34	55	210	4	13	6	18	6	<LLD	5	<LLD
ARCH1-23	7	31	57	191	4	12	6	19	6	<LLD	4	<LLD
ARCH1-25	9	52	58	283	7	25	9	32	8	<LLD	7	<LLD
ARCH1-25A	6	37	50	172	4	17	7	21	6	<LLD	4	1
ARCH1-27	8	64	64	171	7	22	9	30	9	<LLD	15	1
ARCH1-29	9	60	62	339	7	25	9	30	9	<LLD	4	<LLD
ARCH1-31	8	63	67	174	7	24	8	24	10	<LLD	6	<LLD
ARCH2-5	12	103	99	225	12	63	24	80	17	<LLD	10	3
ARCH2-14	12	102	101	209	10	39	13	58	17	<LLD	12	1
ARCH2-25	14	125	97	181	18	40	17	46	19	<LLD	10	<LLD

Echant.	Sr	Y	Zr	Nb	Mo	Ag	Cd	Sn	Sb	Te	I	Cs
	(ppm)											
LLD	1	1	1	1	1	3	3	2	3	3	3	2
ARCH1-2	245	19	322	8	<LLD	<LLD	<LLD	2	<LLD	<LLD	<LLD	<LLD
ARCH1-11	182	25	185	10	2	<LLD	<LLD	<LLD	<LLD	<LLD	<LLD	4
ARCH1-19	130	21	344	8	<LLD	<LLD	<LLD	3	<LLD	<LLD	<LLD	3
ARCH1-23	139	21	329	7	<LLD	<LLD	4	3	<LLD	<LLD	<LLD	4
ARCH1-25	158	23	205	8	<LLD	<LLD	<LLD	3	<LLD	<LLD	<LLD	6
ARCH1-25A	148	25	314	8	2	<LLD	<LLD	2	<LLD	<LLD	<LLD	5
ARCH1-27	176	22	204	8	1	<LLD	<LLD	2	<LLD	<LLD	<LLD	6
ARCH1-29	201	17	144	8	2	<LLD	<LLD	<LLD	<LLD	<LLD	4	7
ARCH1-31	316	11	60	6	3	<LLD	<LLD	<LLD	<LLD	<LLD	<LLD	6
ARCH2-5	160	26	132	12	4	<LLD	4	5	<LLD	<LLD	4	8
ARCH2-14	194	25	153	12	4	<LLD	<LLD	4	<LLD	<LLD	<LLD	9
ARCH2-25	161	24	275	14	<LLD	<LLD	3	6	<LLD	<LLD	4	7

Concentrations en éléments traces ppm-Argiles de Châtillon- Cap Gris Nez

Echant.	La	Ce	Nd	Sm	Yb	Hf	Ta	W	Hg	Tl	Rb	Pb
	(ppm)											
LLD	7	5	3	3	2	2	1	1	4	2	1	1
ARCH1-2	23	35	15	<LLD	3	8	<LLD	<LLD	<LLD	<LLD	33	7
ARCH1-11	37	53	25	5	2	5	1	1	<LLD	<LLD	90	11
ARCH1-19	26	37	18	<LLD	3	9	<LLD	<LLD	<LLD	<LLD	51	8
ARCH1-23	25	44	18	<LLD	<LLD	8	1	<LLD	<LLD	<LLD	50	8
ARCH1-25	35	43	21	6	3	5	2	1	<LLD	<LLD	62	10
ARCH1-25A	25	42	23	<LLD	3	7	1	<LLD	<LLD	<LLD	55	8
ARCH1-27	27	44	22	5	<LLD	3	<LLD	<LLD	<LLD	<LLD	68	10
ARCH1-29	29	35	18	<LLD	3	3	2	1	<LLD	<LLD	67	8
ARCH1-31	29	38	15	<LLD	<LLD	4	<LLD	<LLD	<LLD	<LLD	67	7
ARCH2-5	42	58	27	3	2	4	1	1	<LLD	<LLD	124	19
ARCH2-14	46	62	28	<LLD	2	4	1	2	<LLD	<LLD	118	15
ARCH2-25	36	70	27	4	3	8	2	2	<LLD	<LLD	123	18

Echant.	Th	U	Br	Bi	Ba
	(ppm)	(ppm)	(ppm)	(ppm)	(ppm)
LLD	1	1	1	1	5
ARCH1-2	6	4	4	<LLD	87
ARCH1-11	9	3	7	<LLD	203
ARCH1-19	7	3	3	<LLD	160
ARCH1-23	7	3	3	<LLD	161
ARCH1-25	7	3	6	<LLD	163
ARCH1-25A	8	4	6	<LLD	176
ARCH1-27	8	3	6	1	176
ARCH1-29	6	4	8	<LLD	153
ARCH1-31	6	3	5	<LLD	146
ARCH2-5	11	4	11	<LLD	246
ARCH2-14	10	4	8	2	225
ARCH2-25	11	4	13	<LLD	289

Tableau 19 : Données de composition de Carbone et oxygène (isotope stable) pour toutes les formations étudiées.

Bancs J. Gris Nez	$\delta^{13}\text{C}$	$\delta^{18}\text{O}$	% CaCO ₃	Bancs J. Wimereux	$\delta^{13}\text{C}$	$\delta^{18}\text{O}$	% CaCO ₃
b1	-1,98	-4,13	27	w03 6.08	0,77	-5,81	31,75
b1	-2,05	-4,23	26	w03 7.74	0,93	-5,75	31,97
b02	-1,59	-2,87	82	w06 15.41	1,10	-4,22	22,86
b02	-1,66	-2,83	65	w06 8.03	0,78	-4,69	22,68
b03	-2,10	-4,04	60	w07 4.09	0,69	-4,37	53,66
b04	0,52	-2,58	12	W07 4.89	0,73	-4,37	52,92
b05	-1,73	-2,34	86	w08 2.96	-1,68	-2,89	77,90
b06	0,16	-2,67	34	w08 3.02	-1,71	-2,94	78,46
b06	0,00	-2,39	29	w09 6.54	0,48	-3,61	26,06
b7	0,48	-2,53	27	w09 7.66	0,62	-3,55	25,62
b7	0,31	-2,55	27	W10 3.75	0,05	-3,61	56,07
b08	-0,67	-2,41	38	W10 4.02	0,27	-3,62	54,51
b8	-0,57	-2,61	33	W11 2.05	-2,60	-3,30	89,71
b09	-4,18	-2,03	85	W11 2.65	-2,53	-3,19	87,30
b09	-3,90	-1,86	90	w12 3.84	0,59	-3,09	41,26
b10	-3,32	-2,62	76	w12 4.10	0,81	-3,06	42,25
b11	-1,92	-3,51	50	w13 4.09	0,63	-2,89	41,49
b12	-4,13	-1,75	86	w13 4.30	0,63	-2,86	40,43
b13	-1,04	-4,12	43	w15 2.92	0,21	-3,57	54,92
b14	-0,57	-4,26	39	w15 3.66	0,22	-3,51	55,10
b15	-2,72	-4,77	27	W16 2.38	-1,05	-2,74	87,53
b16	0,16	-4,01	24	w16 2.64	-1,08	-2,77	84,95
				W17 5.64	1,34	-3,33	30,20
				w17 7.39	1,33	-3,26	25,73
				w18 3.77	1,36	-3,93	43,17
				w18 4.37	1,27	-3,80	44,08
				w19 3.73	1,36	-3,96	54,71
				w19 4.91	1,32	-3,74	56,51
				BJ201 7.01	0,72	-5,01	27,91
				BJ201 8.28	0,66	-5,02	27,65
				Banc inférieur, base du banc avec du sédiment incorporé au calcaire	-3,98	-4,16	77,21
				Banc inférieur	-2,69	-3,13	79,04
				Banc inférieur	-1,21	-2,57	79,26
				Banc inférieur	-0,37	-2,38	78,66
				Banc inférieur	-0,30	-2,46	78,61
				Banc inférieur	-0,29	-2,31	83,80
				Banc inférieur, sommet du banc, "propre"	-1,30	-2,65	89,77
				Banc intermédiaire, intérieur de la bioturbation	-1,41	-2,64	89,37
				Banc intermédiaire, encaissant de la bioturbation	-3,49	-3,84	88,36
				Banc intermédiaire, base ou sommet du banc	-3,28	-3,28	90,89
				Banc intermédiaire, milieu du banc	-1,31	-2,64	89,27
				Banc intermédiaire, base ou sommet du banc	-2,86	-3,35	87,94

Tableau 19 : Données de composition de Carbone et oxygène (isotope stable) pour toutes les formations étudiées.

Patch reefs	$\delta^{13}\text{C}$	$\delta^{18}\text{O}$	% CaCO ₃	Patch reefs 2	$\delta^{13}\text{C}$	$\delta^{18}\text{O}$	% CaCO ₃	Calc. Moulin Wibert (Lot FB)	$\delta^{13}\text{C}$	$\delta^{18}\text{O}$	CaCO ₃ %
NTPR5-2.39	-8,46	-1,160	99					MW-1-01 117	0,75	-2,50	50
NTPR3-1.80	-9,45	-0,893	100	am01ma	-8,87	-0,98	85,79	MW-2-01 124 C	-1,00	-2,34	76
NTPR3-2.69	-9,54	-1,055	100	am01ma2	-8,47	-1,07	87,16	MW-3-01 118 B	0,03	-2,52	72
NTPR8-2.32	-1,95	-1,723	100	am02ma	-6,20	-1,48	82,67	MW-4-01 137 B	-1,31	-2,29	75
NTPR2-2.03	-1,42	-2,244	79	am02ma2	-7,73	-1,09	89,07	MW-5-01 131 A	0,31	-2,25	82
NTPR7-2.55	-1,75	-1,799	100	am03ma	0,03	-1,43	75,02	MW-6-01 122	0,23	-2,29	77
NTPR6-2.30	-9,67	-0,773	100	noirdama	-3,86	-2,17	45,44	MW-7-01 138	0,15	-2,31	86
NTPR10-2.44	-0,67	-2,350	100	noirdacoq	0,26	-2,50	43,52	MW-8-01 125 A	-0,33	-2,19	82
NTPR01-1.98	-1,61	-2,226	100	am03coq	-1,93	-1,70	69,88	MW-9-01 124 D	-0,38	-2,16	83
NTPR01-2.50	-1,54	-2,089	96	am03rem	-2,03	-1,43	73,39	MW-10-01 121 A	-0,60	-2,48	94
NTPR04-2.32	-9,62	-0,794	100	noirdarem	0,55	-5,19	86,02	MW-11-01- 135 A	-1,42	-1,87	70
NTPR04-2.42	-9,69	-0,737	100					MW-12-01 129	-1,06	-2,14	80
NTPR09-2.51	-0,96	-2,607	99					MW-1-02 135 B	0,87	-2,30	50
								MW-2-02 126 A	-1,14	-2,31	76
								MW-3-02 121 B	-0,20	-2,42	72
								MW-4-02 137 C	0,02	-2,34	75
								MW-5-02 121 C	-1,17	-2,31	82
								MW-6-02 134 A	-0,49	-2,43	77
								MW-7-02 127 A	-0,57	-2,45	86
								MW-8-02 123	0,01	-2,47	82
								MW-9-02 137 D	-0,36	-2,45	83
								MW-11-02 127 B	-1,66	-1,93	70
								MW-12-02 126 B	-1,12	-2,25	80
								MW-2-01 133	-1,04	-2,28	76
								MW-7-01 119	0,18	-2,35	86
								MW-2-02 134 B	-1,17	-2,47	76
								MW-10-02 125 B	-0,68	-2,69	94

Tableau 19 : Données de composition de Carbone et oxygène (isotope stable) pour toutes les formations étudiées.

Banc Noduleux AdeC	$\delta^{13}\text{C}$	$\delta^{18}\text{O}$	CaCO ₃ %	Bancs Jumeaux Cap Gris Nez	$\delta^{13}\text{C}$	$\delta^{18}\text{O}$	% CaCO ₃	Bancs calcaires des C. du Moulin Wibert	$\delta^{13}\text{C}$	$\delta^{18}\text{O}$	CaCO ₃ %
AR noirda 01	-5,8	-4,5	76,8	BJ05	-1,7	-2,9	85,8	CMW GN 01	0,3	-3,7	59,0
AR noirda 02	-5,4	-4,7	79,7	BJ09	-3,6	-2,8	89,4	CMW GN 01	0,3	-3,4	58,2
AR noirda 03	-4,2	-4,1	80,8	BJ10	-3,0	-3,1	87,7	CMW GN 02	-0,3	-2,5	74,3
AR noirda 04	-3,4	-3,5	75,2	BJ12	-3,9	-2,3	87,7	CMW GN 03	0,2	-3,2	73,1
AR noirda 04	-3,4	-3,5	82,2					CMW GN 04	-0,1	-2,5	79,7
AR noirda 05	-4,1	-3,4	75,9					CMW GN 05	-0,8	-2,7	101,6
AR noirda 06	-4,3	-2,9	71,8					CMW GN 06	0,4	-2,6	83,5
AR noirda 07	-4,4	-2,8	81,6					CMW GN 07	-0,5	-2,7	85,9
AR noirda 08	-4,2	-3,3	82,7					CMW GN 08	0,1	-2,8	85,1
AR noirda 09	-3,6	-3,7	84,4					CMW GN 09	0,2	-2,5	80,5
AR noirda 10	-5,4	-4,7	84,8					CMW GN 10	0,0	-3,1	80,4
								CMW GN 11	-0,9	-2,3	70,4
								CMW GN 11	-0,9	-2,2	70,9
								CMW GN 12	-0,8	-2,5	69,0
								LCMW 11	-1,7	-1,9	67,7
								LCMW 12	-1,1	-2,3	65,6
								LCMW 2	-0,9	-2,3	73,6
								LCMW 3	0,0	-2,4	70,1
								LCMW 4	-0,1	-2,3	76,5
								LCMW 6	0,4	-2,3	78,6
								LCMW 7	-0,1	-2,4	77,5
								LCMW 8	0,2	-2,1	82,8

Tableau 19 : Données de composition de Carbone et oxygène (isotope stable) pour toutes les formations étudiées.

Bancs calcaires des C. du Moulin Wibert (matrice)	$\delta^{13}\text{C}$	$\delta^{18}\text{O}$	% CaCO ₃	Bancs limites Argiles - Grès de Chatillon	$\delta^{13}\text{C}$	$\delta^{18}\text{O}$	CaCO ₃ %	Patch à huîtres (matrice ?)	$\delta^{13}\text{C}$	$\delta^{18}\text{O}$	CaCO ₃ %
				N1	-11,3	-2,1	86,3	Patch à huître GN	-3,5	-1,6	91,6
				N2	-10,4	-1,8	74,8	Patch à huître N1	-1,4	-2,7	73,6
LCMW 2	-0,9	-2,3	73,6	N3	-0,4	-3,5	83,9	Patch à huître N2	-1,3	-2,6	73,3
LCMW 3	0,0	-2,4	70,1	N4	-2,3	-3,7	64,1	Patch à huître N2	-1,3	-2,5	77,8
LCMW 4	-0,1	-2,3	76,5								
LCMW 6	0,4	-2,3	78,6								
LCMW 7	-0,1	-2,4	77,5								
LCMW 8	0,2	-2,1	82,8								
LCMW 11	-1,7	-1,9	67,7								
LCMW 12	-1,1	-2,3	65,6								